Technical Report No. I.

Analyses of Breaching of MR-GO Reach 2 EBSBs During Hurricane Katrina & The 'Neutral' MR-GO Hurricane Katrina Conditions

Report to

Katrina Canal Breaches Consolidated Litigation

[Civil Action Number: 05-4182 "K" (2)]

United States District Court

Eastern District of Louisiana

Pertains to MR-GO, Robinson

[No. 06-2268)

By

Dr. Robert Bea and Rune Storesund

Risk Assessment and Management Services

Moraga, California

July 11, 2008

TABLE OF CONTENTS

I. Executive Summary 3

II. Introduction 6

III. Document Review 7

IV. MR-GO Historic Overview 8

Project Authorization 8

Design Considerations 10

General MR-GO Soil Conditions 13

IV.1.1. Summary of EBSB Fill Characteristics 19

Construction History 22

IV.1.2. MR-GO First Lift - 1968 24

IV.1.3. Second Lift - 1972 28

IV.1.4. First Enlargement – 1980 33

IV.1.5. 'Levee' Closures – 1982 35

IV.1.6. Second Enlargement – 1985 36

IV.1.7. 'Levee' Closures – 1987 38

IV.1.8. 'Levee' Closures – 1992 38

IV.1.9. Summary of Crest Elevation at Station 497+00 40

V. Study Site and Topography 41

VI. Hydrodynamic Loading 46

VII. Erosion Characterization 49

Erodibility Soil Sampling Locations 50

EBSB Erodibility Curves 54

Effects of Soil Compaction 58

VIII. Wave Impact Modeling 61

Overview 61

Model Units 62

Model Geometry 62

Boundary Conditions and Material Properties 64

Wave Generation 66

Wave Breaking 72

Determination of Interaction Shear Velocities 74

IX. Velocity Simulation Results 74

Analysis for Scenario 1 (0430 CDT) 75

Analysis for Scenario 1 (0530 CDT) 78
Analysis for Scenario 1 (0630 CDT) 81
Analysis for Scenario 1 (0730 CDT) 84
Analysis for Scenario 1 (0830 CDT) 87
Analysis for Scenario 2C (0430 CDT) 90
Analysis for Scenario 2C (0530 CDT) 93
Analysis for Scenario 2C (0630 CDT) 96
Analysis for Scenario 2C (0730 CDT) 99
Analysis for Scenario 2C (0830 CDT) 102
X. Estimation of EBSB Breach due to Wave Impacts 105
Effects of Grass Cover (Turf) 106
Wave-Induced Erosion Estimates 111
EBSB Overtopping-Induced Erosion 120
XI. Parametric Erosion Evaluations 131
XII. Review of Possible MR-GO Wave-Induced Erosion Sites 136
Determination of Wave-Induced Erosion 136
Possible Wave-Induced Erosion Sites 141
XIII. Comparison with USACE Analyses 143
XIV. Model Calibration and Validation 145
XV. References 148
XVI. APPENDIX A – PARAMETRIC STUDIES OF EBSB EROSION 155
IPET and LSU (2007) Hydrodynamic Conditions 155
IPET Hydrodynamics 155
Model Configuration and Conditions 166
IPET and LSU (2007) Velocity Simulation Results 174
Analysis Case I 174
Analysis Case II 177
Analysis Case III 180
Analysis Case IV 183
Analysis Case V 186
Analysis Case VI 189
Analysis Case VII 192
Analysis Case VIII 195
Analysis Case IX 198

Analysis Case X 201
Analysis Case XI 204
Analysis Case XII 207
Estimation of EBSB Breach due to Wave Impacts 210
Wave Damage on EBSBs Constructed with 'Good' Materials 214
Validation 218
Supplemental Wave Impact Modeling (SWAN & LSU (2008) Hydrodynamics) 220
Results 223
Results of Supplementary Simulation Runs 228
Analysis Case A (0400 CDT) 229
Analysis Case B (0430 CDT) 232
Analysis Case C (0500 CDT) 235
Analysis Case D (0530 CDT) 238
Analysis Case E (0600 CDT) 241
Analysis Case F (0630 CDT) 244
Analysis Case G (0700 CDT) 247
Analysis Case H (0730 CDT) 250

I. EXECUTIVE SUMMARY

The purpose of this study was to evaluate the magnitude of erosion resulting from wave-induced scour on the flood side of the Mississippi River Gulf Outlet (MR-GO) earthen berm/spoil bank (EBSB) during Hurricane Katrina in August 2005. The study simulated wave-induced erosion and scour effects at MR-GO Station 497+00. This location was selected due to the high degree of data availability for both pre- and post-Katrina conditions (topography, hydrodynamics, and soil boring data). The model results were validated using post-Katrina topography derived from Aerial LiDAR surveys conducted in September, 2005. A review of historical documentation along the MR-GO was conducted to develop background on construction, materials, and geometric configuration.

Hydrodynamic loading on the EBSBs were based on studies by de Wit et al (2008), Gautier et al (2008a, 2008b), IPET (2007a) and LSU (2007). Erosion Function Apparatus (EFA) test results (ILIT, 2006) were used to characterize the erodibility of EBSB materials. Interaction shear velocities between the storm surge and the EBSBs were evaluated for a selection of storm surge elevations. Simulations were also performed using the design geometric EBSB configuration and the actual EBSB configuration (as determined based on the available Aerial LiDAR data from 2000). These interaction shear velocities were then used to calculate the magnitude of lateral erosion based on the erodibility of the EBSB soils.

Based on the results of our analyses, we conclude that it was very possible (and highly likely) for the EBSB at Station 497+00 to have been breached through the crest solely as a result of wave-

induced erosion of the highly erodible materials used to construct the EBSB. High runup and rundown velocities (greater than 10 feet per second - ft/s) were calculated that exceed design recommendations for vegetated channels (FHWA, 1988). Also, the poorly compacted materials used to construct the EBSB were found to have very high erodibility rates. The combination of poorly compacted materials and high shear velocities results in extensive wave-induced erosion and scour.

We found that an EBSB constructed of 'good' materials with low erodibility would have performed significantly better than one constructed of high erodibility materials. Subjected to the same wave impacts, a levee with 'good' materials would have experienced insignificant erosion. It is also highly likely that the EBSB would have performed very well during overtopping conditions as well.

From the Declaration of Dr. Robert Glenn Bea (2008a):

The term "Levee(s)" refers to a hurricane flood protection structure(s) whose purpose is to protect human population living within urban areas and which are designed and constructed in accordance with pertinent USACE manuals, guidelines, standards, criteria, and policies and/or conform to generally-accepted engineering standards for such man-made features. The "protected side" (back side) of the levee is intended to provide protection from hurricane flood waters. The "unprotected side" (front side) of the levee is exposed to hurricane flood waters. As described below, among other things, these man-made features, in order to qualify as "Levees," must be designed to withstand the specified level of storm surge, waves, and currents that they are intended to contain, and must not be expected to erode or wash away during a hurricane for

which they are intended to serve as flood protection for humans and their property. Towards this end, and as set forth in the USACE publications Coastal Engineering Manual (USACE Pub. EM 1110-2-1100) and the Design and Construction of Levees (USACE Pub. EM 1110-2-1913), to qualify as "Levees" these man-made structures must be either (a) composed mostly of compacted clay-like cohesive soils, or (b) if constructed of more loosely compacted soils, they must be capped or covered with more dense materials that will protect against the underlying soils being washed away by wave action, storm surge, elevated tides and other water related phenomena associated with hurricanes. As noted below, in my opinion there were no "Levees" along virtually all of the MR-GO St. Bernard Parish Reach 2 frontage before Hurricane Katrina. Instead, this frontage had no effective hurricane protection since the USACE decided after 1965 to construct man-made features that were nothing more than miles of embankments comprised of dredged spoil that was not suitable for Levees.

The term "earthen berm / spoil bank" ("EBSB") refers to an embankment comprised of materials composed of sandy, silty, soil containing organic matter and shells and/or uncompacted hydraulic fill that is not suitable for constructing hurricane flood protection structures in urban areas as specified in pertinent USACE manuals, guidelines, standards, criteria and policies and/or generally-accepted engineering standards for such man-made features. As noted below, there were only EBSBs along virtually all of the MR-GO St. Bernard Parish frontage before Hurricane Katrina.

II. INTRODUCTION

The purpose of this study was to evaluate the magnitude of earthen berm/spoil bank (EBSB) erosion resulting from wave-induced scour on the flood side of the Mississippi River Gulf Outlet (MR-GO) EBSB during Hurricane Katrina in August 2005. The study simulated wave-induced erosion and scour effects MR-GO Station 497+00. This location was selected due to the high degree of data availability for both pre- and post-Katrina conditions (topography, hydrodynamics, and soil boring data). The model results were generally confirmed using post-Katrina topography derived from Aerial LiDAR surveys conducted in September, 2005.

Numerical modeling services were provided to simulate wave attack on the MR-GO EBSBs during the Hurricane Katrina storm surge of 2005. The analyses were completed using the LS-DYNA software package. Aerial LiDAR data from before and after Hurricane Katrina was the basis for the geometric configuration before and after the hurricane. Hydrodynamic loading used in the modeling was based on results from modeling completed by de Wit et al (2008), Gautier et al (2008a, 2008b) and parametric studies using hydrodynamic information from the Interagency Performance Evaluation Team (IPET) and Louisiana State University Hurricane Center. Erosion characterization was based on testing performed by the Independent Levee Investigation Team (ILIT, 2006), following Hurricane Katrina.

All information presented in this report centers around the MR-GO EBSBs in the vicinity of the project study area (near Station 497+00). The entire reach of the MR-GO is not treated in this report.

III. DOCUMENT REVIEW

A review of historical documentation along the MR-GO was conducted to develop background on construction, materials, and geometric configuration. Previous soil boring information, laboratory testing, and construction sequencing was evaluated. A summary of the reviewed documents is presented below:

- Coastal Environments, Inc (CEI). 1984. "The Mississippi River Gulf Outlet: A Study of Bank Stabilization." Prepared for: St. Bernard Parish Police Jury, Ashley Henderson, President; U.S. Department of Commerce, National Oceanic and Atmospheric Administration; and State of Louisiana, Department of Natural Resources, Coastal Management Section. Dated December, 1984.
- United States Army Corps of Engineers. 1957. "Mississippi River Gulf Outlet Design Memorandum No. 1-B, Channels, Mile 39.01 to Mile 63.77."
- _____. 1967. "Hurricane Protection Levee, First Lift, Sta 594+00 - Sta 770+11." DACW29-67-B-0136.
- _____. 1967. "Hurricane Protection Levee, First Lift, Sta 368+00 - Sta 570+00." DACW29-67-B-0134.
- _____. 1968. "Hurricane Protection Levee, First Lift, Sta 387+40 - Sta 523+00 (Not Continuous)." DACW29-68-B-0064.
- _____. 1972. "Hurricane Protection Levee, Chalmette Area Plan, Sta 370+00 to Sta 682+00." DACW29-72-B-0137.
- _____. 1972. "Hurricane Protection Levee, Chalmette Area Plan, Sta 370+00 to Sta 682+00." DACW29-72-B-0137.

- _____. 1985. "Hurricane Protection Levee Second Enlargement MR-GO B/L Sta 380+50 to Sta 692+50." DACW29-85-B-0073.
- _____. 1987. "Chalmette Area Plan, Hurricane Protection Levee Closures, MR-GO B/L Sta 367+60 to Sta 1005+49." DACW29-87-B-0014.
- _____. 1992. "Lake Pontchartrain Louisiana and Vicinity Chalmette Area Plan, Hurricane Protection Levee Closures, Sta 366+00 C/L to Sta 1007+91 CL." DACW29-92-B-0061.
- _____. 2005. "Lake Pontchartrain Louisiana and Vicinity Chalmette Area Plan, Hurricane Protection Levee, Emergency Restoration B/L Sta 383+00 to Sta 704+00." Solicitation No. W912P8-05-R-0063.
- _____. 2006. "Lake Pontchartrain Louisiana and Vicinity Chalmette Area Plan Emergency Restoration, Levee Restoration East of Bayou Dupre, MR-GO B/L Sta 714+55 to Sta 1007+91." Solicitation No. W912P8-06-R-0002.
- University of California, Berkeley. 2006. "UC Berkeley ILIT MR-GO Borings." – Unpublished.

IV. MR-GO HISTORIC OVERVIEW

Project Authorization

The construction of the MR-GO EBSBs was a component of the Chalmette Area Plan (USACE, 1966a) and in conjunction with the Lake Pontchartrain, Louisiana and Vicinity hurricane protection project. Authority for the project came from Public Law 298 – 89th Congress, 1st Session, approved 27 October 1965. The proposed work in the MR-GO area, as described by the Chief of Engineers, was:

"*…For the Chalmette area, the reporting officers find that the most suitable plan would consist of about 17.3 miles of new and enlarged levees extending generally along the southerly banks of the Gulf Intracoastal Waterway and the Mississippi River Gulf Outlet channel to Bayou Dupre and thence westerly to the Mississippi River levee at Violet*." (USACE, 1966a)

The full report issued by the Chief of Engineers was dated 4 March 1964 and printed in House Document No. 231, 89th Congress, 1st Session.

The project required a 30 percent cost share from local interests. The total estimated (USACE, 1966a) cost of the Chalmette Area Plan project was $32,830,00 of which $24,290,000 was the Federal first cost and $8,540,000 was the non-Federal first cost. The total estimated costs for the MR-GO EBSB construction (not including utility crossings) was $17,753,428 (USACE, 1966a). The total estimated costs for the Bayou Bienvenue and Dupre control structures was $1,422,465 and $1,364,247, respectively (USACE, 1966a).

A construction period of 20 years was assumed for the project, with initial construction starting in 1967 and 'levee' construction phases completed in 1969 (1st lift), 1971 (1st lift shaping), 1975 (2nd lift), 1983 (final shaping Station 270+00 to 807+00, first shaping Station 807+00 to 978+00), and 1987 (final shaping Station 807+00 to 978+00).

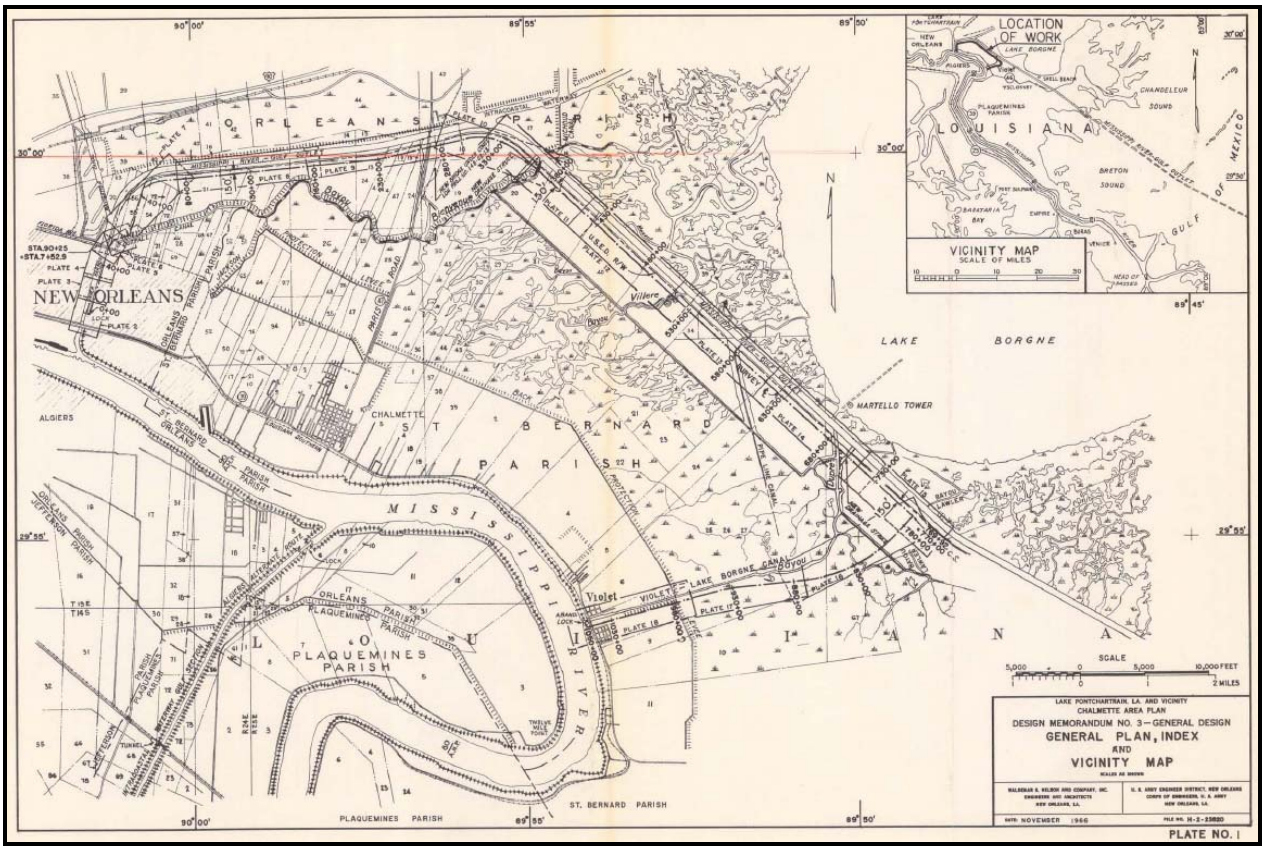


Figure 1**:** An overview of the Chalmette Area Plan (USACE, 1966a)

Figure 1 presents an overview of the planned protection elements associated with the Chalmette Area Plan. A new ring levee would be constructed from the existing navigation lock within the IHNC, along the GIWW, then down the MR-GO until it takes a 90-degree turn to connect to the Mississippi River levees in Violet.

Design Considerations

The EBSB design elevations are presented in the Chalmette Area Plan (USACE, 1966a). These design elevations were based on parameters developed for the Standard Project Hurricane and are summarized in Table 1.

Table 1: Summary of MR-GO 'Levee' Design Parameters

Design Element	Design Value
Storm return period	200-year
Central pressure index	27.5
Maximum 5-minute wind speed	100 mph
Design maximum still water elevation	+13.0 feet MSL
"Freeboard" for wave runup	4.5 feet
Target design elevation (still water + wave runup)	+17.5 feet MSL

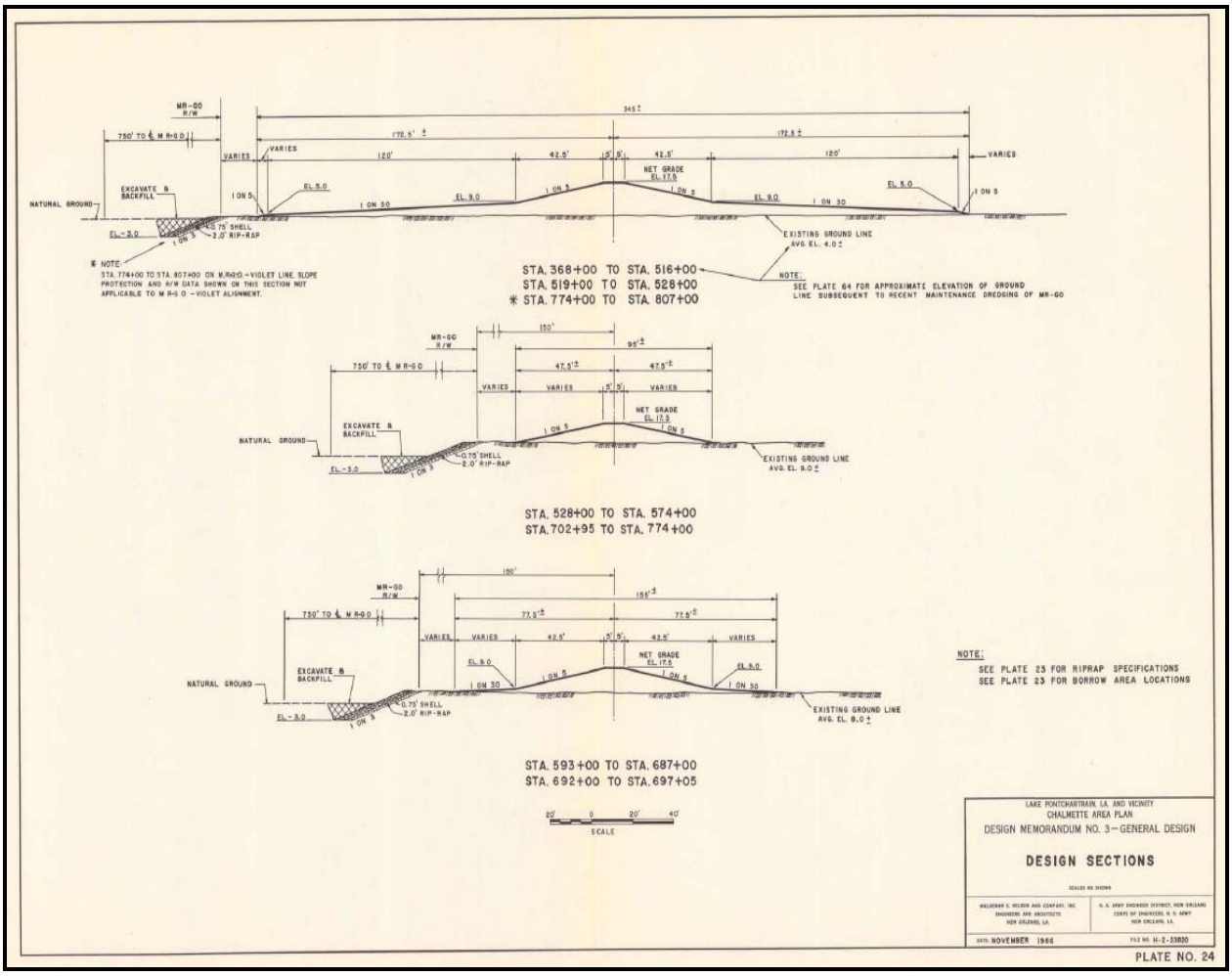


Figure 2: An overview of the Chalmette Area Plan (USACE, 1966a)

Standard design details were developed for the MR-GO EBSBs (Figure 2). The typical outboard and inboard slopes were 5:1 (horizontal:vertical) and 4:1, respectively. The crest width was 10 feet. The target design elevation was El. +17.5 feet (MSL).

Construction 'templates' were also developed to specify how the EBSBs were to be constructed. Sufficient hydraulic fill was placed within the EBSB footprint such that future construction phases could use 'stockpiled' materials within the footprint. Figure 3 presents the construction templates as well as interim construction crest elevations.

Proposed material sources for the construction of elements associated with the Chalmette Area Plan are summarized in Figure 4 (USACE, 1966b).

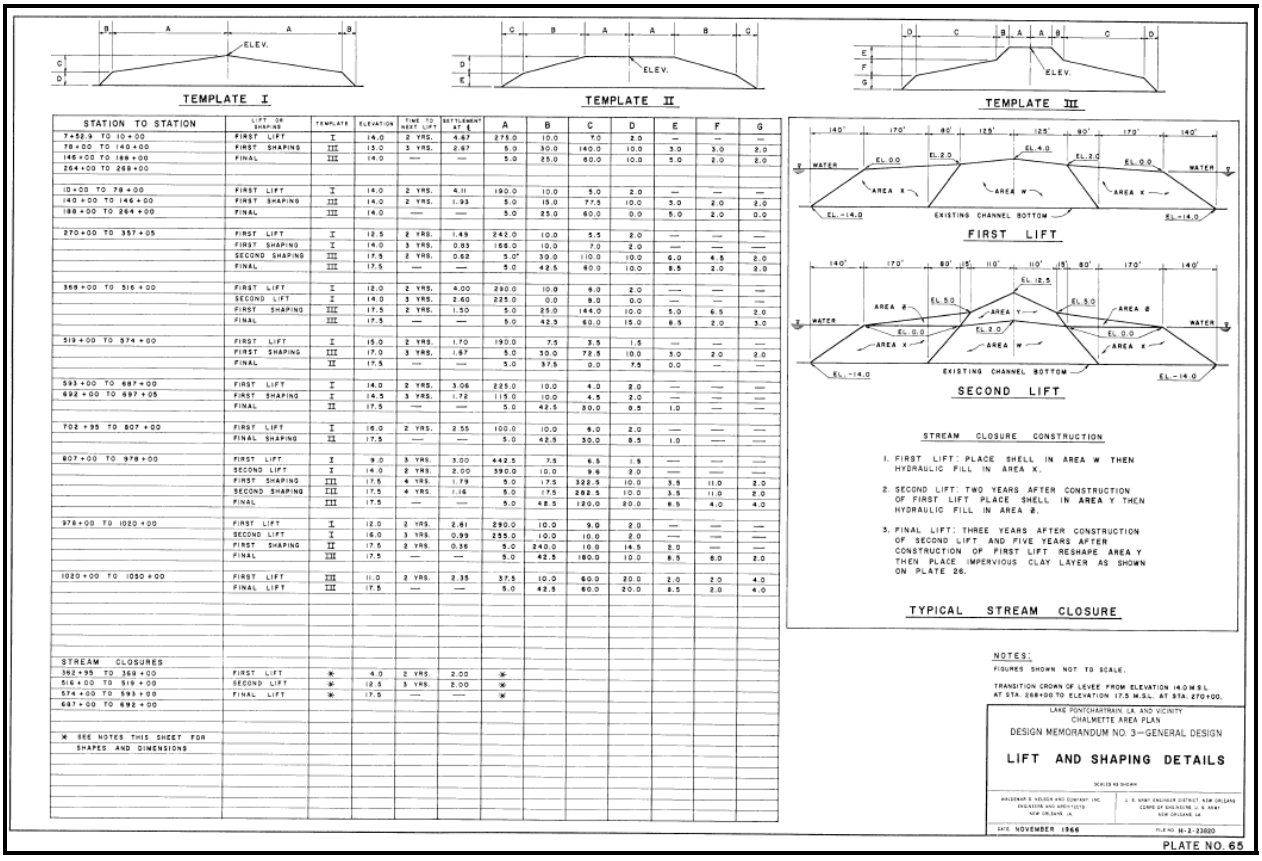


Figure 3: An overview of the Chalmette Area Plan (USACE, 1966a)

TABLE NO. 2

SOURCES OF BACKFILL, SHELL, AND LEVEE MATERIAL

ITEM		SOURCE
CHEF MENTEUR BARRIER STRUCTURE		
	Random backfill	Excavation spoils and approach channel areas
	Clay blankets	Selected excavation spoils and approach channel areas (10 to 20-foot surface layer of fat clay)
	Sand backfill	Selected excavation spoils (10 to 15-foot sand stratum underlies the control structure, navigation channel, and floodgate at -20 to 30 feet)
	Clay cutoffs	Selected excavation spoils (10 to 20-foot surface layer of fat clay found at floodgate site)
	Gulfside levee at west end for highway protection	Gulfside borrow areas in the immediate vicinity of the project
	Tie-in levees and highway approach embankment	Hydraulic pump material (Recent and Pleistocene) from channel and structure excavat ons and adjacent lakeside borrow areas
	Closure dam	Hydraulic pump material (Recent and Pleistocene) from channel and structure excavations and adjacent lakeside borrow areas
	Graded filter	Selected material from sand backfill, and concrete sand from sources on table No. 1.
RIGOLETS BARRIER STRUCTURE		
	Random backfill	Excavation spoils and approach channel areas
	Clay blankets	Selected excavation spoils and approach channel areas (10 to 20-foot surface layer of fat clay)
	Sand backfill	Selected excavation spoils (25-37-foot sand stratum underlies the lock site and part of approach channels -20 feet m.s.l.)
	Clay cutoffs	Selected excavation spoils (10 to 20-foot surface layer of fat clay)
	Gulfside levee on east and west end for highway protection	Gulfside borrow areas in immediate vicinity of the project
	Tie-in levees and highway approach embankment	Hydraulic pump material (Recent and Pleistocene) from channel and structure excavations and adjacent lakeside borrow areas.
	Closure dam	Hydraulic pump material (Recent and Pleistocene) from channel and structure excavations and adjacent lakeside borrow areas
	Graded filter	Selected material from sand backfill, and concrete sand sources on table No. 1
ST. CHARLES PARISH LEVEE		Hydraulic pump material (Pleistocene) from adjacent borrow areas in lake, riprap from sources shown on table No. 1
JEFFERSON PARISH LEVEE		Shell from commercial sources; riprap sources as shown on table No. 1
ORLEANS PARISH LEVEE		
	Jefferson Parish to Inner Harbor Navigation Canal	Hauled material from spillway and/or Mississippi River batture; shell from commercial sources; riprap sources as shown on table No. 1
	Citrus Area	Hydraulic pump material (Pleistocene) from adjacent borrow areas in lake; hauled material from spillway or Mississippi River batture; riprap as on table No. 1
	New Orleans East	Hydraulic pump material (Pleistocene) from adjacent borrow areas in lake; riprap sources as shown on table No. 1
CHALMETTE		
	Along Gulf Intracoastal Waterway and Mississippi River-Gulf Outlet	Existing spoil along Mississippi River-Gulf Outlet on the south and material resulting from enlargement of Mississippi River-Gulf Outlet; riprap as shown on table No. 1
	Mississippi River-Gulf Outlet to Violet Lock	Hydraulic pump material from borrow areas on Lake Borgne side of Bayou Dupre
MANDEVILLE		Shell from commercial sources; riprap from sources as shown on table No. 1
SEABROOK LOCK		Shell from commercial sources; riprap and derrick stone as shown on table No. 1
SHELL		Shell for the entire project may be obtained from nearby commercial sources.

PLATE 5

Figure 4: Proposed material sources for the Chalmette Area Plan construction (USACE, 1966b)

General MR-GO Soil Conditions

A geology report prepared for the MR-GO in 1957-1958 by the Kolb and Van Lopik (USACE, 1958a) found that the upper 2 to 5 feet of the MR-GO alignment was mainly fibrous peat, with some highly organic marsh deposits extending to depths of 5 to 15 feet (USACE, 1958a). The peats and marsh deposits were identified as being highly compressible. The marsh deposits were underlain by interdistributary and intratidal complex silts and clays over a majority of the MR-GO alignment (USACE, 1958a). Three material classification schemes were developed: soft

marsh (500 to 900% water content), firm marsh (100 to 500% water content), and swamp substrate (600 to 800 % water content).

It was noted that the soft marsh and swamp substrate materials would be unable to provide competent foundations for the hurricane protection levees bordering the channel and these materials would be unsuitable for use in levee embankments (USACE, 1958a).

Figure 5 presents the northeast corner of a 1953 USGS Topographic Map which documents site conditions prior to work on the MR-GO. At this time, extensive marsh and a network of bayou channels traverse the MR-GO alignment. The future GIWW can be seen in the very top left corner of the USGS Topographic map.

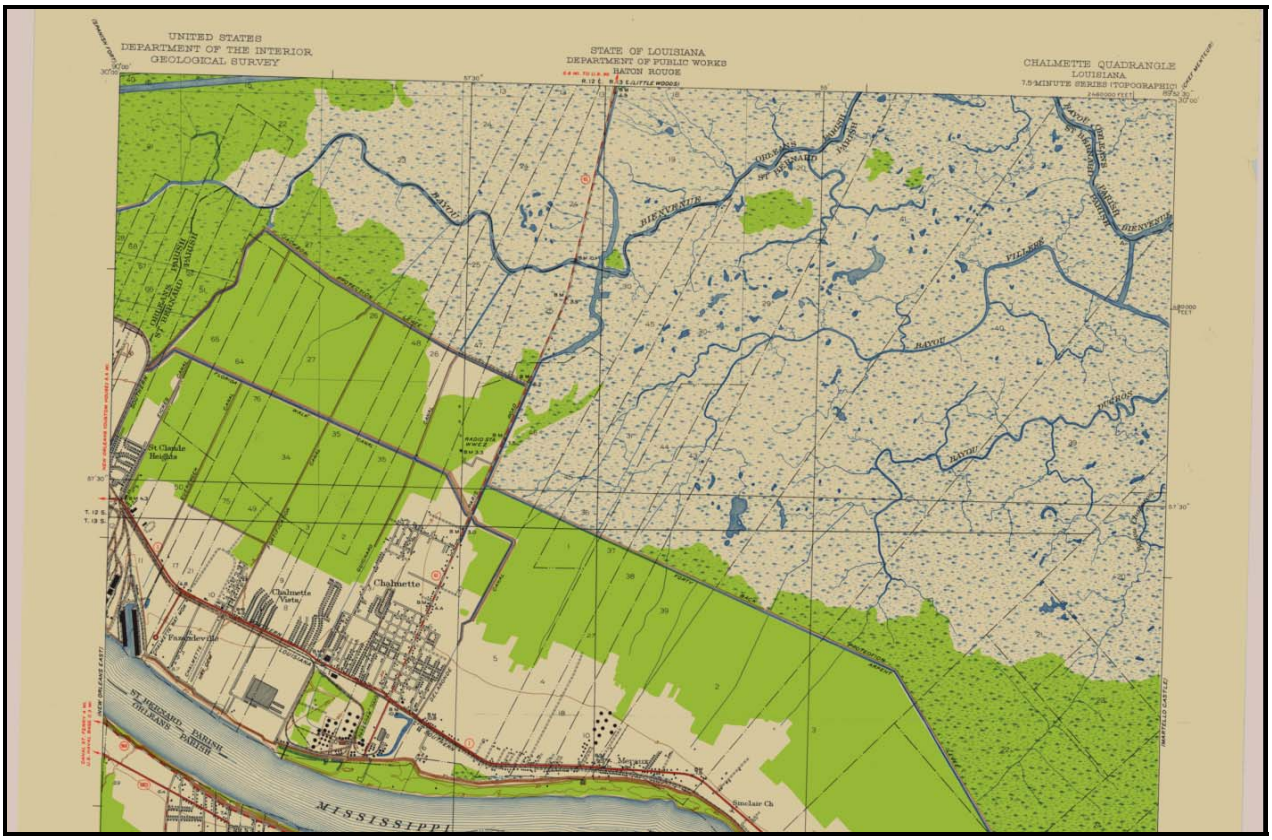


Figure 5: Site conditions in the MR-GO area prior to construction (USGS, 1951).

Figure 6 shows a table from CEI (1984) that summarizes general engineering properties of the depositional units within the MR-GO project reach. Figure 7 shows a spatial distribution of foundation conditions along the MR-GO alignment. Soft marsh conditions were identified in the region where the wave-induced erosion analyses were performed for this study. Figure 8 shows a generalized cross section along the MR-GO alignment.

Table 1. Physical Characteristics of Depositional Types Found in the MRGO Landcut (Modified from Kolb 1958).

Depositional Type	Lithology	Natural Water Content Per Cent Dry Weight	Liquid Limit[1]	Plasticity Index[1]	Shear Strength[(2)] Cohesive Strength (lb/ft^2)	Shear Strength[(2)] Angle of Internal Friction in degrees	Remarks
Prodelta	95% Clay 5% Silt	40-80	70-120	30-55	200-600	0	Underlies entire deltaic sequence as homogeneous unit. Slopes and thickens toward the southeast.
Intradelta Complex	35% Clay 40% Silt 25% Sand	15-40	Non-plastic to 110	Non-plastic to 60	Moderate	Moderate	Relatively coarse portion of subaqueous delta. Intricately interfingered deposits. Disposed in broad wedges about abandoned courses and major distributaries.
Interdistributary	80% Clay 10% Silt 6% Sand 4% Organic	50-160	60-160	30-75	150-300	0	Disposed in clay wedges between major distributaries. Clay sequence interrupted by silty or sandy materials associated with myriad small distributaries, but otherwise fairly homogeneous. Material will probably displace laterally under fairly light load.
Natural Levee	55% Clay 40% Silt 5% Sand	20-40	Non-plastic to 75	Non-plastic to 30	800-1200	15-35	Disposed in irregular belts along abandoned courses and distributaries. Thickness averages 15 ft or less.
Swamp	75% Clay 5% Silt 20% Organic	60-200	60-150	30-60	Low	---	Relatively small areas.
Marsh	33% Clay 2% Silt 65% Organic	80-800	70-250	—	Very Low	—	Forms 90 per cent of land surface within study area. Average thickness 10 ft. Very high water content. Subject to rapid compaction under load.

(1) Atterberg limits do not reflect water content of highly organic materials

(2) Cohesive strength of clays based on unconfined compression test

Figure 6: Table summarizing physical characteristics of the MR-GO deposits (CEI, 1984).

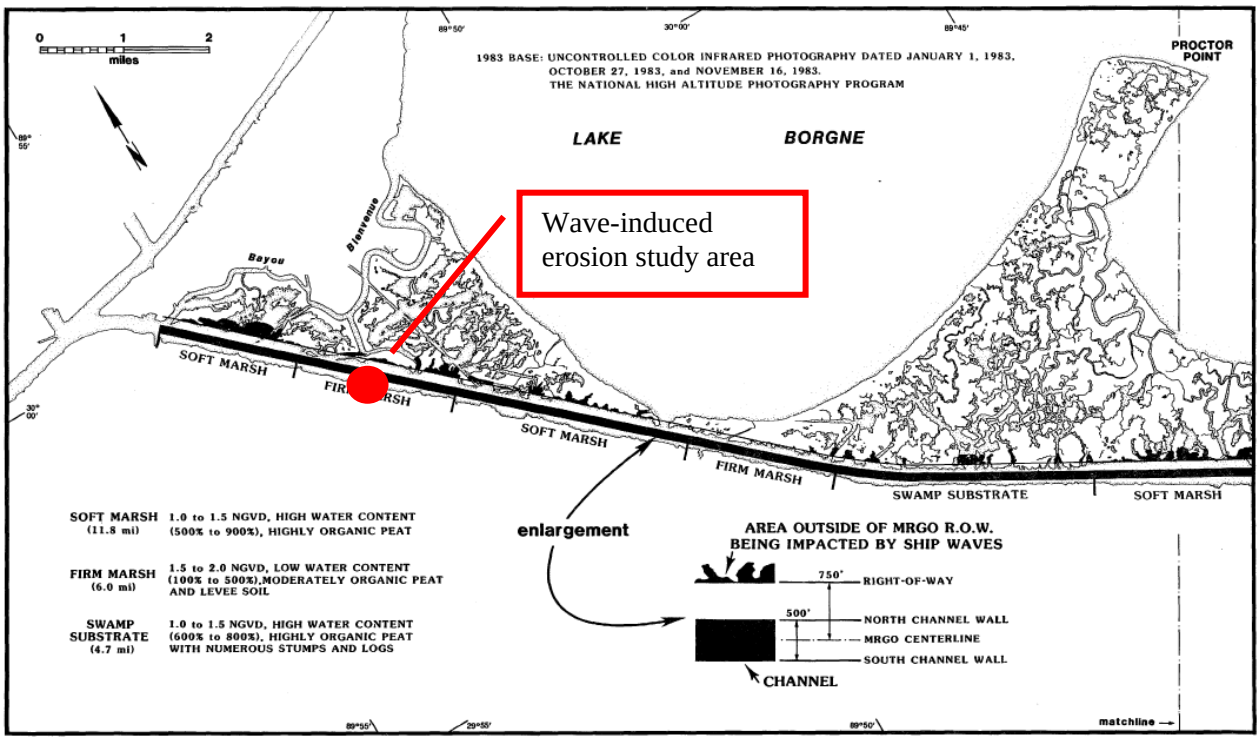


Figure 7: An overview of depositional units along the MR-GO alignment. Firm marsh in the study area (CEI, 1984).

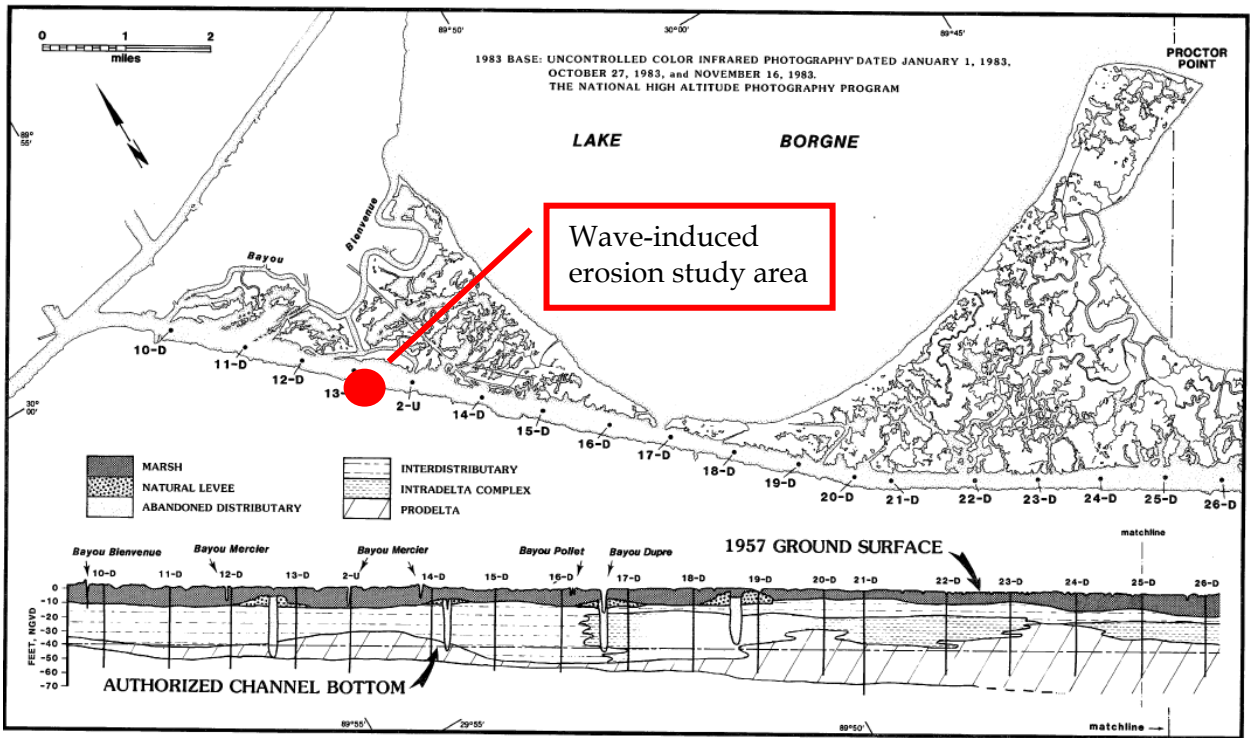


Figure 8: A generalized cross section as presented in CEI (1984) and originally created by Kolb and Van Lobik. The study area for this wave-induced erosion/scour analyses is located between soil borings 13-D and 2-U (CEI, 1984).

A number of soil boring exploration studies were performed along the MR-GO alignment. In the wave-induced study area, borings were taken in 1956 (soil boring 13-D), 1966 (soil boring G-43), 1984 (soil boring 11-UBD), and 2005 (soil boring MR-GO-10). Figure 9 shows an overview of soil borings near the study area. Actual soil boring logs used for this study are presented in the Appendix.

The majority of the soils used to construct the MR-GO EBSB in this reach came from hydraulic fill placed from dredge materials within the MR-GO channel, primarily between El. –42 feet and –70 feet. These materials are described in part by soil boring 13-D, which was situated within the centerline of the proposed MR-GO channel (El. +2 feet, MSL). Soil boring 13-D identifies primarily fat clay to exist within the zone of planned excavation, with in-situ moisture contents between 39% to 117%, with most moisture contents falling within the range of 50% to 80%. Near surface soils (above the excavation zone) were classified as peats, with moisture contents in the range of 300% to 700% (USACE, 1958a).

Soil boring G-43 (El. +4 feet, NGVD), which was drilled between the centerline of the MR-GO EBSB and western edge of MR-GO channel and indicates that subsurface soils primarily consist of very soft fat clays. No peats were logged in this soil boring. In-situ moisture contents between 37% to 106%, with most moisture contents falling within the range of 50% to 80%. Silt strada - lenses and sand strada - lenses were identified within the bottom half of the soil boring (USACE, 1967b).

Soil boring 11-UBD (El. +14 feet, NGVD) was drilled near the centerline of the MR-GO EBSB. This boring documents not only native subsurface soil conditions, but physical characteristics of the placed hydraulic fill as well. Some consolidation and subsidence has occurred since the initial construction of the EBSB, so some interpretation is required to determine the "fill/native" transition, however it is anticipated to occur near El. +0 feet. No density information was presented for this soil boring, so direct correlations to in-situ density are difficult. Moisture content information, however is given, so some conclusions can be drawn on density based on in-situ water contents and relations to maximum dry densities (per ASTM D1557 or D698). The top 10 feet of the soil boring consist of lean clay and silty sand with moisture contents in the range of 25% to 35%. At approximately El. +4 feet, the material type changes to fat clay, with much higher moisture contents ranging from 31% to 60%. A peat layer (moisture contents between 259% and 313%) was observed between El. -6 feet and El. -8 feet (NGVD). The zone between El. +4 feet and El. -6 feet is very likely the transition from native materials (marsh deposits) and EBSB hydraulic fill materials.

Soil boring MR-GO-10 was performed in a potential borrow site (USACE, 2005) for repair materials following Hurricanes Katrina and Rita. The top of boring was reported as being at El. +0 feet (NGVD). A very thin layer (about one foot) of silt and fat clay with sand lenses (about one foot) was found to overlie approximately 10 feet of native peat materials.

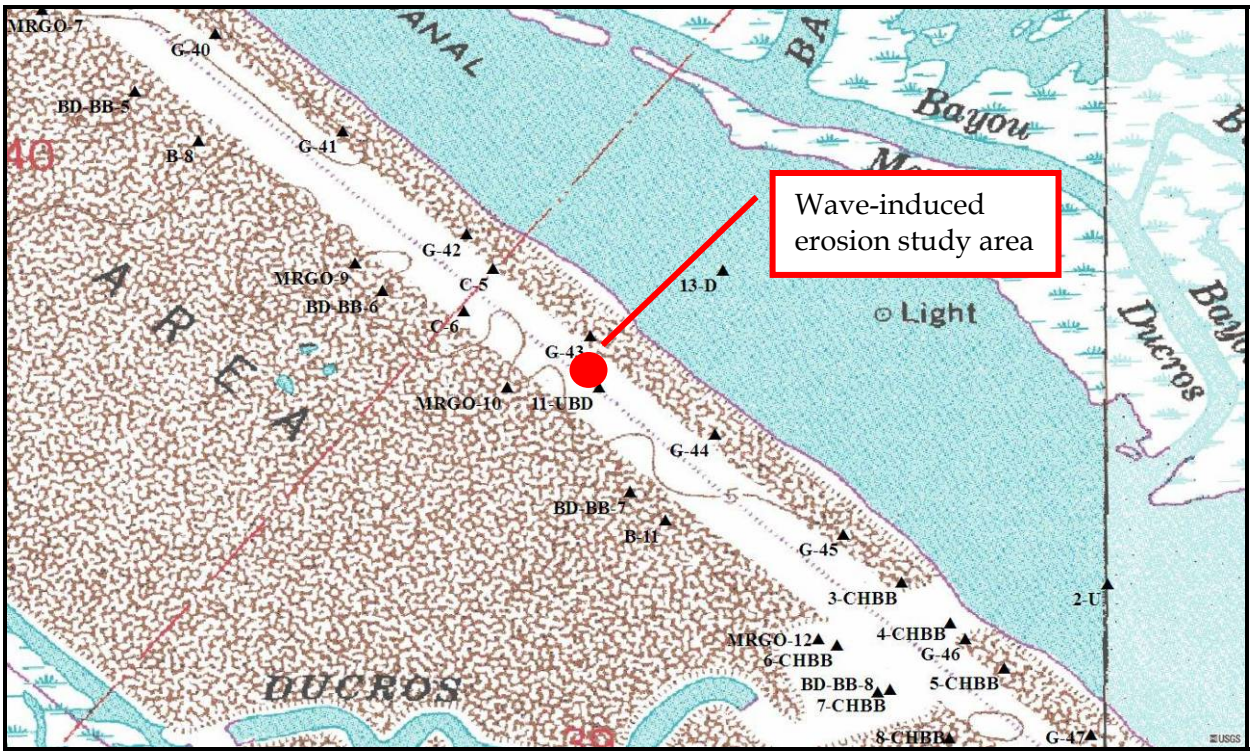


Figure 9: An overview of soil borings (designated by black triangles) near the wave-induced erosion study area.

IV.1.1. Summary of EBSB Fill Characteristics

Based on the available geologic and soil boring investigations at the site, the EBSB fill materials are hydraulic fills derived from Interdistributary and Prodelta complex soils. These soils generally have predominant clay contents (80-95%) with natural water contents (percent of dry weight) of 40 to 160 percent, liquid limits of 60-160, plasticity indices between 30 and 75, and cohesive strengths on the order of 150 to 500 psf. Once placed, the hydraulic fill construction method is anticipated to introduce soil segregation (clays and silts separating from the sands), distinct layering, and a reduction of water contents (from the drying process following placement), liquid limit, plasticity index, and also a decrease in the cohesive strength. No density information was available from the soil boring logs.



Figure 10: Field visits made to the MR-GO alignment in October 2005, following Hurricane Katrina, indicated that sections of the hurricane protection EBSB were made of cohesionless materials.


Figure 11: A cross-sectional view of the MR-GO EBSB at a breach site. The materials used to construct the actual section are quite heterogeneous, and at this location, there are distinct layers of shells.



Figure 12: These photos were taken during a site visit for the MR-GO 'levee' reconstruction work in April 2006. Silts and fine sands result in a dust cloud when subjected to vehicular traffic (Photos 1 and 2), while cohesive clays do not (Photo 3).

Site visits were made to the MR-GO EBSB alignment in October 2005 and April 2006. Figures 10 and 11 show that there were locations encountered where cohesionless materials were encountered. Figure 11 also shows the cross-sectional profile of the MR-GO EBSB at a location where the materials used to construct the EBSB were very heterogeneous.

Photos 1 and 2 (Figure 12) were taken while driving on original sections of the MR-GO EBSB in April 2006. Note that there is a distinct presence of cohesionless materials (silts and fine sands) that are 'kicked up' by the vehicular traffic traversing the EBSB. Photo 3 (Figure 12) shows imported lean and fat clays. No 'dust cloud' is observed, implying that the materials are predominantly cohesive. Thus, based on the site observations, there is strong indication that portions of the MR-GO EBSB was constructed from materials with significant amounts of cohesionless materials such as fine sands and silt.

Construction History

The construction history of the MR-GO EBSBs have a direct impact on their performance. Construction methods (such as hydraulic fill placement), borrow material excavation depths (which correspond to general material soil types), and soil borings (which aid in determining the degree of EBSB soil compaction and site specific soil composition) were used in this study to aid in the characterization of the EBSB material erodibility.

In addition to the general erosion characteristics of the soils from the construction phase, erodibility testing on discrete samples from the MR-GO (ILIT, 2006) was also used to develop erodibility characteristics of the EBSB material at the study section. A description of the erodibility testing from ILIT (2006) is presented later in this paper.

Excerpts from the CEI (1984) comprehensive history of the MR-GO is presented below:

> *The Mississippi River Gulf Outlet (MR-GO) is a 76-mile long, man-made waterway that extends from the City of New Orleans to the Gulf of Mexico. This ship canal was authorized by the U.S. Congress in 1956, and was undertaken as a full-scale project in 1958. Most of the canal was built through the ecologically sensitive wetlands of St. Bernard Parish during an era of low environmental awareness. The project brought on a litany of environmental problems, including habitat change, marsh loss, and severe shoreline erosion. These problems evolved immediately following construction, and are continuing largely unabated to this day….The U.S. Army Corps of Engineers (USACE), the Federal agency responsible for design and construction of the MR-GO, has only recently recognized MR-GO-related*

problems. They have finally characterized the MR-GO as one of eight areas in south Louisiana where "erosion stabilization measures are urgently needed."

The MR-GO was authorized by the Rivers and Harbor Act of March 29, 1956 (Public Law 455, 84th Congress, 2nd Session)…Work commenced in detailed planning of the MR-GO in July 1956. The final design incorporated a 36-feet deep, 500-feet wide canal extending 76 miles to the 38-ft contour in the Gulf of Mexico. The landcut was maximized to extend 42.8 mi from the Inner Harbor Navigation Canal to Gardner Island. Canal walls were designed with 2:1 slope, and the right-of-way extended 750 feet from the center line into the marsh on the northeast side…All dredged material in the landcut was to be used to build a 4,000 ft wide, 10-ft high spoil bank on the southwest shore of the canal.

Actual construction began in March 1958 with the first dredging contract awarded March 12, 1958 for excavation of a 2.5 mi section at the New Orleans Terminus. The remaining MR-GO channel was dredged in sections, each of which was dredged in three phases: (1) an "access channel" (18 ft x 140 ft), (2) an "interim channel (36 ft x 250 ft), and (3) the final "project channel" (36 ft x 500 ft). Some sections were completed to full project channel dimensions before other sections had an access channel dredged.

The MR-GO was constructed under 35 different contracts. The complete access channel was finished in March 1961. The complete interim channel was finished July 5, 1963, and was dedicated July 25, 1963, at which time the first commercial ship was allowed to travel from

New Orleans to the Gulf of Mexico. The full project channel was completed in January 1968.

Full project dimensions were completed <between Bayou Bienvenue to Bayou La Loutre> in October 1963, but later the full project dimensions were exceeded when the hurricane protection levee project authorized channel deepening to allow for additional 'levee' material. Between Bayou Bienvenue and Bayou Dupree, dredging in some locales reached -80 feet. Some shoaling has occurred since these dredging activities, but this portion of the MR-GO to this day has depths that reach 70 ft.

Unfortunately, no bathymetry data was available (for incorporation into this study) following completion of the MR-GO EBSB construction to further describe how much borrow material (quantities and corresponding dredge depth) was utilized.

IV.1.2. MR-GO First Lift - 1968

The first lift was placed in the late 1960s. Construction documentation was not available to confirm actual construction dates, however, the project plans were dated March 1967 (USACE, 1967a), so it is assumed that construction initiated following completion of the plans. The interim MR-GO channel was completed in 1963, so it is also assumed that all borrow materials for the MR-GO EBSB s were from deposits outside the interim channel.

It is important to note that the interim channel had dimensions of 36 feet by 250 feet and the final MR-GO channel had dimensions of 36 feet by 500 feet. The primary enlargement for the MR-GO was enlarging the width of the channel, not the depth. EBSB construction occurred in zones

and was not continuous throughout the entire EBSB alignment. The target design elevation for this phase of work was El 12.0 feet (MSL).

The plans for the initial lift (USACE, 1967a) identify the borrow materials for the first lift of the EBSB coming from excavations within the MR-GO channel ranging from El. -42 feet to El. -60 feet (MSL). Dredge spoils from the enlargement of the MR-GO channel width, therefore, fall outside the range of identified borrow. Figure 13 shows the schematic shown in the project plans (USACE, 1967a).

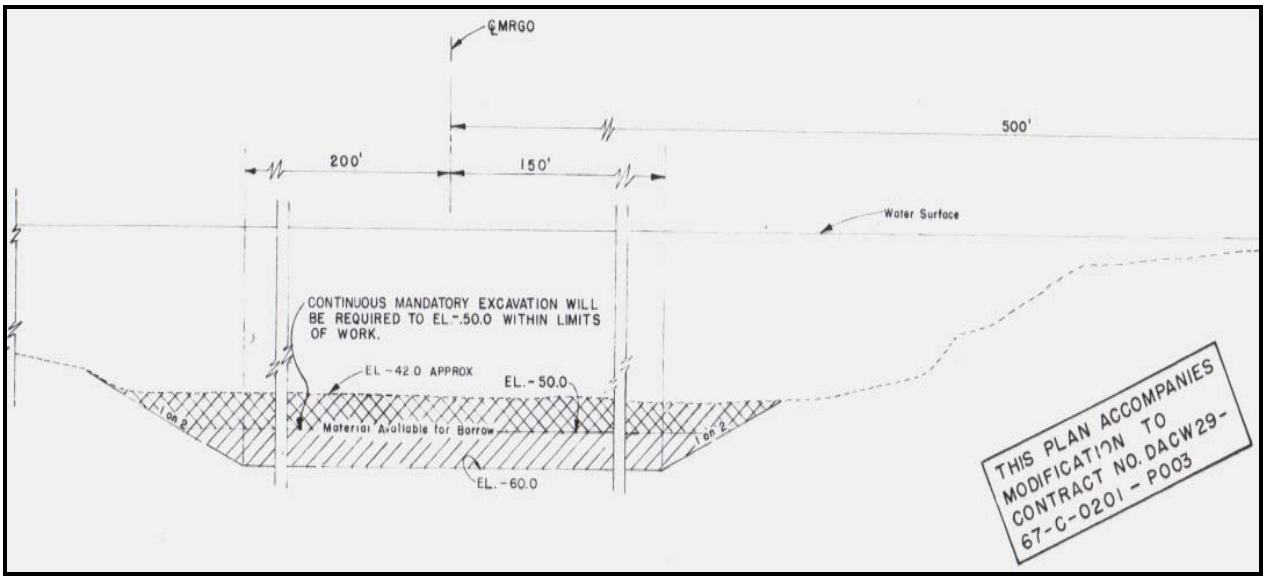


Figure 13: Identified borrow source for the first lift of the MR-GO levee. The borrow material ranged in elevation from El. -42 feet to El. -60 feet (USACE, 1967a).

The initial MR-GO channel construction method used hydraulic dredging to remove sediments within the MR-GO channel and 'disposed' of these material in a spoil bank, west of the MR-GO channel (USACE, 1967a), implying that fill materials were placed within the footprint of the EBSB as a fluid and no compactive effort was employed to densify the EBSB materials. Temporary dikes were constructed on either side of the 'levee' toes to contain the hydraulic fill

as it was placed within the spoil disposal area. Figure 14 shows the hydraulic section as specified on the project plans (USACE, 1967a).

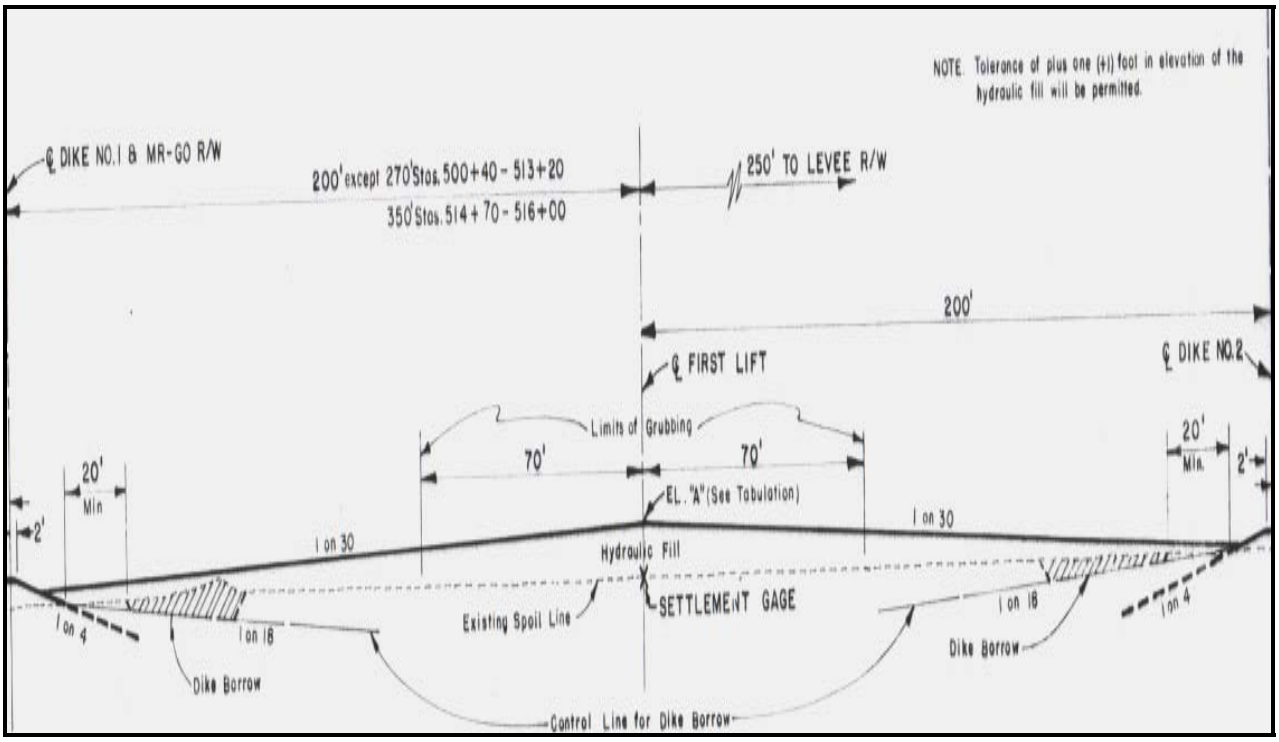


Figure 14: The hydraulic fill section as specified on the project design plans (USACE, 1967a).

This material collection technique naturally promotes segregation of soils with cohesionless materials (sands, gravels, shells, etc.) settling in stratigraphic units distinct from fines such as clays and silts. Organics will tend to 'float' to the top of the hydraulic fill unit. The resulting stratigraphy is highly heterogeneous and variable in composition.

Bayou Villere, however, was in the process of being closed during this phase of work. The first lift was placed in the summer of 1967 (USACE, 1968). Materials used to fill the bayou channel were not described. Figure 15 shows the design detail from the 1968 USACE plans.

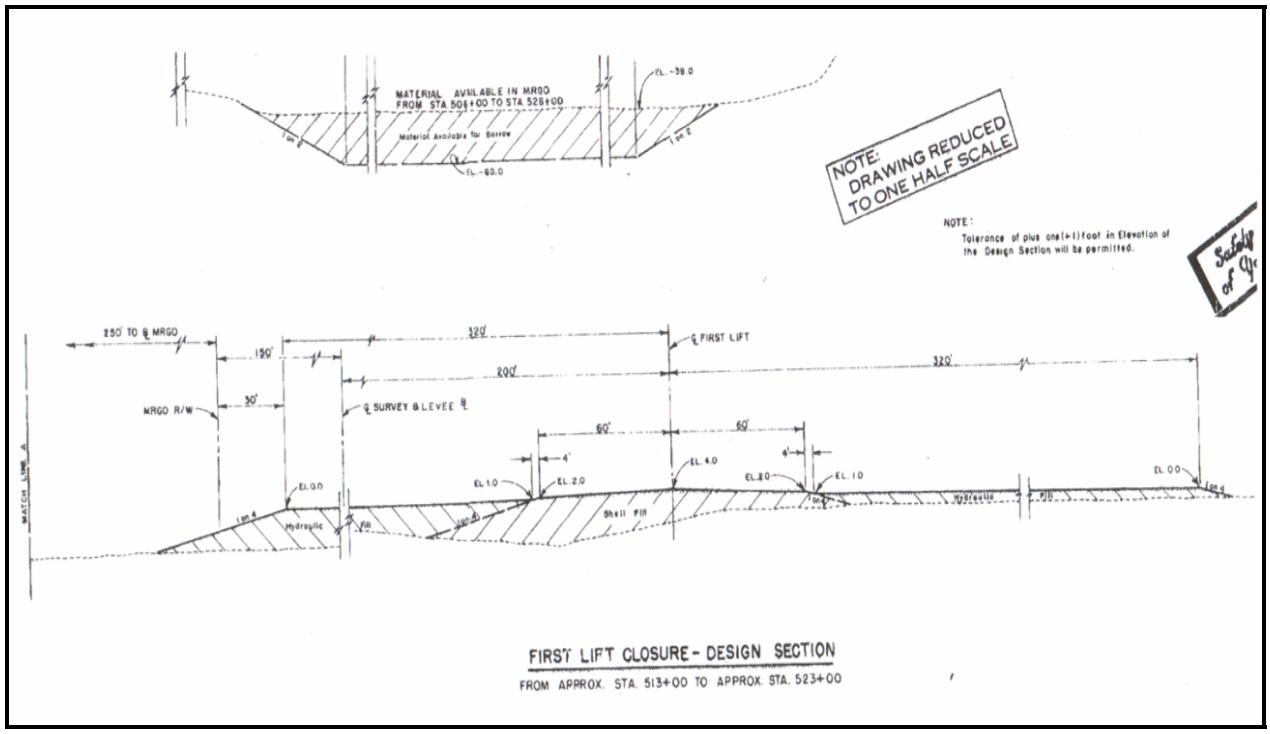


Figure 15**:** The hydraulic fill section as specified on the project design plans (USACE, 1968).

Shell fill was used as the core of the closure section with hydraulic fill on the inboard and outboard toes. The design elevation for this lift was El. +4.0 feet (NGVD).

No work on the Bayou Bienvenue and Bayou Dupre control structures had occurred at this time and the natural channels were functioning in an unaltered manner. The pipeline canal (near Station 580+00) was also not “closed” and future plans included construction of a ‘levee’ over this region.

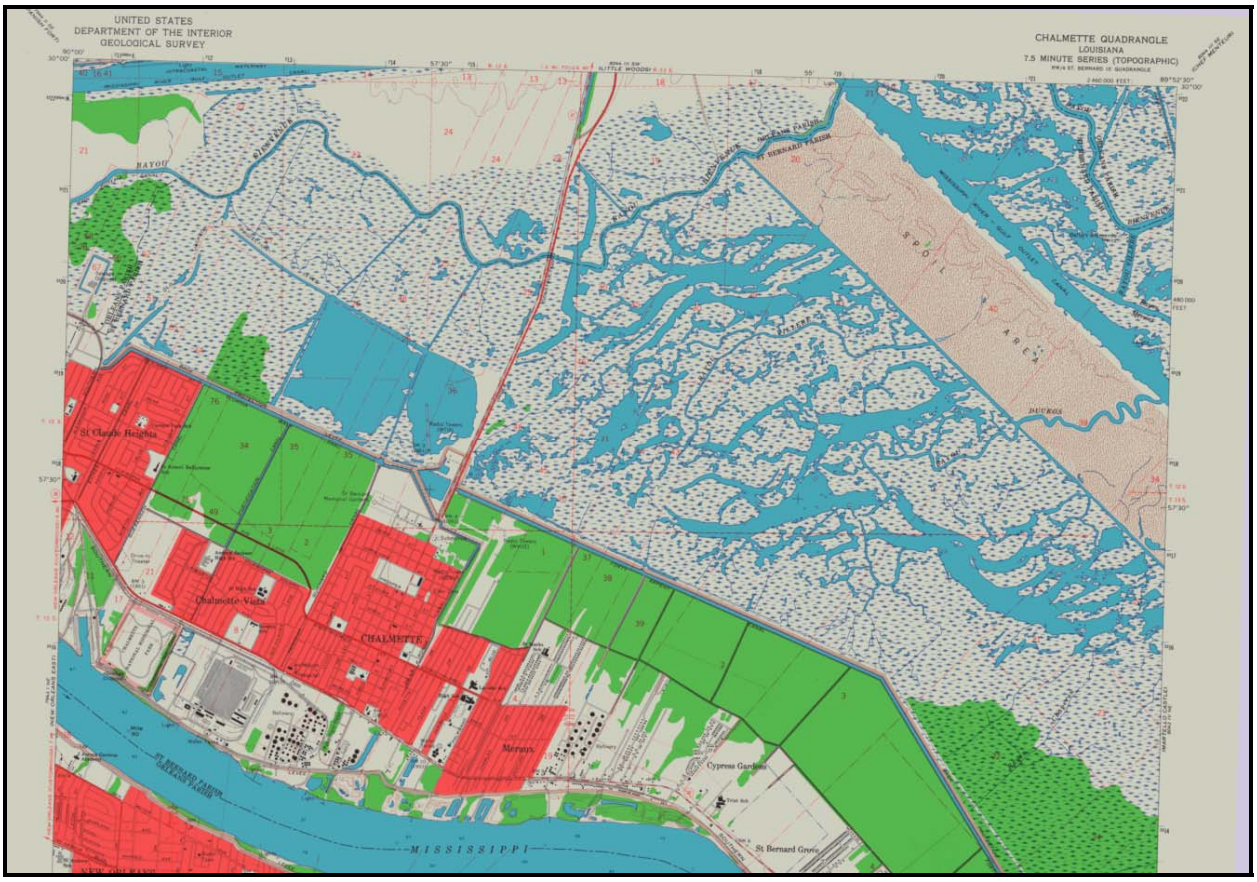


Figure 16**:** Site conditions in the MR-GO area following initiation of construction. The spoil area is clearly identified and Bayou Bievenue is still unaltered (USGS, 1967).

Figure 16 shows the project area as mapped by the USGS in 1967. The spoil area associated with the hydraulic fill placement can be seen and the MR-GO and GIWW channels have also been mapped.

IV.1.3. Second Lift - 1972

Plans for the second lift of the MR-GO EBSBs were issued in April 1972 (USACE, 1972). The construction work consisted of raising the EBSB crest to El. +18.0 feet (MSL) and closing Bayou Viellere and the Pipeline Canal. Centerline EBSB profiles indicate that site grades had settled as much as 5 feet to approximately El. +7 feet to El. +10 feet, with some locations along the EBSB alignment still at El. +12 feet (MSL).

The design elevations at Bayou Viellere and the Pipeline Canal were El. +14.0 feet and +10.5 feet (MSL) respectively. The Bayou Viellere and Pipeline Canal design closure sections consisted of shell backfill within the channel and a capping of hydraulically placed Pleistocene clay (USACE, 1972). Figure 17 presents a cross sectional view of the Bayou Viellere channel closure and Figure 18 presents a cross sectional view of the Pipeline Canal closure.

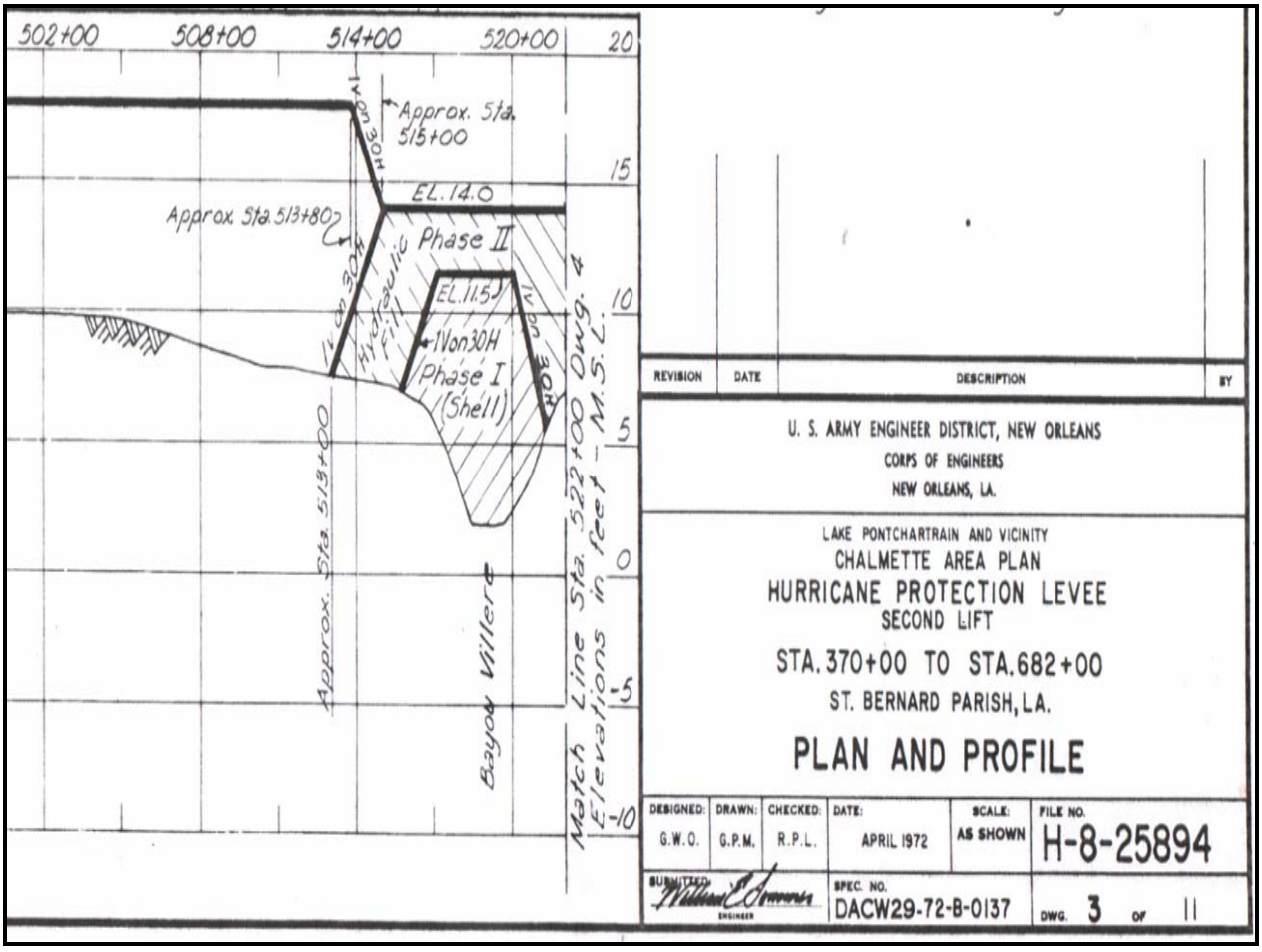


Figure 17**:** Closure details for the Bayou Villere channel (USACE, 1972).

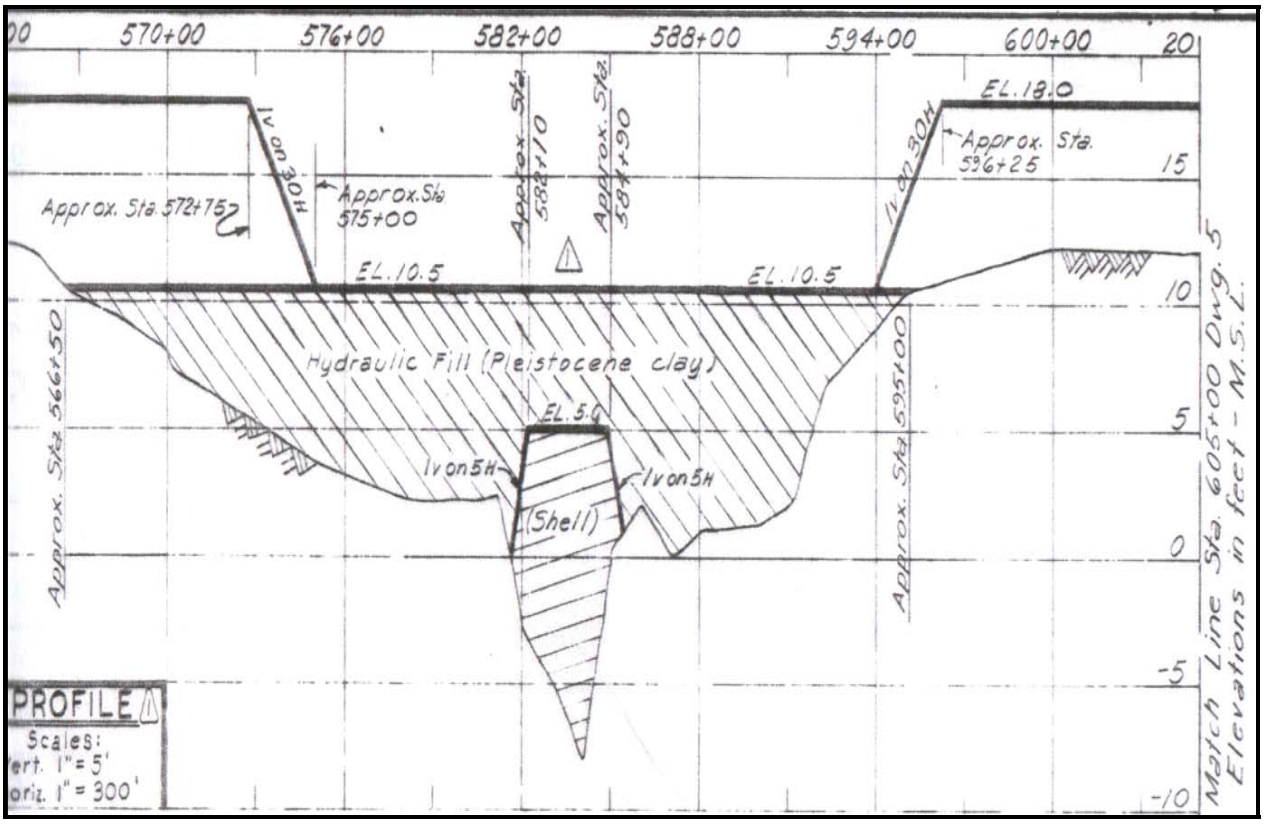


Figure 18: Closure details for the Pipeline Canal (USACE, 1972).

The ‘levee’ construction method was hydraulic fill (USACE, 1972), implying that fill materials were placed within the footprint of the ‘levee’ as a fluid and no compactive effort was employed to densify the EBSB materials. Temporary dikes were constructed on either side of the EBSB toes to contain the hydraulic fill as it was placed within the EBSB footprint. Materials for this phase of work came from the MR-GO channel, excavated from El. -47 feet to El. -70 feet (MSL). Figure 19 presents the design section for this phase of work (USACE, 1972).

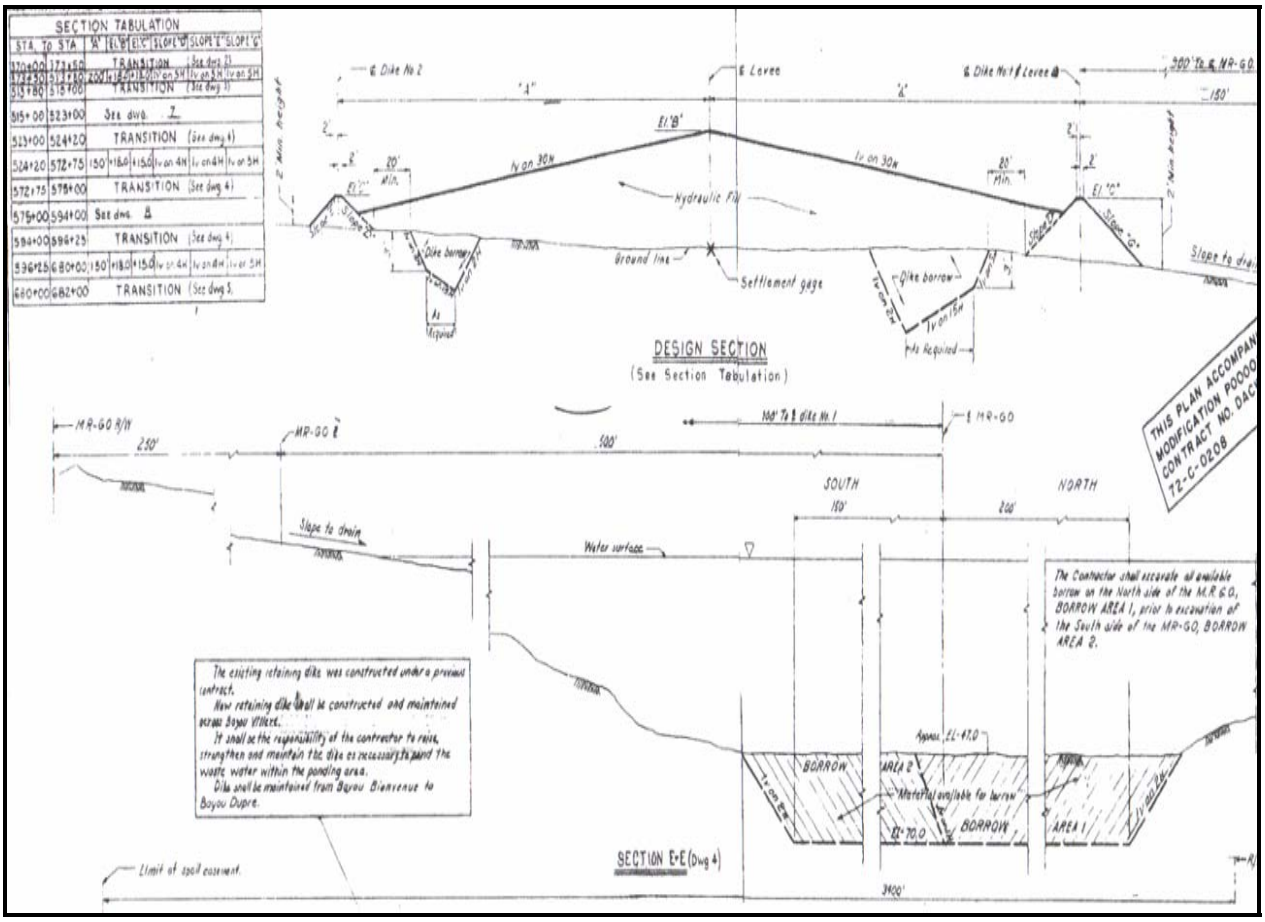


Figure 19**:** The hydraulic fill section as specified on the project design plans (USACE, 1972).

No work on the Bayou Bienvenue and Bayou Dupre control structures had occurred at this time and were functioning in an unaltered manner. Aerial photos from 1974 do show both the Bayou Bienvenue and Dupre control structures, so construction on these flood protection components occurred between 1972 and 1974. Aerial photographs from 1974 are presented in Figures 20 and 21 that show these two control structures.



Figure 20**:** Aerial photograph of the Bayou Bienvenue Control Structure site in 1974 (Gulf Coast Aerial).



Figure 21: Aerial photograph of the Bayou Bienvenue Control Structure site in 1974 (Gulf Coast Aerial).

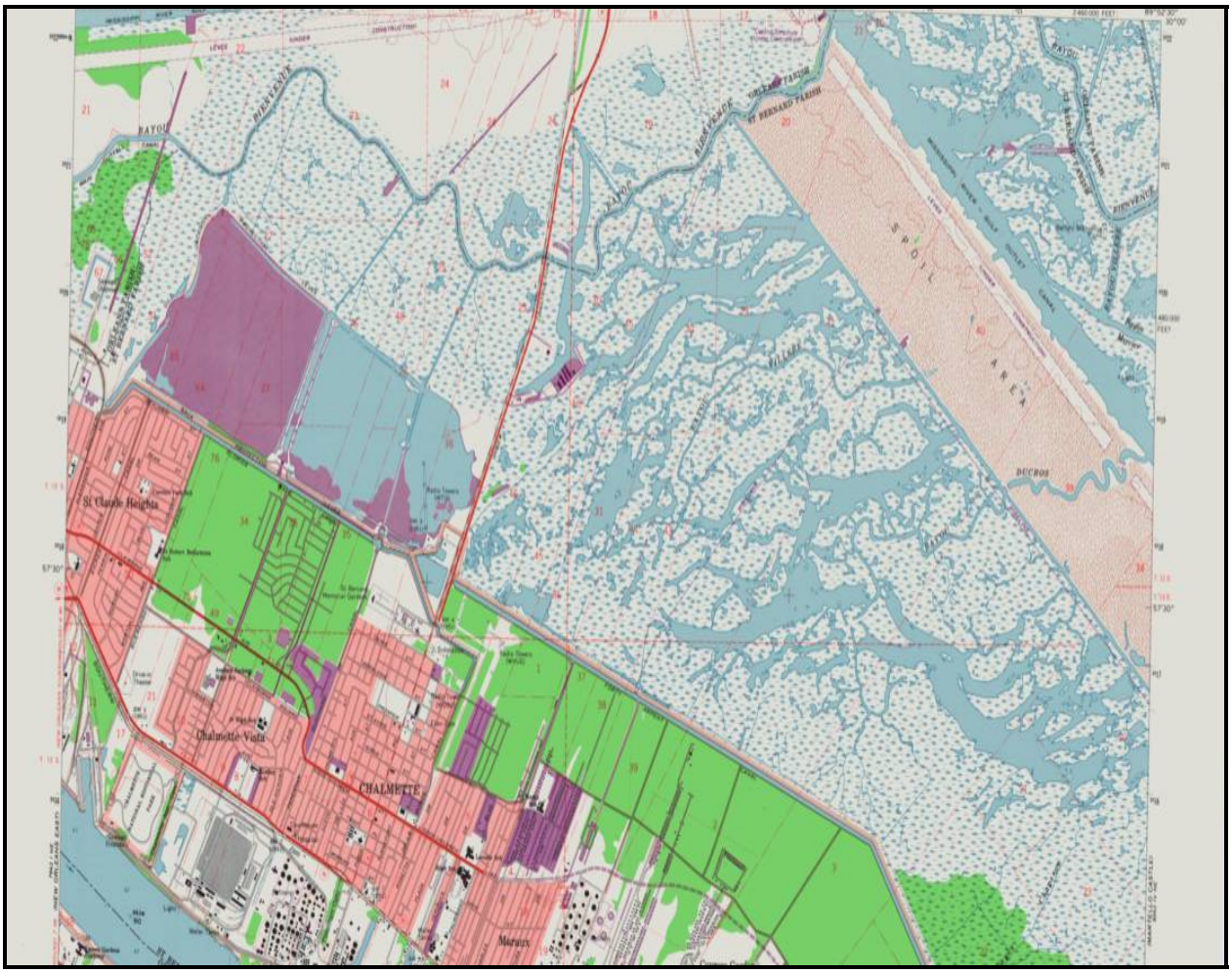


Figure 22: Site conditions in the MR-GO area following initiation of construction. The spoil area is clearly identified and Bayou Bievenue is still unaltered (USGS, 1972).

Figure 22 shows the project area as mapped by the USGS in 1972. A note is present on the topographic map that the Bayou Bienvenue control structure is under construction.

IV.1.4. First Enlargement – 1980

Plans for the first enlargement of the MR-GO EBSBs were issued in July 1980 (USACE, 1980). The construction work consisted of raising the EBSB crest to El. +18.0 feet (MSL). Centerline EBSB profiles indicate that site grades had settled as much as 8 feet to approximately El. +10

feet to El. +15 feet. The majority of the EBSB alignment was surveyed (USACE, 1980) to be approximately El +14 feet (MSL).

Unlike previous construction approaches, the first enlargement used borrow from the inboard and outboard EBSB toes, not from the MR-GO channel. Site grades in this area were approximately El. +4 feet (MSL), which were most likely soils from previous hydraulic fill operations as the natural site grades in the area were on the order of El. +0 feet (MSL).

There were no criteria for compacting the EBSB materials (USACE, 1980). The project plans called for the EBSB slopes to be fertilized and seeded following completion of construction (USACE, 1980). Figure 23 presents the design section for this phase of work.

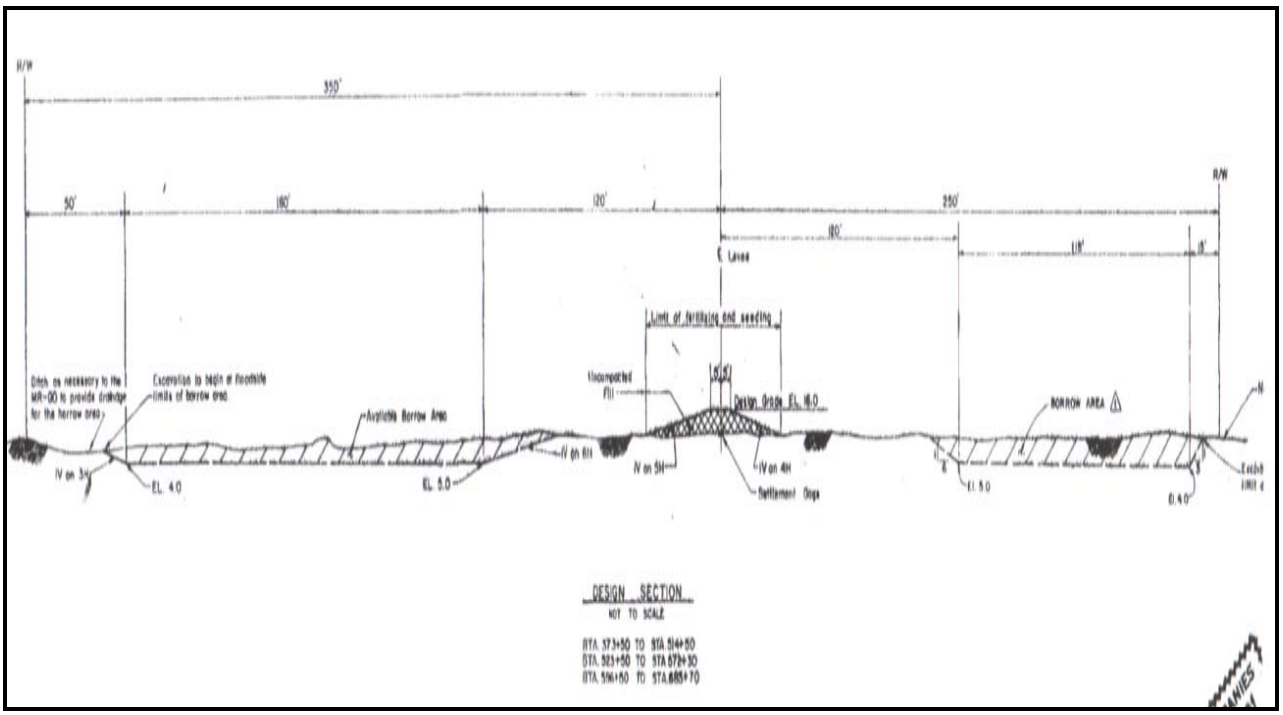


Figure 23: The typical design section for the first enlargement phase as specified on the project plans (USACE, 1980).

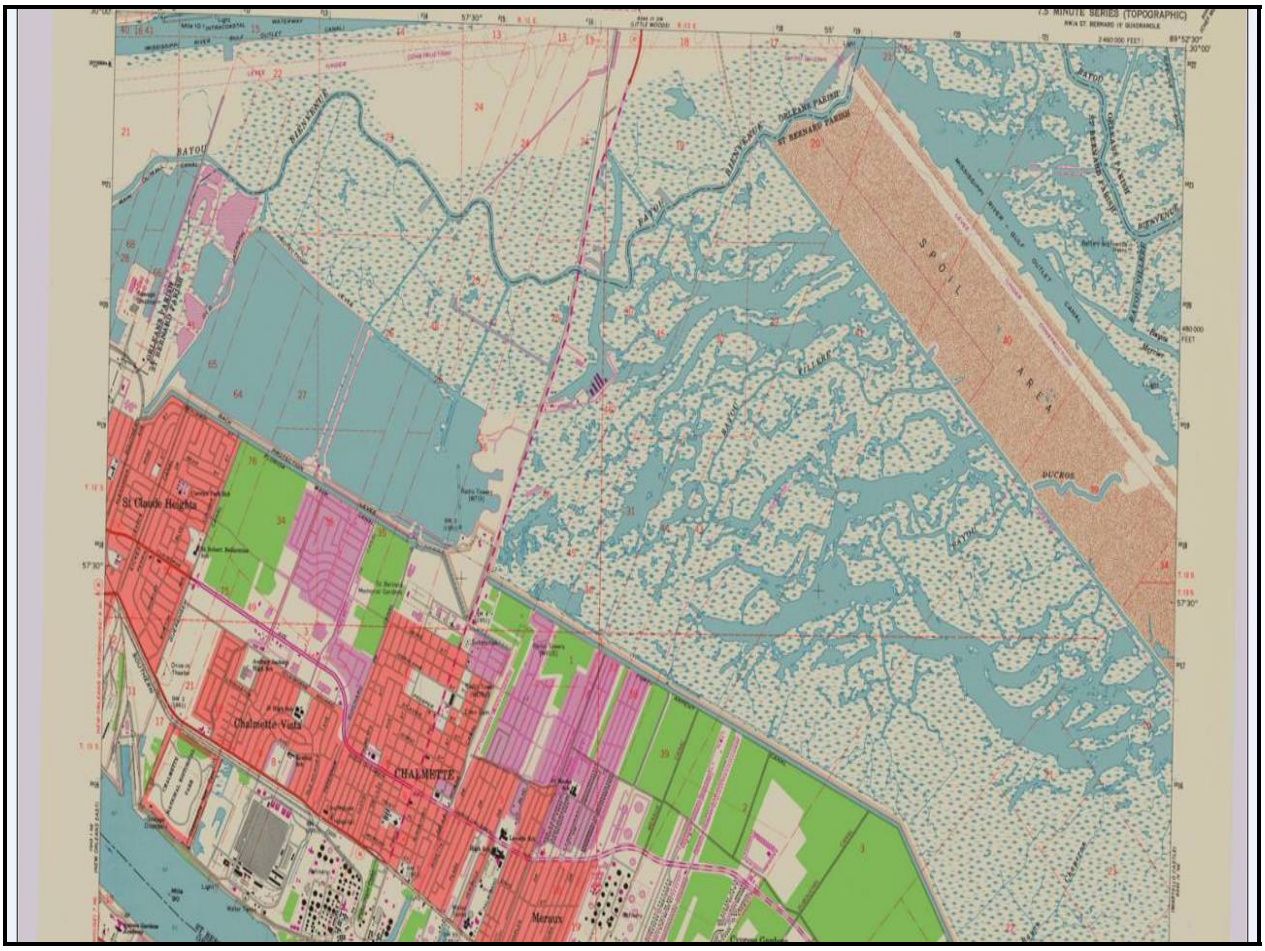


Figure 24: MR-GO as mapped by USGS in 1979. The channel for the Bayou Bienvenue control structure has been excavated and the control structure installed (USGS, 1979).

Figure 24 shows the project area as mapped by the USGS in 1979. The Bayou Bienvenue control structure has been completed and the control structure channel has been excavated. The historic Bayou Bievenue channel has been filled.

IV.1.5. 'Levee' Closures – 1982

Plans were developed by the USACE (1983) to close the historic Bayou Bienvenue and Dupre channels and to construct 'levees' connecting the previously constructed MR-GO EBSB to the completed Bienvenue and Dupre control structures. In addition to closures at the control structures, these plans also addressed the Bayou Villere and southern pipeline crossing locations.

It appears from the plans that fill materials came from a combination of MR-GO channel excavations and utilization of hydraulic fill materials previously placed at the site, outside the 'footprint' of the design section EBSB.

IV.1.6. Second Enlargement – 1985

Plans for the first enlargement of the MR-GO EBSBs were dated May 1985. The construction work consisted of raising the crest to El. +20.5 feet (NGVD). Centerline EBSB profile surveys from 1983 (USACE, 1985) indicate that the EBSB had settled as much as 3 feet to El. +15 feet (NGVD), with the majority of the EBSB alignment had a crest elevation of approximately El +16 feet (NGVD).

The specified design elevation was lower than El. +20.5 feet (NGVD) at pipeline crossing locations, at Bayou Villere, and at a slope failure location. A slide was identified to have occurred in the MR-GO EBSB between Station 480+50 to 486+50. The exact extents or mechanism of the slide were not described.

Borrow materials appear to have come from excess hydraulic fill located at the inboard and outboard toes of the MR-GO EBSB. There were no criteria for compacting the EBSB materials (USACE, 1985). The project plans called for the EBSB slopes to be fertilized and seeded following completion of construction. Figure 25 presents the design section for this phase of work.

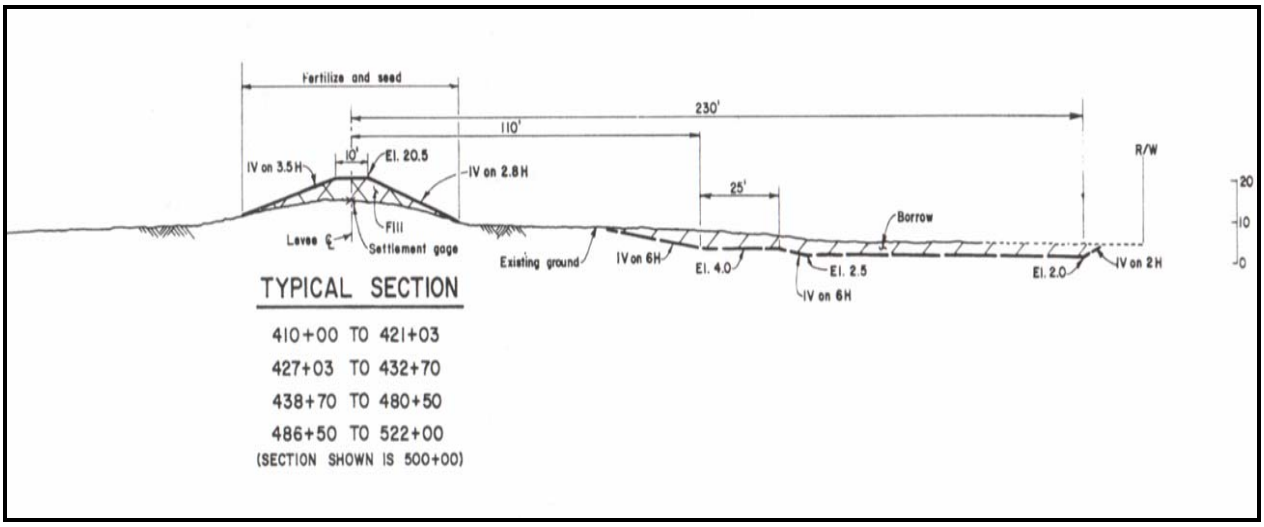


Figure 25**:** Typical design section for the second enlargement construction phase (USACE, 1985).

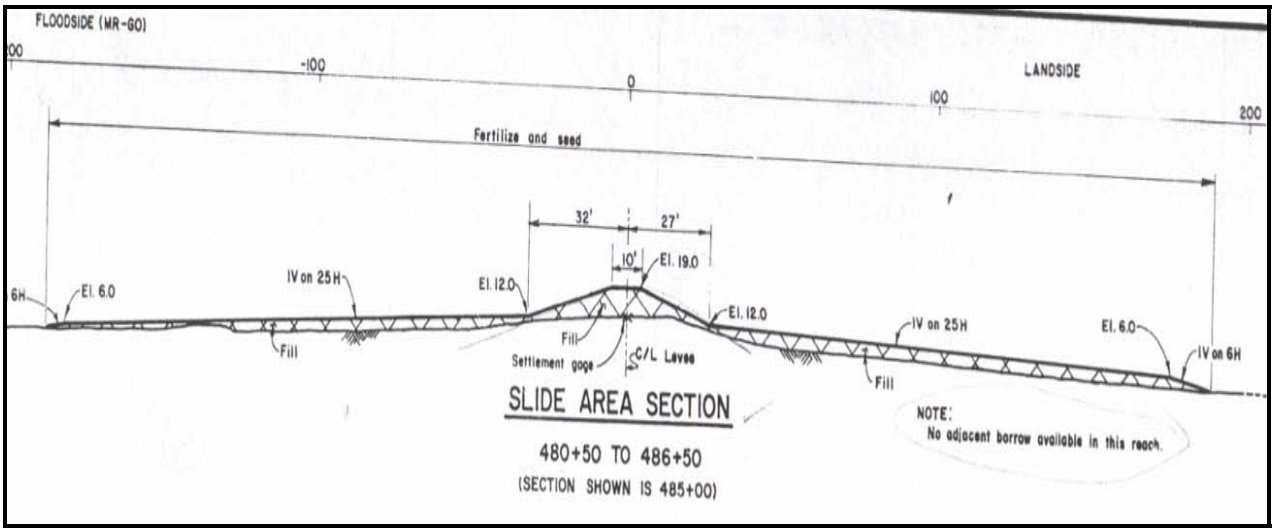


Figure 26**:** Construction details for the slope failure that occurred between Stations 480+15 to 486+50 (USACE, 1985).

Figure 24 shows the construction repair details for the slope failure that occurred between Stations 480+15 and 486+50. From the drawing, it appears that as much as 6 feet of crest elevation was lost as a result of the slide, consolidation, and regional subsidence since the EBSB segment was constructed.

IV.1.7. 'Levee' Closures – 1987

In 1987, the USACE (1987) implemented a plan to raise EBSB elevations at the previous 1982 closure locations: the historic Bayou Bienvenue and Dupre channels, Bayou Villere and the southern pipeline crossing locations. Additionally, a section of EBSB was also repaired between Stations 964+00 and 978+00. It appears from the plans that fill materials came from materials outside the 'footprint' of the design section EBSB.

IV.1.8. 'Levee' Closures – 1992

Plans were developed by the USACE (1992) to install sheet piles at select locations along the MR-GO EBSB where excessive settlements occurred. An EBSB crest elevation survey performed in 1990 (USACE, 1992) indicated that crest elevations had dropped to approximately El. +18 feet (NGVD), below the target design level of El. + 20.5 feet (NGVD). A summary of repair sections including EBSB elevation prior to repair and target repair elevation are summarized in Table 2, below.

Table 2: Summary of Sheet Pile Repair Locations (Elevation datum NGVD)

Start Station	End Station	Repair Type	Initial Elevation	Target Elevation
369+22	381+30	PZ-22 Sheet Pile	+14 feet	+18.5 feet
479+95	487+18	PZ-22 Sheet Pile	+17 feet	+18.5 feet
579+90	604+15	PZ-22 Sheet Pile, 'Levee' Fill	+14 feet	+18.5 feet
621+60	647+20	PZ-22 Sheet Pile, 'Levee' Fill	+15 feet	+18.5 feet
652+86	656+45	PZ-22 Sheet Pile, 'Levee' Fill	+16 feet	+18.5 feet
966+10	980+75	Sheet Pile, 'Levee' Fill	+15 feet	+18.5 feet

The average MR-GO EBSB crest elevation based on the 1990 survey (USACE, 1992) was approximately El. +18 feet (NGVD).

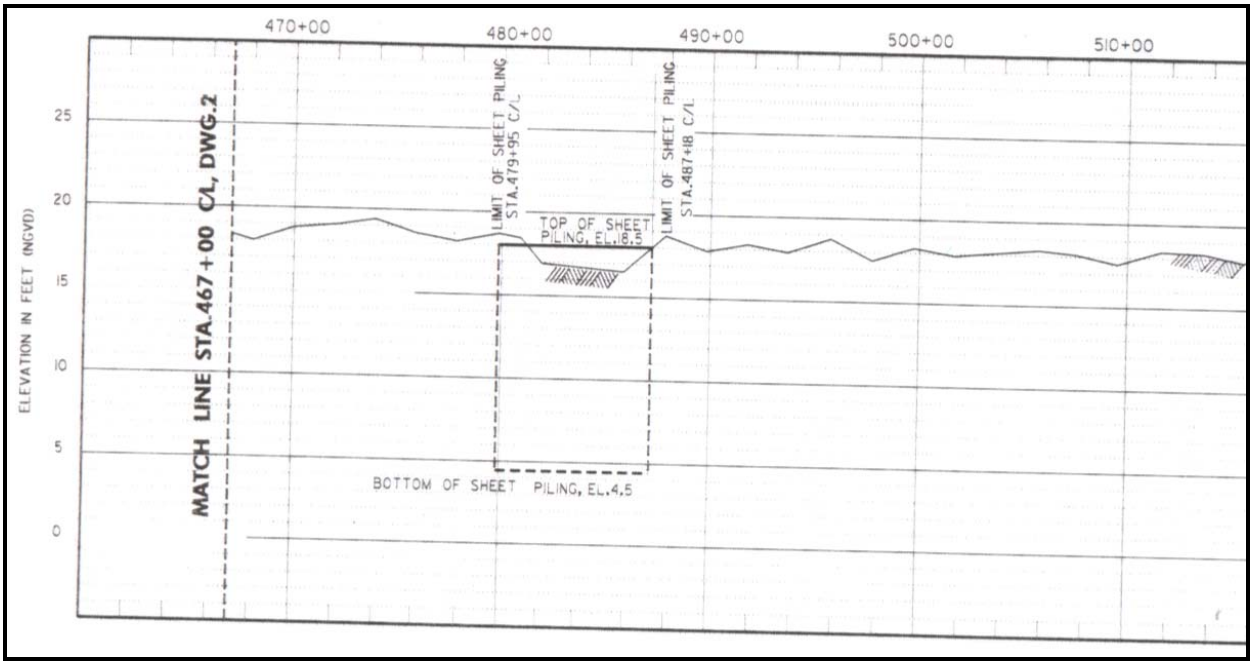


Figure 27**:** Example construction detail where sheet piles were specified to be installed to achieve the desired crest elevation of +18.5 feet (NGVD) (USACE, 1992).

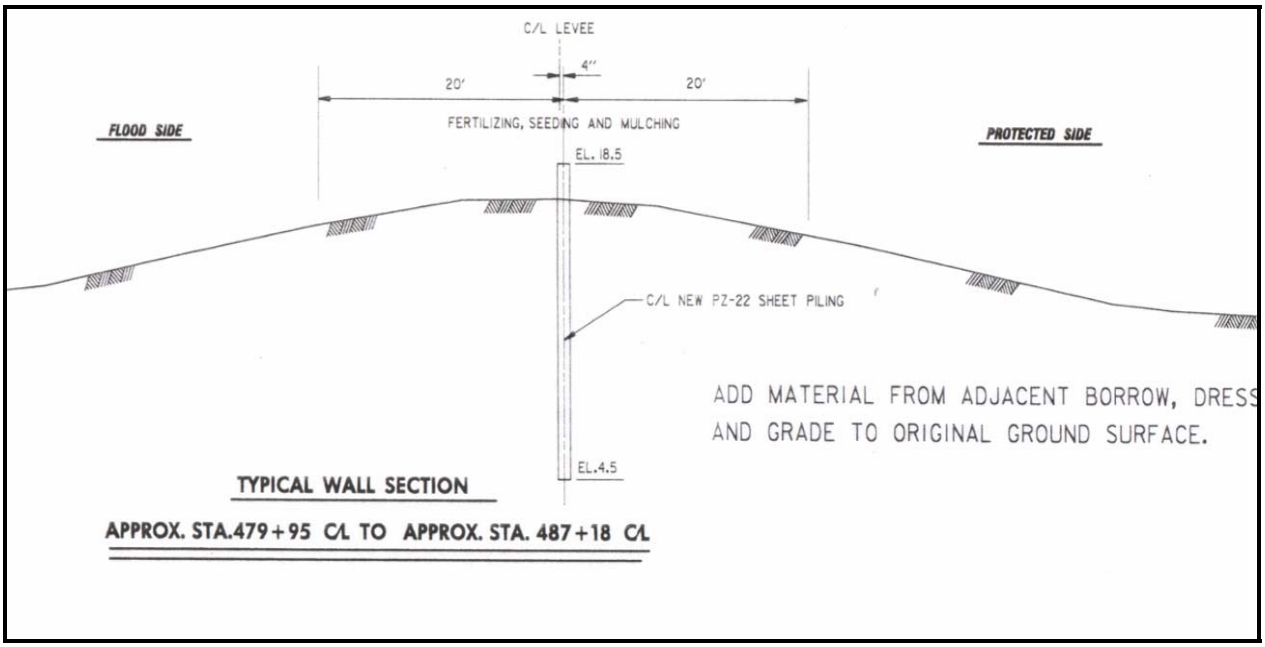


Figure 28**:** Cross sectional view of the sheet pile EBSB repair approach (USACE, 1992).

Figures 27 and 28 present a profile and cross sectional view of the proposed sheet pile EBSB repair approach. PZ-22 sheet piles were installed to attain the design EBSB crest elevation of +18.5 feet (NGVD). No design analyses (lateral stability, seepage, etc.) were presented with the project plans.

IV.1.9. Summary of Crest Elevation at Station 497+00

A chronological timeline of EBSB crest elevation was developed at Station 497+00 to evaluate actual achieved EBSB crest elevation versus time. The crest elevations were obtained from construction plans developed by the USACE and issued for each of the different construction phases.

The original Chalmette Area Plan (USACE, 1966a) had a target completion date of 1983 for the EBSBs in the vicinity of Station 497+00. As constructed, however, the design target elevation was not achieved until 1987. Shortly after, the actual EBSB crest elevation fell below the target design elevation.

Figure 29 presents a timeline of the EBSB crest elevation at Station 497+00 from 1966 to 2007. At the time Hurricane Katrina hit the MR-GO area, the EBSB crest elevation had settled approximately 1.5 feet below the target crest elevation of +17.5 feet (NGVD). Also included on this plot are approximations of storm surge elevations (high water marks not necessarily including wave runup) near Station 497+00 from observations following Hurricanes Betsy (USACE, 1965) and Camille (USACE, 1970).

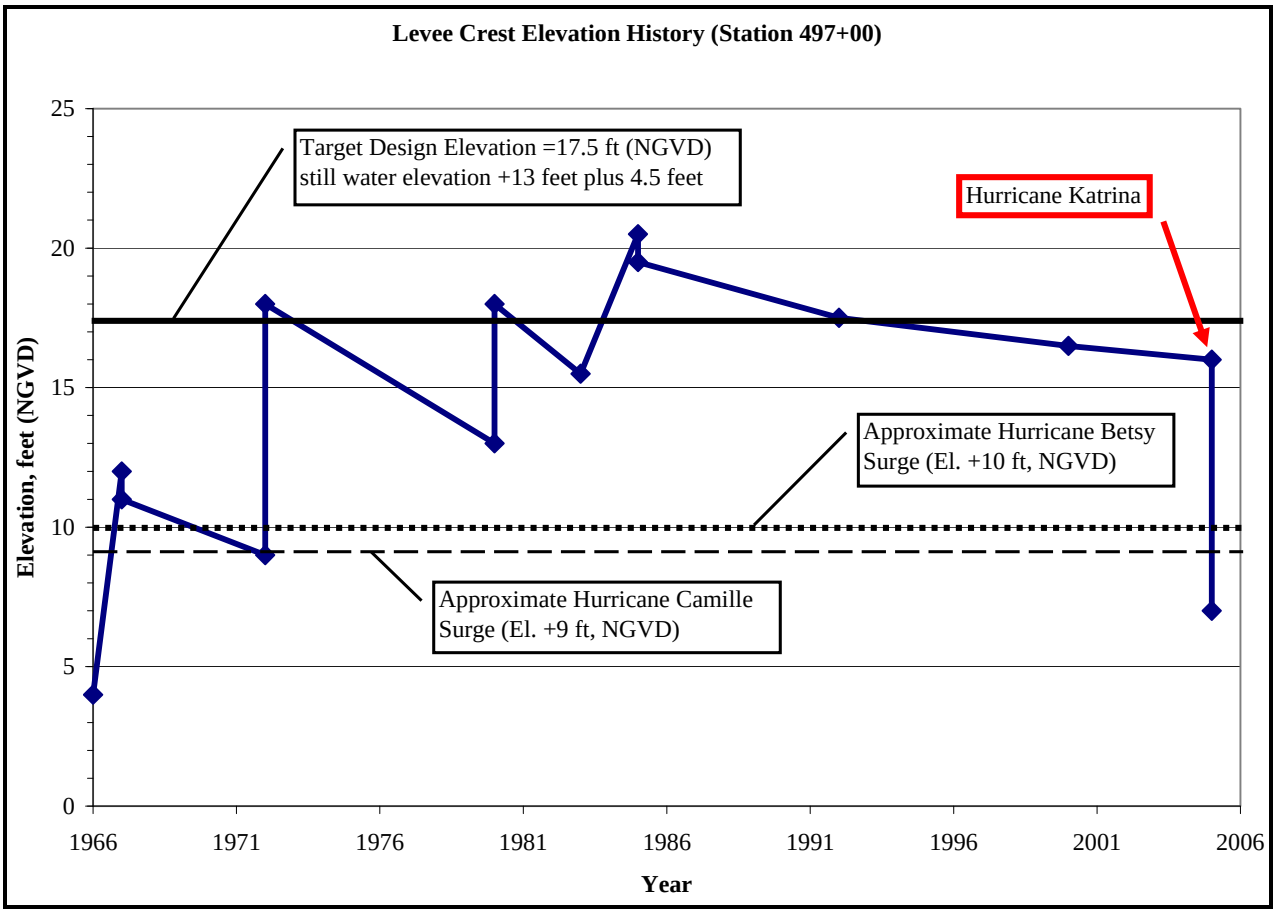


Figure 29**:** Plot of EBSB crest elevation from 1966 to 2007, when Hurricane Katrina hit New Orleans.

V. STUDY SITE AND TOPOGRAPHY

Aerial LiDAR surveys were performed in 2000 and 2005 by Chance Surveys. The datums used for the 2000 and 2005 survey were NAVD88 (vertical) and Louisiana 1702, Southern Zone (1983, US Survey feet)(horizontal). These were obtained from the IPET spatial data website, available from https://ipet.wes.army.mil. The 2000 survey data was used to define the surface geometry for the study site. The 2005 survey data was used to confirm the magnitude of erosion as determined per the numerical modeling results.

Figure 30 presents a comparison of the 2000 EBSB topography with the post-Katrina topography in September 2005 prepared by IPET and presented in their report (USACE, 2007a).

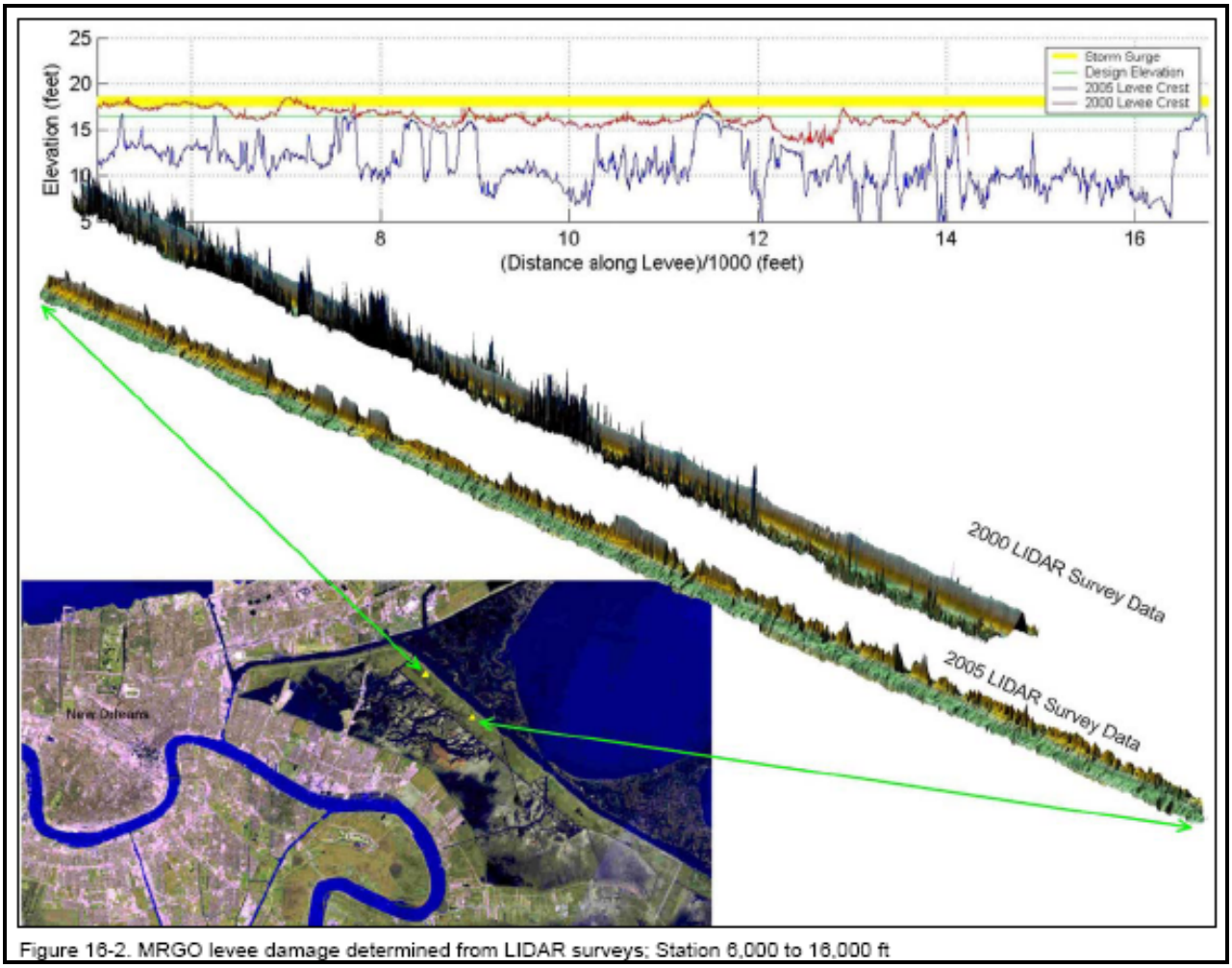


Figure 30**:** Comparison of the pre (2000) and post (2005) EBSB profiles based on aerial LiDAR surveys (IPET, 2007a).

As can be seen in this picture, this region of the MR-GO EBSB experienced variable performance. Some locations experienced very little erosion, while other locations experienced catastrophic erosion. A close-up view of the 2000 LiDAR survey in the vicinity of Station 497+00 is presented in Figure 31. This figure shows the "pre-Katrina" condition of the EBSB. Figure 32 shows the Aerial LiDAR results following Hurricane Katrina. Significant scour and

erosion can be seen. The aerial oblique photograph included in Figure 32 also shows the "post-Katrina" EBSB condition.

Figure 33 shows a comparison (in plan view) of the 2000 and 2005 condition of the MR-GO EBSB at Station 497+00. Significant erosion (as much as 12 feet) occurred along this section of the levee. Figure 34 shows a difference map between the two surveys.

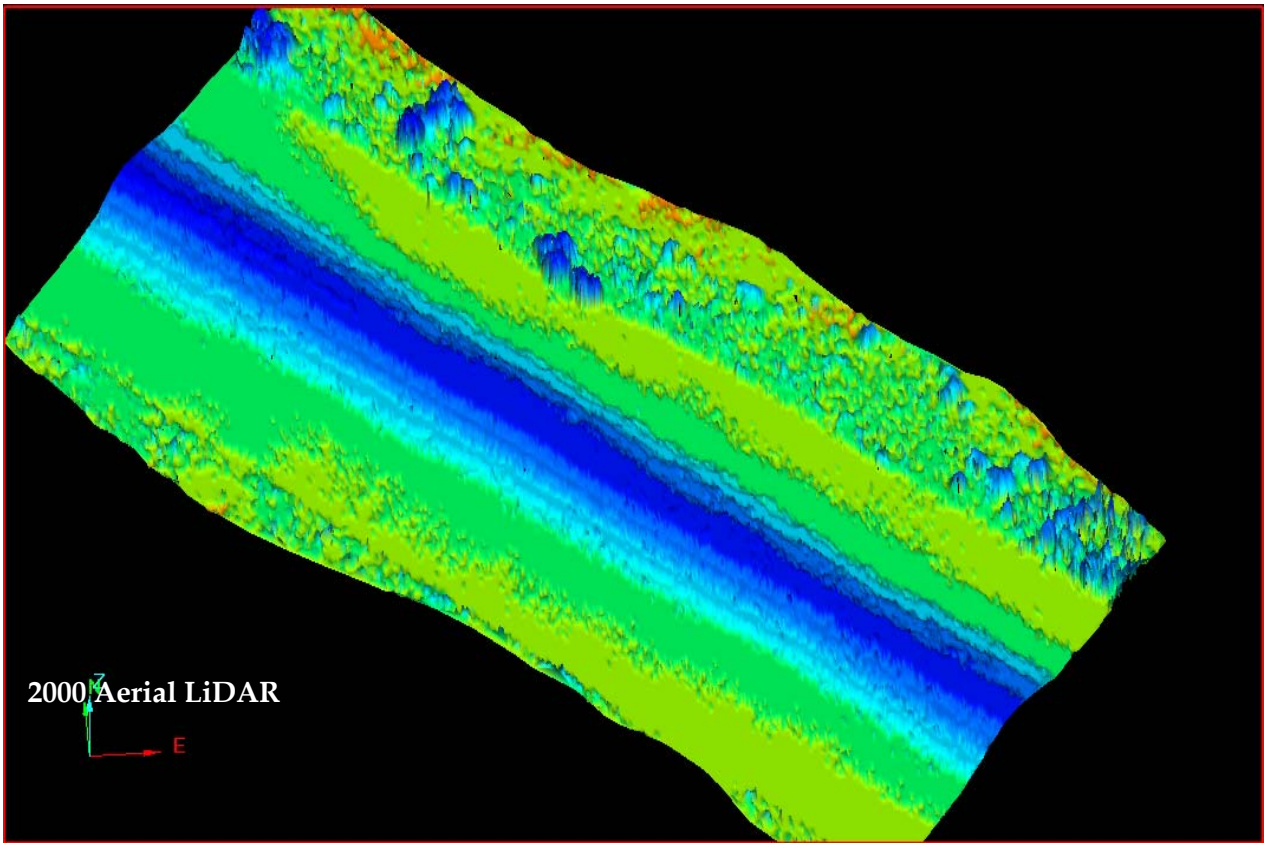


Figure 31**:** Pre-Hurricane Katrina Aerial LiDAR data will be used as the geometric initial conditions for the erosion/scour analyses.

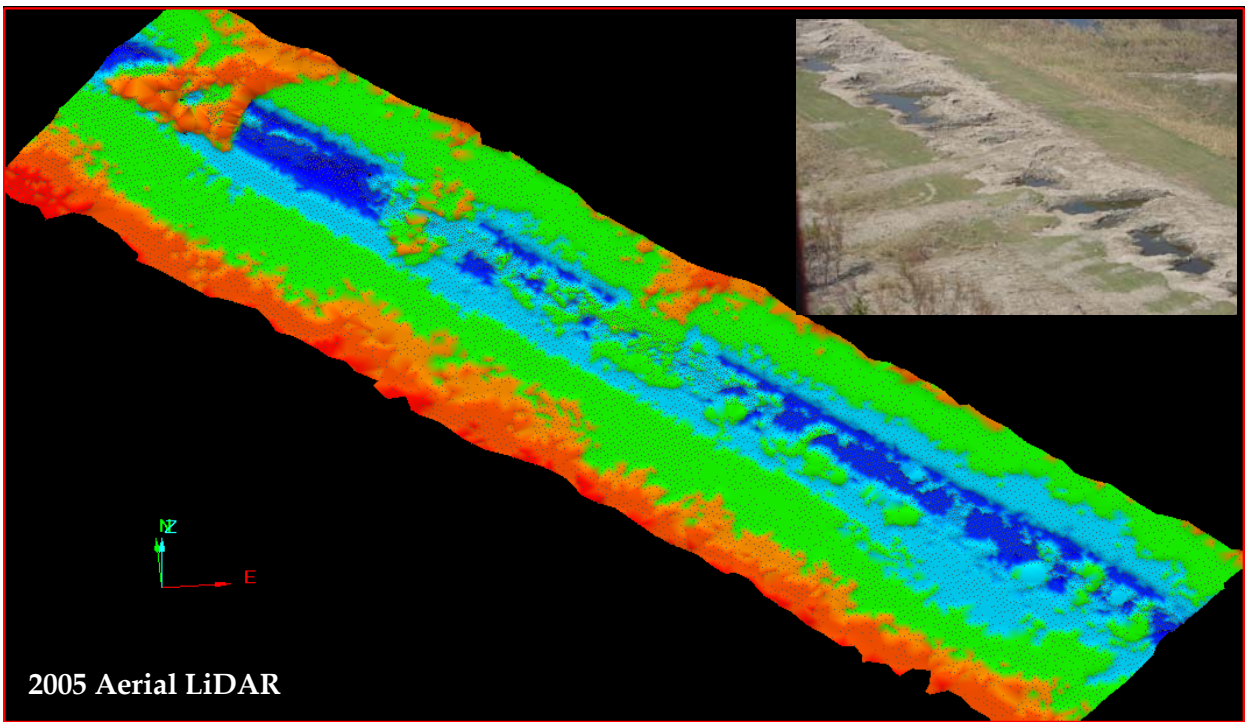


Figure 32**:** Aerial LiDAR surveys captured the erosion features of the MR-GO EBSBs following Hurricane Katrina. Elevations are colored from red (low) to blue (high). Above is an aerial oblique photograph showing erosion and scour as depicted in the Aerial LiDAR survey.

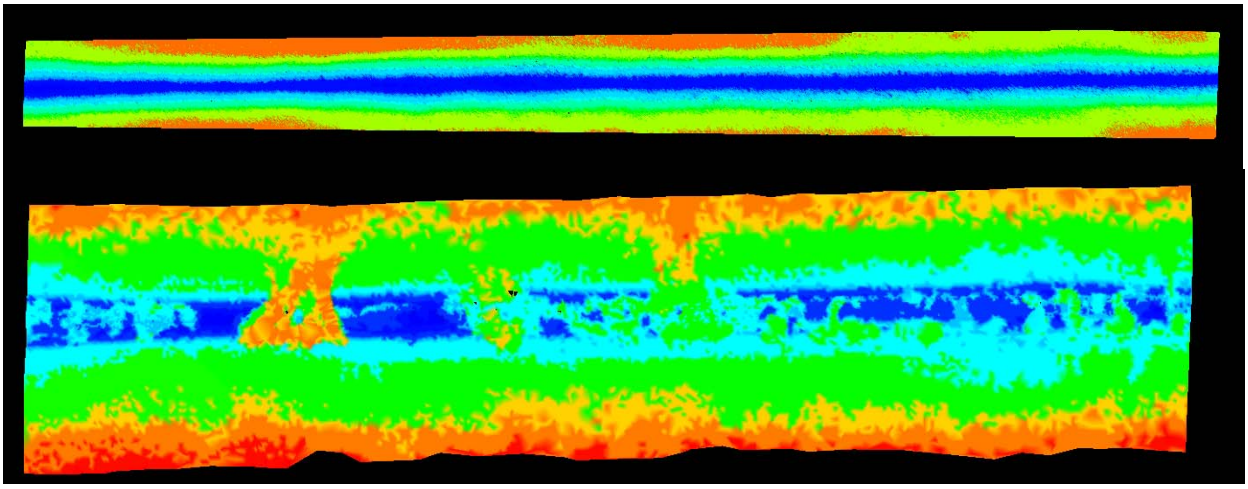


Figure 33**:** A plan view comparison of the 2000 (top) and 2005 (bottom) EBSB condition at Station 497+00.

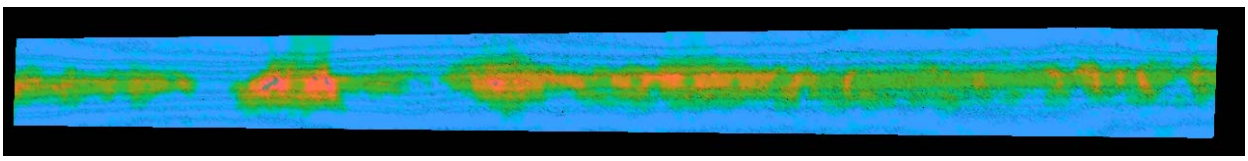


Figure 34**:** This 'difference map' was generated by calculating the elevation difference between the 2000 and 2005 EBSB geometry.

In addition to EBSB configuration and elevation information, Aerial LiDAR is also useful to identify the presence of vegetation that may reduce the height of wind-generated storm waves onto the EBSB. At locations where the vegetation is higher than the maximum wave elevation, significant damping is expected to occur. The degree of vegetation at this site was moderate, so a moderate degree of damping is likely to have occurred at this site during the actual passing of Hurricane Katrina. Standard numerical modeling analyses, however, do not directly capture damping effects of the vegetation and additional research and development is required to refine these analyses.

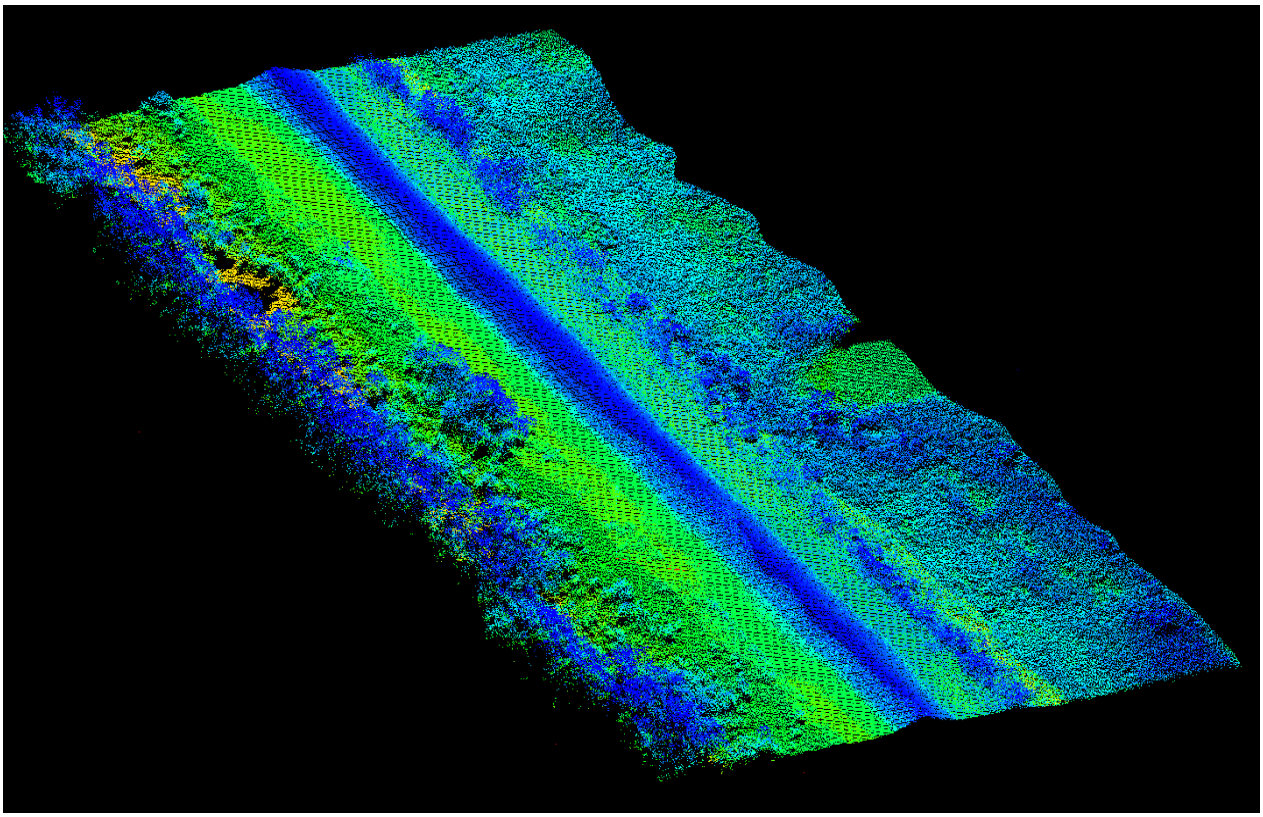


Figure 35**:** A view of the raw LiDAR data points showing vegetation on either side of the MR-GO EBSB in the vicinity of Station 497+00.

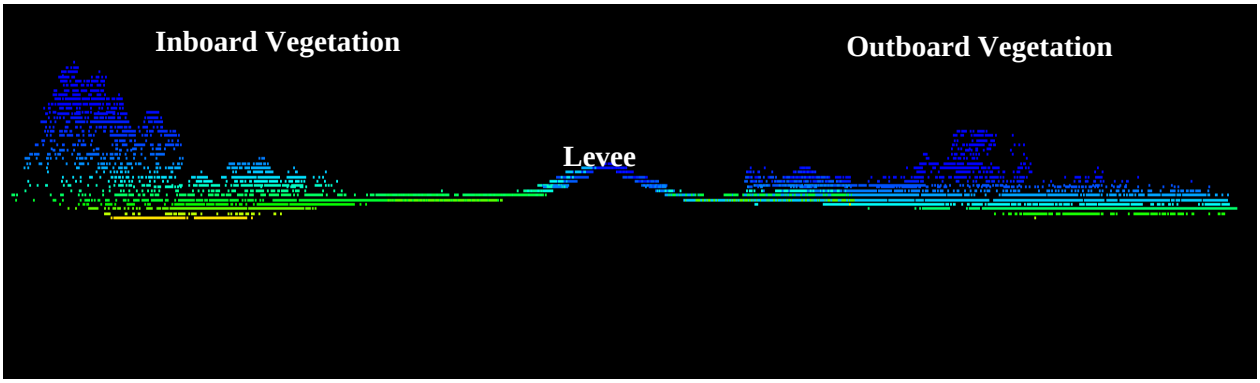


Figure 36**:** A cross sectional view of the EBSB section at Station 497+00. Note the height of the vegetation on the inboard and outboard sides of the EBSB.

Figures 35 and 36 provide a view of the raw Aerial LiDAR scans performed near Station 497+00. Figure 35 is an aerial oblique view that is color coded based on elevation. Red colors are low elevation and blue colors are higher elevations. Figure 36 provides a cross sectional view of the EBSB. Note the heights of the vegetation on the outboard side of the EBSB. Some patches of vegetation are actually higher than the crest of the EBSB, implying some degree of wave attenuation as the waves pass from the open Lake Borgne region towards the hurricane protection 'levee.'

VI. HYDRODYNAMIC LOADING

Hydrodynamic loading considered for these analyses were based on studies by de Wit et al (2008), Gautier et al (2008a, 2008b). Two scenarios were considered for wave-induced erosion analyses in this report; the first (Scenario 1), modeled the actual conditions along the Lake Borgne/MR-GO region at the time of Hurricane Katrina and the second scenario (Scenario 2C, also referred to as Scenario 2Ci in some figures) considered a Neutral MR-GO with no navigation channel and no degradation of the wetlands and surrounding marshes at the time of Hurricane Katrina. Scenario 3 (not evaluated in this study) was an analysis to calculate

hydrodynamics in the Lake Borgne/MR-GO region assuming that the MR-GO navigation channel was constructed and the original wetlands/marshes were in perfect condition, with no reduction in spatial extents from the documented 1956 wetland/marsh conditions.

Hydrodynamic information for Scenario 1 and Scenario 2C was provided (de Wit et al., 2008; Gautier et al., 2008a; 2008b) on an hourly basis between 0400 (CDT) and 0900 (CDT). The study site (Station 497+00) is described as Location 3 in the de Wit et al (2008), Gautier et al (2008a, 2008b) reports.

The simulations performed in this study used one-hour time steps, with interpolated hydrodynamic values between the hourly reported values used to approximate wave-induced erosion on the flood face of the MR-GO EBSBs. For example, the reported hydrodynamic values at 0400 (CDT) and 0500 (CDT) were used to calculate interpolated hydrodynamic values at 0530 (CDT). The interpolated hydrodynamic values at 0530 (CDT) were then used to simulate wave-induced erosion between 0400 and 0500 (CDT). Storm surge elevations were based on FINEL models (Gautier et al., 2008a; 2008b), not ADCIRC models. Table 3 presents a summary of the hydrodynamic values used in the Scenario 1. The values in italics were hydrodynamic values from Gautier et al (2008a) used to interpolate the simulation hydrodynamics (on the half-hour).

Table 3: Summary of Scenario 1 Hydrodynamic Values at Station 497+00 (Actual MR-GO)

Time (CDT)	Storm Surge (ft) NAVD88	Significant Wave Height (ft)	Wave Period (s)	Overtopping ($ft^3/s/ft$)
0400	*9.2*	*1.9*	*3.8*	*0.0*
0430	10.1	2.0	4.0	0.0
0500	*11.0*	*2.1*	*4.2*	*0.0*
0530	12.0	2.7	4.5	0.0
0600	*13.0*	*3.3*	*4.7*	*0.0*
0630	14.2	4.1	4.9	0.0
0700	*15.4*	*4.9*	*5.1*	*0.0*
0730	16.6	5.5	5.4	0.2
0800	*17.8*	*6.0*	*5.6*	- - -
0830	16.1	4.8	5.2	0.2
0900	*14.3*	*3.6*	*4.7*	- - -

Table 4 presents a summary of the hydrodynamic values used in the Scenario 2C simulations. The values in italics were hydrodynamic values from Gautier et al (2008b) used to interpolate the simulation hydrodynamics (on the half-hour).

Table 4: Summary of Scenario 2C Hydrodynamic Values at Station 497+00 (Neutral MR-GO)

Time (CDT)	Storm Surge (ft) NAVD88	Significant Wave Height (ft)	Wave Period (s)	Overtopping ($ft^3/s/ft$)
0400	*9.0*	*0.5*	*2.4*	*0.0*
0430	9.9	0.6	2.7	0.0
0500	*10.7*	*0.8*	*2.9*	*0.0*
0530	11.8	1.0	3.1	0.0
0600	*12.8*	*1.3*	*3.2*	*0.0*
0630	14.0	1.5	3.4	0.0
0700	*15.2*	*1.8*	*3.5*	*0.0*
0730	16.2	2.0	3.5	0.2
0800	*17.1*	*2.2*	*3.5*	- - -
0830	16.0	1.7	3.5	0.2
0900	*14.9*	*1.2*	*3.4*	- - -

VII. EROSION CHARACTERIZATION

The constitutive model of the EBSB erosion (the amount of realized erosion based on applied shear velocity from wave impact) was defined using erodibility characterization of the EBSB materials. The erodibility of a soil is defined as the relationship between the erosion rate of a soil and the shear velocity induced at the soil/water interface. A state of the art Erosion Function Apparatus (EFA) testing method was used by ILIT (2006) to characterize the erodibility of 'levee' materials throughout the greater New Orleans area. Testing was performed under the direction of Dr. Jean Luis Briaud of Texas A&M University.

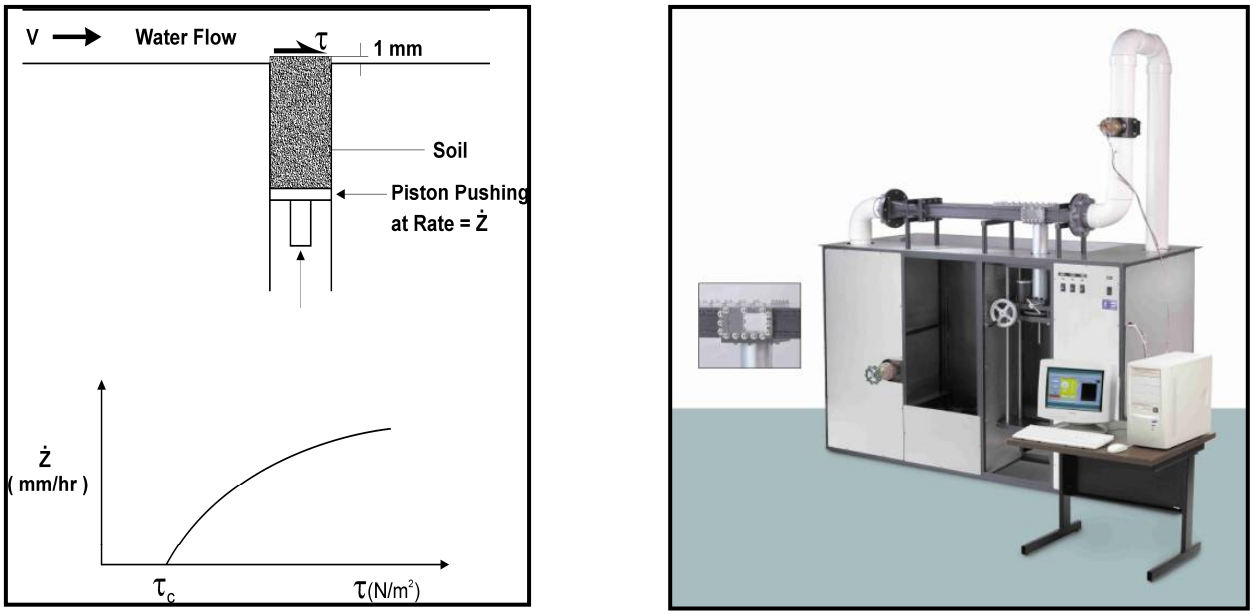


Figure 37: A view of the EFA and testing procedure (ILIT, 2006).

The EFA test consists of eroding a soil sample by pushing it out of a thin walled Shelby tube and recording the erosion rate for a given velocity of water flowing past the sample. Several velocities are used in order to define the erosion function curve. See Figure 37 for a diagram of the EFA machine and loading mechanism.

Erodibility Soil Sampling Locations

Five erodibility samples were collected along the MR-GO EBSBs, these samples are shown on Figure 38.

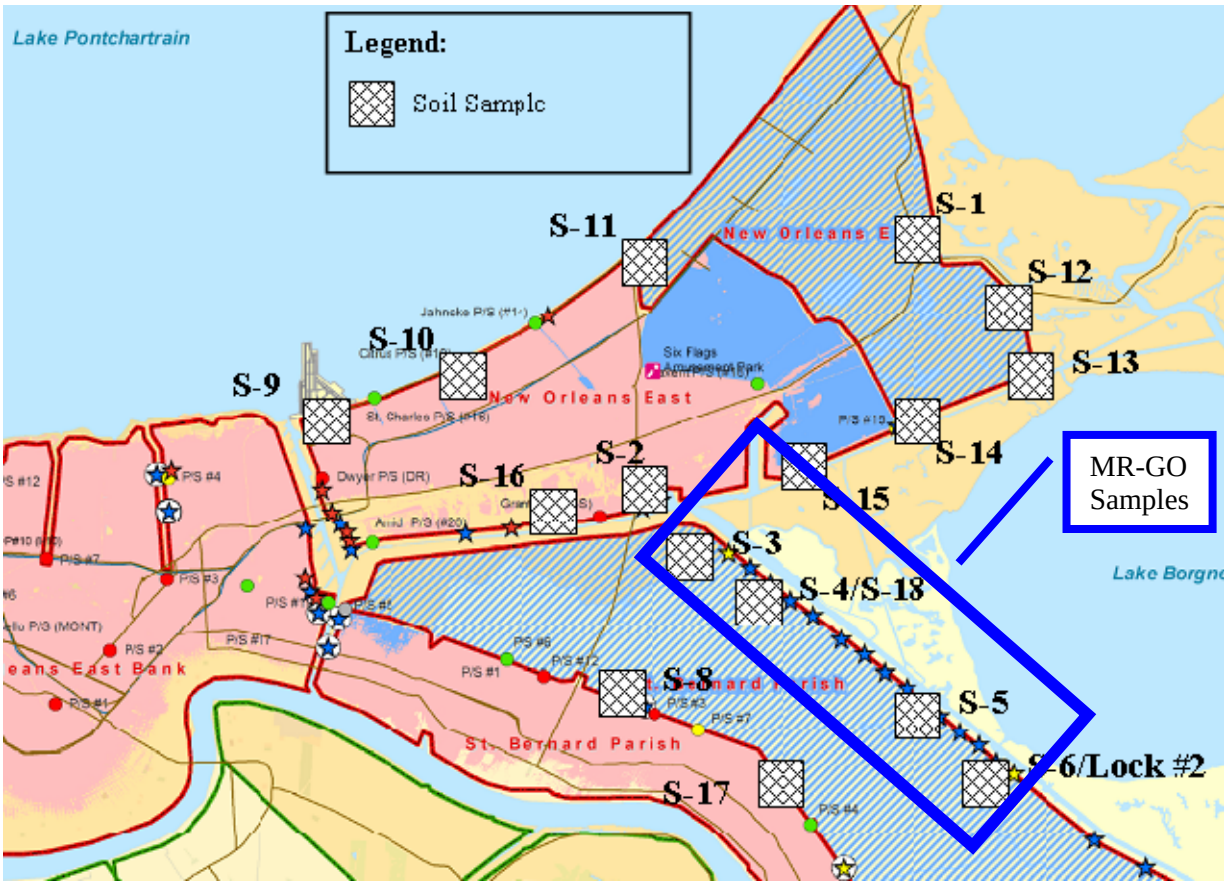


Figure 38**:** Five erodibility samples were collected along the MR-GO EBSB alignment (S3, S4, S5, S6, S18) (ILIT, 2006).

No actual in-situ samples were available for testing from the EBSB at Station 497+00 prior to Hurricane Katrina, so reconstituted soil samples were created from samples collected from the MR-GO EBSBs during field visits (ILIT, 2006) in October 2005, following Hurricane Katrina. These reconstituted samples were compacted with light compactive effort to match the assumed in-situ material density based on design drawing specifications and available soil boring information and critical velocity values were obtained based on the EFA testing. Results from the EFA testing of samples collected from the MR-GO EBSBs are presented in Figure 39.

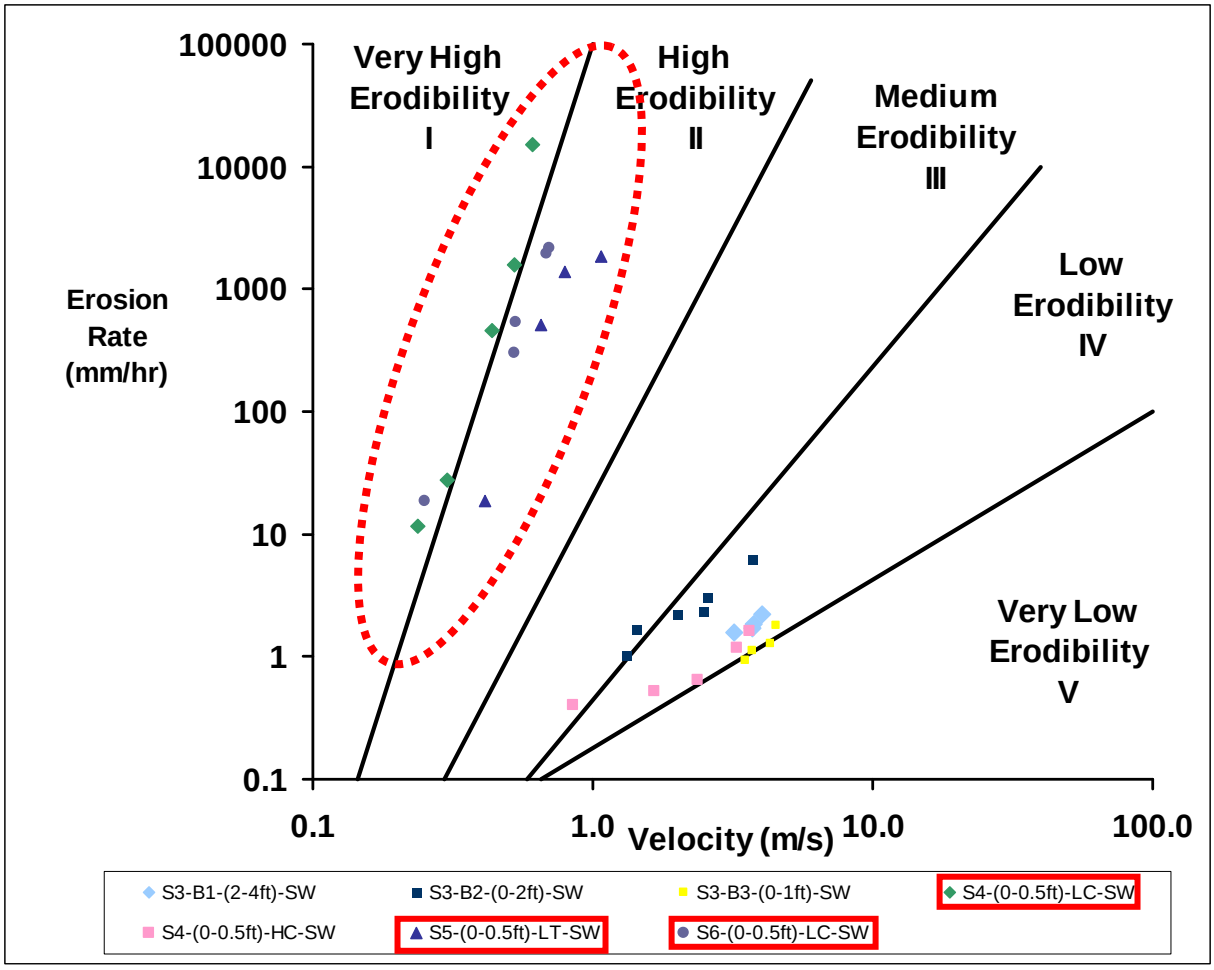


Figure 39**:** Samples (red boxes) obtained and tested from the MR-GO were found to have high to very high erodibility based on the EFA testing performed by ILIT (2006).

Three soil erodibility profiles were considered in these analyses to evaluate the magnitude of wave-induced erosion on the levees; Very High Erodibility (Sample S-4), High Erodibility (Sample S-5), and Low Erodibility (Sample S-6). Soil samples for the Very High Erodibility and High Erodibility were collected from the MR-GO alignment between Bayou Bievenue and Bayou Dupre (Figure 38). The Low Erodibility soil sample was collected from the MR-GO alignment just north of Bayou Bievenue (Figure 41).

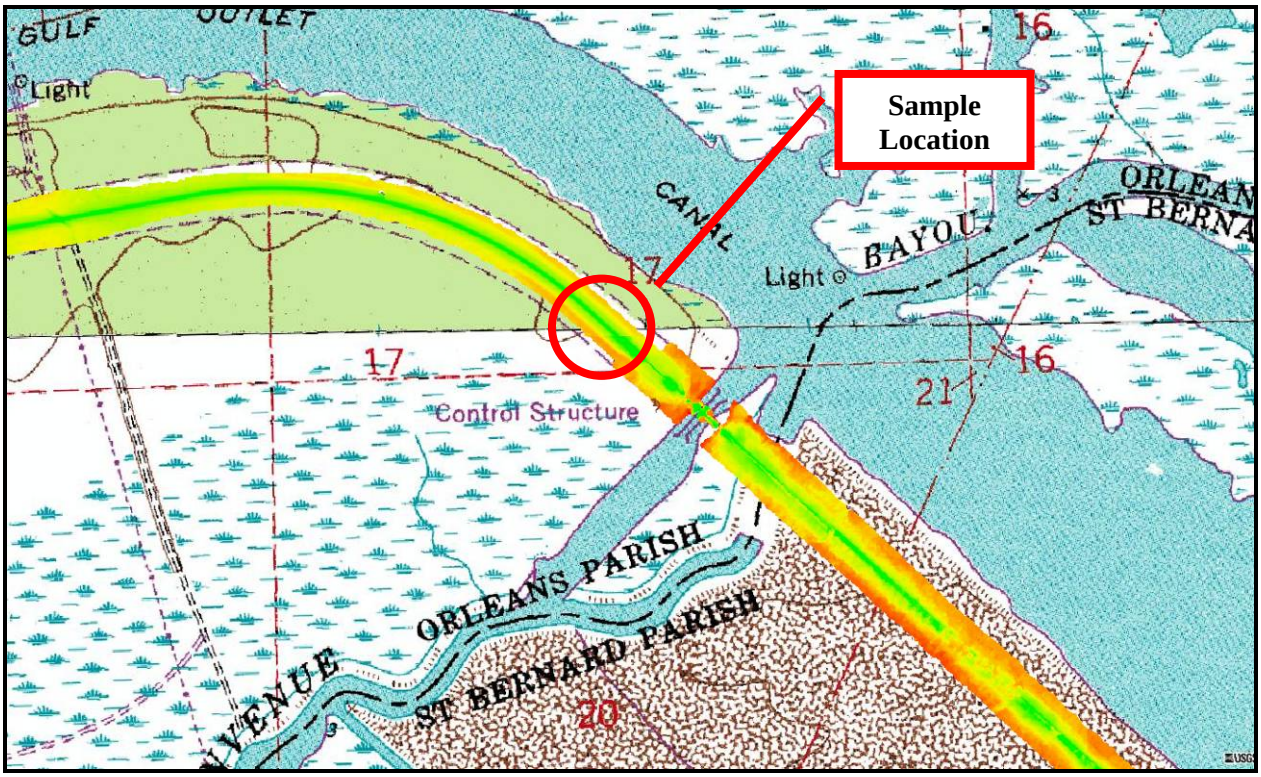


Figure 40: The sample used to determine 'good' levee material erodibility was collected from the MR-GO EBSBs north of Bayou Bienvenue. This location did not experience significant wave-induced erosion.

The region (north of the Bayou Bienvenue Control Structure) where the Low Erodibility soil sample used for the EFA testing was collected, did not experience any significant wave-induced erosion, in fact, a concrete barge/platform collided with the levee and no significant damage was incurred by the levee (Figure 41).



Figure 41: Levees north of Bayou Bievenue were constructed of 'good' materials that were both erosion resistant and impact resistant, as can be seen by this barge that came to rest on top of the earthen levee during the storm.

EBSB Erodibility Curves

Erodibility characterization selected to represent the EBSB materials at Station 497+00 was based on testing performed on soil samples collected from MR-GO. Erodibility test results from the EFA testing of samples S-3, S-4, and S-5 (presented in Figures 42, 43, and 44, respectively) were used to develop erosion curves based on velocities.

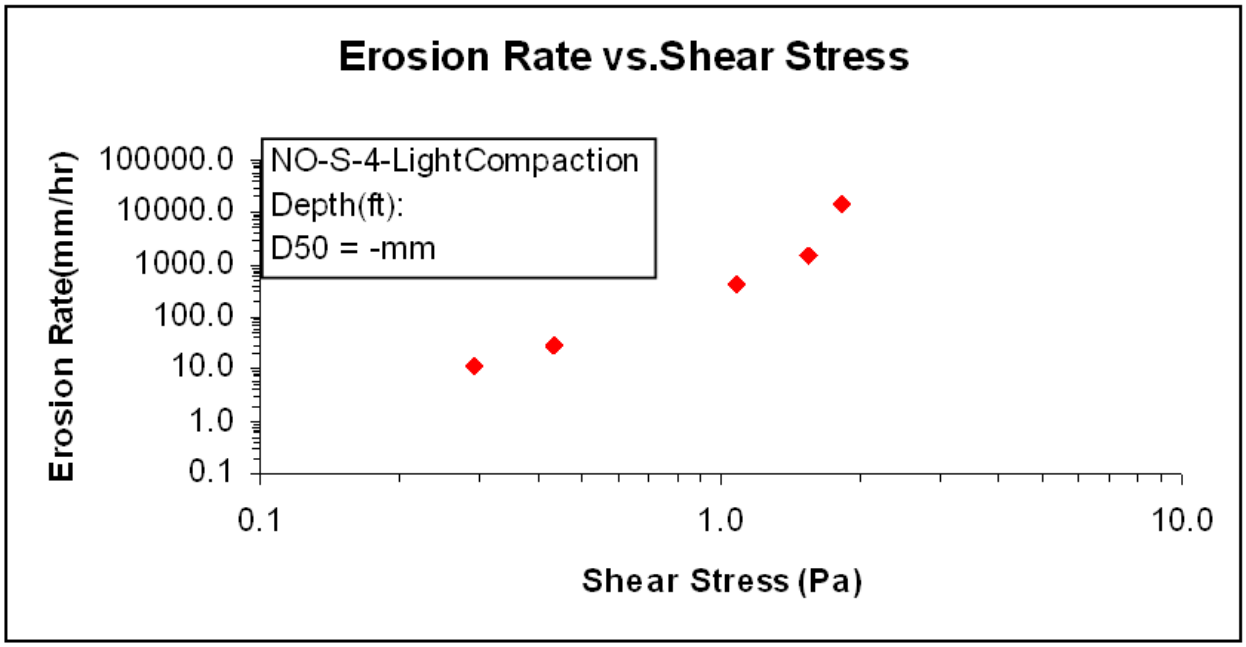


Figure 42**:** Erodibility test results on bulk soil samples (S-4) from the MR-GO EBSBs (ILIT, 2006) with Very High Erodibility.

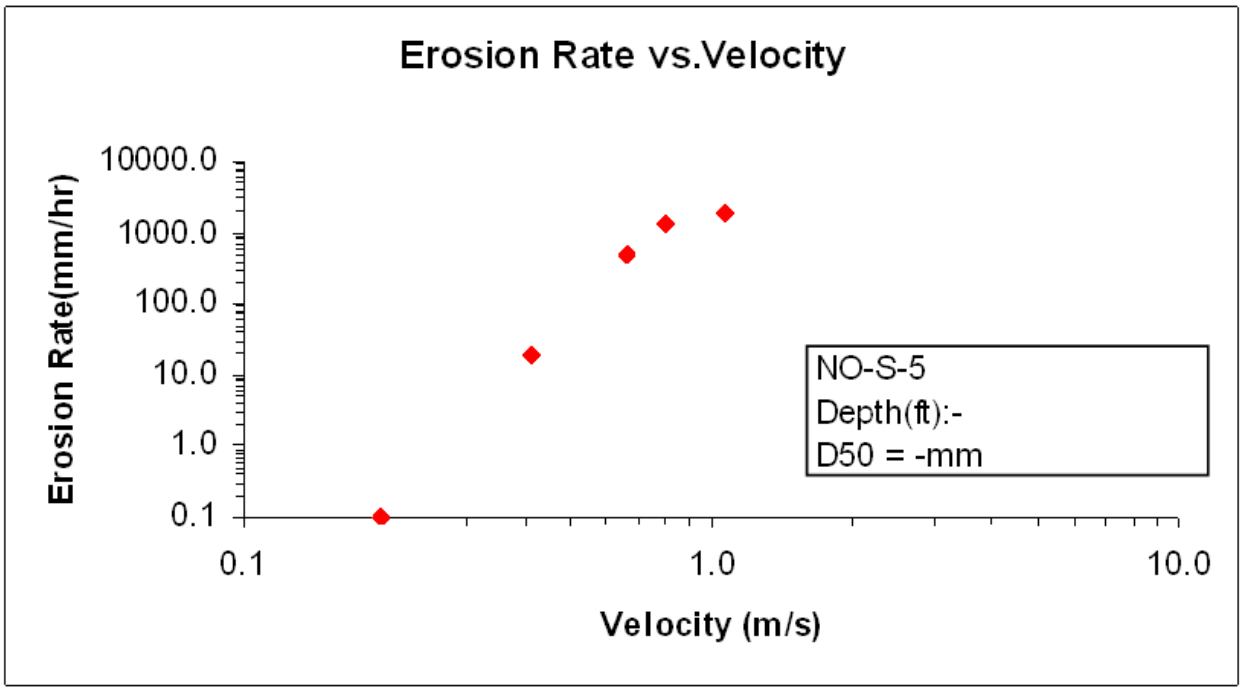


Figure 43**:** Erodibility test results on bulk soil samples (S-5) from the MR-GO EBSBs (ILIT, 2006) with High Erodibility.

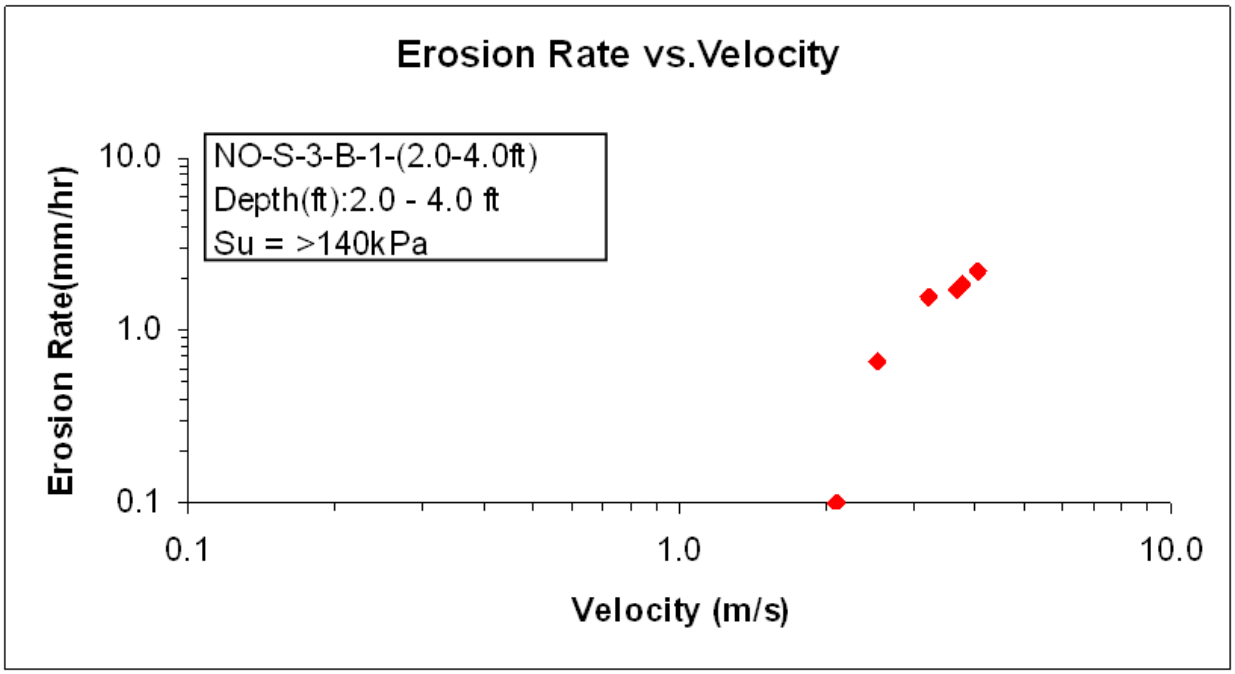


Figure 44**:** Erodibility test results on bulk soil samples (S-3) from the MR-GO EBSBs (ILIT, 2006) with Low Erodibility.

An exponential function was developed to correlate erodibility with shear velocity imposed on the EBSB face as a result of wave-induced uprush and downrush. These relations are presented in Figures 45 through 47 (Very High Erodibility <Category I>, High Erodibility <Category II>, and Low Erodibility <Category IV>, respectively). Based on the maximum amount of suspended soil that can be transported, the maximum erodibility rate was 'capped' at a value of twice the maximum EFA test result value. The ceiling erodibilty rate was imposed to limit the amount of potential erosion as water has a maximum sediment carrying capacity. The exact ceiling value for sediment transport using the EFA testing machine has not been established to date, however, all data points obtained using the EFA test procedure are assumed to be possible. Further testing should be performed to evaluate erodibility rates outside the testing range identified to validate the actual erodibility rate ceiling for this material.

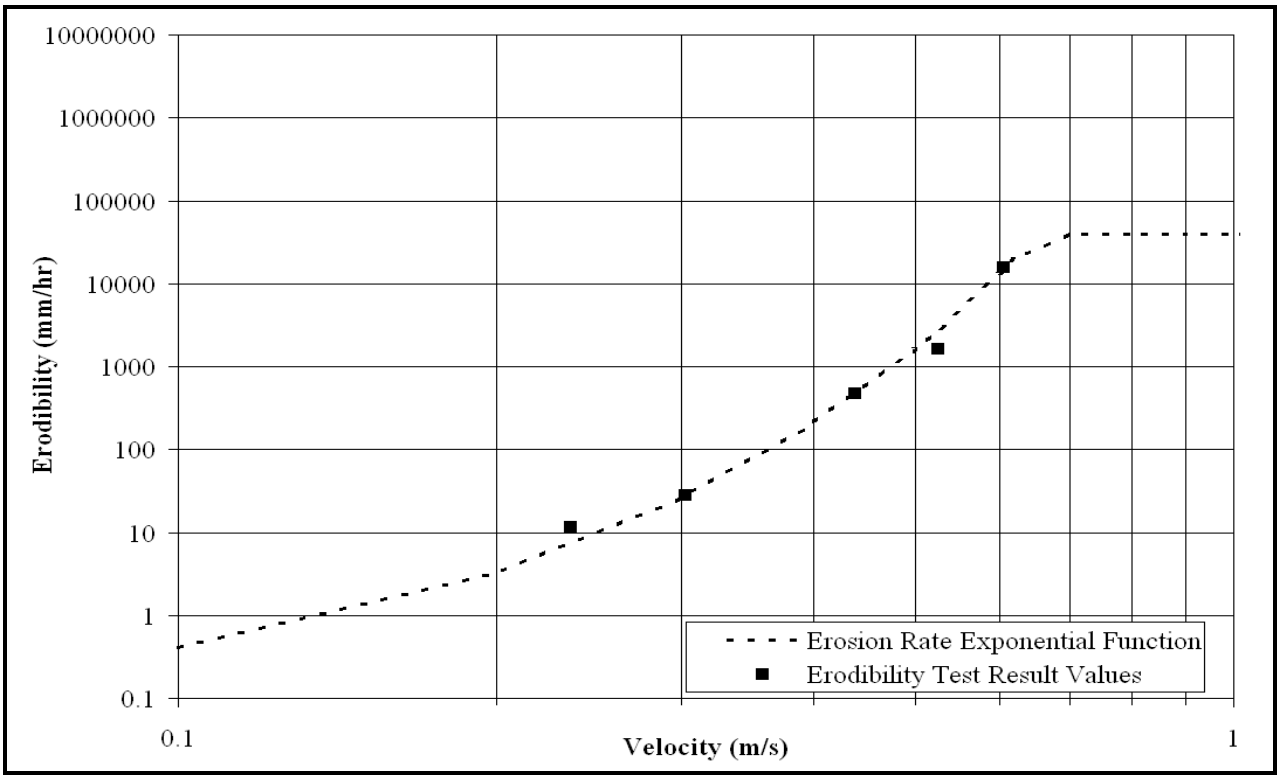


Figure 45: Exponential function used to characterize erodibility for Very High Erodibility (Category I) materials.

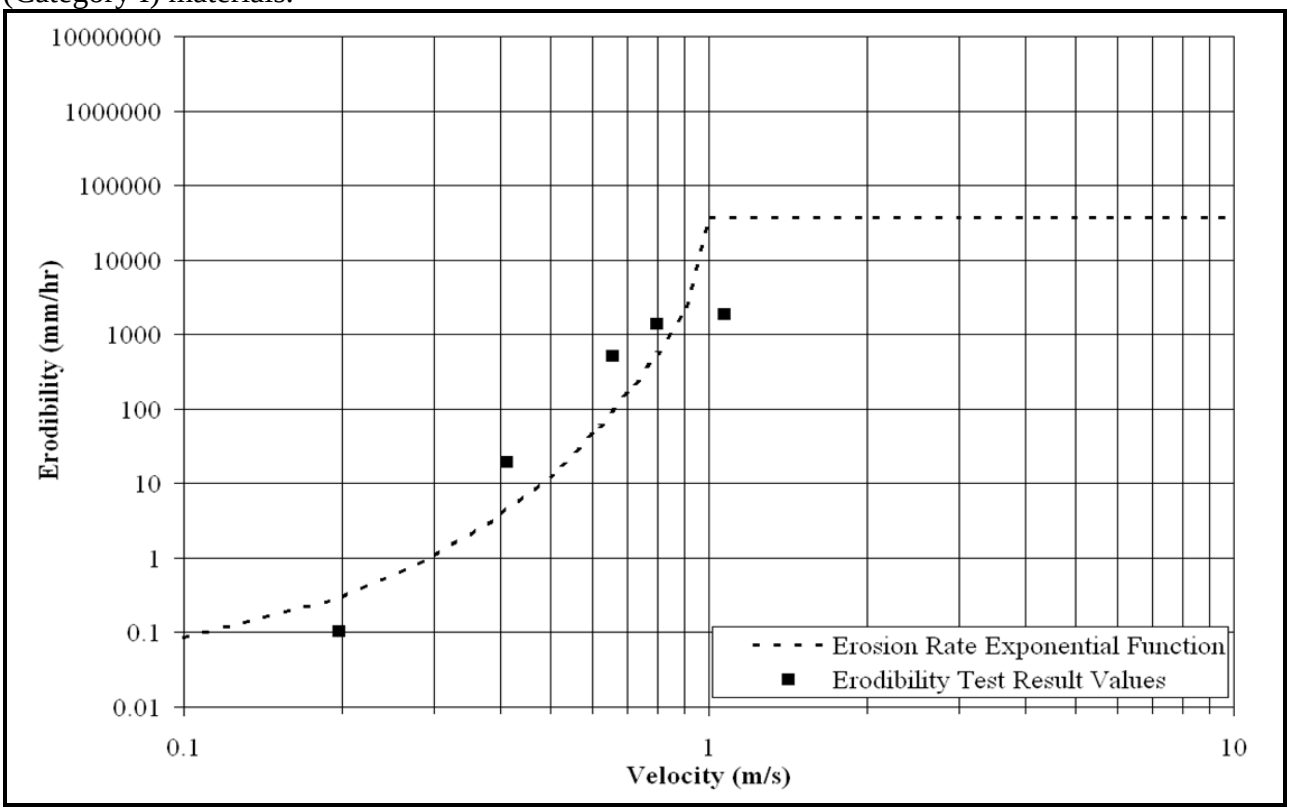


Figure 46: Exponential function used to characterize erodibility for High Erodibility (Category II) materials.

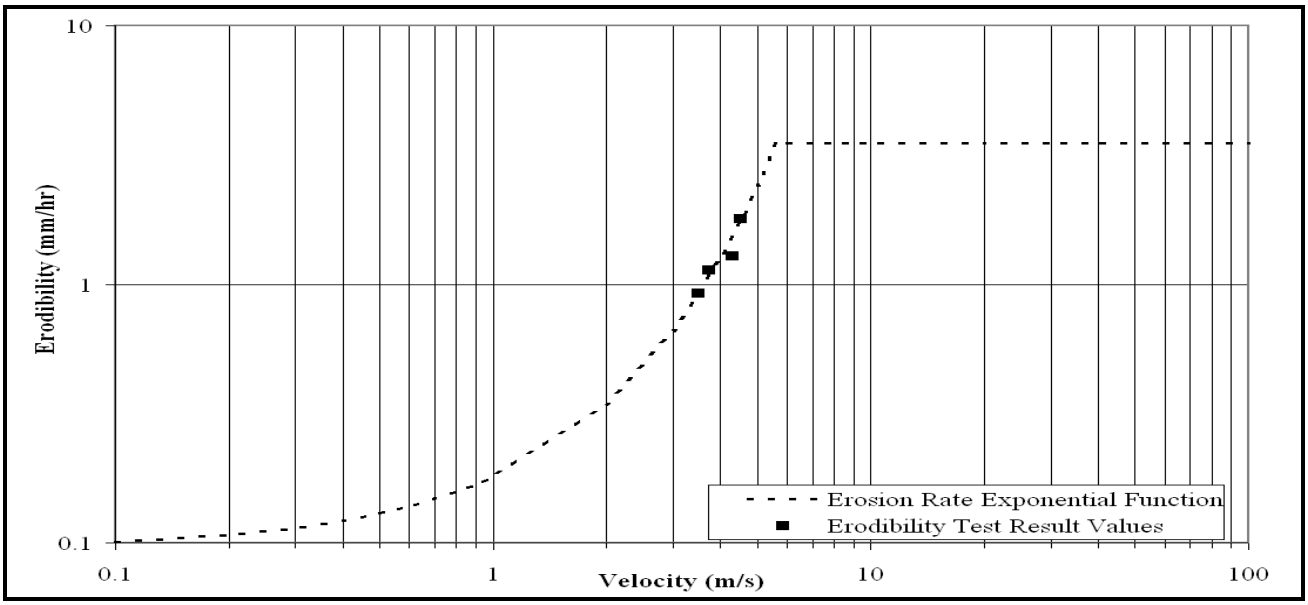


Figure 47: Exponential function used to characterize erodibility for Low Erodibility (Category IV) materials.

Erosion rates for the wave-induced erosion analysis were based on these velocity profiles. As can be see in Figure 47, the velocity capacity of 'good' levee materials (Low Erodibility) is two to three orders of magnitude greater than 'poor' levee materials (Very High Erodibility).

Estimates of wave-induced erosion extents based on the three soil erodibility profiles are presented in *Section XI. Estimation of EBSB Breach due to Wave Impacts.*

Effects of Soil Compaction

An evaluation was performed to assess the influence of compaction on erodibility of the soils (Figure 48). Two samples of soils collected from sample location S-4 were prepared and tested in the EFA. One sample was lightly compacted and the other sample was highly compacted. The highly compacted sampled exhibited several orders of magnitude difference in erodibility, registering as a Low Erodibility material (Category IV), whereas the lightly compacted sample

registered primarily as a Very High Erodibility material (Category I). This comparison confirms that the degree of compaction makes a LARGE difference in the performance of the 'levee' materials. Semi-compacted or no-compaction materials behave VERY differently from highly compacted soil materials. Utilization of clay (CH, CL) materials without proper compaction will not ensure low erodibility rates.

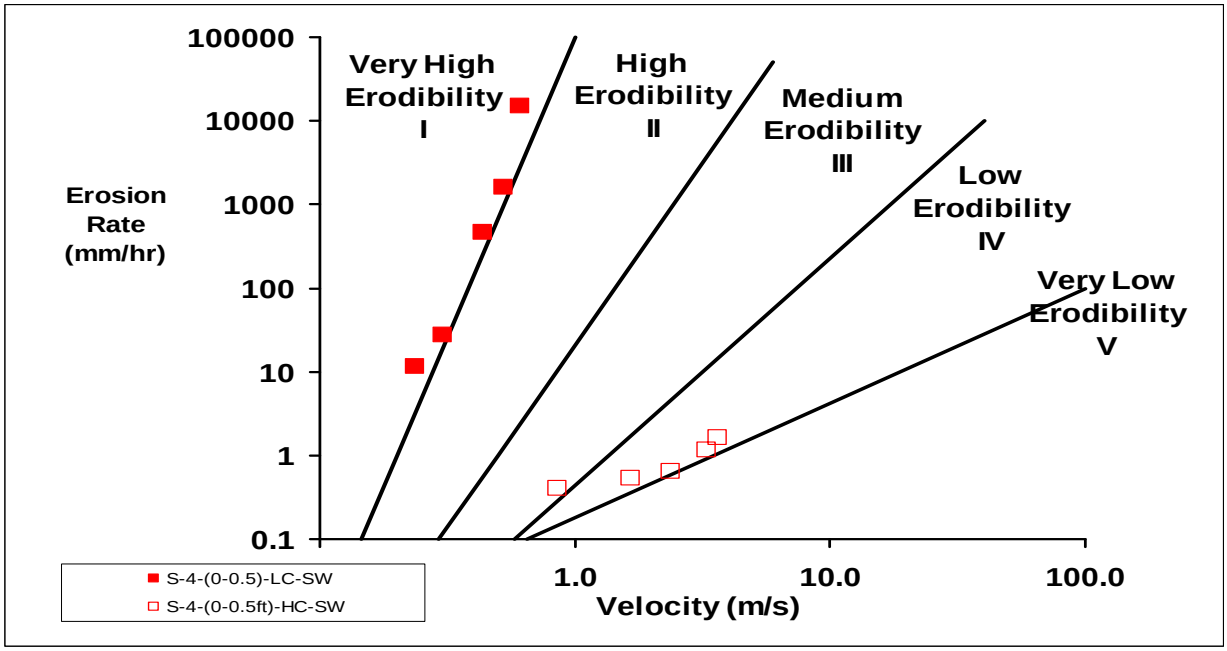


Figure 48: Degree of compaction makes a LARGE difference in the performance of the 'levee' materials. Semi-compacted or no-compaction materials behave VERY differently from highly compacted soil materials. Utilization of clay (CH, CL) materials without proper compaction will not ensure low erodibility rates (ILIT, 2006).

Erodibility evaluations were performed by IPET following Hurricanes Katrina and Rita (Figure 49). The results of their study are presented as an appendix in Volume V of the IPET report series. Four samples were collected from the same general vicinity as examined in this study. Only one of the four test locations was on an existing EBSB (M3). Two of the test locations were reconstructed EBSB sections that had undergone some degree of compaction. One test location (M2-2) was at a local borrow pit which was in an uncompacted state (hydraulic fill materials from the MR-GO channel excavations).

These tests found that the (pre and post) materials used to construct the MR-GO EBSB ranged from resistant to erosion to very erodible. The local borrow pit (site M2-2 consisting of uncompacted hydraulic fill used to construct the original MR-GO EBSB) was characterized as erodible and very erodible. The existing EBSB location (M3) had test results that were very erodible and resistant.

It should be noted, that some materials as part of the reconstruction efforts (M2-1) were found to be erodible. Use of 'erodible' materials should be strongly discouraged and is contrary to recommendations by IPET.

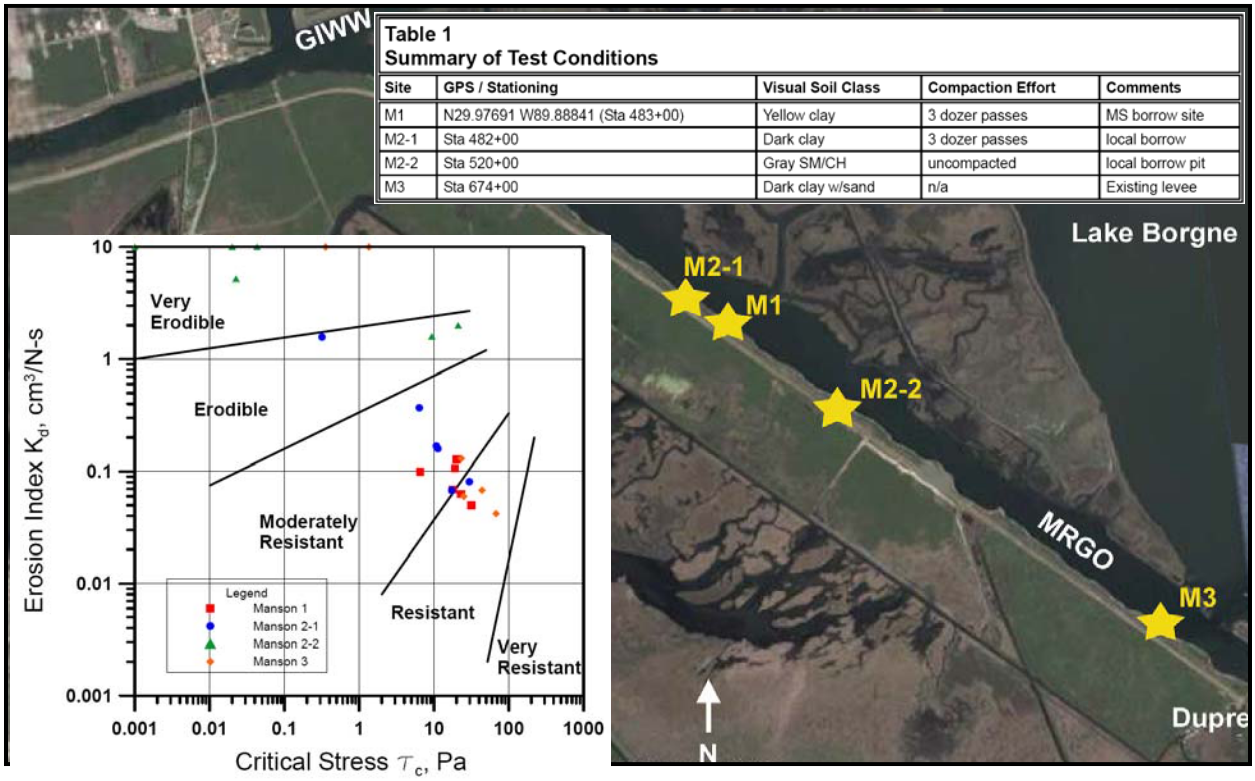


Figure 49: Results from erodibility evaluations performed by IPET following Hurricane Katrina found samples along the MR-GO to be very erodible and erodible (IPET, 2007e).

VIII. WAVE IMPACT MODELING

Overview

LS-DYNA (LSTC, 2007) is a general purpose finite element code for analyzing the large deformation static and dynamic response of structures and structures coupled to fluids. The main solution methodology is based on explicit time integration. LS-DYNA's capabilities include non linear dynamics, fluid analysis, and smooth particle hydrodynamics. The contact algorithms include flexible body to rigid body contact, eroding contact, and CAD surfaces. LS-DYNA contains approximately one-hundred constitutive models and ten equations of state to cover a wide range of material behavior. In addition to the standard constitutive models, user-defined models are also available.

Interaction shear velocities between the storm surge and the earthen levees were evaluated for a selection of storm surge elevations. Simulations were also performed using the actual EBSB configuration (as determined based on the available Aerial LiDAR data from 2000). For each storm surge elevation a numerical simulation was conducted for 150 seconds using the specified hydrodynamic characteristics (Gautier et al., 2008a, 2008b). This simulation time was selected in order to optimize computing time, while achieving 'steady state' wave impact conditions (interaction shear stresses and velocities) in the model. The initial 20 seconds of numerical simulation were dedicated to 'initializing' the run (gravity initialization and generating the hurricane waves).

Model Units

LSDYNA allows for a variety of units to be used in development of the numerical model, however the units must be specified by the model developer. Table 5 presents a summary of the units utilized in these numerical simulations.

Table 5: Summary of Model Parameter Units

Mass	Length	Time	Density	Force	Stress	Velocity	Energy
slugs	ft	s	slugs/ft^3	lbf	psf	ft/s	lbf-ft

LSDYNA does not directly label units, so it is critical to ensure the proper units are assigned to the correct parameters.

Model Geometry

As previously mentioned, the design EBSB configuration was not the actual configuration of the EBSB at the time Hurricane Katrina hit the New Orleans area. The crest elevation at Station 497+00 was approximately +16 feet, 1.5 feet lower than the target design elevation.

The development of the actual geometric configuration of the EBSB (Figure 50) was based on available Aerial LiDAR data. The flood side EBSB toe begins at Elevation +5 feet, runs at a slope of about 1 on 66 for 130 feet to Elevation + 7 feet, then runs on a slope of 1 on 3.5 for 31 feet to Elevation + 16 feet,. The crest has a width of 10 feet. The protected side EBSB slope runs on a slope of 1 on 3.6 to Elevation +9 feet (NAVD88). For these analyses, the model was terminated at Elevation +9 (NAVD88).

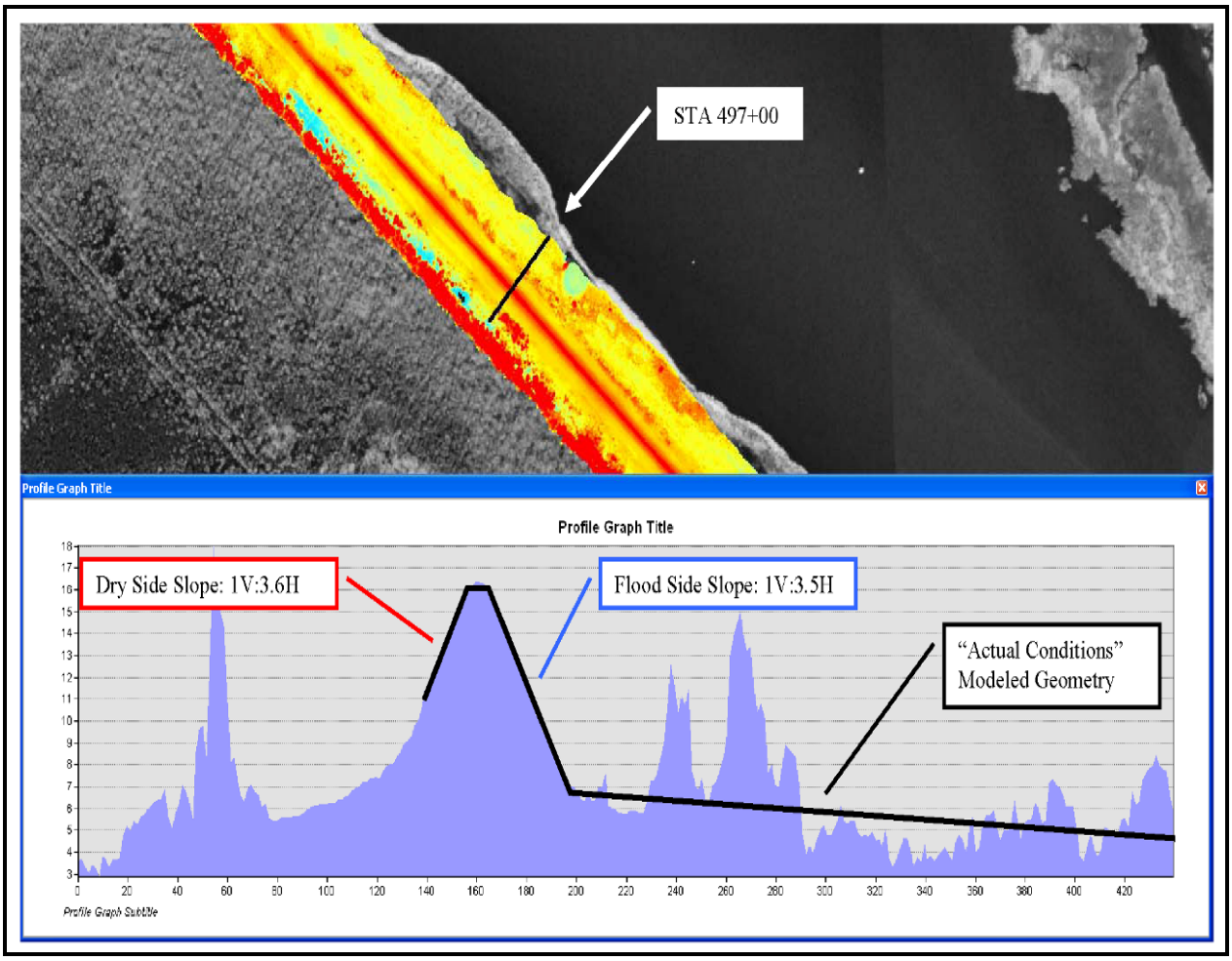


Figure 50: The EBSB profile used to model 'actual' geometry.

In order to fully develop the hurricane waves, a portion of the MR-GO channel was incorporated in to the model to provide additional depth adjacent to the wave generator. The actual distance from the edge of the MR-GO channel to the flood side toe of the EBSB is approximately 258 feet, however, for this simulation the modeled distance was 50 feet (to reduce the numerical computation time). This modification is not expected to have a significant impact to the calculated interaction shear velocities since wave damping is not implemented in the model. It is important to note that the presence of flood side vegetation acts to attenuate and damp incident wave energy (it was not accounted for in the hydrodynamic characterization developed by IPET).

The model was created using a grid size of approximately 1.0 foot (meaning a node was located at a spacing of one foot). The x-axis runs longitudinal and the y-axis represents the model elevation. The z-axis runs along the width of the model (which was set to be one-foot).

Boundary Conditions and Material Properties

The numerical model consisted of four components: the EBSB, water, void space, and the wave generation/water inflow mechanism (for overtopping conditions). Figure 51 presents an overview of the model.

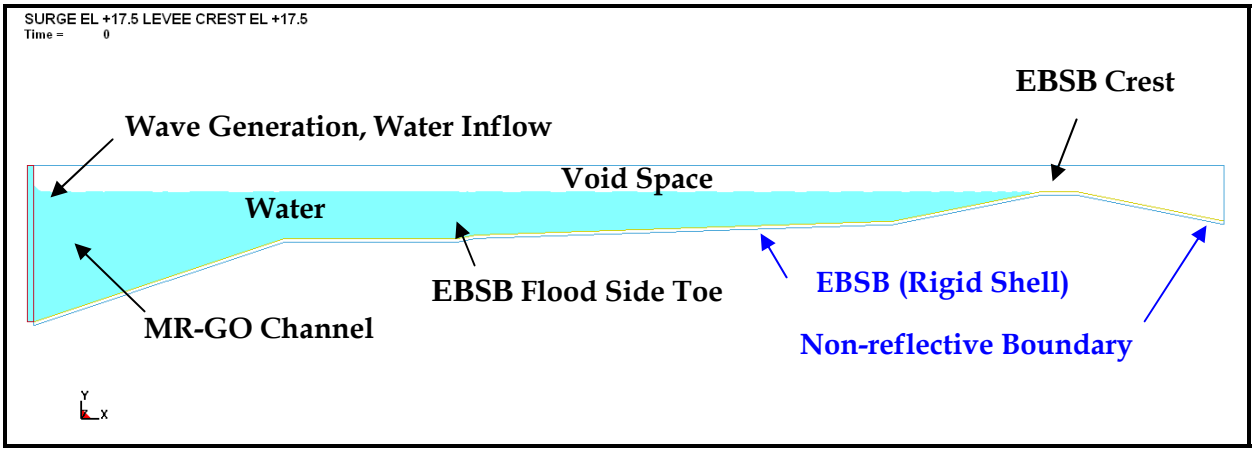


Figure 51: An overview of the model used for the numerical simulation.

A non-reflective boundary was established inboard of the EBSB. The EBSB was modeled as a (non-pervious) rigid shell. For analyses where the EBSB was overtopped, inflow rates were estimated based on Gautier et al. (2008a, 2008b) overtopping rates. These inflow rates were used to maintain the 'still water' elevation over which the storm waves were generated.

A detailed description of the model components is presented below:

EBSB – The EBSB was modeled as a non-porous, rigid shell element (*MAT_020), Lagrangian surface, allowing for coupling forces between the fluid and EBSB to be calculated. No material properties (Young's modulus, Poisson ratio, etc.) were required for this material type.

Fluid/Water – The fluid was modeled as 'generic' material (*MAT_009) allowing equations of state to be considered without computing deviatoric stresses. The water was assigned a mass density of 1.99 slugs/ft^3 (Munson et al, 1998), a pressure cutoff of -1.0E+11 psf (i.e. no pressure cutoff), and a dynamic viscosity coefficient of 2.5E-5 (Munson et al, 1998). Equations of state were used (*EOS_GRUNEISEN) as a constitutive equation to provide a mathematical relationship between state functions of the fluid (such as pressure, volume, and internal energy) along with hourglass controls (*HOURGLASS) to maintain mesh stability.

Void Space – Void space was included in the numerical model to extend the model space above the still water elevation so that the storm surge waves would remain within the model boundary. The void space was modeled as 'vacuum' material (*MAT_140), which is a 'dummy' material representing a vacuum in a multi material Euler/ALE model. Void space was used instead of 'air' in order to simplify the numerical computations and this approximation has very little impact on the calculated values as the interaction between air and the water has minimal damping effects on the incident wave shape and form.

Wave Generator/Water Source – Waves were generated from water elements with a time-dependent velocity profile. The fluid was modeled as 'generic' material (*MAT_009) allowing equations of state to be considered without computing deviatoric stresses. The water was assigned a mass density of 1.99 slugs/ft^3 (Munson et al, 1998), a pressure cutoff of -1.0E+11 psf i.e. no pressure cutoff), and a dynamic viscosity coefficient of 2.5E-5 (Munson et al, 1998). Equations of state were used (*EOS_GRUNEISEN) as a constitutive equation to provide a mathematical relationship between state functions of the fluid (such as pressure, volume, and internal energy). The boundary is a prescribed-velocity boundary.

Wave Generation

Waves were generated by specifying a velocity profile for the model nodes located within the 'wave generator' part. The velocity profile has a time-dependent 'circular' shape to it that simulates the circular orbits of the water particles (Figure 52).

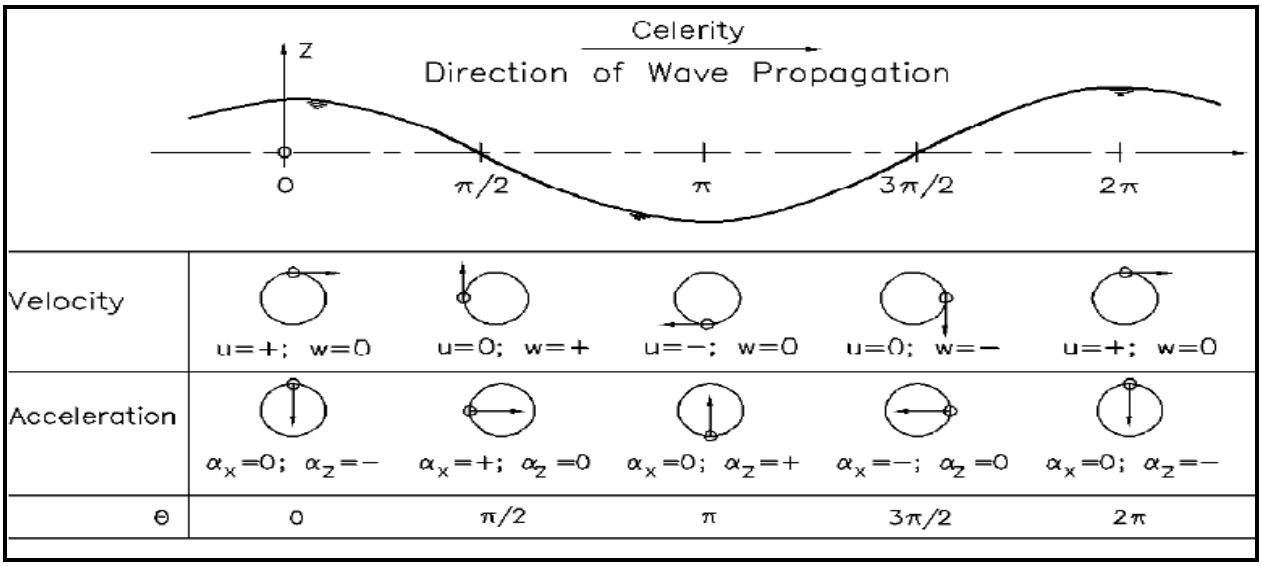


Figure 52**:** An overview of the water velocity field and relative water displacement as a function of time (USACE, 2006b).

The velocity profile (Figure 53) was described within LSDYNA by equations 1 and 2 (below), using the parameters v and ω, where v is the velocity parameter (used to generate the correct wave height) and ω is the circular rate frequency (where the wave Period (T)=2 π/ω), was used to develop the period of the wave. The overtopping rate equivalent velocity (overtopping_velocity) was used to maintain the specified still water elevation for conditions where overtopping of the EBSB occurred.

The wave generation equations are listed below:

Horizontal Velocity: v*sin(ω*time)+overtopping_velocity [Eq 1]

Vertical Velocity: v*cos(ω*time) [Eq 2]

Equation parameters used for the evaluated Scenario 1 time intervals are summarized in Table 6 and equation parameters for Scenario 2C simulations are presented in Table 7.

Table 6: Wave Generation Parameters for Scenario 1 (Actual MR-GO Conditions)

Time (CDT)	**Storm Surge Elevation (ft)**	**Wave Height Parameter (v)**	**Wave Period Parameter (ω)**	**Overtopping_ Velocity**
0430	10.1	1.531	1.57	0.0
0530	12.0	2.070	1.35	0.0
0630	14.2	1.960	1.25	0.0
0730	16.6	2.648	1.16	0.2
0830	16.1	2.311	1.21	0.2

Table 7: Wave Generation Parameters for Scenario 2C (Neutral MR-GO)

Time (CDT)	**Storm Surge Elevation (ft)**	**Wave Height Parameter (v)**	**Wave Period Parameter (ω)**	**Overtopping_ Velocity**
0430	9.9	0.318	2.33	0.0
0530	11.8	0.530	2.03	0.0
0630	14.0	0.800	1.85	0.0
0730	16.2	1.531	1.80	0.1
0830	16.0	1.185	1.85	0.1

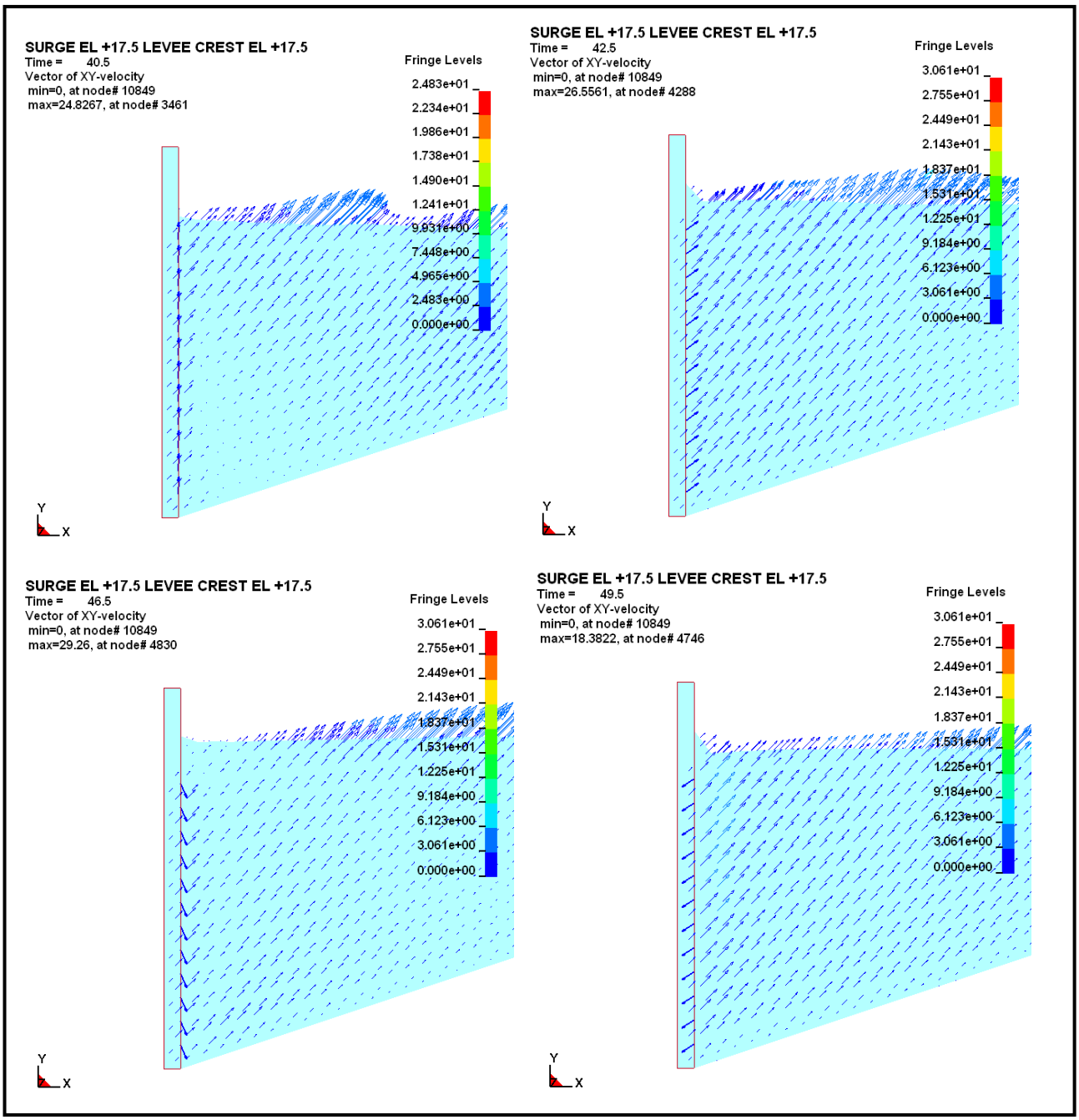


Figure 53: An example view of the changing velocity field resulting in waves with the specified characteristics.

The generated waves were checked by visual inspection to ensure conformance with the target characteristics through an evaluation of the wave heights over time (the specified period of the wave) at a specified node.

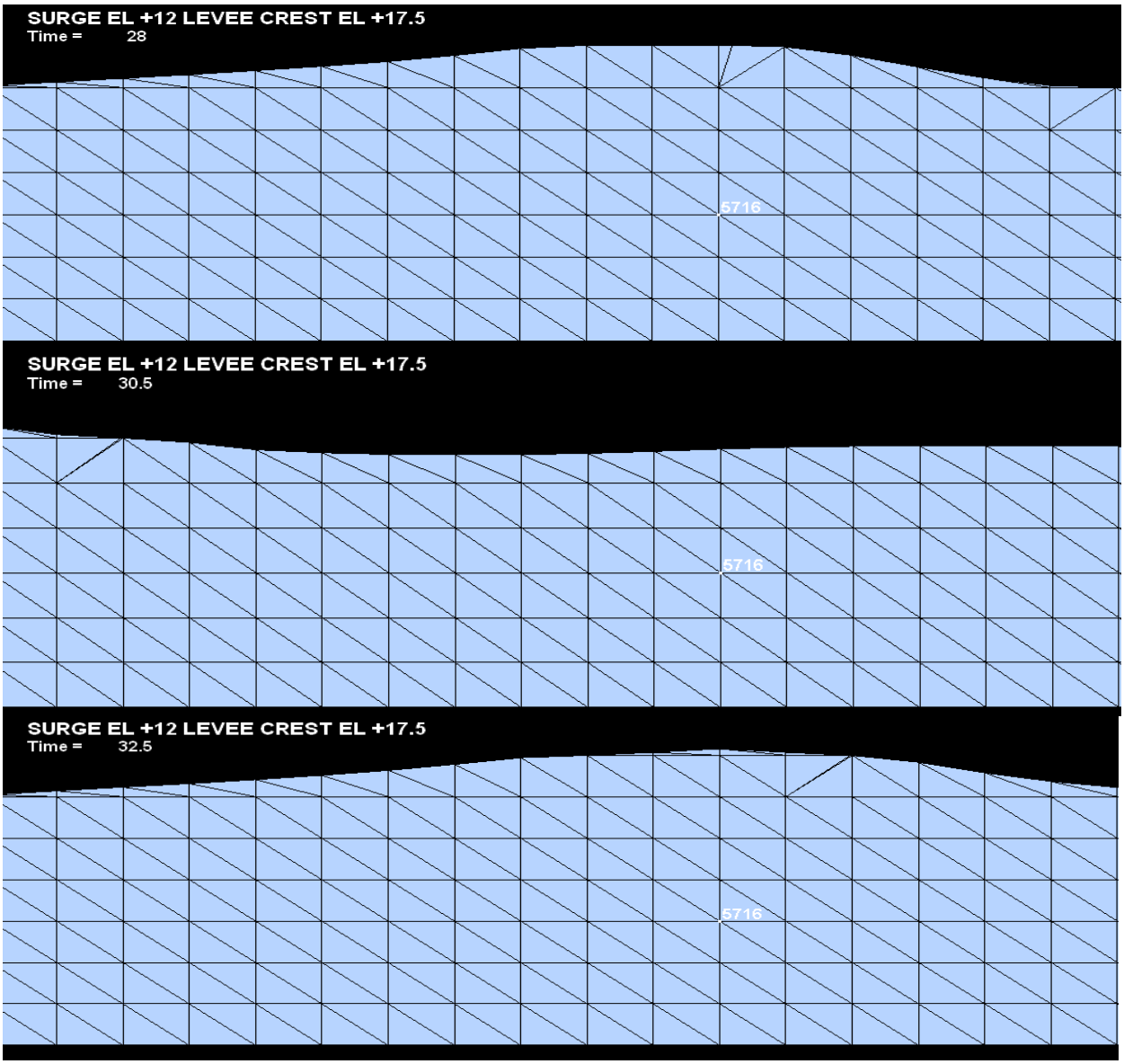


Figure 54**:** An example view of the monitoring node to validate the characteristics of the simulated waves.

Figure 54 presents an example of the method used to validate wave characteristics. At this monitoring node (node 5716), the starting time was 28 seconds with a water 'height' of 5.3 feet (each 'node' has a 1.312-foot spacing in this mesh). The 'low' water was observed at 30.5 seconds with a water 'height of 3.6 feet. Another wave peak was observed at 32.5 seconds with a water 'height' of 5.3 feet. This visual inspection process yields a significant wave height of 1.7 feet (5.3 feet – 3.6 feet) with a period of 4.5 seconds (32.5 seconds – 28 seconds).

The difference between the elevation at the wave minimum and maximum heights was used to validate the significant wave height and the difference in the time between the occurrence of the wave peak and trough was used to calculate the period of the wave for all simulation cases. These values were then compared against the wave characteristics, significant wave height and wave period defined by Gautier et al (2008a, 2008b). The relative error between the simulated DYNA waves and the specified Gautier et al (2008a, 2008b) waves is presented in Table 8 (Scenario 1) and Table 9 (Scenario 2C). In general, there was very close (less than 15% error) agreement between the modeled and specified wave (note that relative error for wave period is presented in "()"). Relative error was calculated as:

$$\text{Percent Error} = (H_s - H_{DYNA}/H_{DYNA})x100\% \quad \text{[Eq 3]}$$

Table 8: Error Determination of DYNA Generated Waves for Scenario 1 Hydrodynamics

Time (CDT)	**Storm Surge Elevation (ft)**	**Significant Wave Height (ft)**	**Wave Period (s)**	**DYNA Wave Height (ft)**	**DYNA Wave Period (s)**	**Percent Error**
0430	10.1	2.0	4.0	2.1	4.0	5% (0%)
0530	12.0	2.7	4.5	2.9	4.5	7% (0%)
0630	14.2	4.1	4.9	4.0	5.0	3% (2%)
0730	16.6	5.5	5.4	6.1	5.5	10% (2%)
0830	16.1	4.8	5.2	5.0	5.5	4% (5%)

Table 9: Error Determination of DYNA Generated Waves for Scenario 2C Hydrodynamics

Time (CDT)	Storm Surge Elevation (ft)	Significant Wave Height (ft)	Wave Period (s)	DYNA Wave Height (ft)	DYNA Wave Period (s)	Percent Error
0430	9.9	0.6	2.7	0.5	2.5	20% (8%)
0530	11.8	1.0	3.1	1.1	3.0	9% (3%)
0630	14.0	1.5	3.4	1.6	3.5	6% (3%)
0730	16.2	2.0	3.5	2.0	3.5	0% (0%)
0830	16.0	1.7	3.4	1.6	3.5	6% (3%)

Wave Breaking

The wave breaking type (Figure 55) anticipated to occur on the EBSB flood face was calculated (USACE, 2006c) and compared with the numerical simulation results from LSDYNA.

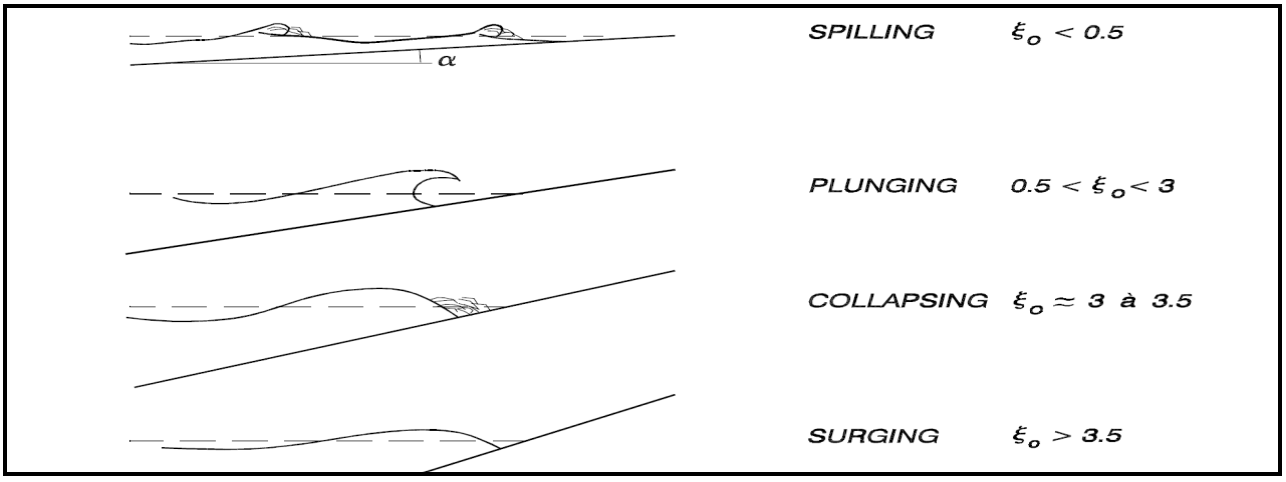


Figure 55: Wave breaking types and shapes as defined in the Coastal Engineering Manual (USACE, 2006c).

Table 10 presents a summary of the anticipated wave breaking types at Station 497+00 based on the storm surge elevation for Scenario 1 and Table 11 presents a summary of the anticipated wave breaking types for Scenario 2C.

Table 10: Wave Breaking Types for Scenario 1 Hydrodynamics (Actual MR-GO)

Time (CDT)	**Slope Angle (α)**	**Wave Height (H_0)**	**Wavelength (L_0)**	**Wave Period (T)**	**Breaker Parameter (ξ)**	**Breaking Type**
0430	16	2.0	82	4.0	1.8	Plunging
0530	16	2.7	104	4.5	1.8	Plunging
0630	16	4.1	123	4.9	1.6	Plunging
0730	16	5.5	149	5.4	1.5	Plunging
0830	16	4.8	138	5.2	1.5	Plunging

Table 11: Wave Breaking Types for Scenario 2C Hydrodynamics (Perfect MR-GO)

Time (CDT)	**Slope Angle (α)**	**Wave Height (H_0)**	**Wavelength (L_0)**	**Wave Period (T)**	**Breaker Parameter (ξ)**	**Breaking Type**
0430	16	0.6	37	2.7	2.3	Plunging
0530	16	1.0	49	3.1	2.0	Plunging
0630	16	1.5	59	3.4	1.8	Plunging
0730	16	2.0	63	3.5	1.6	Plunging
0800	16	2.2	63	3.5	1.5	Plunging
0830	16	1.7	59	3.4	1.7	Plunging

The observed results from LSDYNA were in close agreement with these calculated wave breaking types.

Determination of Interaction Shear Velocities

Velocities were determined by tracking the velocity profiles at selected nodes using the *DATABASE_HISTORY_NODE option (nodout) for the actual (Figure 56) EBSB geometry. This option generates an ASCII database output with a time-history summary of velocity components and resultants for the selected nodes. The location of the velocity corresponds to the location of the node.

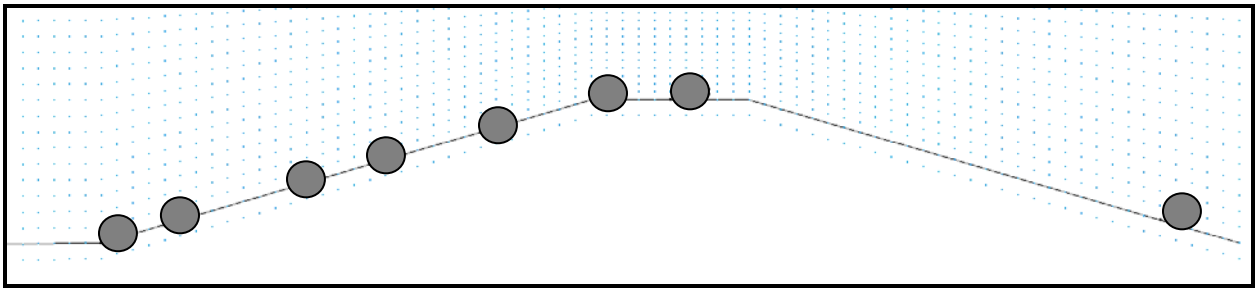


Figure 56: An overview of 'monitoring' nodes used to calculate shear velocities for the actual EBSB configuration.

IX. VELOCITY SIMULATION RESULTS

The imposed interaction shear velocities calculated by the LSDYNA numerical simulation were compared against the erosion/scour soil limits (capacity) as estimated based on the Erodibility Function Apparatus and EBSB soil composition. Soil samples collected from the ESBSs south of Bayou Bievenue and north of Bayou Dupre were found to generally be Very High and High Erodibility materials (hydraulic fill derived from the MR-GO navigation channel excavations).

The analyses were oriented to determining the likelihood of EBSB breaching due primarily to wave impact prior to EBSB overtopping. As a result, the analysis time frame was limited to the time before the storm surge overtopped the EBSB. Once overtopping occurred, the high-erodibility materials would have been extremely susceptible to erosion due to the high velocities and low material erosion resistance.

A discussion of the simulated shear velocities for the evaluated Scenario 1 (Hurricane Katrina 'as was' Conditions) and Scenario 2C ('Neutral' MR-GO Hurricane Katrina Conditions) cases is presented below at each of the simulation time steps (0430 CDT, 0530 CDT, 0630 CDT, 0730 CDT, and 0830 CDT).

Analysis for Scenario 1 (0430 CDT)

Scenario 1 at 0430 CDT (Figure 57) consisted of an EBSB crest Elevation of +16 feet (NAVD88) and hydrodynamics consisting of a storm surge Elevation of +10.1 feet (NAVD88), a wave period of 4.0 seconds and a significant wave height of 2.0 feet. There was no overtopping.

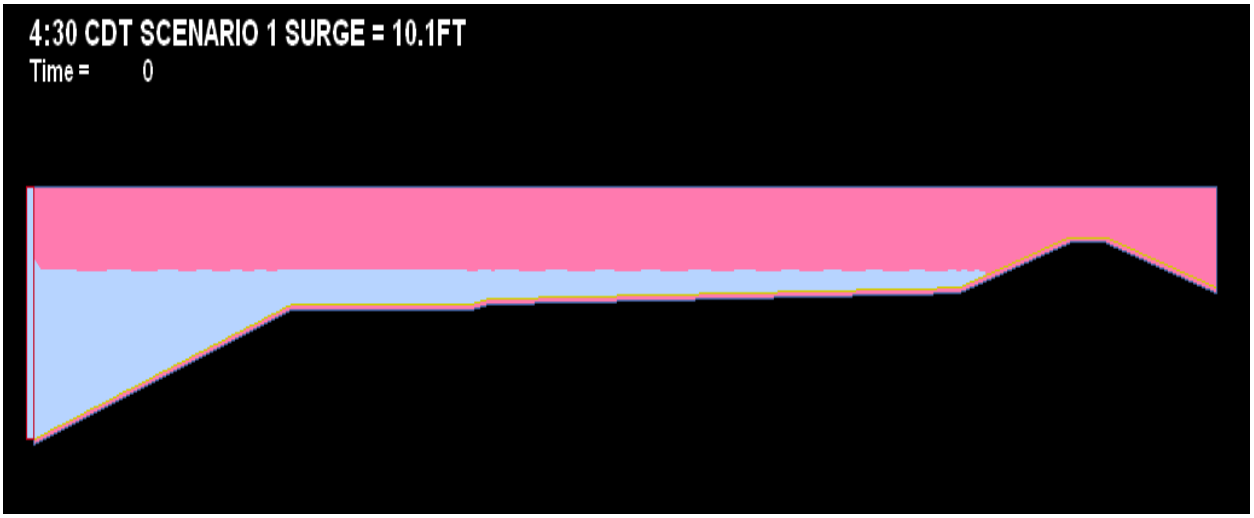


Figure 57: Initial conditions for Scenario 1 at 0430 CDT.

At Elevation +10.1 feet (NAVD88), the storm surge reached the flood side toe of the EBSB. A plot of the shear velocities is presented in Figure 58. The peak shear velocity at the storm surge elevation was determined to be 10 ft/s.

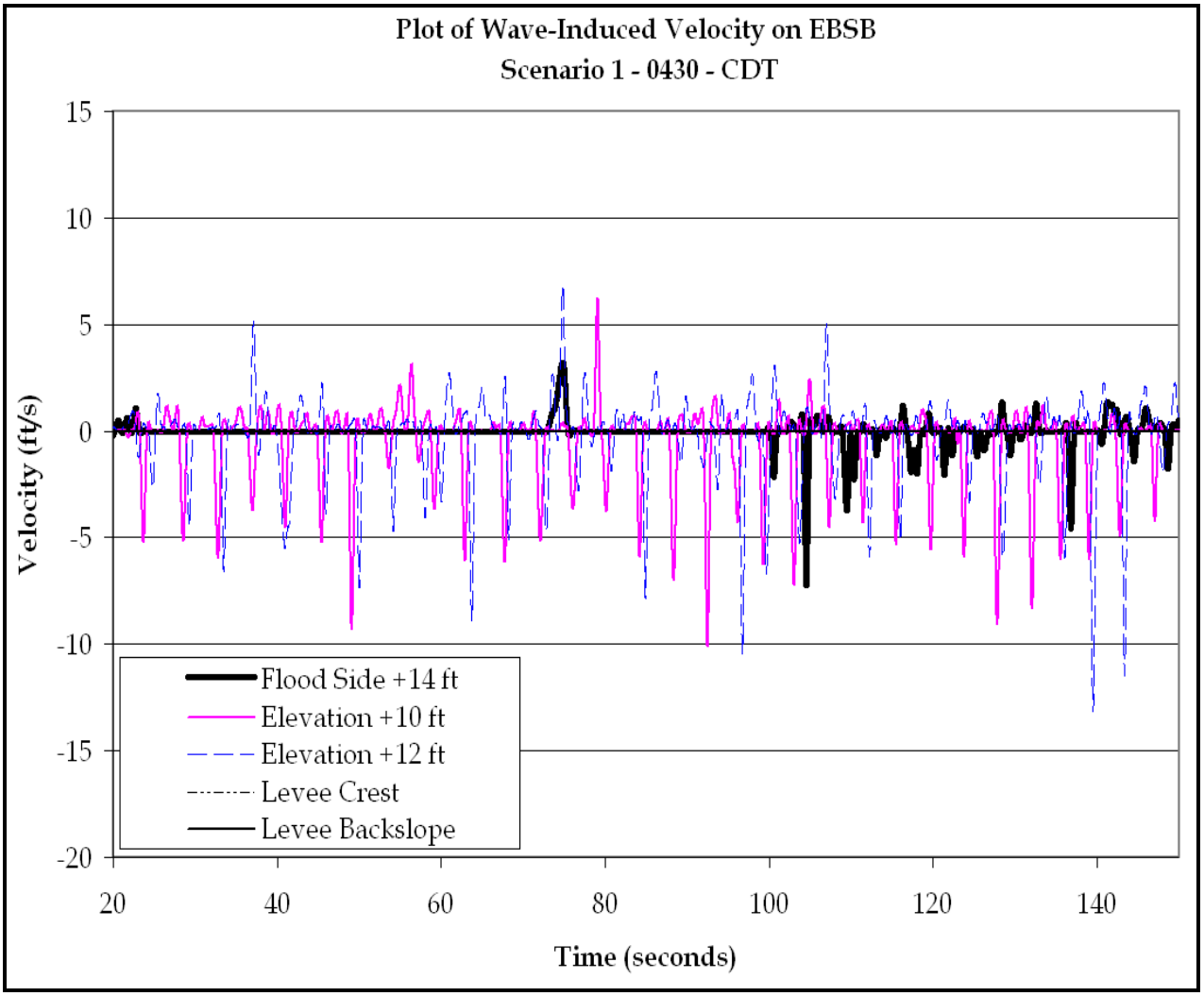


Figure 58**:** A plot of the velocity time history on the flood side face of the EBSB with the storm surge at 0430 CDT.

Figure 59 (below) provides a graphical representation of water movement over time. With the hurricane storm surge at El. +10.1 feet (NAVD88), the actual geometric configuration of the EBSB induces a tendency for the waves to exhibit a primarily 'runup' and 'rundown' behavior.

Storm Surge Elevation: +10.1 feet Crest Elevation: +16 feet

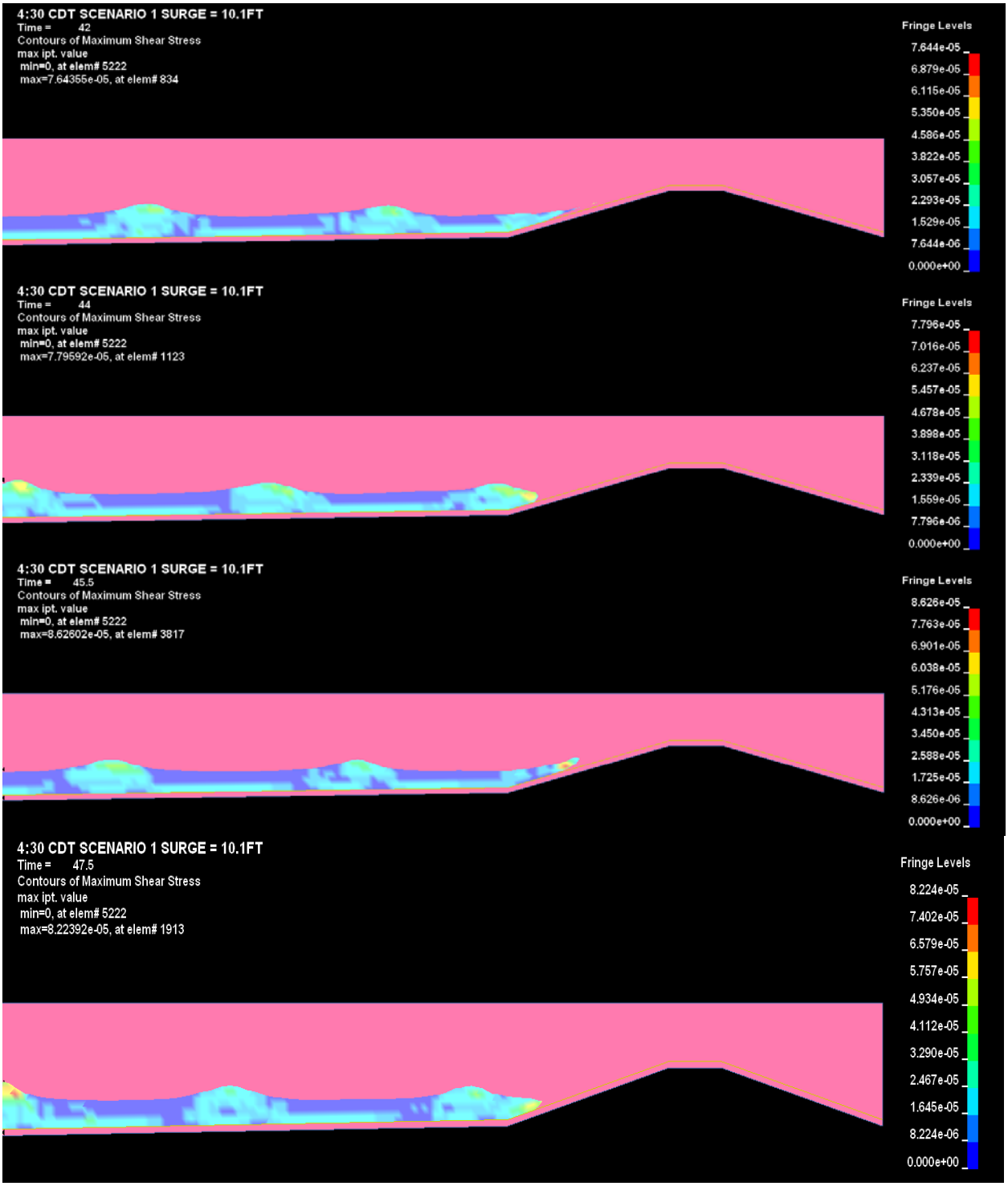


Figure 59**:** With the hurricane storm surge at El. +10.1 feet (NAVD88), the actual geometric configuration of the EBSB induces a tendency for the waves to exhibit a primarily 'runup' and 'rundown' behavior (fringe level units in psf).

Analysis for Scenario 1 (0530 CDT)

Scenario 1 at 0530 CDT (Figure 60) consisted of a crest Elevation of +16 feet (NAVD88) and hydrodynamics consisting of a storm surge Elevation of +12.0 feet (NAVD88), a wave period of 4.5 seconds, and a significant wave height of 2.7 feet. There was no overtopping.

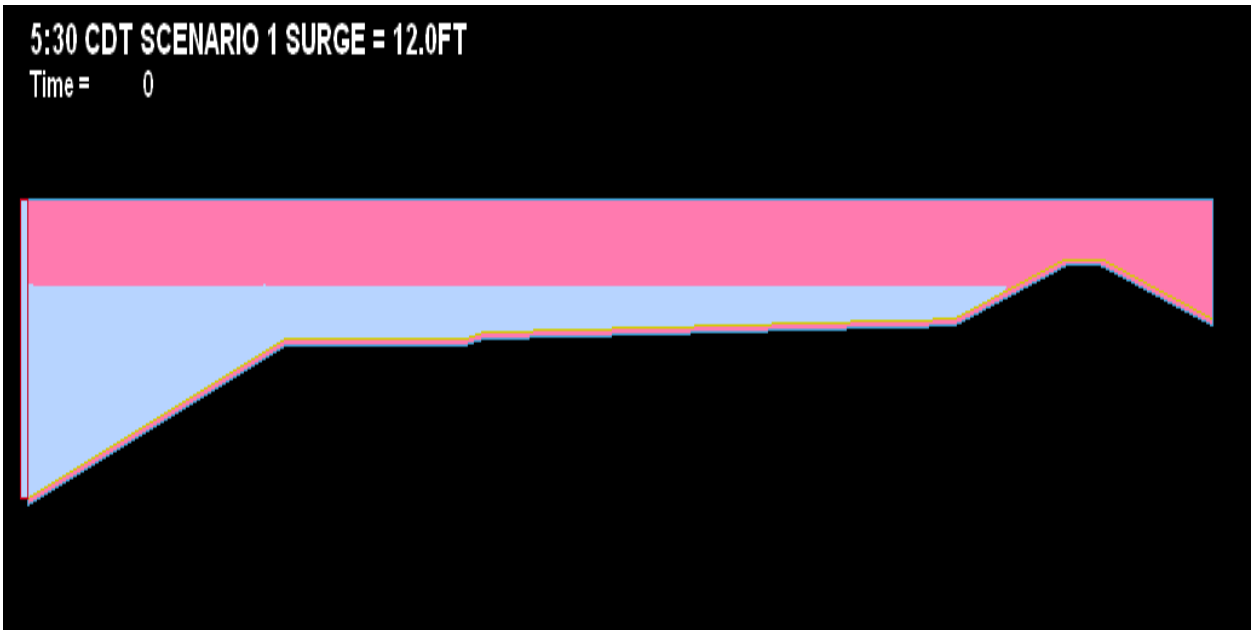


Figure 60: Initial conditions for Scenario 1 at 0530 CDT.

At Elevation +12.0 feet (NAVD88), the storm surge had reached the main EBSB 1 on 3.5 flood side slope. A plot of shear velocities is presented in Figure 61. The peak velocity was determined to be 12 ft/s.

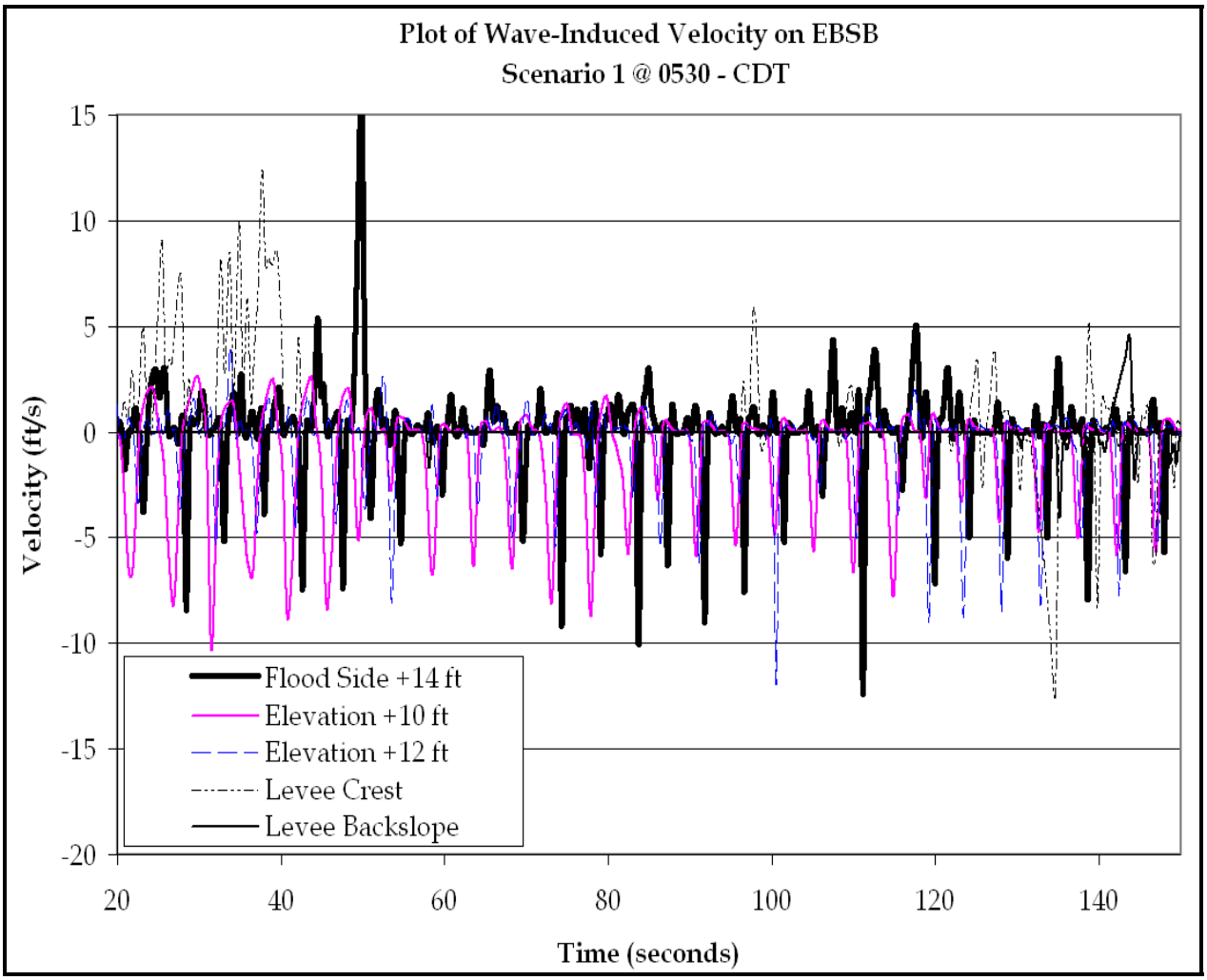


Figure 61: Time history plot of shear velocities for the storm surge at 0530 CDT.

Figure 62 (below) provides a graphical representation of water movement over time. With the hurricane storm surge at El. +12.0 feet (NAVD88), the geometric configuration of the EBSB induces a tendency for the waves to exhibit a primarily 'runup' and 'rundown' behavior, with moderate to major wave impacts as well as wave-induced overtopping.

Storm Surge Elevation: +12.0 feet Crest Elevation: +16 feet

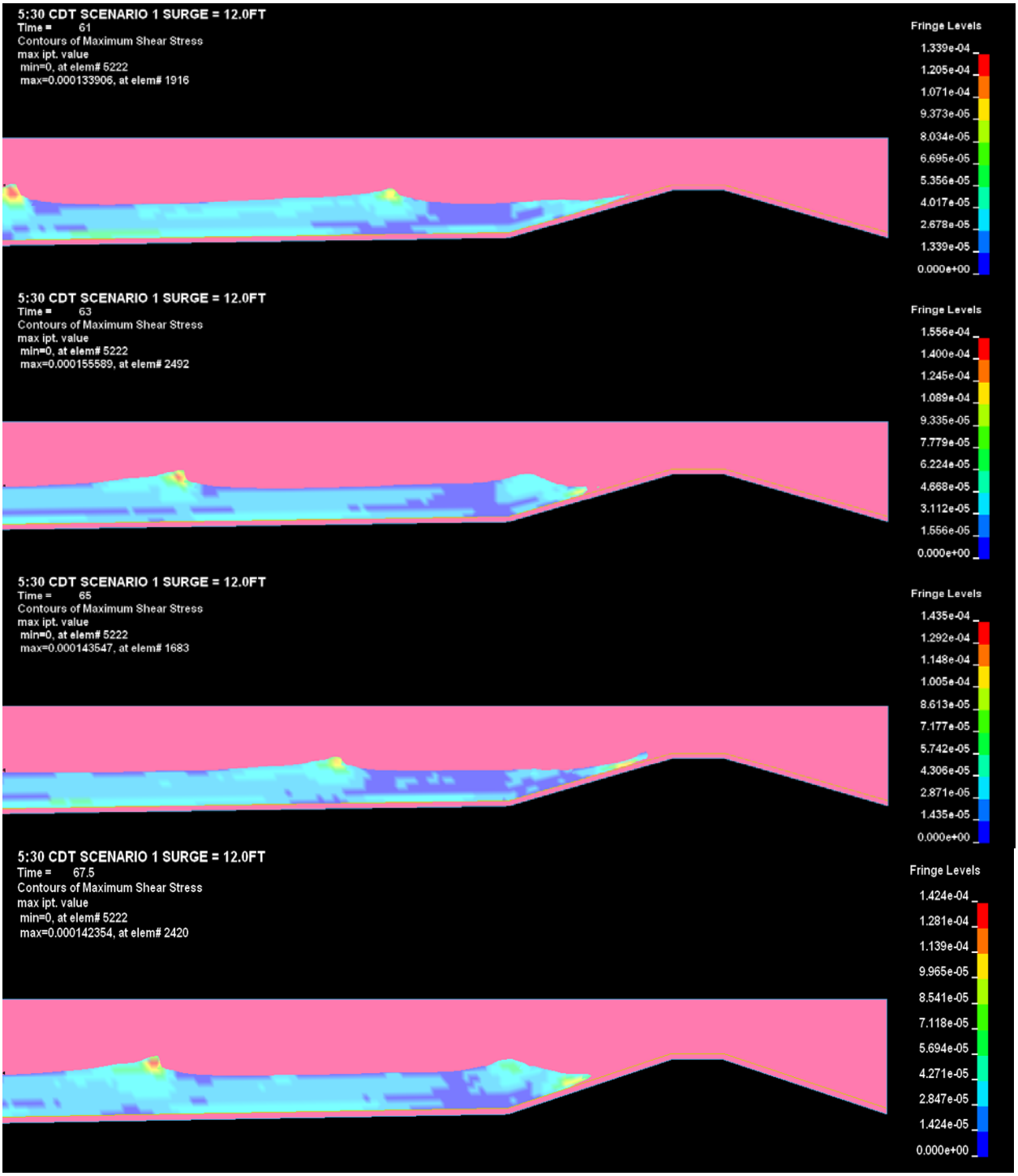


Figure 62**:** With the hurricane storm surge at El. +12.0 feet (NAVD88), the actual geometric configuration of the EBSB induces a tendency for the waves to exhibit a primarily 'runup' and 'rundown' behavior with moderate to major wave impacts (fringe level units in psf).

Analysis for Scenario 1 (0630 CDT)

Scenario 1 at 0630 CDT (Figure 63) consisted of a crest Elevation of +16 feet (NAVD88) and hydrodynamics consisting of a storm surge Elevation of +14.2 feet (NAVD88), a wave period of 4.9 seconds, and a significant wave height of 4.1 feet. There was limited overtopping.

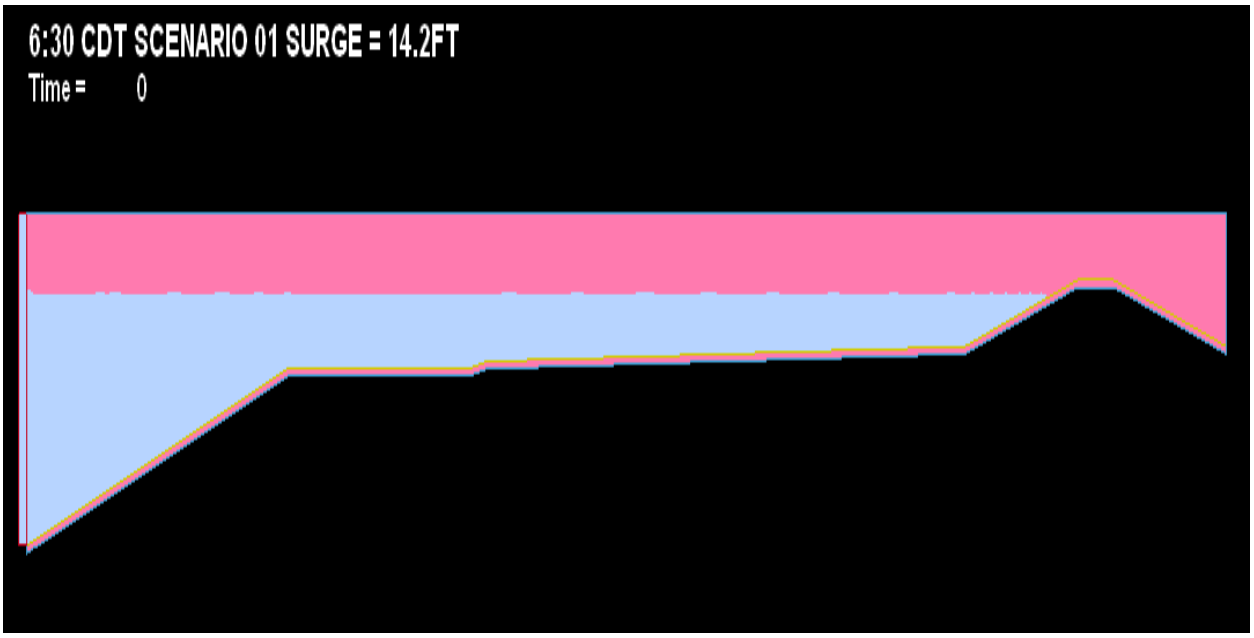


Figure 63**:** Initial conditions for Scenario 1 at 0630 CDT.

At Elevation +14.2 feet (NAVD88), the storm surge was nearing the crest of the EBSB and limited (wave-induced) overtopping was occurring. A plot of shear velocities is presented in Figure 64. The peak velocity was determined to be 15 ft/s.

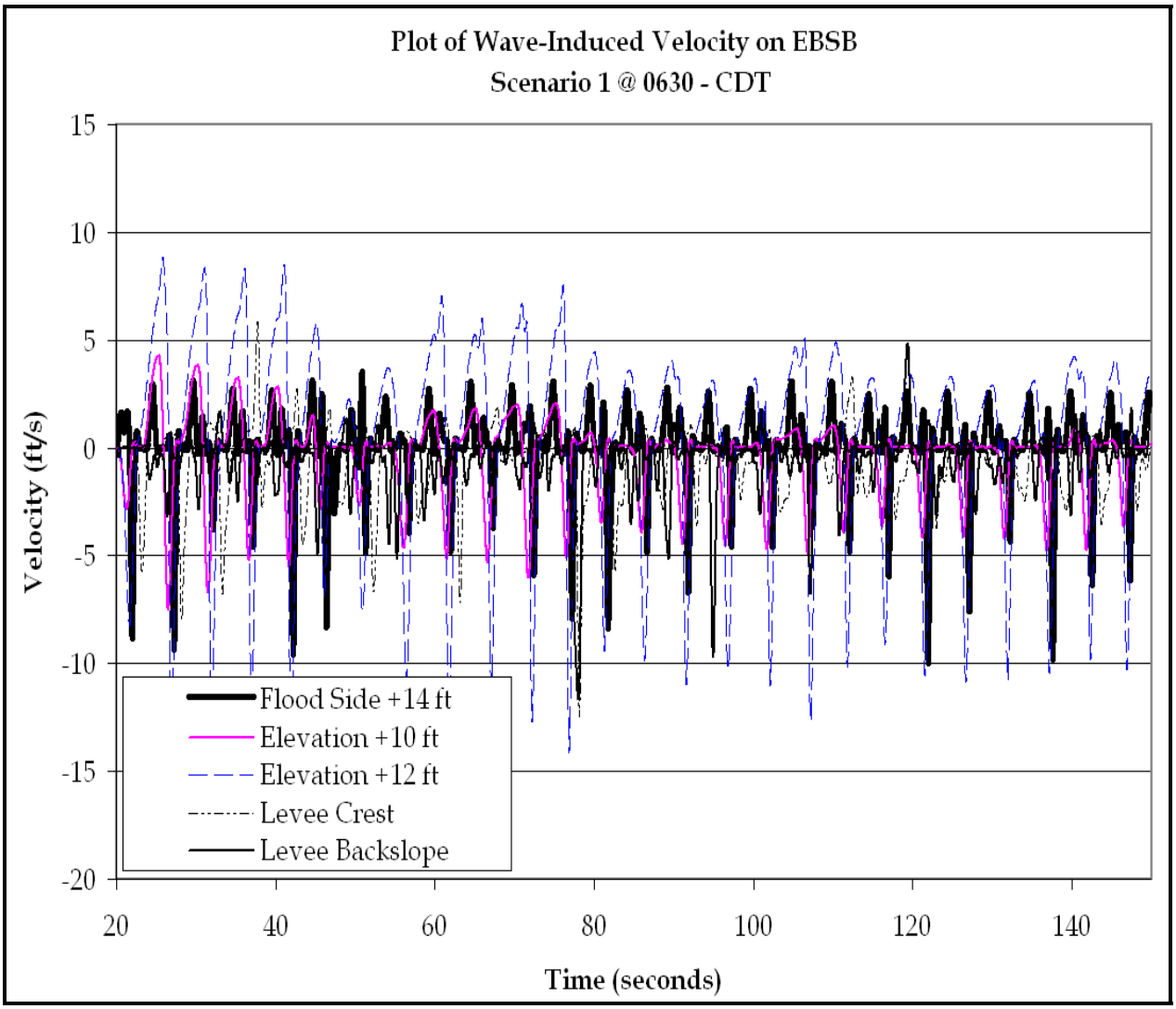


Figure 64: Time history plot of shear velocities for the storm surge at 0630 CDT.

Figure 65 (below) provides a graphical representation of water movement over time. With the hurricane storm surge at El. +14.2 feet (NAVD88), the geometric configuration of the EBSB appears to not promote direct wave impacts, but rather induces a tendency for the waves to 'spill over' the top of the EBSB, contributing significantly to run-up and run-down erosion with overtopping.

Storm Surge Elevation: +14.2 feet Crest Elevation: +16 feet

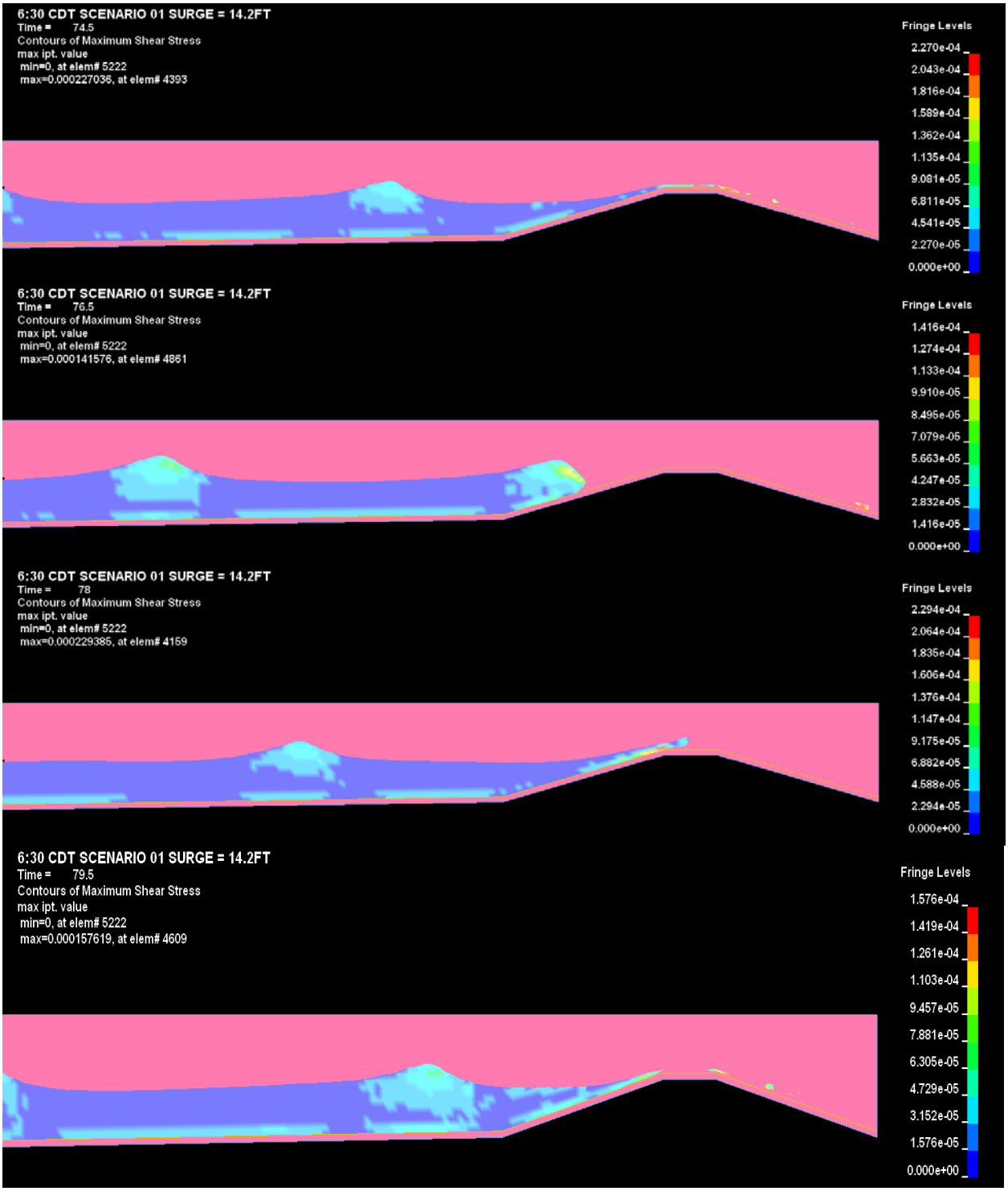


Figure 65**:** With the hurricane storm surge at El. +14.2 feet (NAVD88), waves induce predominantly run-up and run-down erosion with some overtopping (fringe level units in psf).

Analysis for Scenario 1 (0730 CDT)

Scenario 1 at 0730 CDT (Figure 66) consisted of a crest Elevation of +16 feet (NAVD88) and hydrodynamics consisting of a storm surge Elevation of +16.6 feet (NAVD88), a wave period of 5.4 seconds, and a significant wave height of 5.5 feet. There was active overtopping.

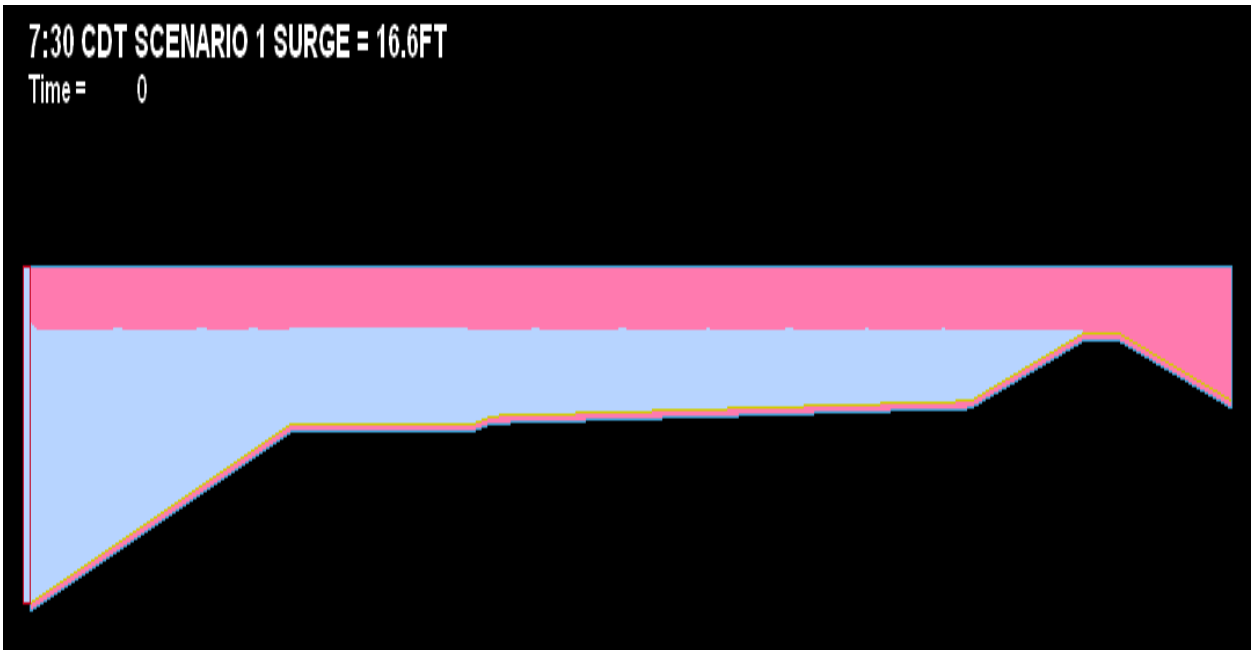


Figure 66: Initial conditions for Scenario 1 at 0730 CDT.

At Elevation +16.6 feet (NAVD88), the storm surge had reached the crest of the EBSB. A plot of the shear velocities is presented in Figure 67. The peak shear velocity was determined to be 14 ft/s. At this storm surge elevation and wave action results in active overtopping of the levee.

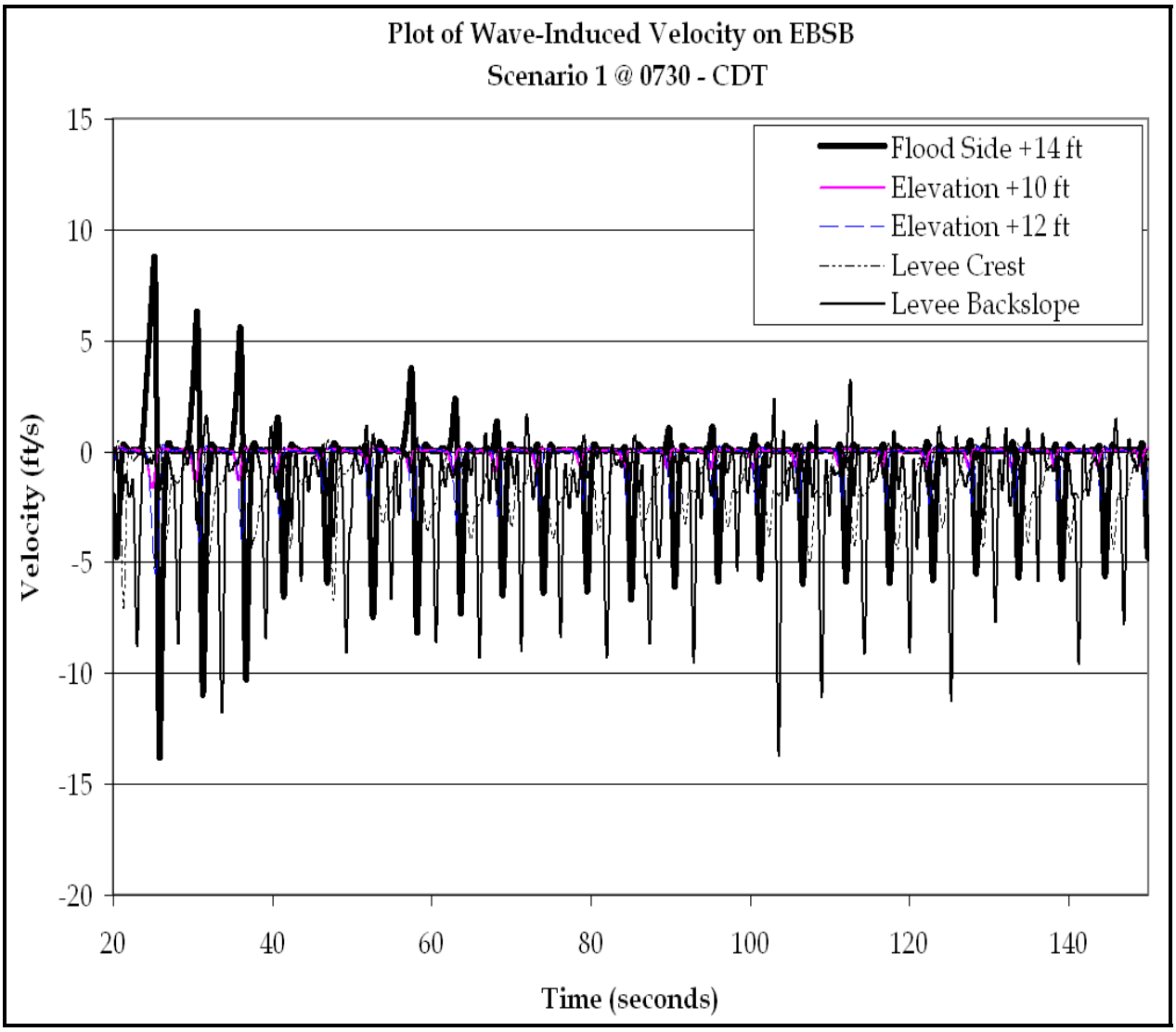


Figure 67: Time history plot of shear velocities for the storm surge at 0730 CDT.

Figure 68 (below) provides a graphical representation of water movement over time. With the hurricane storm surge at El. +16.6 feet (NAVD88), the geometric configuration of the EBSB induces a tendency for the waves to exhibit a primarily overtopping behavior, with moderate wave impacts.

Storm Surge Elevation: +16.6 feet Crest Elevation: +16 feet

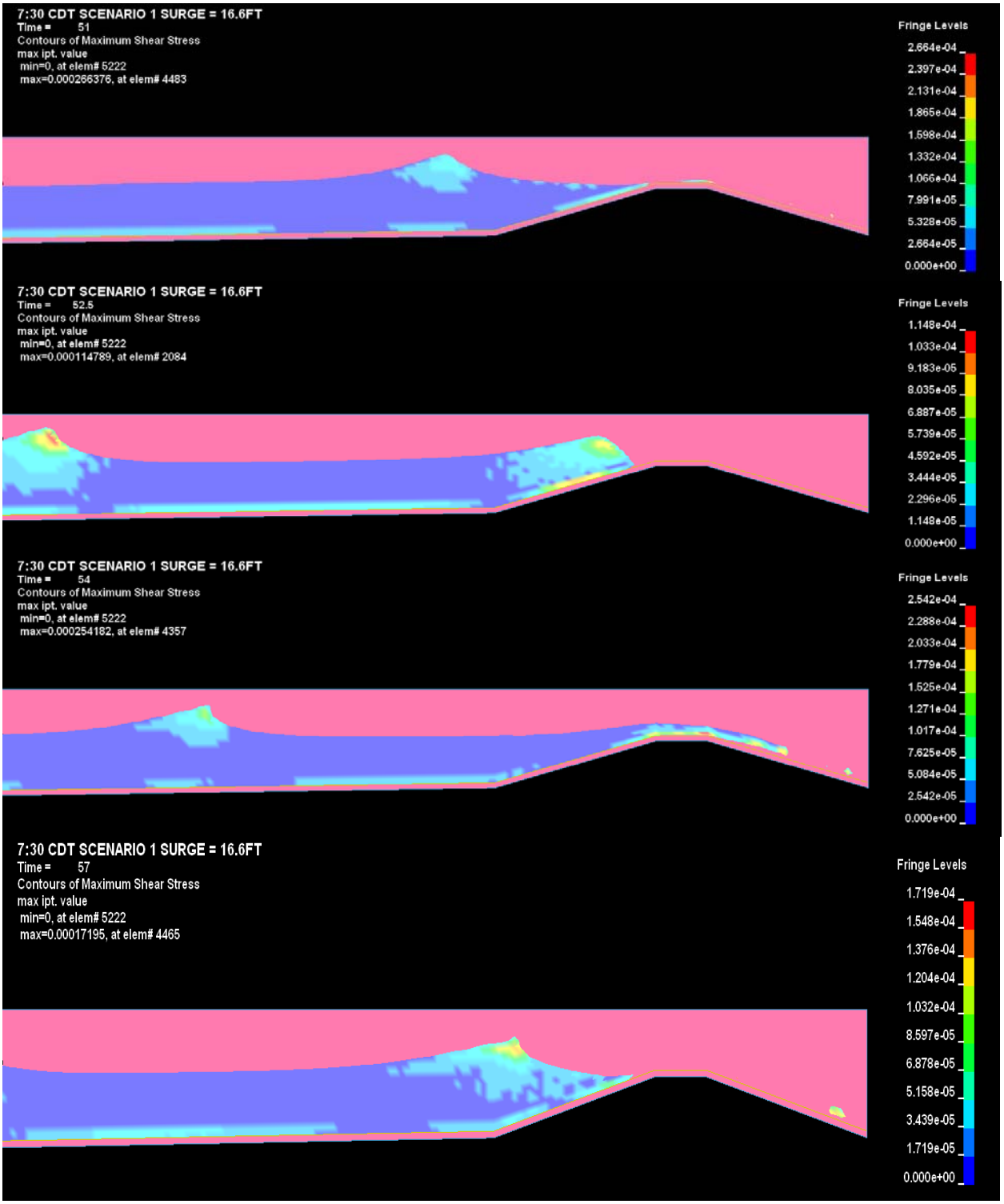


Figure 68**:** With the hurricane storm surge at El. +16.6 feet (NAVD88), the waves to exhibit a primarily overtopping condition with negligible wave impacts (fringe level units in psf).

Analysis for Scenario 1 (0830 CDT)

Scenario 1 at 0830 CDT (Figure 69) consisted of a crest Elevation of +16 feet (NAVD88) and hydrodynamics consisting of a storm surge Elevation of +16.1 feet (NAVD88), a wave period of 5.2 seconds, and a significant wave height of 4.8 feet. There was wave-induced overtopping.

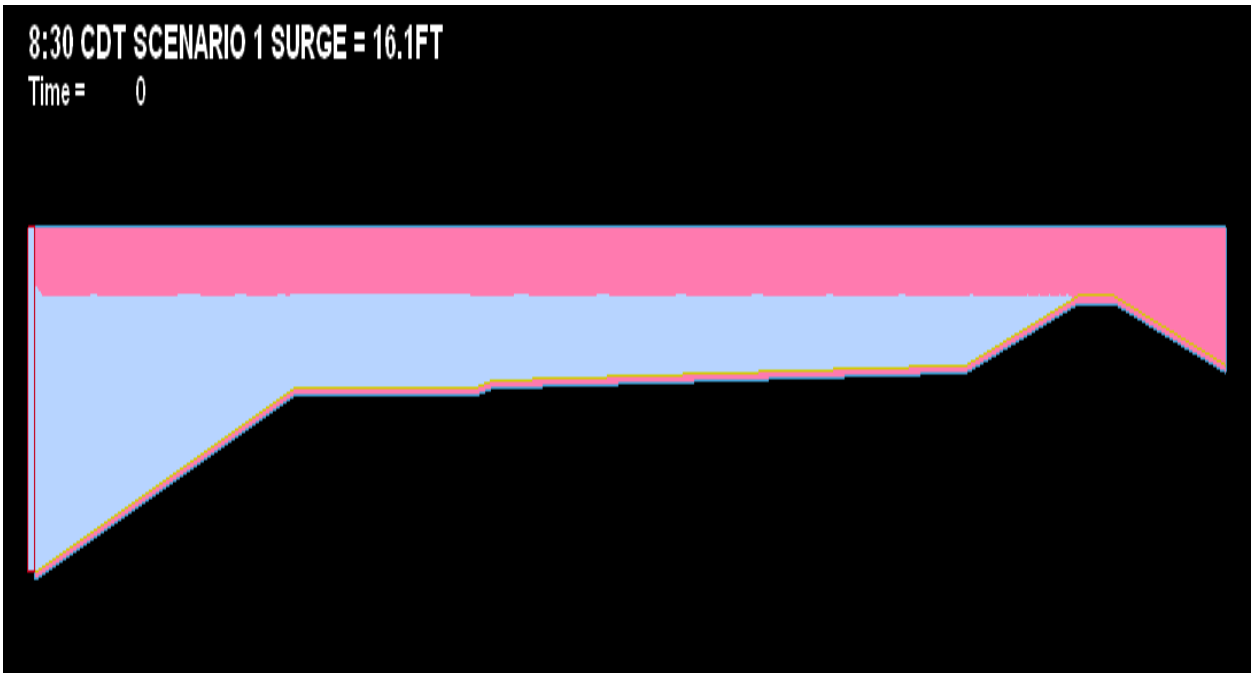


Figure 69: Initial conditions for Scenario 1 at 0830 CDT.

A plot of shear velocities is presented in Figure 70. The peak velocity was determined to be 14 ft/s.

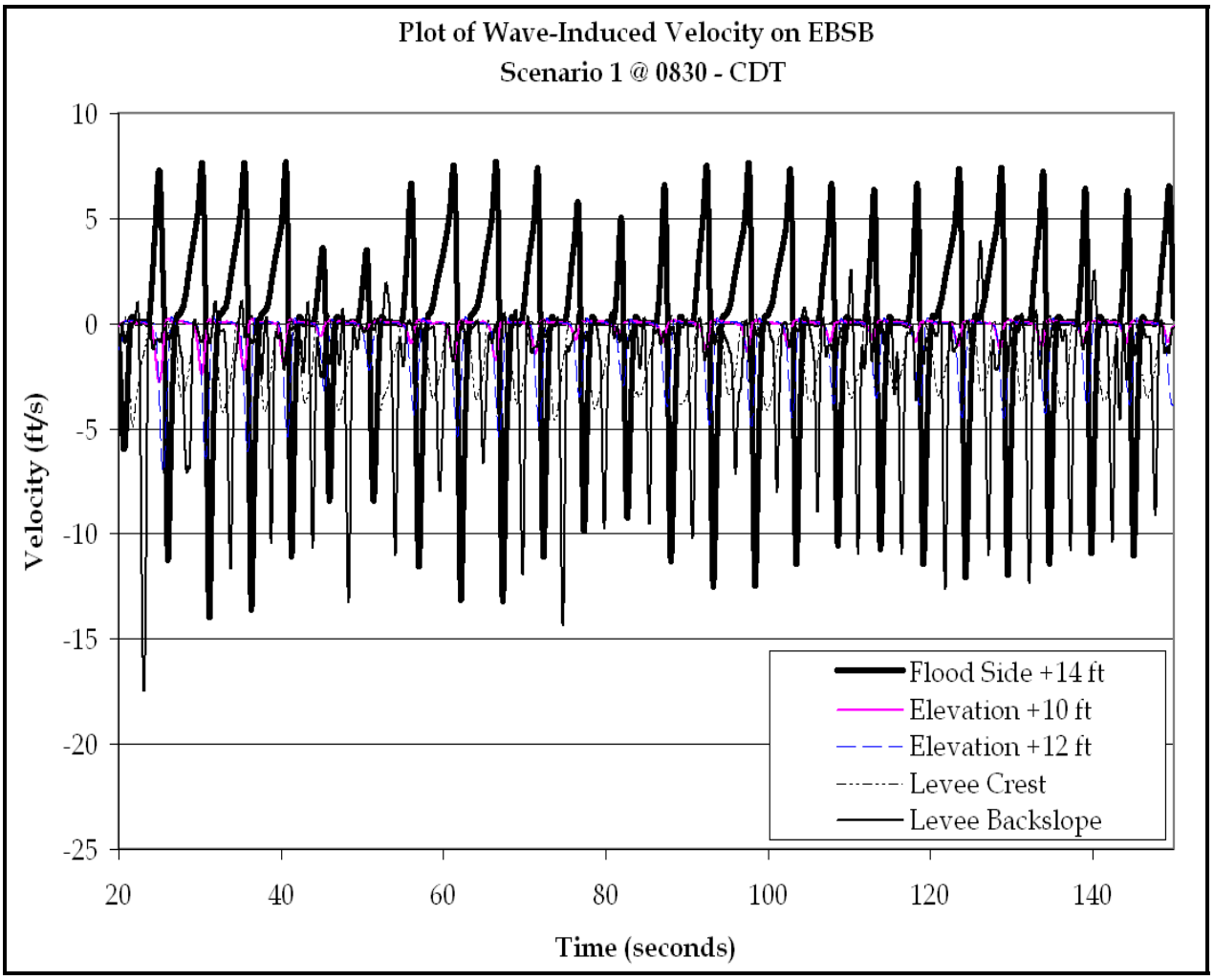


Figure 70: Time history plot of shear velocities for the storm surge at 0830 CDT.

Figure 71 (below) provides a graphical representation of water movement over time. With the hurricane storm surge at El. +16.1 feet (NAVD88), the design geometric configuration of the EBSB induces a tendency for the waves to exhibit a primarily overtopping behavior, with minor wave impacts.

Storm Surge Elevation: +16.1 feet Crest Elevation: +16 feet

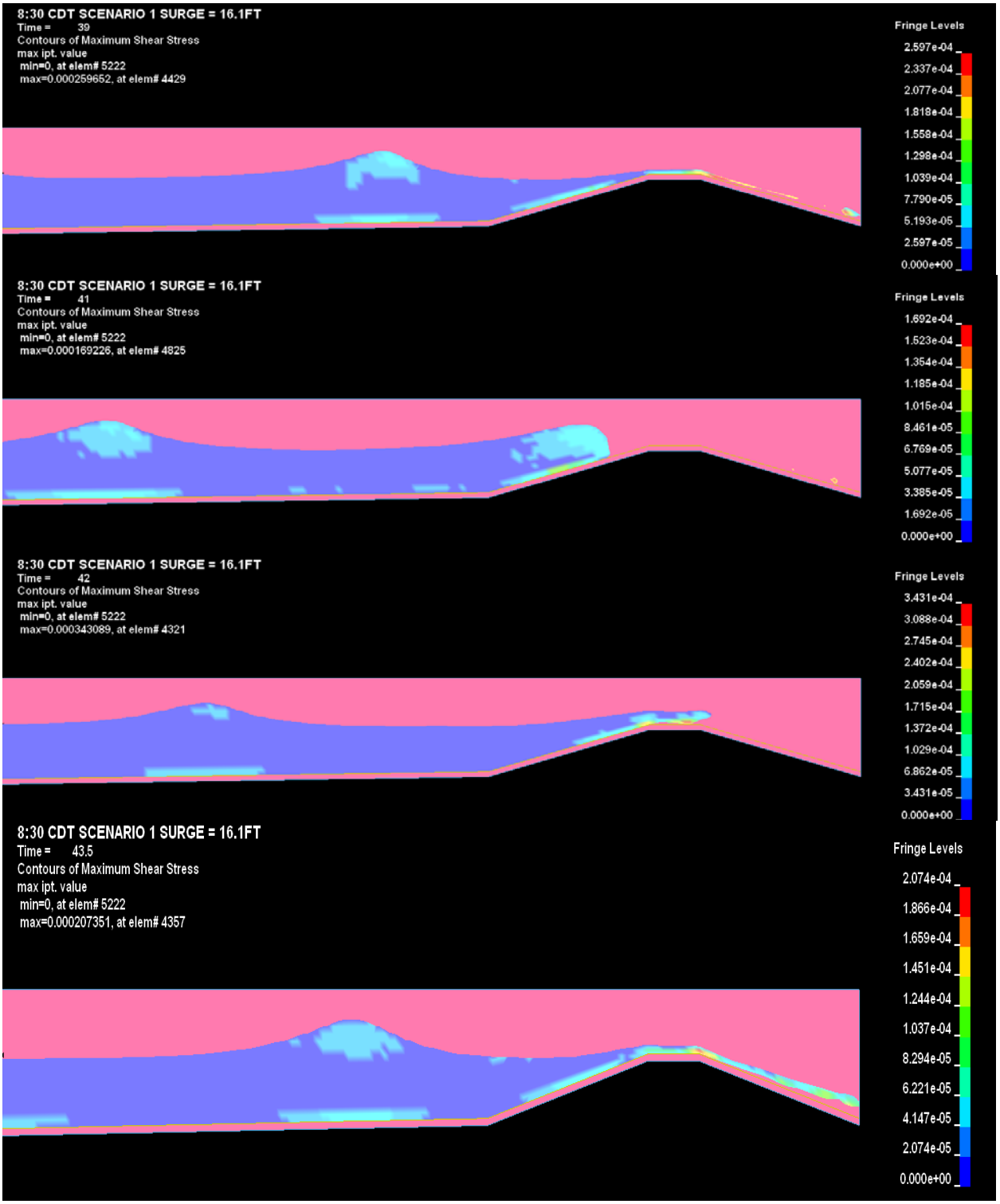


Figure 71**:** With the hurricane storm surge at El. +16.1 feet (NAVD88), the design geometric configuration of the EBSB induces a tendency for the waves to exhibit a primarily an overtopping behavior with minor wave impacts (fringe level units are psf).

Analysis for Scenario 2C (0430 CDT)

Scenario 2C – the 'Neutral' MR-GO Hurricane Katrina Conditions - at 0430 CDT (Figure 72) consisted of a crest Elevation of +16 feet (NAVD88) and hydrodynamics consisting of a storm surge elevation of +9.9 feet, a wave period of 2.7 seconds, and a significant wave height of 0.6 feet. There was no overtopping.

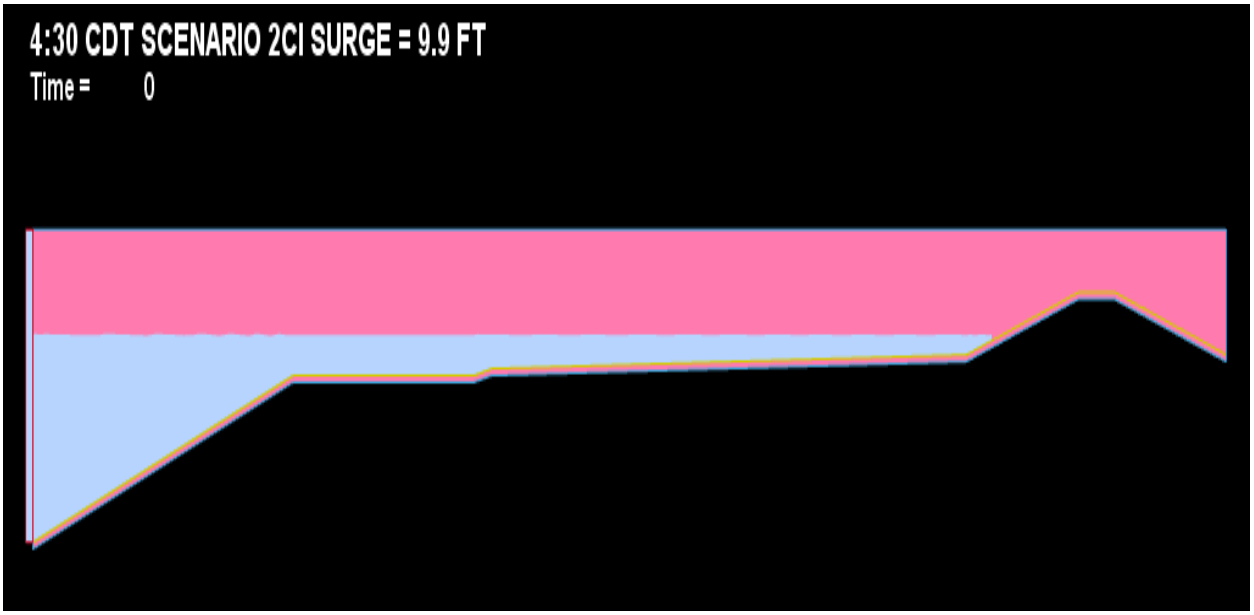


Figure 72: Initial conditions for Scenario 2C at 0430 CDT.

At Elevation +9.9 feet (NAVD88), the storm surge reached the flood side toe of the EBSB. A plot of shear velocities is presented in Figure 73. The peak velocity at Elevation +10 feet (NAVD88) was determined to be 4 ft/s.

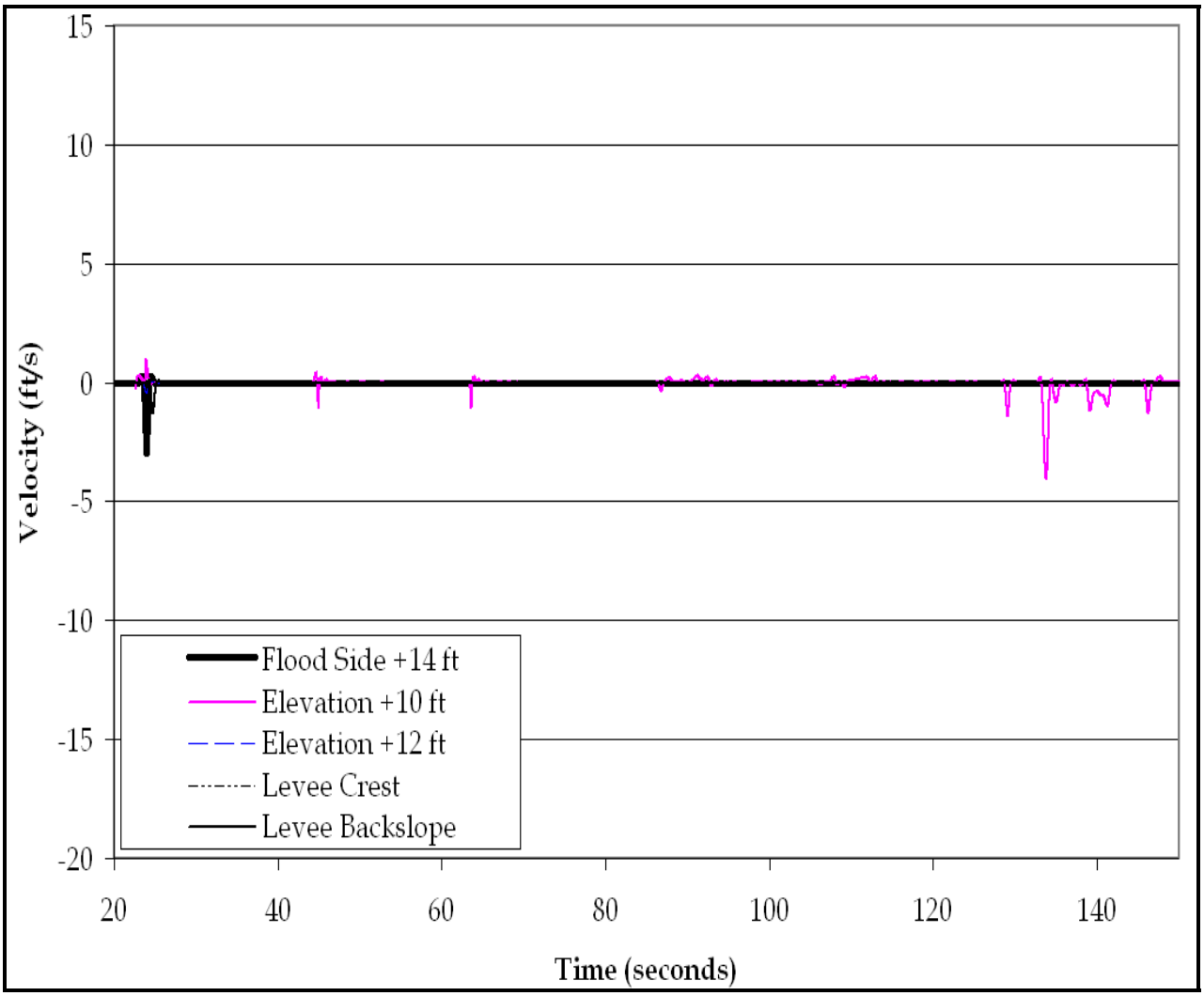


Figure 73**:** Time history plot of shear velocities for the storm surge at 0430 CDT.

Figure 74 (below) provides a graphical representation of water movement over time. With the hurricane storm surge at El. +9.9 feet (NAVD88), the geometric configuration of the EBSB appears to exhibit primarily 'runup' and 'rundown'erosion.

Storm Surge Elevation: +9.9 feet Crest Elevation: +16 feet

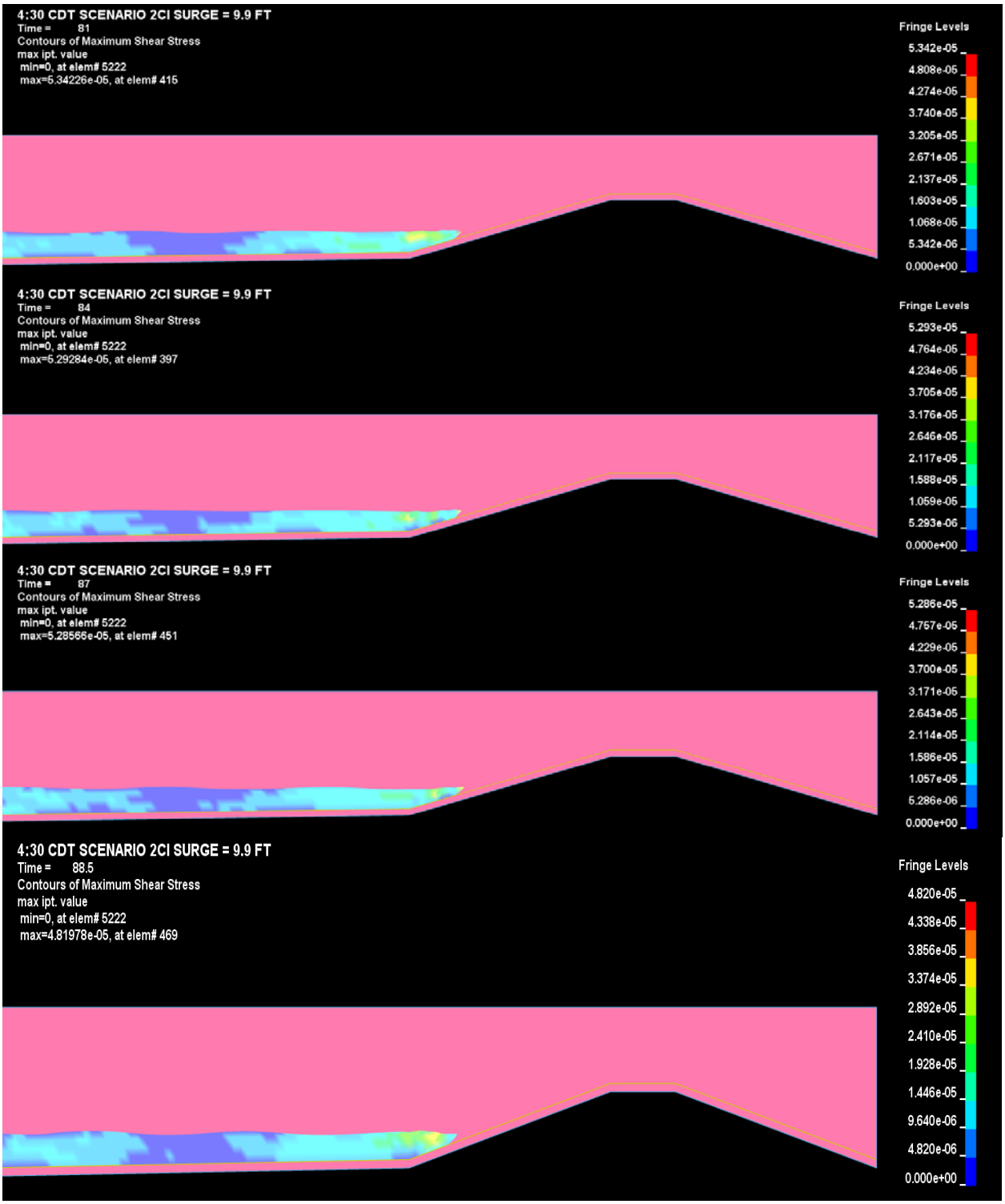


Figure 74**:** With the hurricane storm surge at El. +9.9 feet (NAVD88), waves predominantly 'runup' and 'rundown' the ESBS face (fringe level units are psf).

Analysis for Scenario 2C (0530 CDT)

Scenario 2C at 0530 CDT (Figure 75) consisted of a crest Elevation of +16 feet (NAVD88) and hydrodynamics consisting of a storm surge Elevation of +11.8 feet (NAVD88), a wave period of 3.1 seconds, and a significant wave height of 1.0 feet. There was no overtopping.

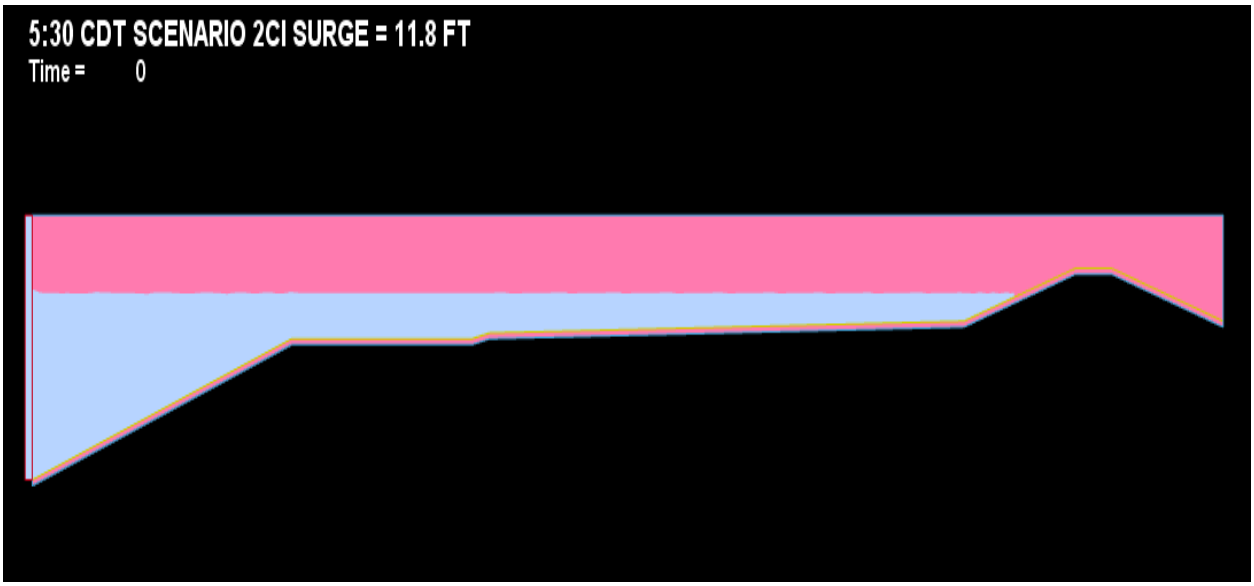


Figure 75: Initial conditions for Scenario 2C at 0530 CDT.

At Elevation +11.8 feet (NAVD88), the storm surge is in contact with the flood face of the EBSB. A plot of shear velocities is presented in Figure 76. The peak velocity at Elevation +12 feet (NAVD88) was determined to be 6.2 ft/s. A nodal velocity output malfunction was detected at Elevation +14 feet (NAVD88) and the cause for this output error was not identified prior to required submittal of this report, however, the data from this node was not directly used in these analyses.

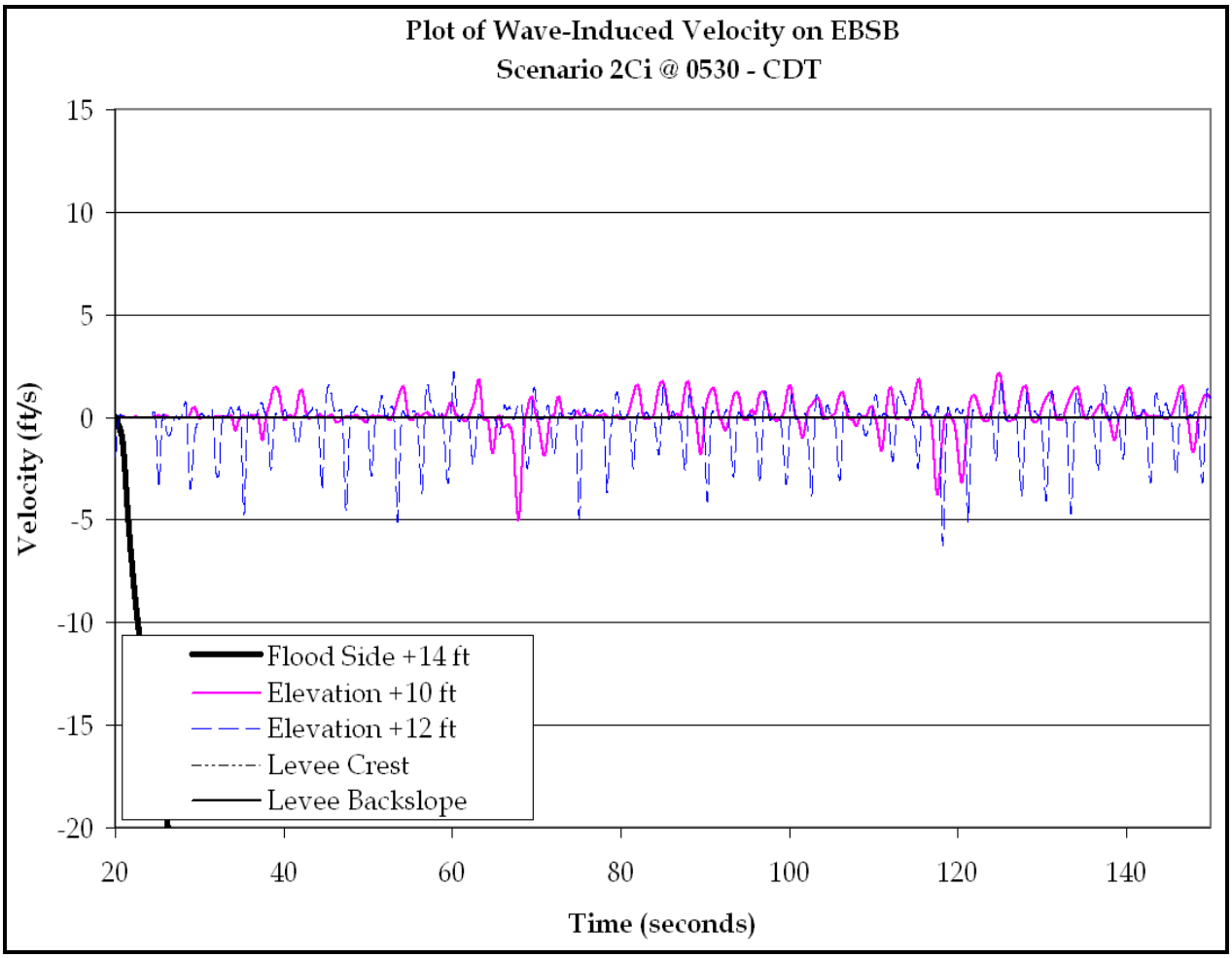


Figure 76**:** Time history plot of shear velocities for the storm surge at 0530 CDT.

Figure 77 (below) provides a graphical representation of water movement over time. With the hurricane storm surge at El. +11.8 feet (NAVD88), the design geometric configuration of the EBSB induces a tendency for the waves to exhibit a primarily 'runup' and 'rundown' behavior, with minimal wave impacts.

Storm Surge Elevation: +11.8 feet Crest Elevation: +16 feet

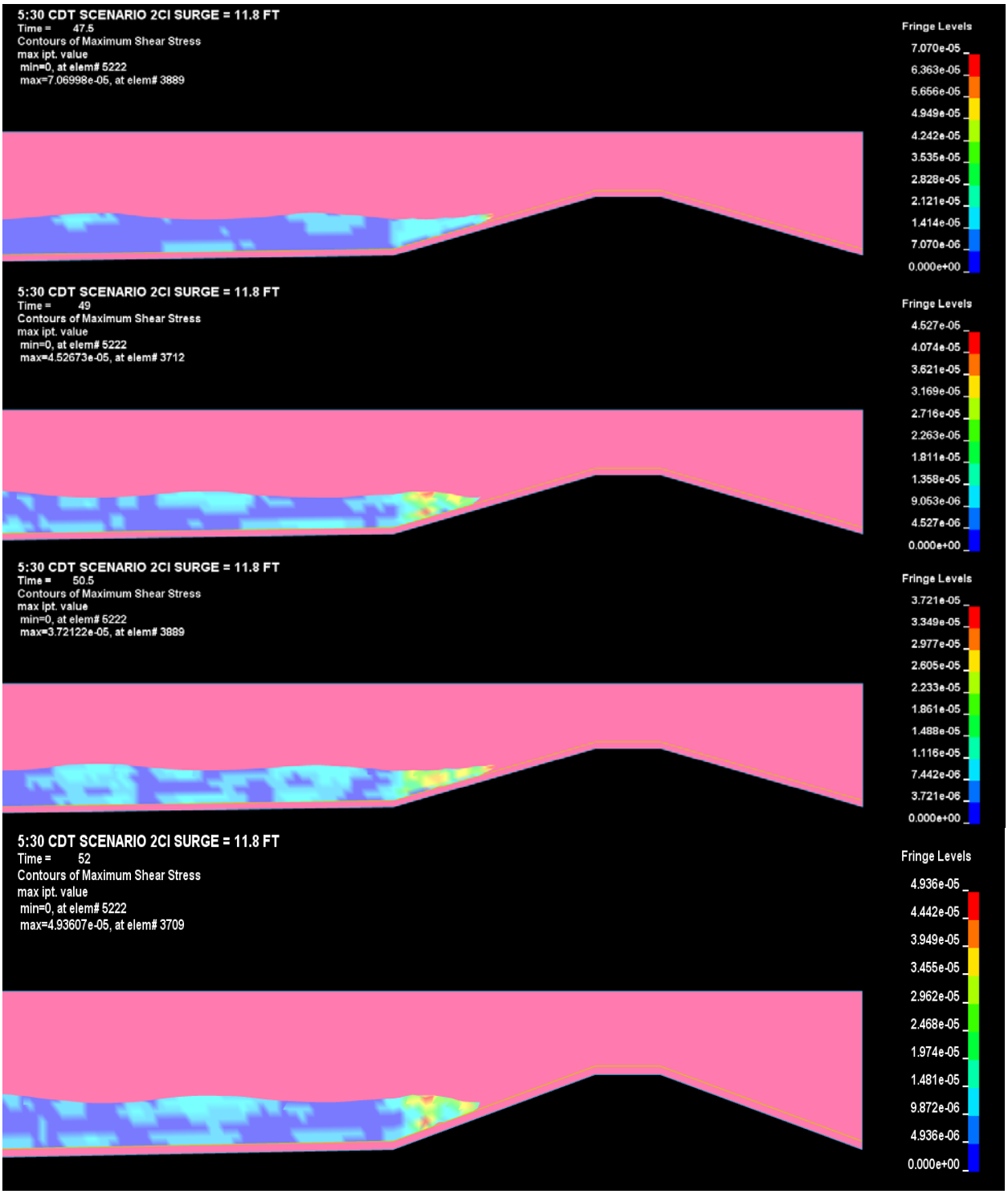


Figure 77**:** With the hurricane storm surge at El. +11.8 feet (NAVD88), the waves to exhibit primarily a 'runup' and 'rundown' behavior (fringe level units are psf).

Analysis for Scenario 2C (0630 CDT)

Scenario 2C at 0630 CDT (Figure 78) consisted of a crest Elevation of +16 feet (NAVD88) and hydrodynamics consisting of a storm surge Elevation of +14.0 feet (NAVD88), a wave period of 3.4 seconds, and a significant wave height of 1.5 feet. There was no active overtopping.

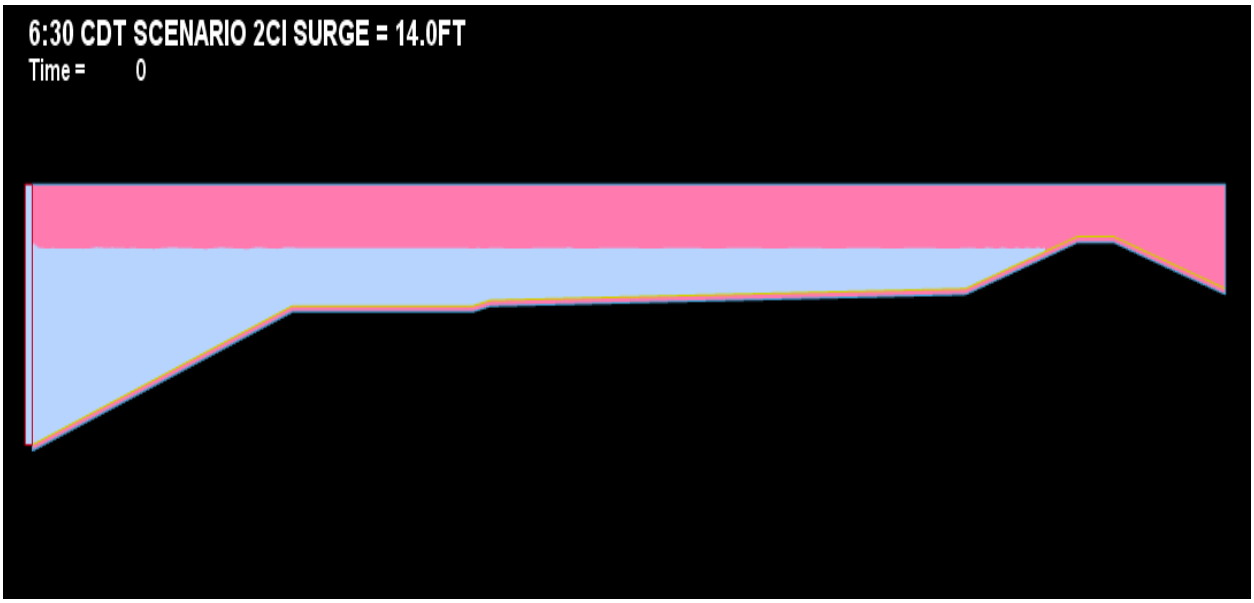


Figure 78: Initial conditions for Scenario 2C at 0630 CDT.

At Elevation +14.0 feet (NAVD88), the storm surge reaches the main EBSB flood side face. A plot of shear velocities is presented in Figure 79. The peak velocity at Elevation +14 feet (NAVD88) was determined to be 4.3 ft/s.

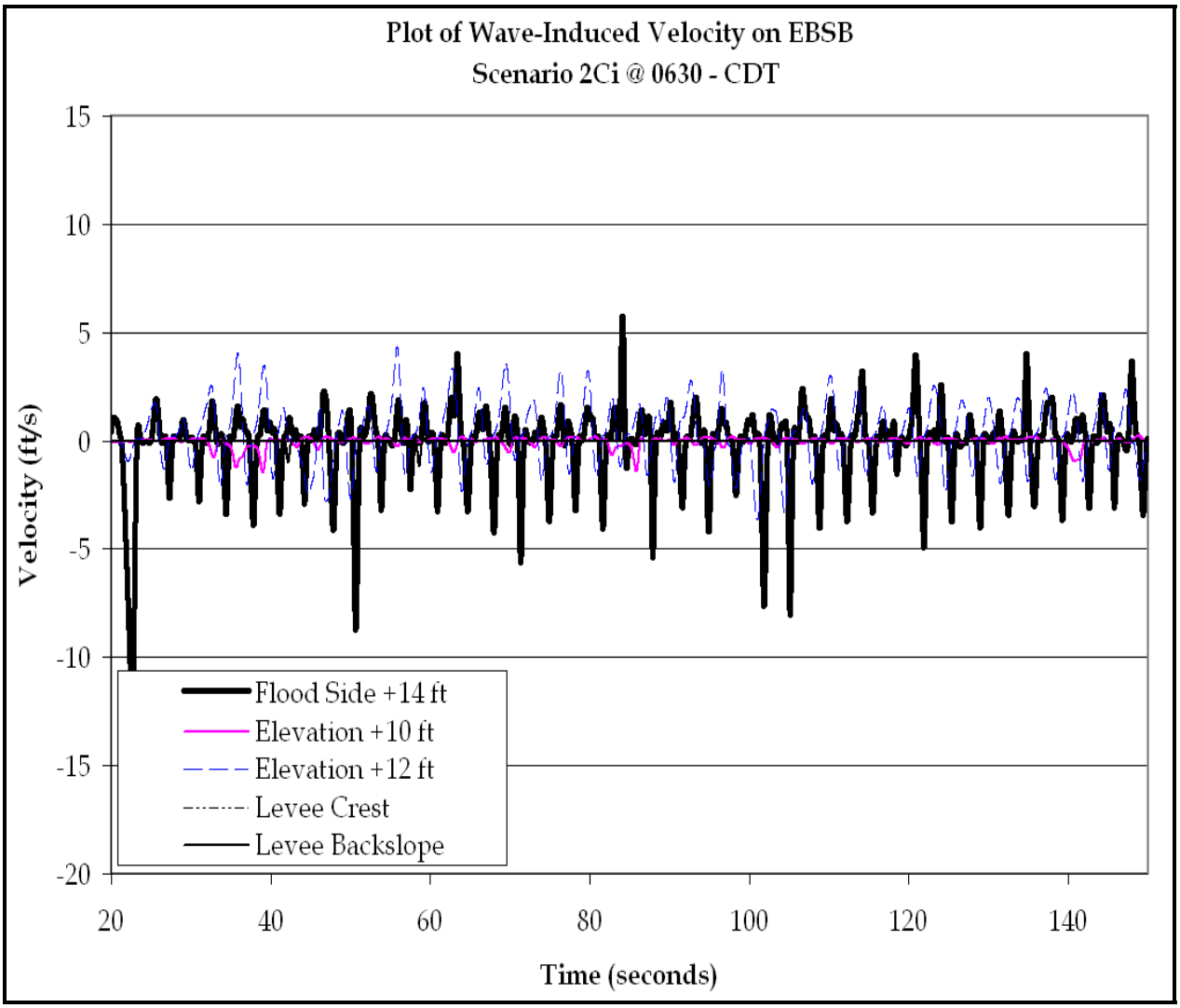


Figure 79**:** Time history plot of shear velocities for the storm surge at 0630 CDT.

Figure 80 (below) provides a graphical representation of water movement over time. With the hurricane storm surge at El. +14.0 feet (NAVD88), the configuration of the EBSB induces a tendency for the waves to exhibit a primarily 'runup' and 'rundown' behavior, with minor to moderate wave impacts.

Storm Surge Elevation: +14.0 feet Crest Elevation: +16 feet

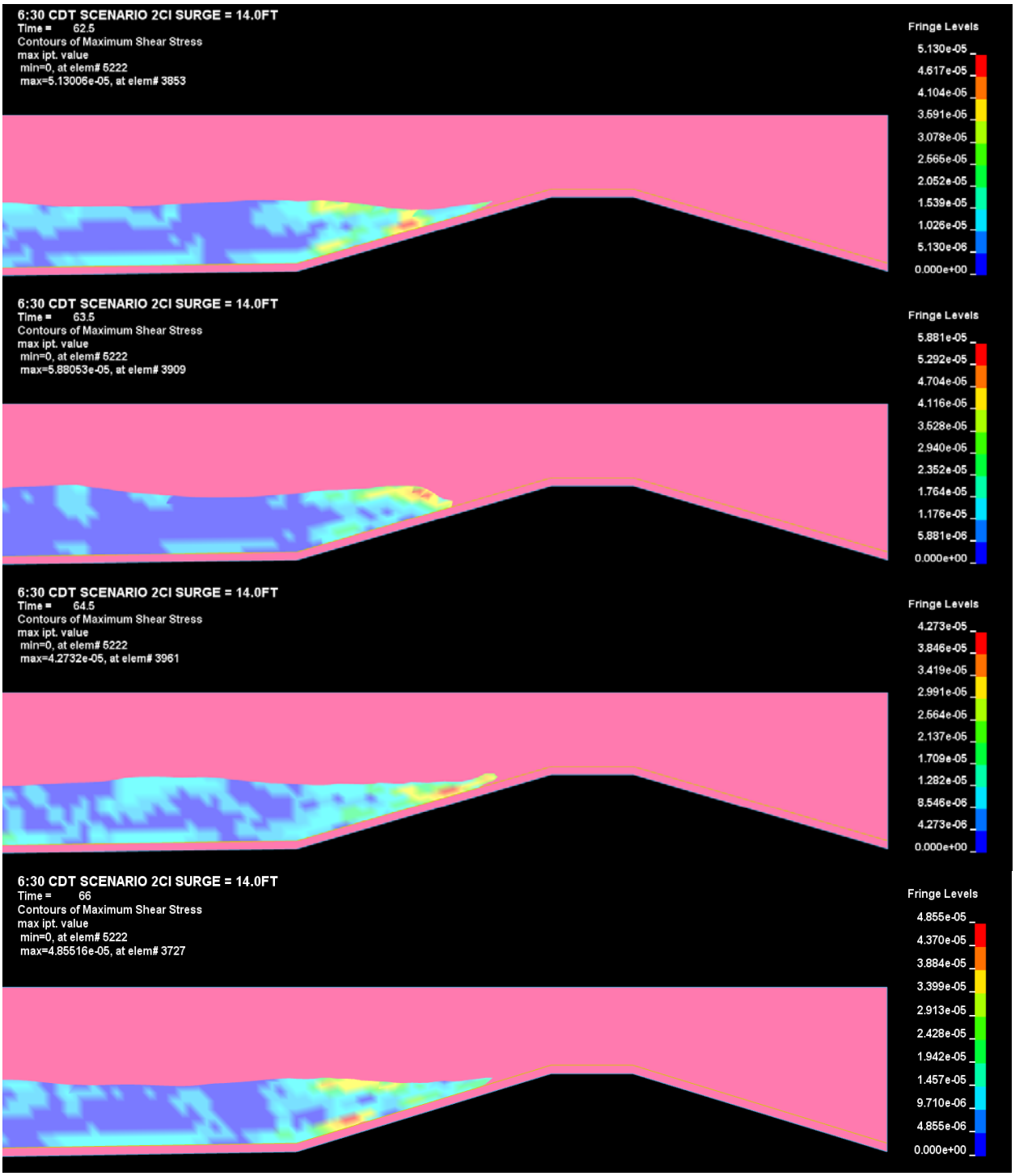


Figure 80**:** With the hurricane storm surge at El. +14.0 feet (NAVD88), the waves to exhibit a plunging behavior with minor to moderate wave impacts and wave-induced overtopping (fringe level units are psf).

Analysis for Scenario 2C (0730 CDT)

Scenario 2C at 0730 CDT (Figure 81) consisted of a crest Elevation of +16 feet (NAVD88) and hydrodynamics consisting of a storm surge Elevation of +16.2 feet (NAVD88), a wave period of 3.5 seconds, and a significant wave height of 2.0 feet. Active overtopping was also included in the modeling.

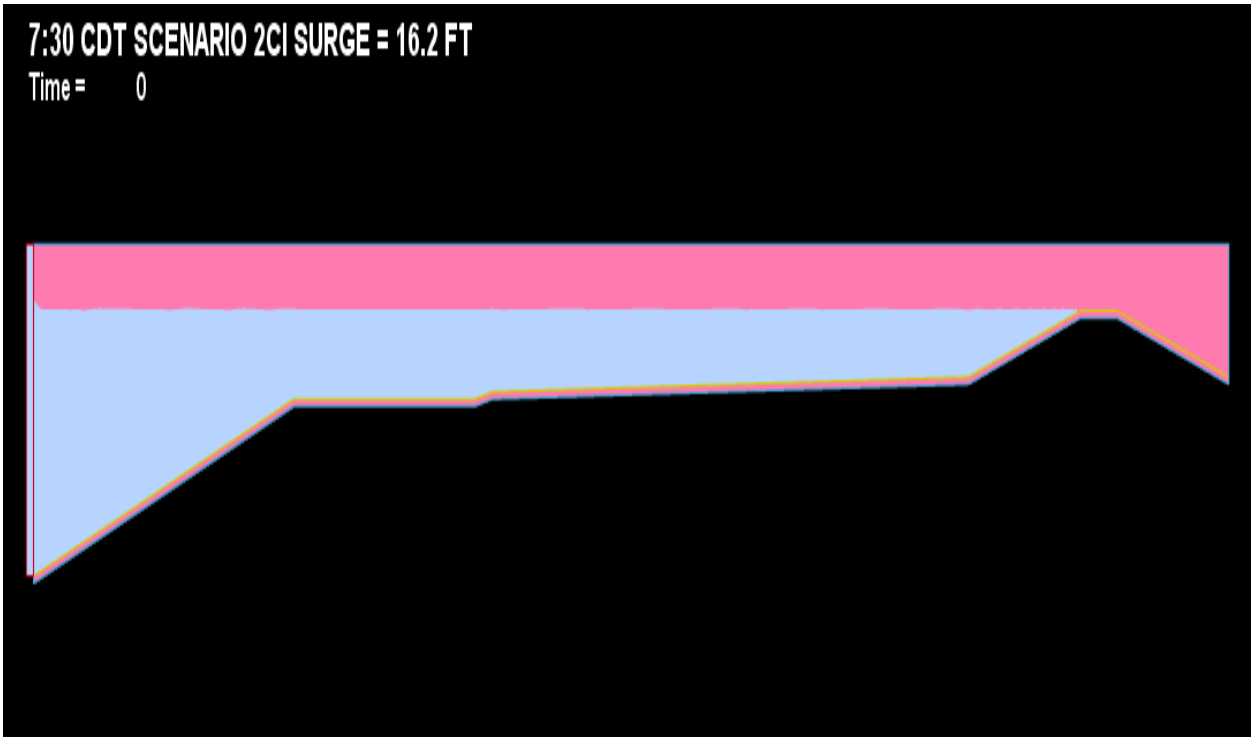


Figure 81**:** Initial conditions for Scenario 2C at 0730 CDT.

At Elevation +16.2 feet (NAVD88), the storm surge reaches the EBSB crest. A plot of shear velocities is presented in Figure 82. The peak velocity at Elevation +14 feet (NAVD88) was determined to be 3.4 ft/s.

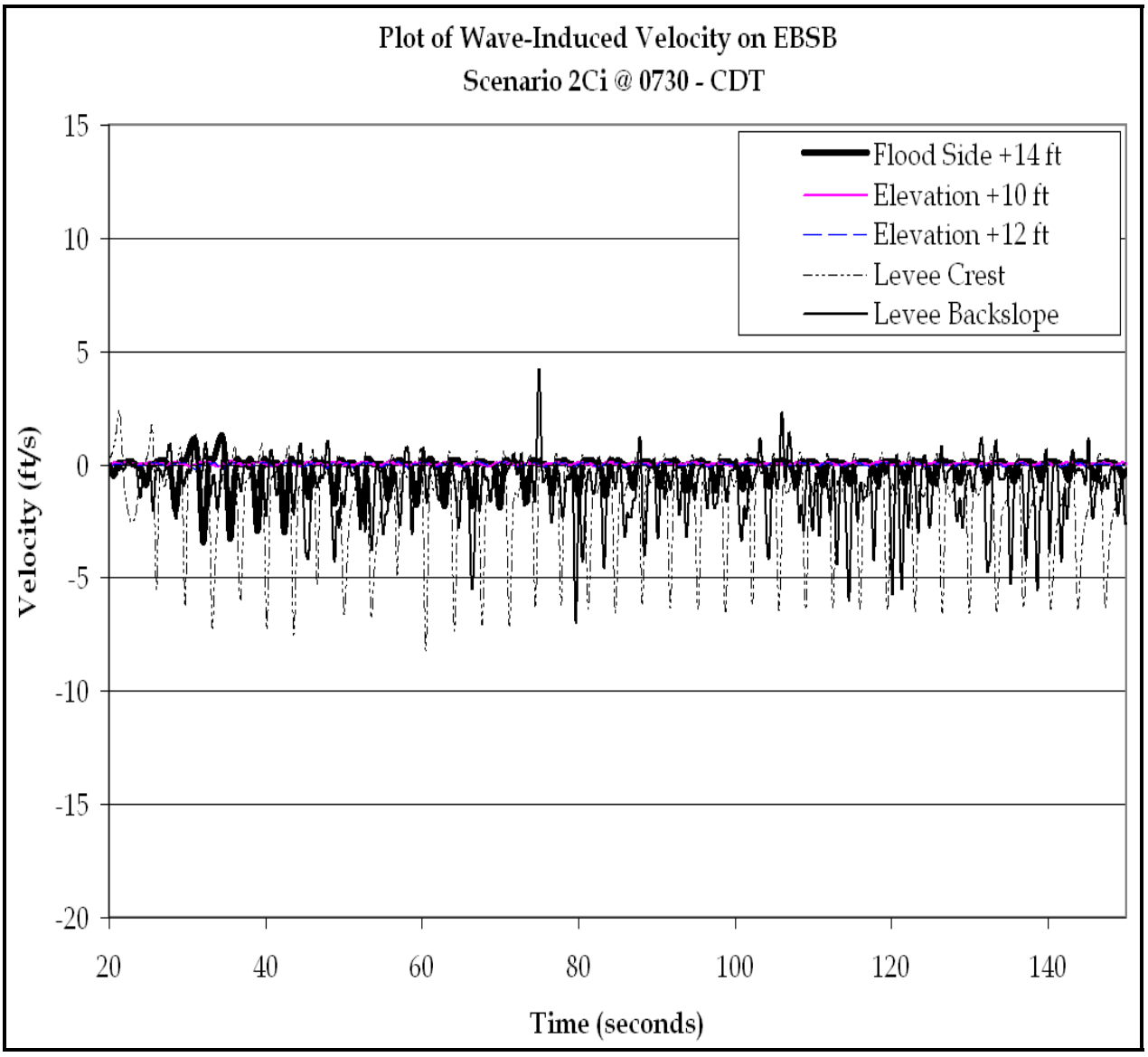


Figure 82: Time history plot of shear velocities for the storm surge at Elevation +16.2 feet.

Figure 83 (below) provides a graphical representation of water movement over time. With the hurricane storm surge at El. +16.5 feet (NAVD88), waves break on the EBSB face and spill over the crest until the wave pulse cascades down the back slope of the EBSB.

Storm Surge Elevation: +16.2 feet Crest Elevation: +16 feet

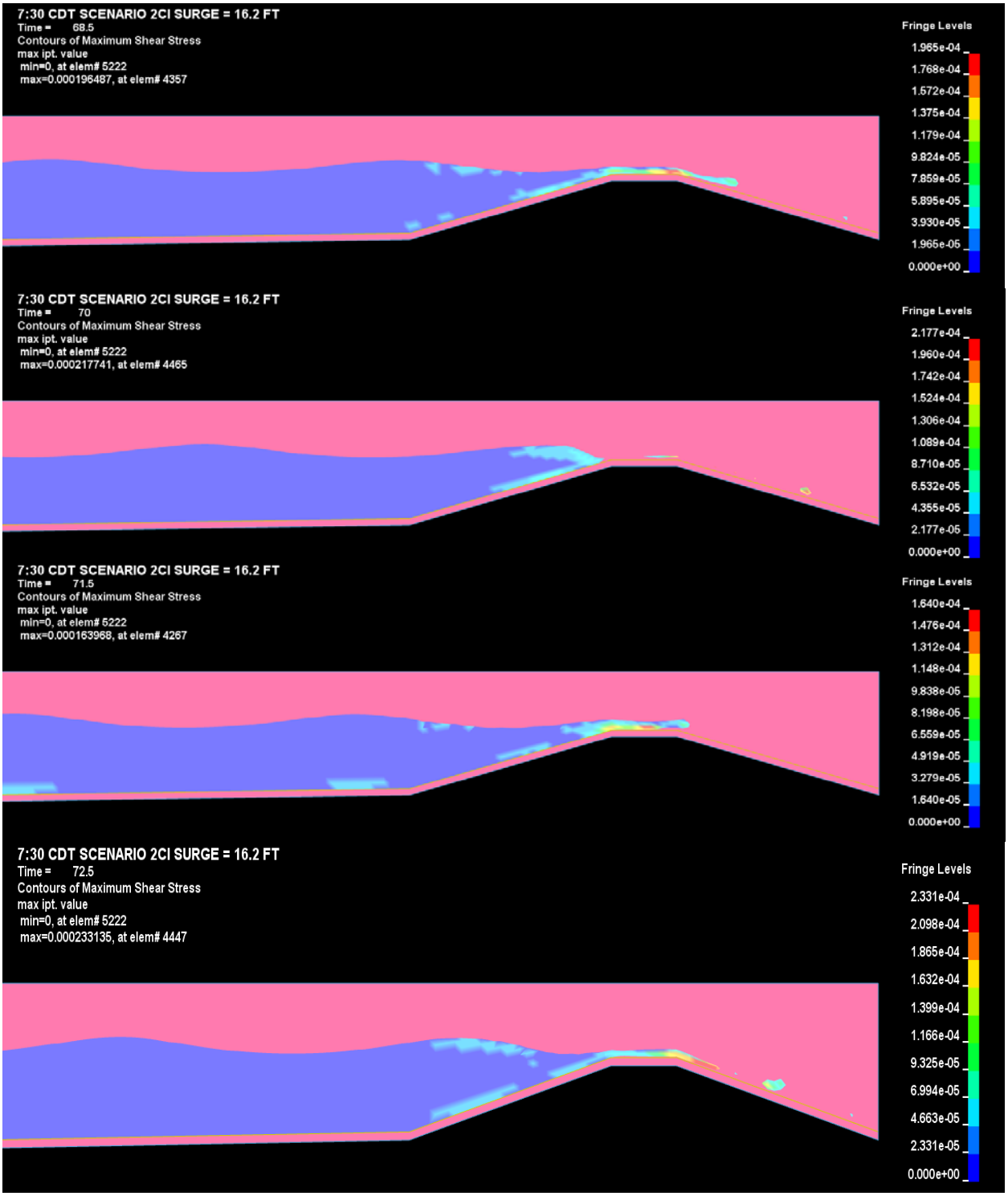


Figure 83**:** With the hurricane storm surge at El. +16.2 feet (NAVD88), waves break on the EBSB face and spill over the crest until the wave pulse cascades down the back slope of the EBSB (fringe level units are psf).

Analysis for Scenario 2C (0830 CDT)

Scenario 2C at 0830 CDT (Figure 84) consisted of a crest Elevation of +16 feet (NAVD88) and hydrodynamics consisting of a storm surge Elevation of +16.0 feet (NAVD88), a wave period of 3.4 seconds, and a significant wave height of 1.7 feet. Active overtopping was also included in the modeling and this time period was after the peak of the storm surge (at this time the storm surge is receding).

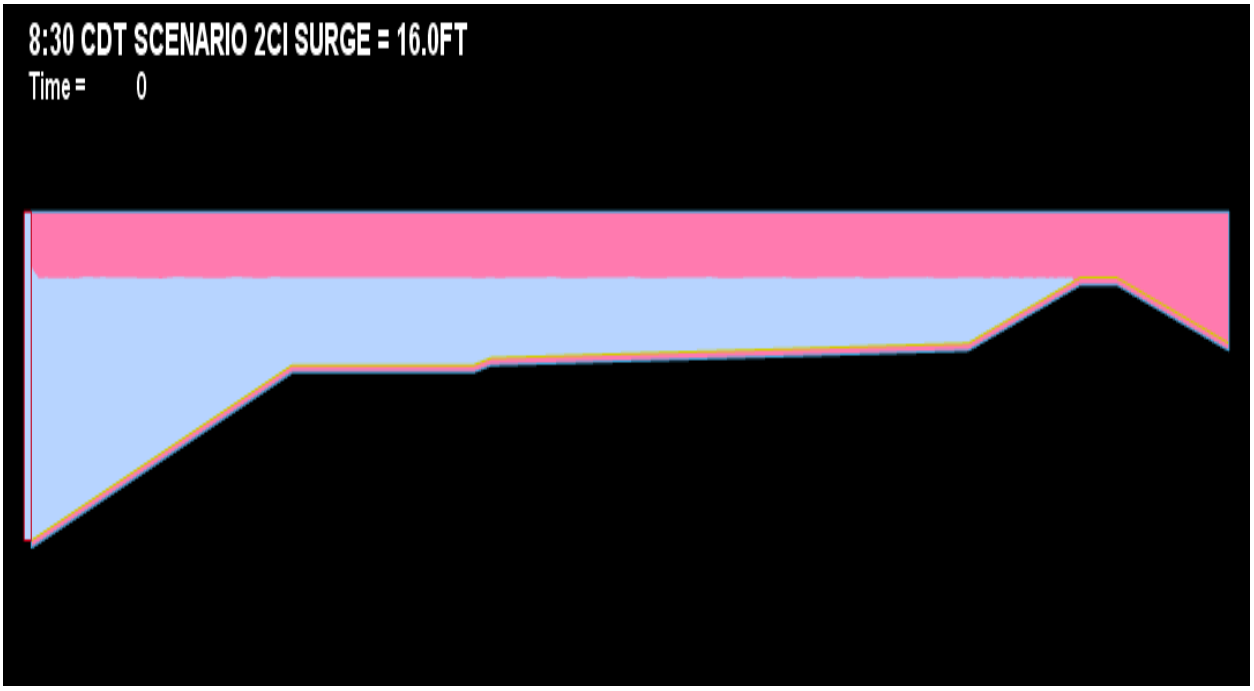


Figure 84**:** Initial conditions for Scenario 2C at 0830 CDT.

At Elevation +16.0 feet (NAVD88), the storm surge reaches the EBSB crest. A plot of shear velocities is presented in Figure 85. The peak velocity at Elevation +14 feet (NAVD88) was determined to be 4.2 ft/s.

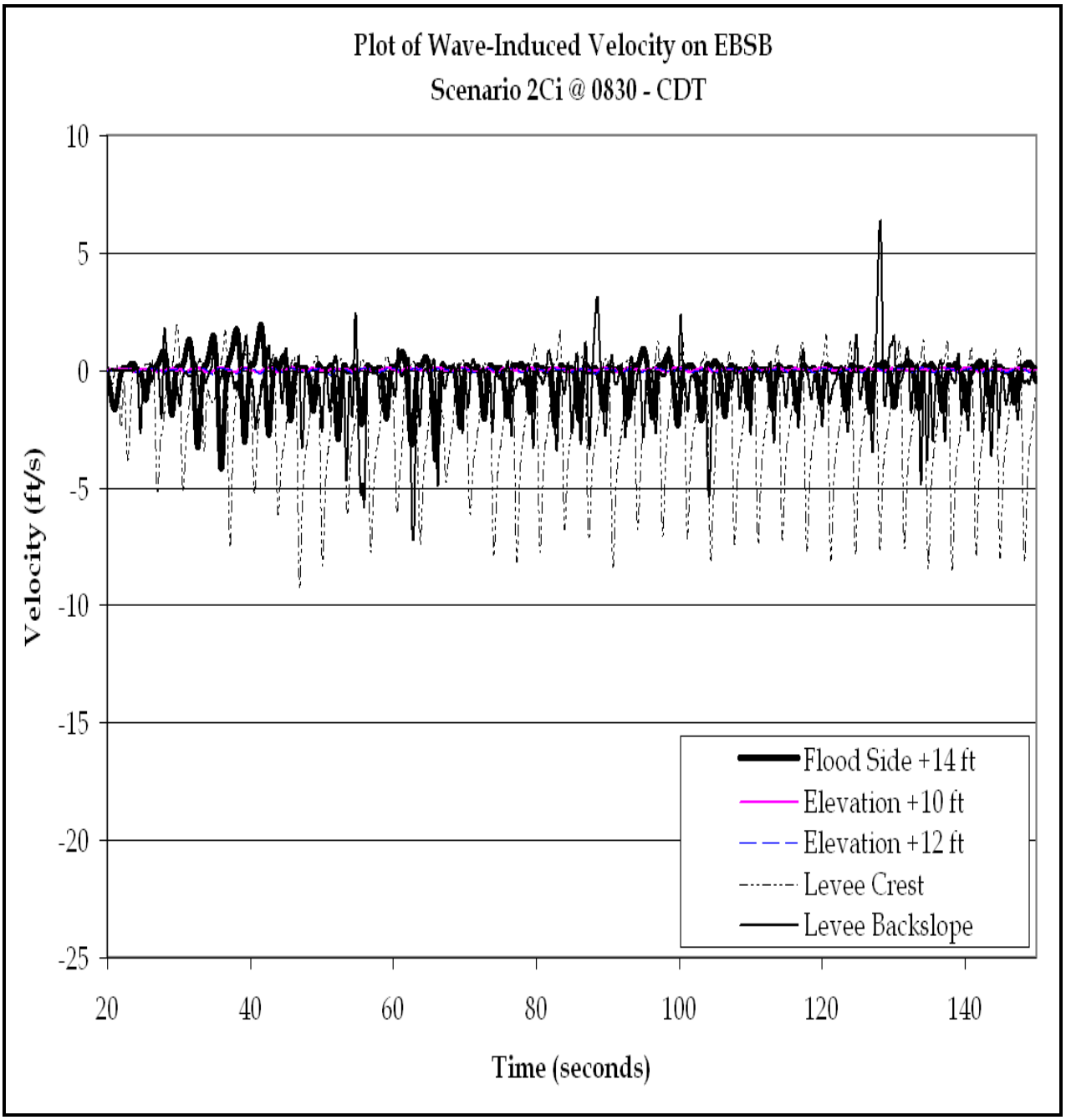


Figure 85: Time history plot of shear velocities for the storm surge at 0830 CDT.

At Elevation +16.0 feet (NAVD88), the storm surge reaches the EBSB crest with the waves breaking on the levee crest and resulting in active overtopping. A plot of shear velocities is presented in Figure 82.

Storm Surge Elevation: +16.2 feet Crest Elevation: +16 feet

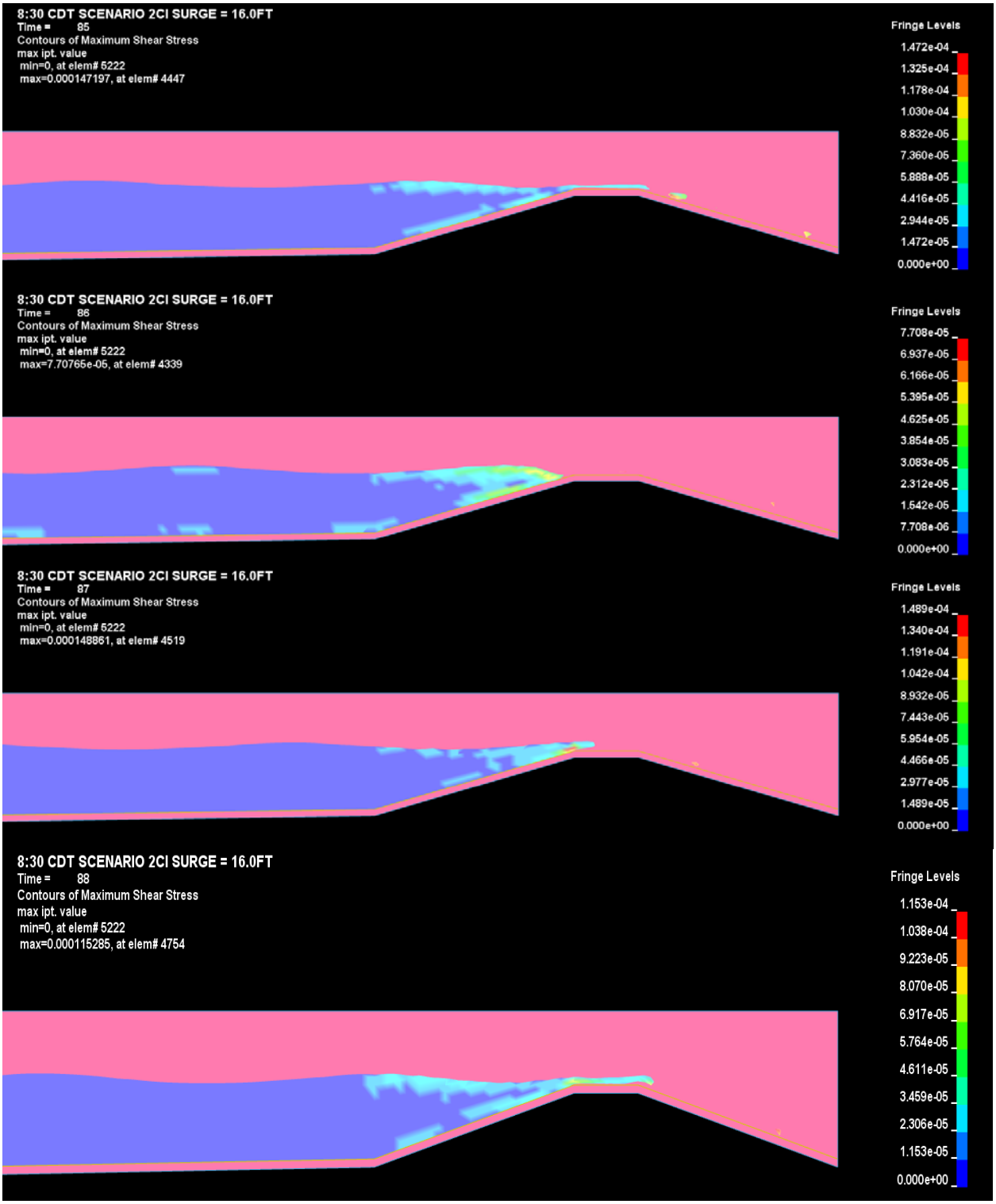


Figure 86: With the hurricane storm surge at El. +16.0 feet (NAVD88), waves break on the EBSB face and spill over the crest until the wave pulse cascades down the back slope of the EBSB (fringe level units are psf).

X. ESTIMATION OF EBSB BREACH DUE TO WAVE IMPACTS

This section of the report presents estimates of EBSB breaching based on the wave up-rush and down-rush velocities, EBSB soil erodibility characteristics, and presence of grass cover (turf). Lateral EBSB erosion was evaluated based on a three-step process: (1) velocity profiles were generated using LSDYNA (assuming actual geometric configuration) at discrete time intervals; (2) resistance to wave-induced erosion as a result of grass cover (turf) on the flood face of the EBSB was estimated and no wave-induced erosion was applied until the grass cover protection failed, and (3) estimated soil erodibility characteristics were used, in combination with the estimated wave-induced flood face velocities, to estimate the magnitude of lateral erosion.

The analytical model used for the lateral erosion calculation used in this report is presented in Figure 87. Once the grass cover protection has been compromised, the estimated lateral erosion (as determined by the LSDYNA velocity results coupled with erodibility characteristics of the EBSB) results in an erosion notch that migrates laterally (towards the protected side of the EBSB).

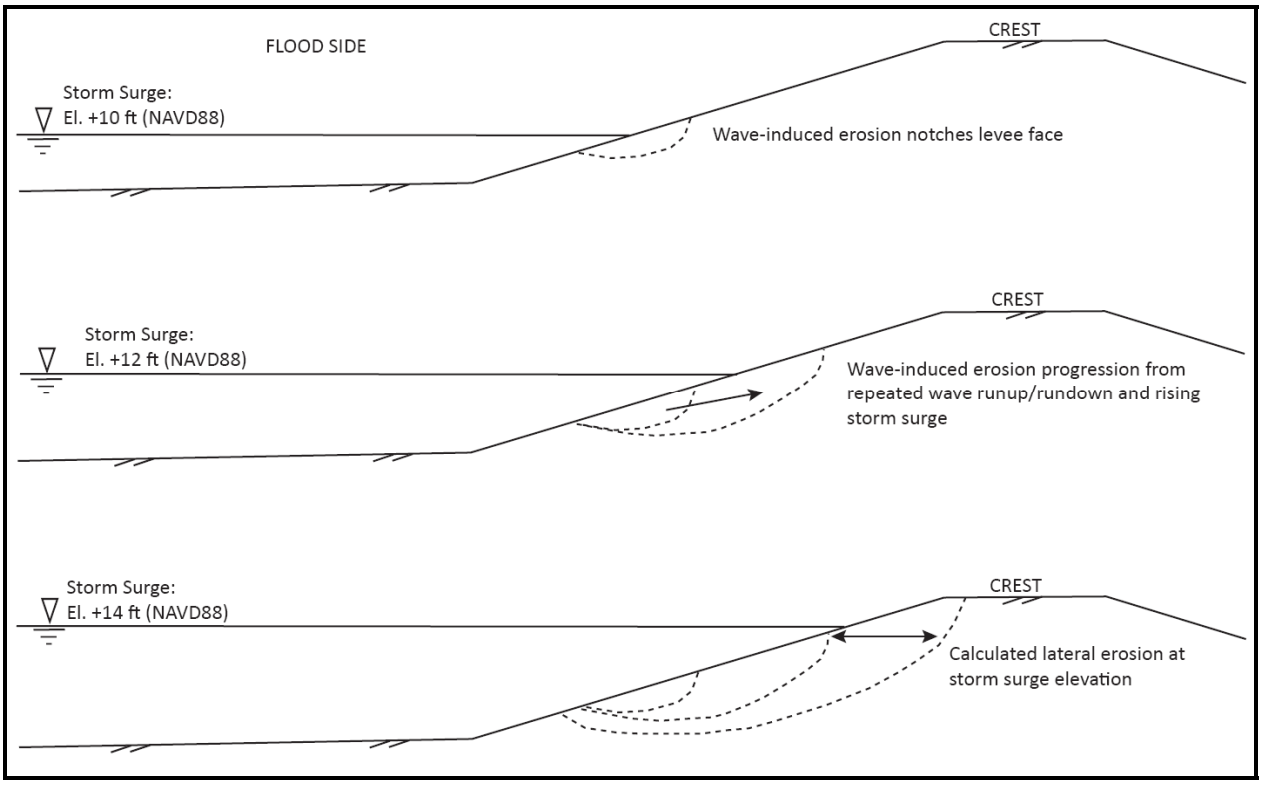


Figure 87: Development of wave-induced erosion on the flood face of the EBSB as a result of wave runup and rundown velocities on very high and highly erodible EBSB materials.

Effects of Grass Cover (Turf)

The presence of grass cover (turf) on the side slopes of the EBSBs, provides some protection against immediate erosion due to wave-induced uprush and downrush water velocities. A detailed technical background of erosion resistance on levee faces subjected to wave loadings is presented in Bea (2008a). Figure 88 presents a schematic of the grass cover structure that provides some resistance to uprush - downrush wave-induced velocities. The type of grass, grass root structure, and substrate impact the performance and durability of the grass cover.

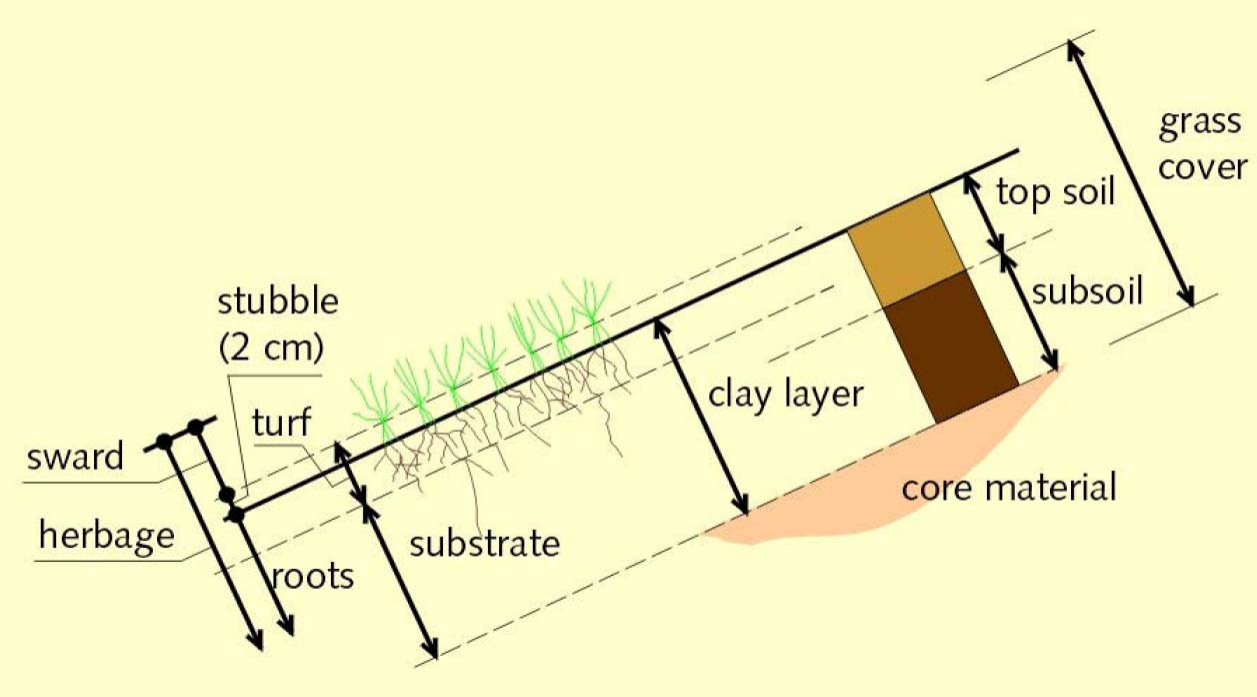


Figure 88: Schematic of grass cover structure providing erosion resistance when subjected to flowing water (TAW, 1999).

Bea (2008a) developed, based on Seijffert and Verheij (1999), a correlation between incident significant wave height and duration until breaching of the grass cover and initiation of active erosion of the EBSB soil. Figure 89 presents the correlation between grass turf protection duration and incident significant wave height (as determined by Bea, 2008a).

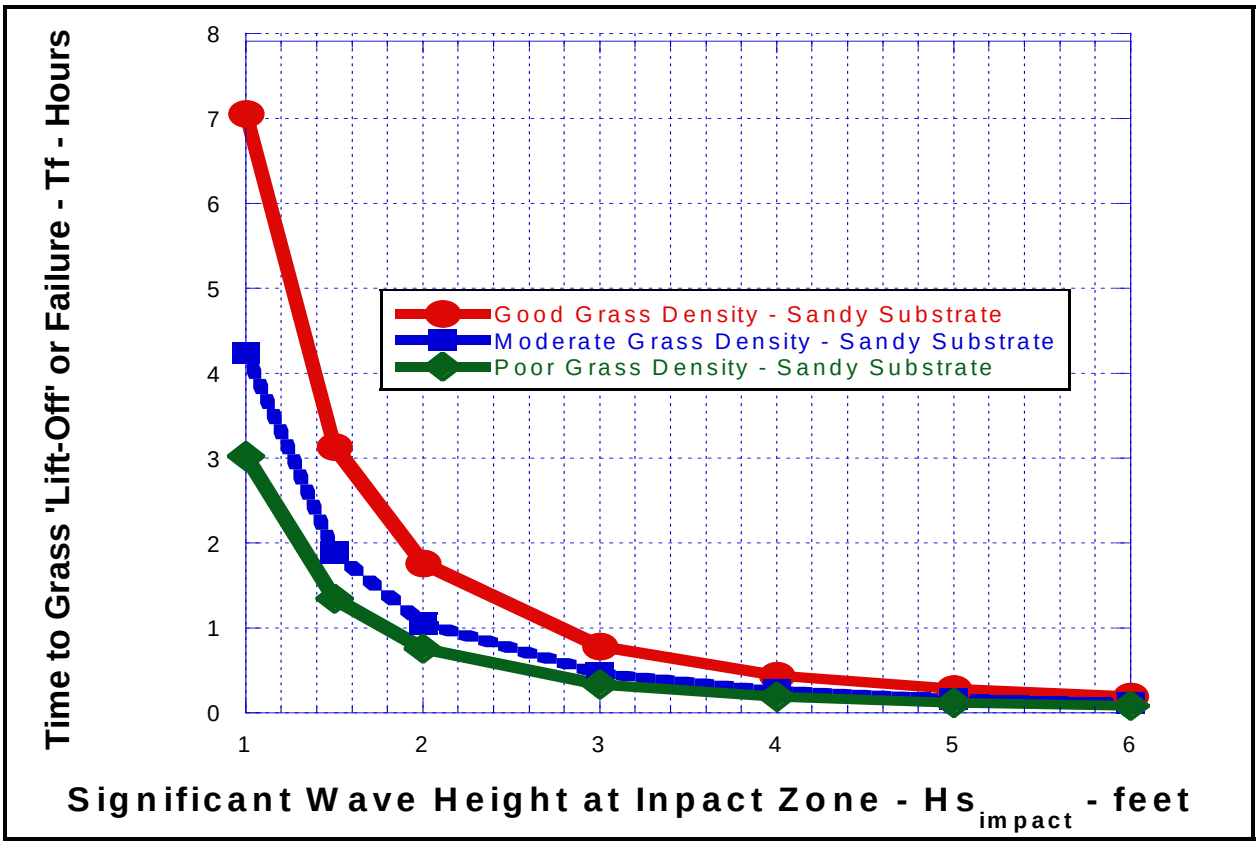


Figure 89: A correlation chart between grass cover protection duration and incident significant wave height onto the EBSB flood side face (Bea, 2008a).

A linear "Miner's fatigue damage accumulation" model (Lematire and Desmorat 2005) was used to determine the duration (hours) of wave-induced uprush/downrush loading until compromise of the grass cover and exposure of the EBSB soils. In this model the damage at which 'failure' (grass lift-off) develops is when the total damage (D) reaches unity (D = 1.0). The total damage is computed as the summation of the time the grass is exposed to each of 'n' time intervals (t_{gi} - time grass exposed to given 'ith' time interval) divided by the time to grass lift-off in that time interval (Tf_{gi}):

$$D = \sum_{i=1}^{n} \frac{t_{gi}}{Tf_{gi}} \leq 1.0 \text{ (when D = 1 failure occurs)} \qquad \text{Eq [4]}$$

For the Scenario 1 hydrodynamics, it was determined that good grass density on sandy substrate was compromised by 0530 CDT and poor grass density on sandy substrate was compromised by 0500 CDT. For the Scenario 2C hydrodynamics, it was determined that good grass density on sandy substrate was compromised by 0800 CDT and poor grass density on sandy substrate was compromised by 0645 CDT. The grass turf compromise calculations are presented in Tables 12 through 15.

Table 12: Calculation of 'good' grass cover (sandy substrate) for Scenario 1.

Scenario 1 - Good Grass Density, Sandy Substrate

Time (CDT)	Hs (ft)	Maximum Turf Erosion Duration (hrs)	Turf Exposure Period (hrs)	Interval Turf Damage (%)	Cumulative Turf Damage (%)
430	2.0	1.8	1.00	56%	56%
515	2.3	1.5	0.25	17%	72%
530	2.6	1.3	0.25	20%	92%
545	2.9	0.9	0.25	28%	120%
600	3.2	0.8	0.25	31%	151%
630	4.1	0.5	1.00	200%	351%

Table 13: Calculation of 'poor' grass cover (sandy substrate) for Scenario 1.

Scenario 1 - Poor Grass Density, Sandy Substrate

Time (CDT)	Hs (ft)	Maximum Turf Erosion Duration (hrs)	Turf Exposure Period (hrs)	Interval Turf Damage (%)	Cumulative Turf Damage (%)
415	1.9	0.9	0.25	28%	28%
430	2.0	0.8	0.25	31%	59%
445	2.0	0.8	0.25	31%	90%
500	2.1	0.8	0.25	31%	122%
530	2.6	0.6	1.00	167%	288%
630	4.1	0.1	1.00	1000%	1288%
730	5.5	0.1	1.00	1000%	2288%

Table 14: Calculation of 'good' grass cover (sandy substrate) for Scenario 2C.

Scenario 2C - Good Grass Density, Sandy Substrate

Time (CDT)	Hs (ft)	Maximum Turf Erosion Duration (hrs)	Turf Exposure Period (hrs)	Interval Turf Damage (%)	Cumulative Turf Damage (%)
430	0.6	11.0	1.00	9%	9%
530	1.0	7.0	1.00	14%	23%
630	1.5	3.1	1.00	32%	56%
715	1.9	1.8	0.25	14%	70%
730	2.0	1.8	0.25	14%	84%
745	2.1	1.7	0.25	15%	85%
800	2.2	1.6	0.25	16%	99%
830	1.7	2.5	1.00	40%	124%

Table 15: Calculation of 'poor' grass cover (sandy substrate) for Scenario 2C.

Scenario 2C - Poor Grass Density, Sandy Substrate

Time (CDT)	Hs (ft)	Maximum Turf Erosion Duration (hrs)	Turf Exposure Period (hrs)	Interval Turf Damage (%)	Cumulative Turf Damage (%)
430	0.6	4.5	1.00	22%	22%
530	1.0	3.0	1.00	33%	56%
615	1.4	1.6	0.25	16%	71%
630	1.5	1.3	0.25	19%	90%
645	1.6	1.2	0.25	21%	111%
700	1.7	1.3	0.25	19%	130%
730	2.0	0.8	1.00	125%	255%
830	1.7	1.0	1.00	100%	355%

To account for the protection afforded the EBSB by the grass cover (good grass density on sandy substrate), no lateral erosion was accumulated until the compromise of the cover.

Wave-Induced Erosion Estimates

Wave-induced cumulative erosion of EBSB materials (E) was calculated using an integrated time-step function (Eq 5) based on the erodibility of the EBSB material at the time step being evaluated (where the erodibility of the time step is determined by the time-average shear velocities calculated at the defined storm surge elevations). The erodibility at the time step ($\dot{e}(v)$) is then multiplied by the value of the time step to calculate the lateral extent of erosion.

$$E = \sum \dot{e}(v(t))\Delta t \qquad \text{[Eq 5]}$$

Since the numerical simulation only has an effective time duration of 130 seconds (eliminating the first 20 numerical simulation time required to 'initiate' the model), the cumulative erosion for the 130 second period was extrapolated to the remainder of the time interval (i.e. multiplied by 3600s/130s or 27.74).

Tables 16-18 presents a summary of the estimated lateral erosion between 0430 and 0730 (CDT) for the Scenario 1 hydrodynamics (assuming actual MR-GO channel configuration at the time of Hurricane Katrina) with EBSB materials rated as Very High, High, and Low Erodibility, respectively.

Tables 19-21 presents a summary of the estimated lateral erosion between 0430 and 0730 (CDT) for the Scenario 2C hydrodynamics (assuming a neutral MR-GO configuration) with EBSB materials rated as Very High, High, and Low Erodibility, respectively.

For the purposes of erosion protection provided by the EBSB grass cover, a sandy substrate was assumed, however, we note that this may not be realistic for 'low erodibility' materials and the information provided is for 'informational purposes' only. Additionally, for overtopping conditions, erosion over the EBSB crest and overtopping induced erosion were not included in the lateral erosion calculations presented below.

Table 16: Determination of Erosion on EBSB Flood Face for Scenario 1 hydrodynamics (Actual MR-GO) and Very High Erodibility EBSB materials (sandy grass substrate)

Scenario 1 - Lateral Erosion Results (Very High Erodibility, 'sandy' substrate)

Time (CDT)	Grass Cover	Storm Surge Elev. (ft)	Lateral Erosion (ft)	Cumulative Erosion (ft)
430	Good	10.1	20.7	N/A
530		12.0	20.8	10.4
630		14.2	88.7	99.1
730		16.6	25.9	125.0
430	Poor	10.1	20.7	N/A
530		12.0	20.8	20.8
630		14.2	88.7	109.5
730		16.6	25.9	135.4
430	None	10.1	20.7	20.7
530		12.0	20.8	41.5
630		14.2	88.7	130.2
730		16.6	25.9	156.1

Table 17: Determination of Erosion on EBSB Flood Face for Scenario 1 hydrodynamics (Actual MR-GO) and High Erodibility EBSB materials (sandy grass substrate)

Scenario 1 - Lateral Erosion Results (High Erodibility)

Time (CDT)	Grass Cover	Storm Surge Elev. (ft)	Lateral Erosion (ft)	Cumulative Erosion (ft)
430	Good	10.1	12.6	N/A
530		12.0	10.9	5.5
630		14.2	53.7	59.2
730		16.6	17.7	76.9
430	Poor	10.1	12.6	N/A
530		12.0	10.9	10.9
630		14.2	53.7	64.6
730		16.6	17.7	82.3
430	None	10.1	12.6	12.6
530		12.0	10.9	23.5
630		14.2	53.7	77.2
730		16.6	17.7	94.9

Table 18: Determination of Erosion on EBSB Flood Face for Scenario 1 hydrodynamics (Actual MR-GO) and Low Erodibility EBSB materials (sandy grass substrate)

Scenario 1 - Lateral Erosion Results (Low Erodibility)

Time (CDT)	Grass Cover	Storm Surge Elev. (ft)	Lateral Erosion (ft)	Cumulative Erosion (ft)
430	Good	10.1	0.0	N/A
530		12.0	0.0	0.0
630		14.2	0.0	0.0
730		16.6	0.0	0.0
430	Poor	10.1	0.0	N/A
530		12.0	0.0	0.0
630		14.2	0.0	0.0
730		16.6	0.0	0.0
430	None	10.1	0.0	0.0
530		12.0	0.0	0.0
630		14.2	0.0	0.0
730		16.6	0.0	0.0

Table 19: Determination of Erosion on EBSB Flood Face for Scenario 2C hydrodynamics (Neutral MR-GO) and Very High Erodibility EBSB materials (sandy grass substrate)

Scenario 2C - Lateral Erosion Results (Very High Erodibility, 'sandy' substrate)

Time (CDT)	Grass Cover	Storm Surge Elev. (ft)	Lateral Erosion (ft)	Cumulative Erosion (ft)
430	Good	9.9	0.6	N/A
530		11.8	16.4	N/A
630		14	23.3	N/A
730		16.2	3.3	N/A
430	Poor	9.9	0.6	N/A
530		11.8	16.4	N/A
630		14	23.3	5.83
730		16.2	3.3	9.13
430	None	9.9	0.6	0.6
530		11.8	16.4	17.0
630		14	23.3	40.3
730		16.2	3.3	43.6

Table 20: Determination of Erosion on EBSB Flood Face for Scenario 2C hydrodynamics (Neutral MR-GO) and High Erodibility EBSB materials (sandy grass substrate)

Scenario 2C - Lateral Erosion Results (High Erodibility, 'sandy' substrate)

Time (CDT)	Grass Cover	Storm Surge Elev. (ft)	Lateral Erosion (ft)	Cumulative Erosion (ft)
430	Good	9.9	0.3	N/A
530		11.8	4.3	N/A
630		14	2.8	N/A
730		16.2	0.3	N/A
430	Poor	9.9	0.3	N/A
530		11.8	4.3	N/A
630		14	2.8	0.70
730		16.2	0.3	1.00
430	None	9.9	0.3	0.3
530		11.8	4.3	4.6
630		14	2.8	7.4
730		16.2	0.3	7.7

Table 21: Determination of Erosion on EBSB Flood Face for Scenario 2C hydrodynamics (Neutral MR-GO) and Low Erodibility EBSB materials (sandy grass substrate)

Scenario 2C - Lateral Erosion Results (Low Erodibility, 'sandy' substrate)

Time (CDT)	Grass Cover	Storm Surge Elev. (ft)	Lateral Erosion (ft)	Cumulative Erosion (ft)
430	Good	9.9	0.0	N/A
530		11.8	0.0	N/A
630		14	0.0	N/A
730		16.2	0.0	N/A
430	Poor	9.9	0.0	N/A
530		11.8	0.0	N/A
630		14	0.0	0.0
730		16.2	0.0	0.0
430	None	9.9	0.0	0.0
530		11.8	0.0	0.0
630		14	0.0	0.0
730		16.2	0.0	0.0

Figures 90 through 92 show plots of lateral erosion induced from wave-attack on the MR-GO EBSB during Scenario 1 hydrodynamic conditions and an EBSB constructed from ‘very high erodibility,’ ‘high erodibility,’ and ‘low erodibility’ materials, respectively. Each plot shows the erosion protection afforded based on ‘good,’ ‘poor,’ and no grass cover.

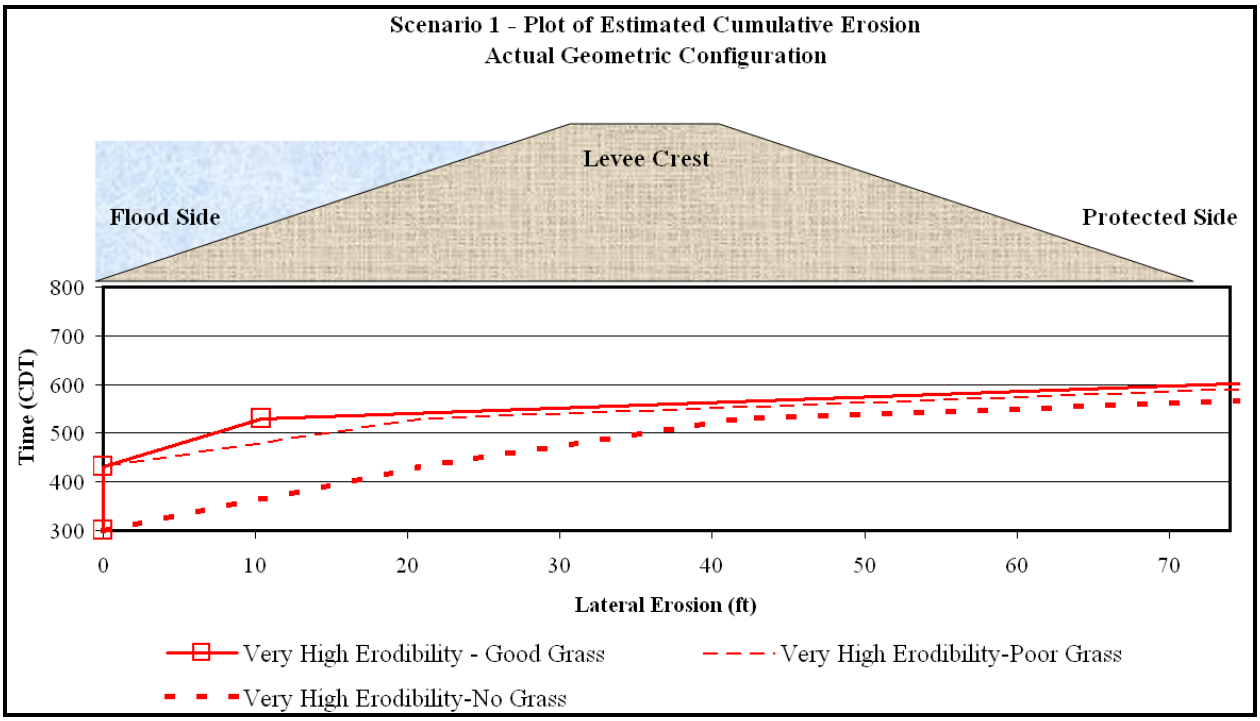


Figure 90: A plot of lateral erosion induced from wave-attack on the MR-GO EBSB for the Scenario 1 hydrodynamic conditions with very high erodibility materials and different levels of grass armor (good grass turf, poor grass turf, and no grass turf).

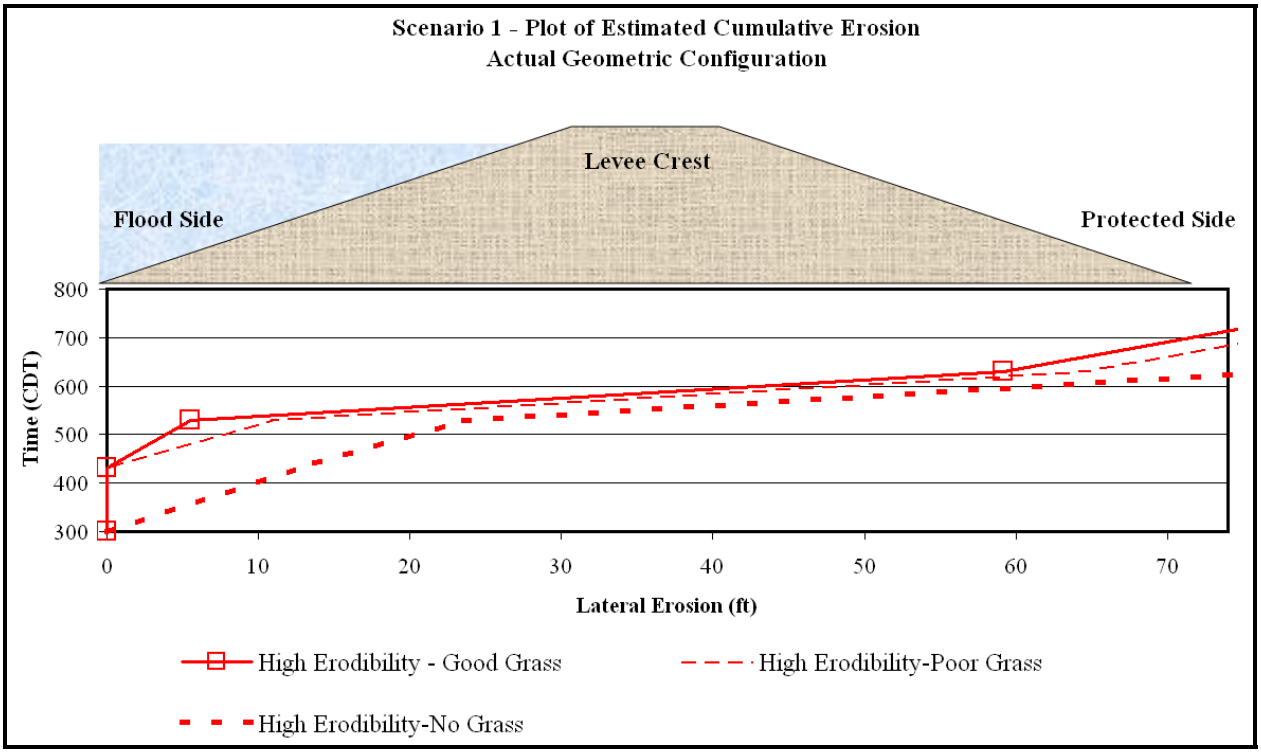


Figure 91: A plot of lateral erosion induced from wave-attack on the MR-GO EBSB for the Scenario 1 hydrodynamic conditions with high erodibility materials and different levels of grass armor (good grass turf, poor grass turf, and no grass turf).

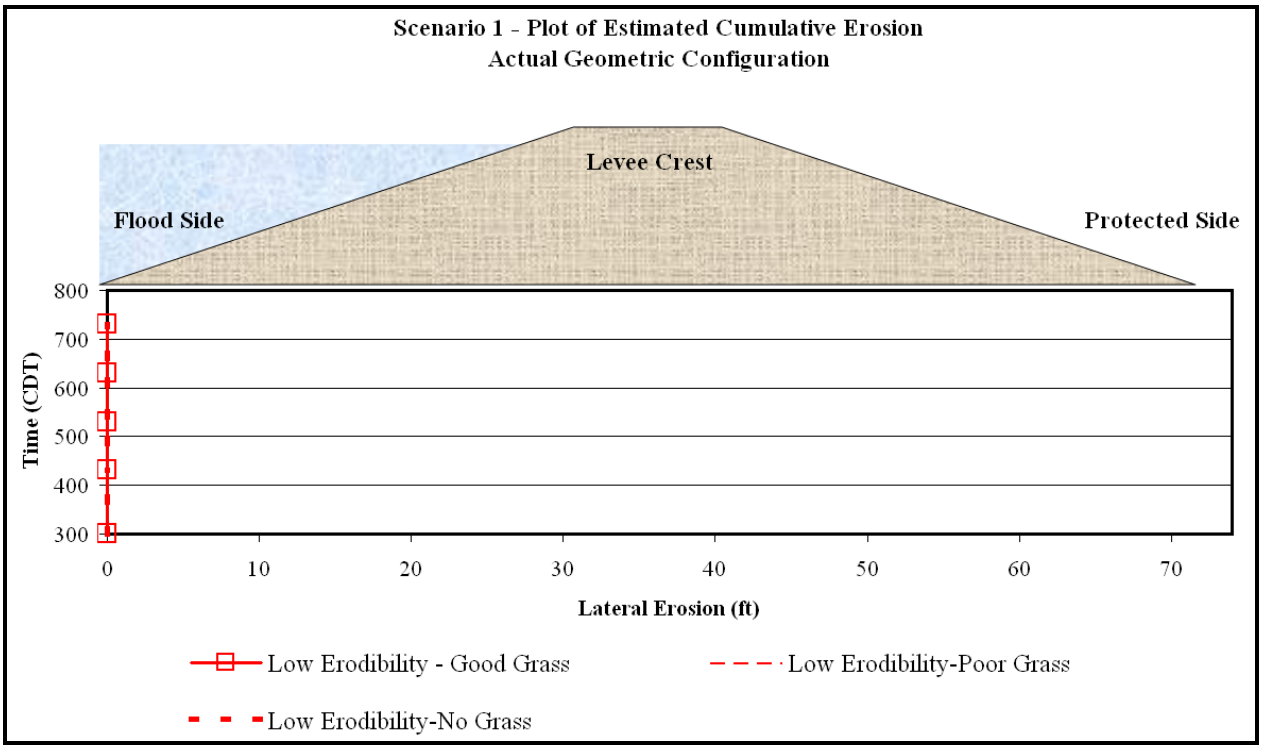


Figure 92: A plot of lateral erosion induced from wave-attack on the MR-GO EBSB for the Scenario 1 hydrodynamic conditions with low erodibility materials and different levels of grass armor (good grass turf, poor grass turf, and no grass turf).

Figures 93 through 95 show plots of lateral erosion induced from wave-attack on the MR-GO EBSB during Scenario 2C hydrodynamic conditions and an EBSB constructed from 'very high erodibility,' 'high erodibility,' and 'low erodibility' materials, respectively. Each plot shows the erosion protection afforded based on 'good,' 'poor,' and no grass cover.

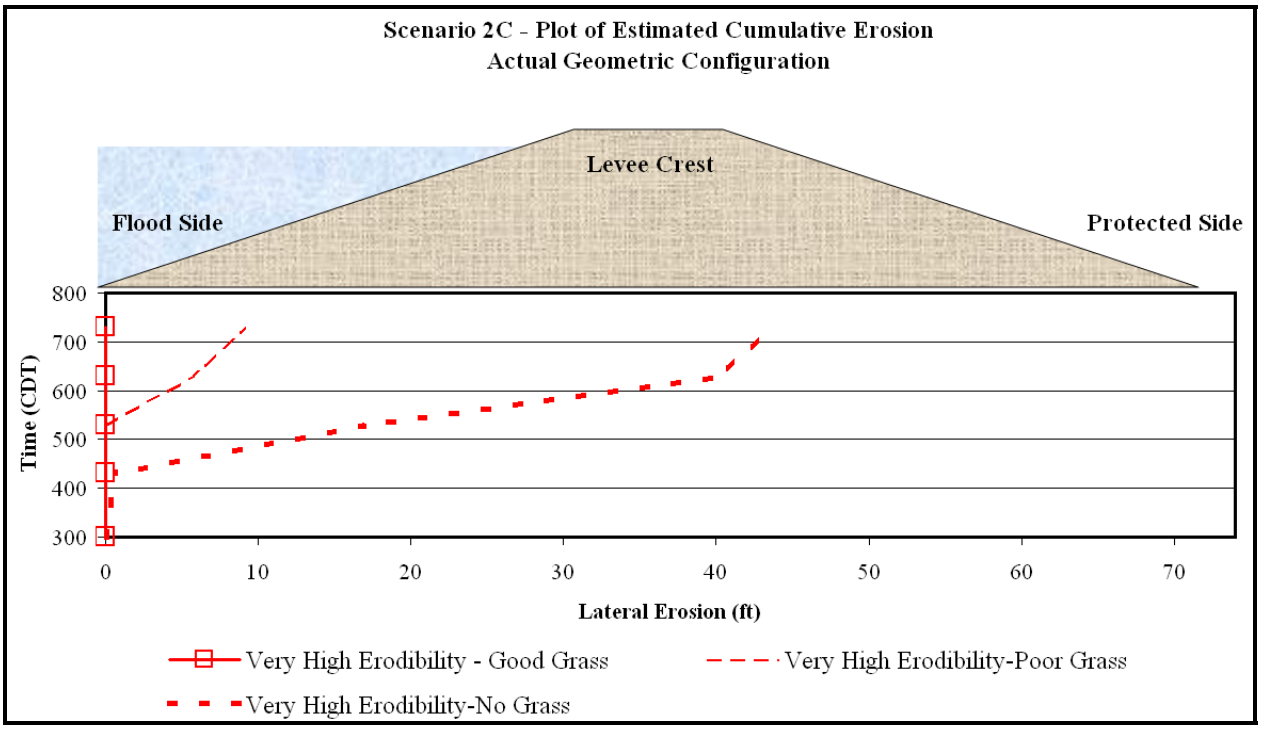


Figure 93: A plot of lateral erosion induced from wave-attack on the MR-GO EBSB for the Scenario 2C hydrodynamic conditions with very high erodibility materials and different levels of grass armor (good grass turf, poor grass turf, and no grass turf).

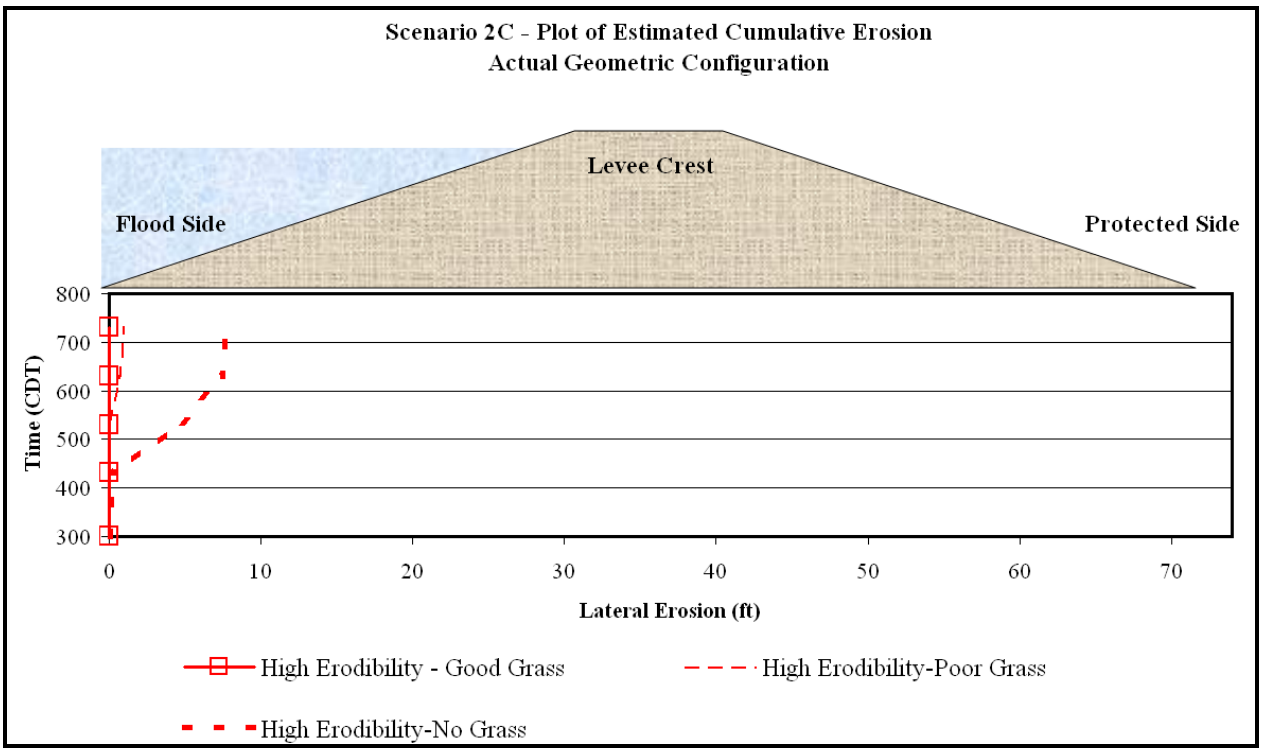


Figure 94: A plot of lateral erosion induced from wave-attack on the MR-GO EBSB for the Scenario 2C hydrodynamic conditions with high erodibility materials and different levels of grass armor (good grass turf, poor grass turf, and no grass turf).

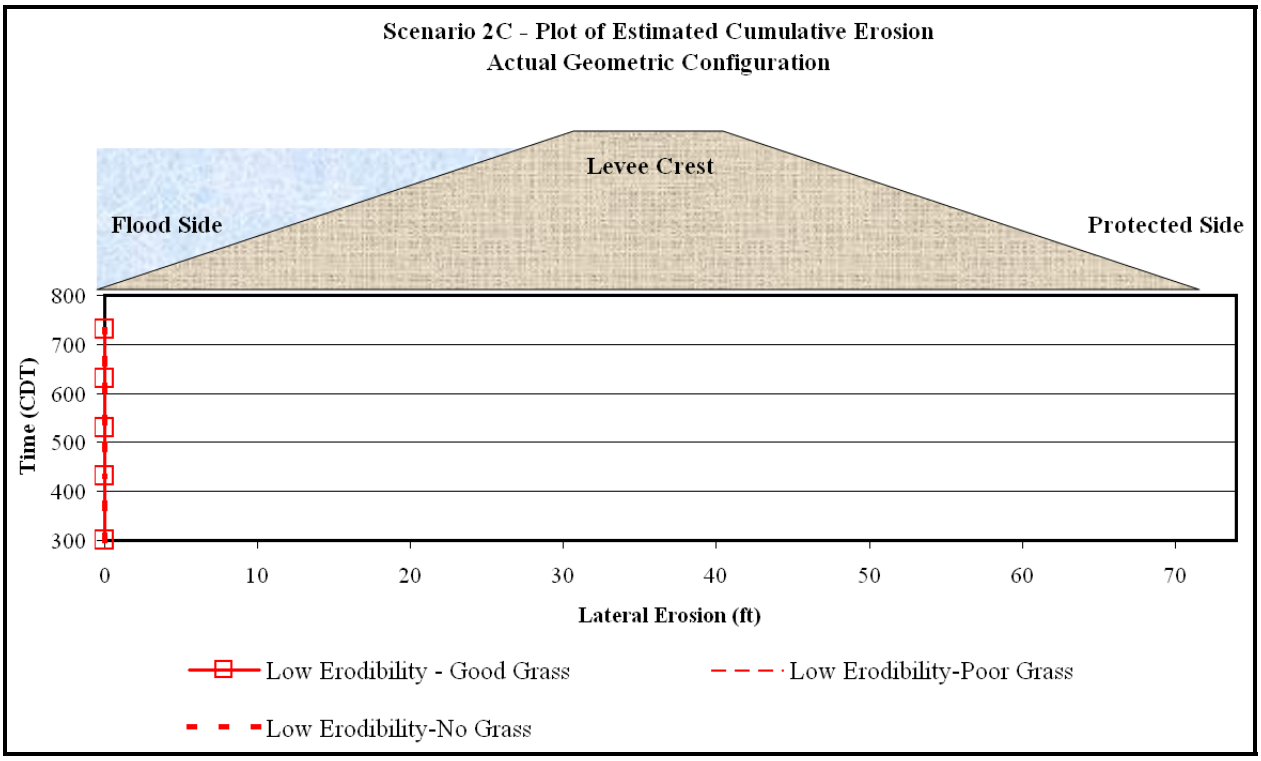


Figure 95: A plot of lateral erosion induced from wave-attack on the MR-GO EBSB for the Scenario 2C hydrodynamic conditions with low erodibility materials and different levels of grass armor (good grass turf, poor grass turf, and no grass turf).

Based on these analyses, we can conclude that for Scenario 1 hydrodynamics – the Hurricane Katrina 'as was' Conditions, it was very possible for the EBSB to have been breached through the crest solely as a result of wave-induced erosion of the very high and high erodible materials used to construct the EBSB (no significant erosion would be anticipated had low erodibility materials been used to construct the EBSB).

For the Scenario 2C hydrodynamics – the 'Neutral' MR-GO Hurricane Katrina Conditions - wave-induced breaching of the EBSB is only anticipated if the EBSB were constructed from highly erodible materials and had no protective grass cover at the time of the hurricane.

It is also quite apparent that a levee constructed of 'good' materials with low erodibility would have performed significantly better than one constructed of very high erodibility materials. Subjected to the same wave impacts, the levee with 'good' materials would have experienced insignificant erosion. It is also highly likely that the levee would have performed very well during overtopping conditions as well.

EBSB Overtopping-Induced Erosion

Similar to flood side erosion due to incident storm waves, the presence of grass cover (turf) on the 'protected' (or landward) side slopes of the EBSBs provides some protection against immediate erosion due to overtopping conditions with water cascading down the backside of the EBSB. A detailed technical background of overtopping erosion resistance is presented in Bea (2008). As mentioned earlier, the type of grass, grass root structure, and substrate impact the performance and durability of the grass cover.

Bea (2008a) developed, based on Seijffert and Verheij (1999), a correlation between overtopping limiting velocity and duration until breaching of the grass cover and initiation of active erosion of the EBSB soil. Figure 96 presents the correlation between grass turf protection duration and overtopping velocity on the backside of the EBSB (as determined by Bea, 2008a).

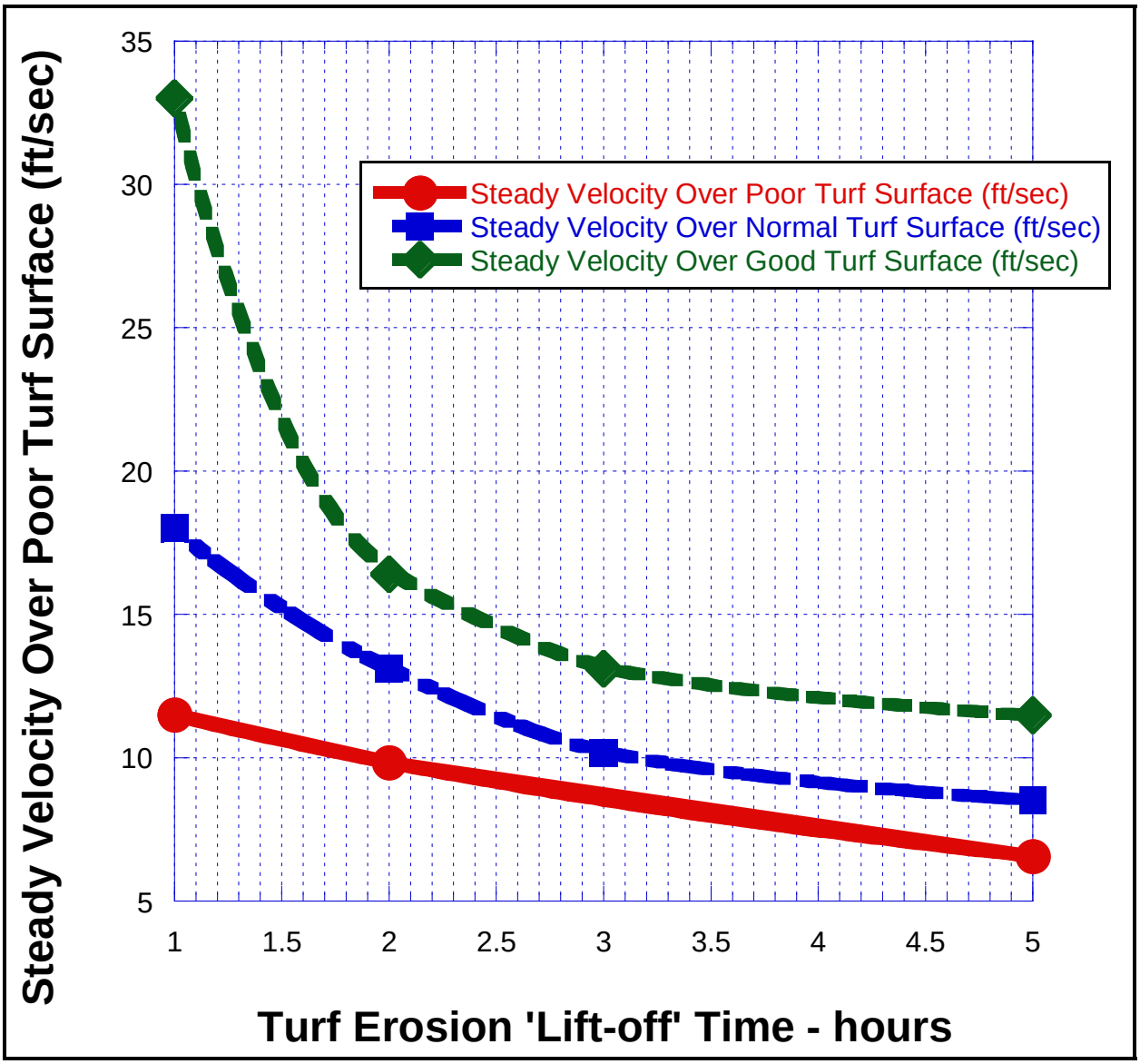


Figure 96: A correlation chart between grass cover protection duration and overtopping velocity on backside of EBSB (Bea, 2008).

Terminal velocity values were determined based on Hewlett et. al (1987), using the relation of:

$$V = \frac{d^{2/3} S^{1/2}}{n} \qquad \text{Eq [6]}$$

A Manning's coefficient (n) of 0.04 and a slope of (1/3.5 = 0.286) were used in combination with the critical depth (d). Critical depth was calculated based on (2/3)H, where H is the overtopping

head. A maximum erosion duration of 20 hours was used for these analyses. The EBSB crest Elevation was +16.0 feet (NAVD88).

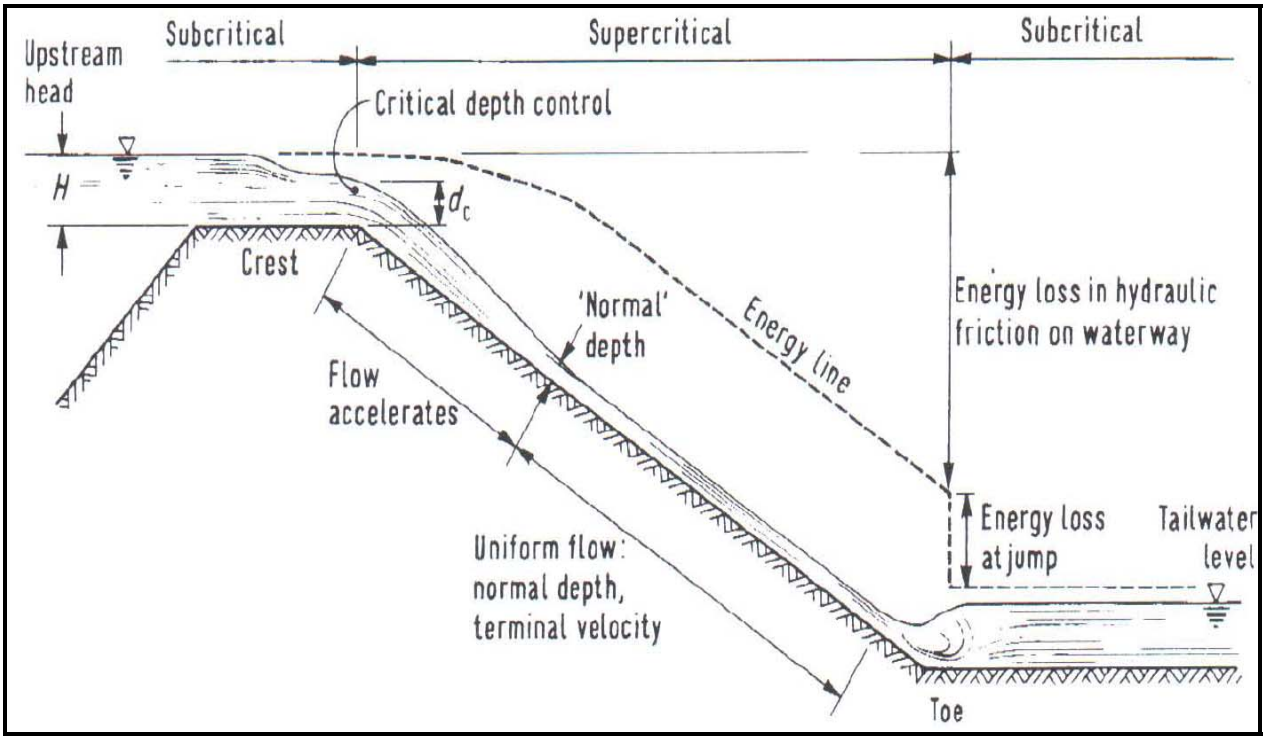


Figure 97: Graphic depiction of flow regimes during overtopping conditions (from Hewlett et al, 1987).

As with the wave-induced erosion calculations, a linear "Miner's fatigue damage accumulation" model (Lematire and Desmorat 2005) was used to determine the duration (hours) of overtopping-induced backside velocity loading until compromise of the grass cover and exposure of the EBSB soils. In this model the damage at which 'failure' (grass lift-off) develops is when the total damage (D) reaches unity (D = 1.0). The total damage is computed as the summation of the time the grass is exposed to each of 'n' time intervals (t_{gi} - time grass exposed to given 'ith' time interval) divided by the time to grass lift-off in that time interval (Tf_{gi}).

For the Scenario 1 hydrodynamics, it was determined that good grass density would not be compromised during overtopping conditions (between 0730 CDT and 0900 CDT), however, compromise of the grass cover protection was anticipated by 0800 for poor grass cover conditions.

For the Scenario 2C hydrodynamics, it was determined that neither the good grass density or poor grass density covers would be compromised during the overtopping conditions (between 0730 CDT and 0900 CDT).

The grass turf compromise calculations are presented in Table 22 (Scenario 1 conditions) and Table 23 (Scenario 2C conditions).

Table 22: Calculation of grass cover compromise time based on Scenario 1 hydrodynamics.

Scenario 1 - Overtopping Resistance due to Grass Cover

Time (CDT)	Grass Cover	Storm Surge Elev. (ft)	Maximum Velocity (ft/s)	Maximum Turf Erosion Duration (hrs)	Turf Exposure Period (hrs)	Interval Turf Damage (%)	Cumulative Turf Damage (%)
730	Good	16.6	7.3	7.0	0.5	7%	7%
800		17.8	15.1	2.3	0.5	22%	29%
830		16.1	2.2	20.0	0.5	3%	31%
900		14.3	N/A	20.0	0.5	3%	34%
730	Poor	16.6	7.3	3.0	0.5	17%	17%
800		17.8	15.1	0.3	0.5	200%	217%
830		16.1	2.2	8.0	0.5	6%	223%
900		14.3	N/A	20.0	0.5	3%	225%

Table 23: Calculation of grass cover compromise time based on Scenario 2C hydrodynamics.

Scenario 2C - Overtopping Resistance due to Grass Cover

Time (CDT)	Grass Cover	Storm Surge Elev. (ft)	Maximum Velocity (ft/s)	Maximum Turf Erosion Duration (hrs)	Turf Exposure Period (hrs)	Interval Turf Damage (%)	Cumulative Turf Damage (%)
730	Good	16.2	3.5	20	0.5	3%	3%
800		17.1	10.9	7	0.5	7%	10%
830		16	N/A	20	0.5	3%	12%
900		14.9	N/A	20	0.5	3%	15%
730	Poor	16.2	3.5	6	0.5	8%	8%
800		17.1	10.9	1	0.5	50%	58%
830		16	N/A	20	0.5	3%	61%
900		14.9	N/A	20	0.5	3%	63%

These calculations indicate that the only evaluated condition that would result in compromise of the grass cover protection and initiation of active overtopping scour was the Scenario 1 ‘poor grass’ cover case, with compromise occurring at approximately 0745 CDT. Assuming an overtopping duration of 45 minutes (0745 CDT to 0830 CDT), it would be expected to incur approximately 100 feet of erosion of Very High Erodibility materials, approximately 90 feet of High Erodibility materials, and no erosion for Low Erodibility materials.

Erosion analyses were also performed on the crest of the EBSB for the Scenario 1 and Scenario 2 hydrodynamics. The analyses considered the effects of Very High Erodibility, High Erodibility, and Low Erodibility EBSB materials with Good, Poor, and No grass cover protection.

Analyses for the Scenario 1 hydrodynamics found that no for Very High Erodibility materials, no crest breach was anticipated for Good grass cover condition, but breaching was anticipated for Poor grass cover condition (starting at approximately 0800 CDT) and for the No grass cover

condition (starting at approximately 0730 CDT), with rapid degradation. For the Scenario 1 High Erodibility material condition, no crest breach was anticipated for Good grass cover condition, but breaching was anticipated for Poor grass cover condition (starting at approximately 0800 CDT) and for the No grass cover condition (starting at approximately 0730 CDT), with moderate degradation. For the Scenario 1 Low Erodibility material condition, no crest breaching was anticipated for the Good, Poor, or No grass cover conditions. Results from the Scenario 1 analyses are presented in Tables 24 through 26.

Table 24. Crest Erosion for Scenario 1 Hydrodynamics and Very High Erodibility Materials

Time (CDT)	Grass Cover	Storm Surge Elev. (ft)	Cumulative Turf Damage (%)	Cumulative Crest Erosion (ft)	Crest Elevation, NAVD88 (ft)
730		16.6	7%	0.0	+16
800	Good	17.8	29%	0.0	+16
830		16.1	31%	0.0	+16
730		16.6	17%	0.0	+16
800	Poor	17.8	217%	28.9	-12.9
830		16.1	223%	51.4	-35.4
730		16.6	100%	17.4	-1.4
800	None	17.8	100%	46.3	-30.3
830		16.1	100%	68.8	-52.8

Table 25. Crest Erosion for Scenario 1 Hydrodynamics and High Erodibility Materials

Time (CDT)	Grass Cover	Storm Surge Elev. (ft)	Cumulative Turf Damage (%)	Cumulative Crest Erosion (ft)	Crest Elevation, NAVD88 (ft)
730		16.6	7%	0.0	+16
800	Good	17.8	29%	0.0	+16
830		16.1	31%	0.0	+16
730		16.6	17%	0.0	+16
800	Poor	17.8	217%	9.0	+7
830		16.1	223%	17.6	-1.6
730		16.6	100%	5.8	+10.2
800	None	17.8	100%	14.8	+1.2
830		16.1	100%	23.4	-7.4

Table 26. Crest Erosion for Scenario 1 Hydrodynamics and Low Erodibility Materials

Time (CDT)	Grass Cover	Storm Surge Elev. (ft)	Cumulative Turf Damage (%)	Cumulative Crest Erosion (ft)	Crest Elevation, NAVD88 (ft)
730		16.6	7%	0.0	+16
800	Good	17.8	29%	0.0	+16
830		16.1	31%	0.0	+16
730		16.6	17%	0.0	+16
800	Poor	17.8	217%	0.0	+16
830		16.1	223%	0.0	+16
730		16.6	100%	0.0	+16
800	None	17.8	100%	0.0	+16
830		16.1	100%	0.0	+16

Analyses for the Scenario 2 hydrodynamics found that no for Very High Erodibility materials, no crest breach was anticipated for Good or Poor grass cover condition, but breaching was anticipated for the No grass cover condition (starting at approximately 0730 CDT), with rapid degradation. For the Scenario 2C High Erodibility material condition, no crest breach was anticipated for the Good or Poor grass cover condition, but breaching was anticipated for the No grass cover condition (starting at approximately 0730 CDT), with moderate degradation. For the Scenario 2C Low Erodibility material condition, no crest breaching was anticipated for the Good, Poor, or No grass cover conditions. Results from the Scenario 2C analyses are presented in Tables 27 through 29.

Table 27. Crest Erosion for Scenario 2C Hydrodynamics and Very High Erodibility Materials

Time (CDT)	Grass Cover	Storm Surge Elev. (ft)	Cumulative Turf Damage (%)	Cumulative Crest Erosion (ft)	Crest Elevation, NAVD88 (ft)
730		16.2	3%	0.0	+16
800	Good	17.1	10%	0.0	+16
830		16	12%	0.0	+16
730		16.2	8%	0.0	+16
800	Poor	17.1	58%	0.0	+16
830		16	61%	0.0	+16
730		16.2	100%	17.0	-1
800	None	17.1	100%	38.2	-22.2
830		16	100%	67.7	-51.7

Table 28. Crest Erosion for Scenario 2C Hydrodynamics and High Erodibility Materials

Time (CDT)	Grass Cover	Storm Surge Elev. (ft)	Cumulative Turf Damage (%)	Cumulative Crest Erosion (ft)	Crest Elevation, NAVD88 (ft)
730		16.2	3%	0.0	+16
800	Good	17.1	10%	0.0	+16
830		16	12%	0.0	+16
730		16.2	8%	0.0	+16
800	Poor	17.1	58%	0.0	+16
830		16	61%	0.0	+16
730		16.2	100%	10.4	+5.6
800	None	17.1	100%	22.8	-6.8
830		16	100%	39.7	-23.7

Table 29. Crest Erosion for Scenario 2C Hydrodynamics and Low Erodibility Materials

Time (CDT)	Grass Cover	Storm Surge Elev. (ft)	Cumulative Turf Damage (%)	Cumulative Crest Erosion (ft)	Crest Elevation, NAVD88 (ft)
730		16.2	3%	0.0	+16
800	Good	17.1	10%	0.0	+16
830		16	12%	0.0	+16
730		16.2	8%	0.0	+16
800	Poor	17.1	58%	0.0	+16
830		16	61%	0.0	+16
730		16.2	100%	0.0	+16
800	None	17.1	100%	0.0	+16
830		16	100%	0.0	+16

Plots of crest elevation degradation for Scenario 1 are presented in Figures 98 through 100. Plots of crest elevation degradation for Scenario 2C are presented in Figures 101 through 103.

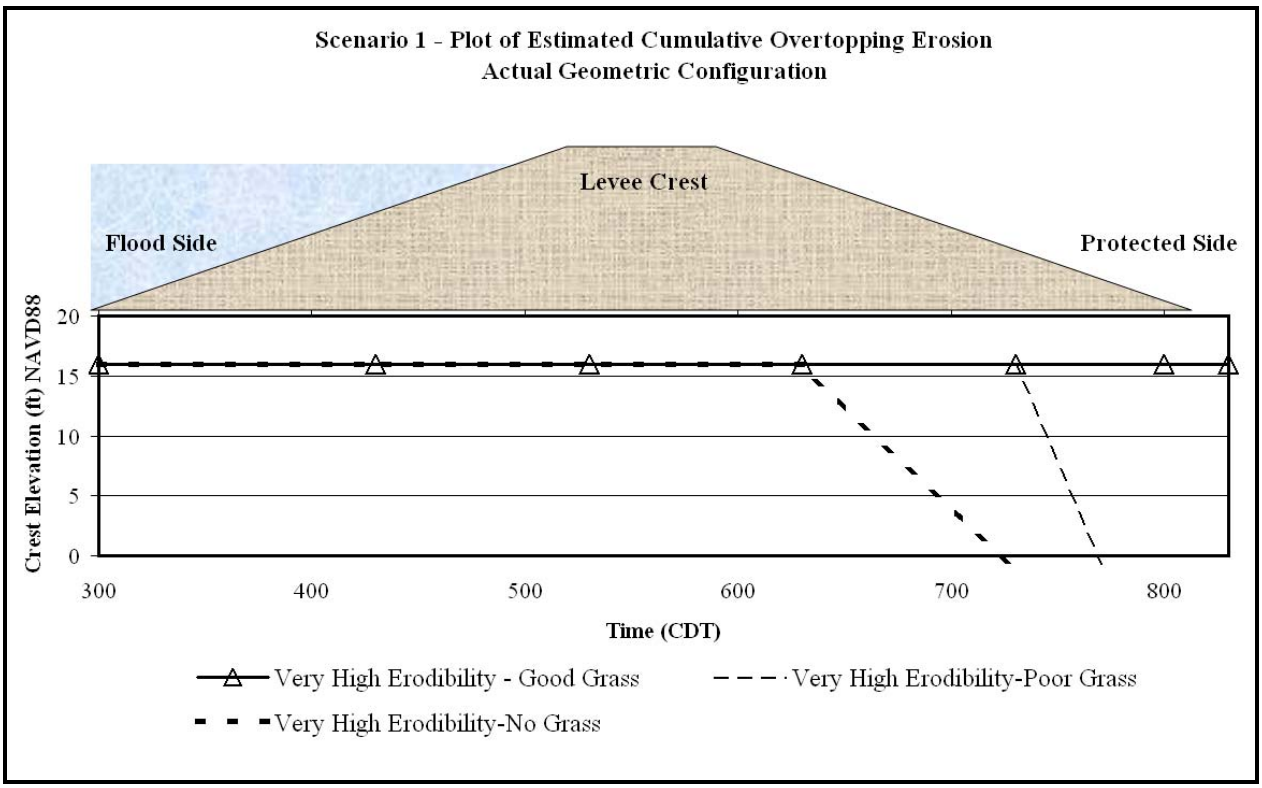


Figure 98: Plots of estimated crest erosion due to overtopping for Scenario 1 hydrodynamics and Very High Erodibility materials.

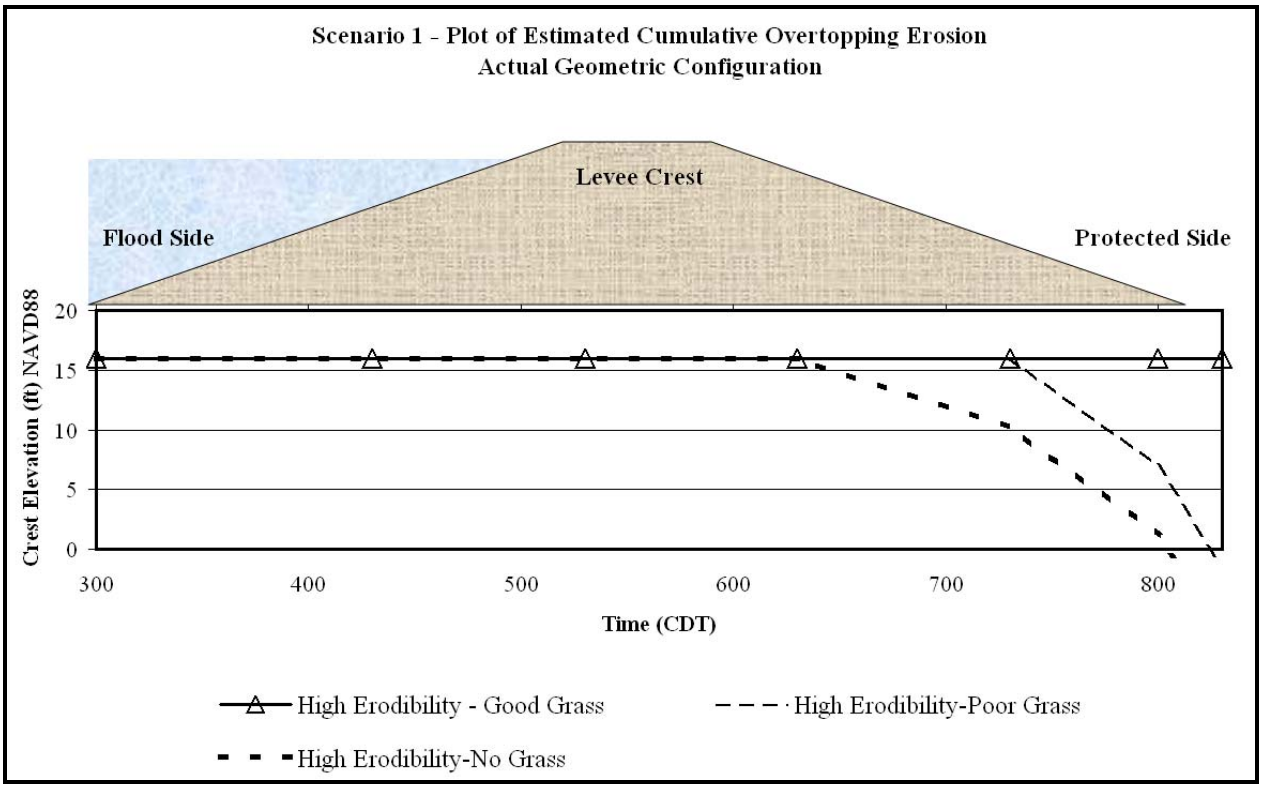


Figure 99: Plots of estimated crest erosion due to overtopping for Scenario 1 hydrodynamics and High Erodibility materials.

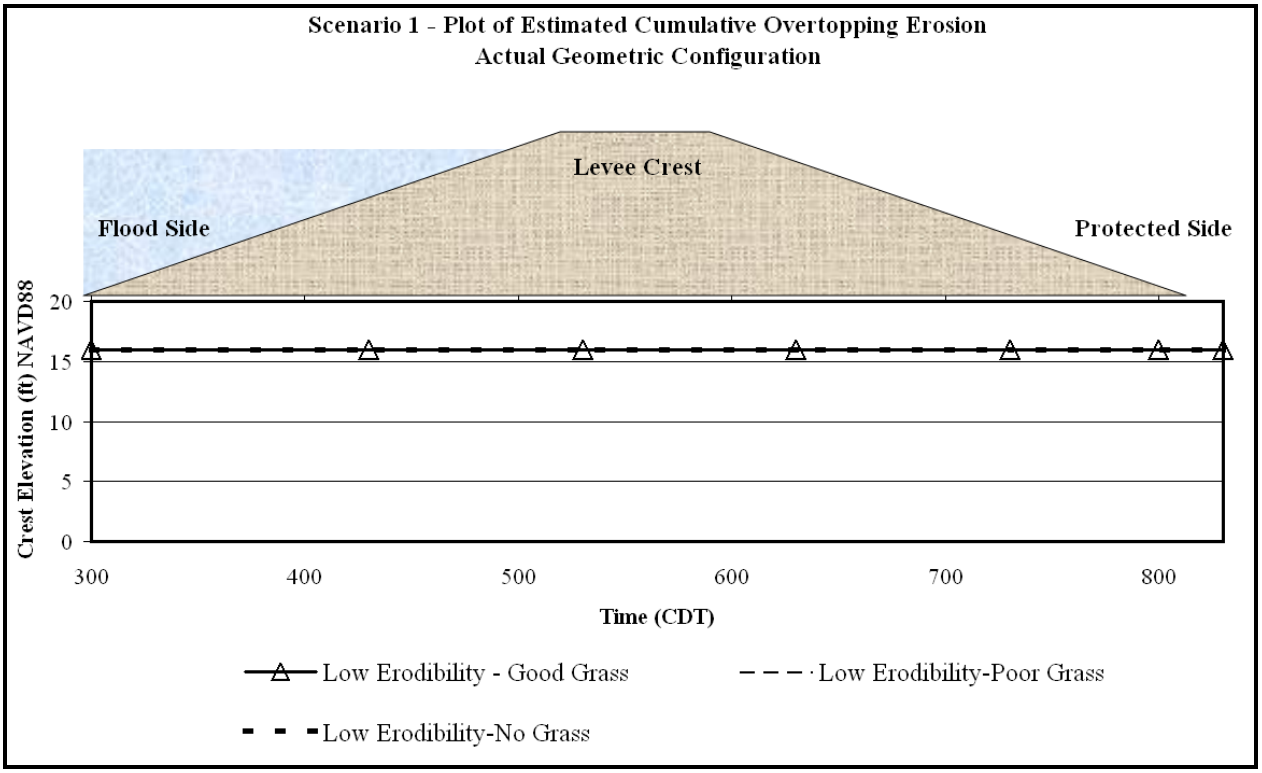


Figure 100: Plots of estimated crest erosion due to overtopping for Scenario 1 hydrodynamics and Low Erodibility materials.

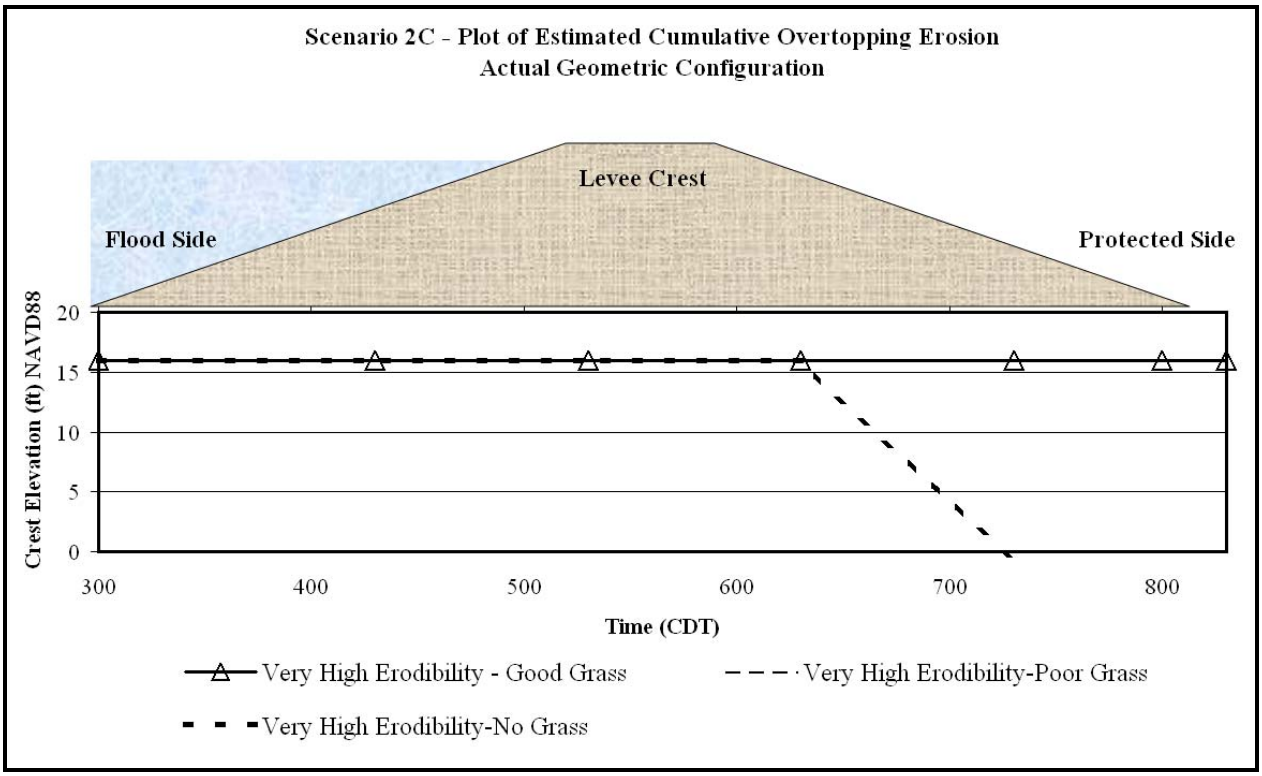


Figure 101: Plots of estimated crest erosion due to overtopping for Scenario 2C hydrodynamics and Very High Erodibility materials.

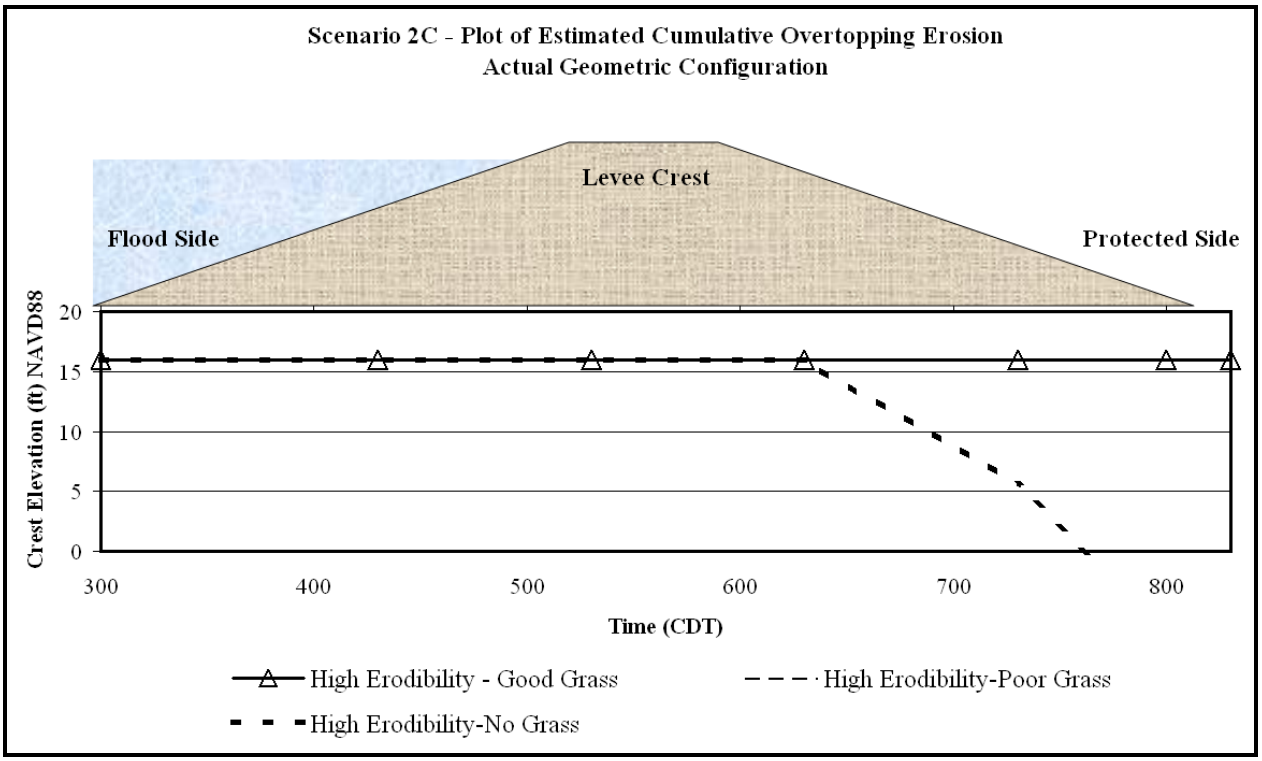


Figure 102: Plots of estimated crest erosion due to overtopping for Scenario 2C hydrodynamics and High Erodibility materials.

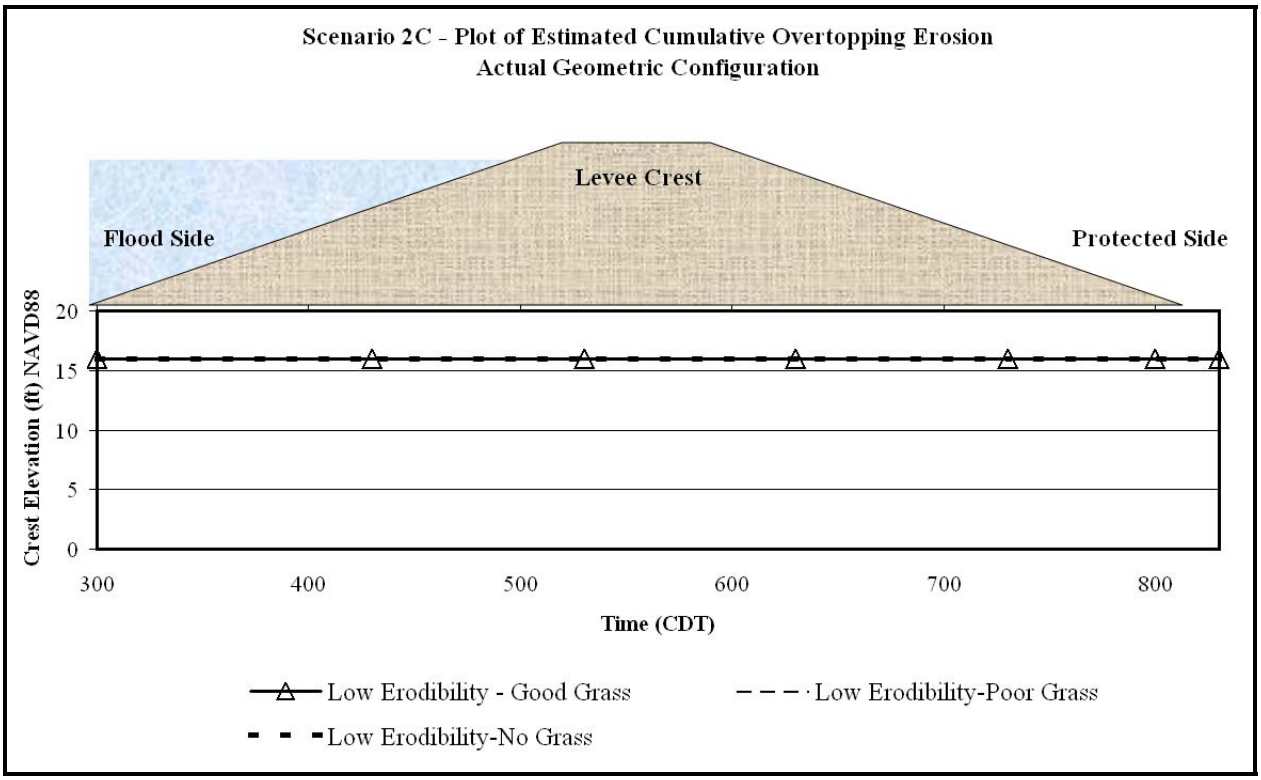


Figure 103: Plots of estimated crest erosion due to overtopping for Scenario 2C hydrodynamics and Low Erodibility materials.

XI. PARAMETRIC EROSION EVALUATIONS

Additional evaluations were also conducted to evaluate EBSB performance. These evaluations are detailed in Appendix III. The evaluations considered a number of hydrodynamic conditions, impact of hurricane storm surge currents running parallel to the shoreline/EBSBs, and design configuration (EBSB side slopes of 1 on 5) vs. actual configuration (EBSB side slopes of 1 on 3.5) of the EBSBs.

Table 30 presents the hydrodynamic conditions for IPET (2007a) and LSU (2007) used in the parametric studies. Table 31 presents the hydrodynamic conditions for Kok et al., (2008). The modeled storm surge elevations varied from Elevation +8 feet to Elevation +17.5 feet

(NAVD88). The significant wave heights varied from 1.1 feet to as much as 7.9 feet with wave periods between 2 seconds and 13.5 seconds.

Table 30: Summary of IPET (2007a) and LSU (2007) Hydrodynamic Conditions

Case	Hydro-dynamics	EBSB Geometry	Storm Surge Elevation	Significant Wave Height (H_{mo})	Wave Period	Overtopping Rate ($ft^3/s/ft$)
I	IPET	Actual	+8 ft	1.1 ft	3.5 s	0.0
II	IPET	Actual	+12 ft	1.6 ft	4.4 s	0.0
III	IPET	Actual	+17.5 ft	2.6 ft	13.5 s	0.19
IV	LSU	Actual	+8 ft	1.3 ft	2.0 s	0.0
V	LSU	Actual	+12 ft	2.0 ft	2.0 s	0.0
VI	LSU	Actual	+17.5 ft	3.2 ft	6.0 s	0.19
VII	IPET	Design	+8 ft	1.1 ft	3.5 s	0.0
VIII	IPET	Design	+12 ft	1.6 ft	4.4 s	0.0
IX	IPET	Design	+17.5 ft	2.6 ft	13.5 s	0.07
X	LSU	Design	+8 ft	1.3 ft	2.0 s	0.0
XI	LSU	Design	+12 ft	2.0 ft	2.0 s	0.0
XII	LSU	Design	+17.5 ft	3.2 ft	6.0 s	0.07

Table 31: Summary of Kok et al. (2008) Hydrodynamic Conditions

Case	Time (CDT)	Storm Surge Elevation (ft) NAVD88	Significant Wave Height, H_{mo} (ft)	Wave Period (s)	Overtopping Rate ($ft^3/s/ft$)
A	04:00	10.2	3.9	3.3	0.0
B	04:30	11.1	4.5	3.5	0.0
C	05:00	12.0	5.2	3.8	0.0
D	05:30	12.8	5.9	4.0	0.0
E	06:00	13.8	6.6	4.2	0.0
F	06:30	14.8	7.3	4.5	0.2
G	07:00	16.0	7.9	4.7	0.3
H	07:30	17.1	7.6	4.9	0.3

Figures 104 and 105 show plots of lateral erosion induced from wave-attack on the actual and design geometric EBSB configurations, respectively. Based on these simulations, and the assumed EBSB geometric configuration and materials, the EBSB crest is breached around 0500 CDT. After 0530 CDT, the magnitude of lateral erosion dramatically reduces as the outboard EBSB face is fully submerged by the storm surge (which occurs around 0600 CDT). Because the EBSB face is submerged, there is no wave-induced runup/rundown, minimizing velocity magnitudes on the EBSB face.

A comparison between the supplemental analysis and previous analyses using IPET and LSU hydrodynamics is presented in Figure 106. The Kok et al. (2008) hydrodynamics imply that more wave-induced erosion occurred on the EBSB than wave-induced erosion as determined by the

LSU (2007) and IPET (2007a) hydrodynamics. However, all three hydrodynamic profiles indicate that the EBSB would have been breached as a result of wave-induced erosion.

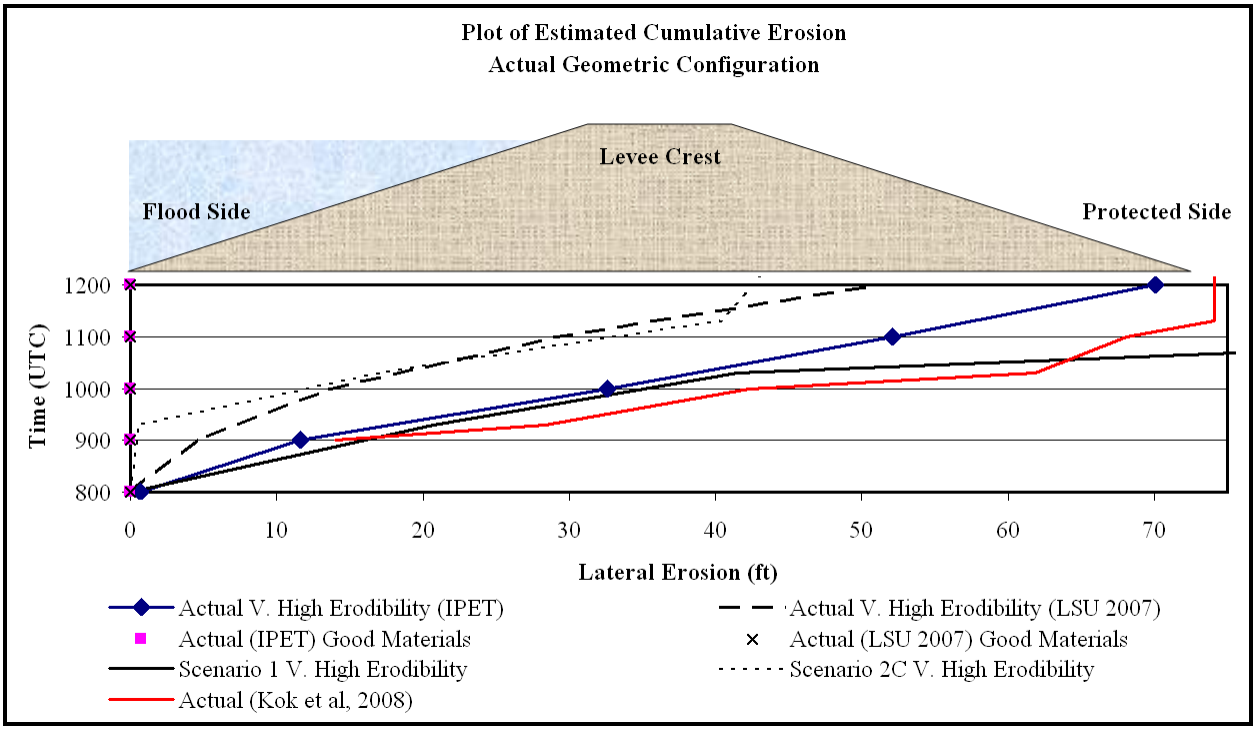


Figure 104: Comparison of lateral erosion for the actual EBSB configuration.

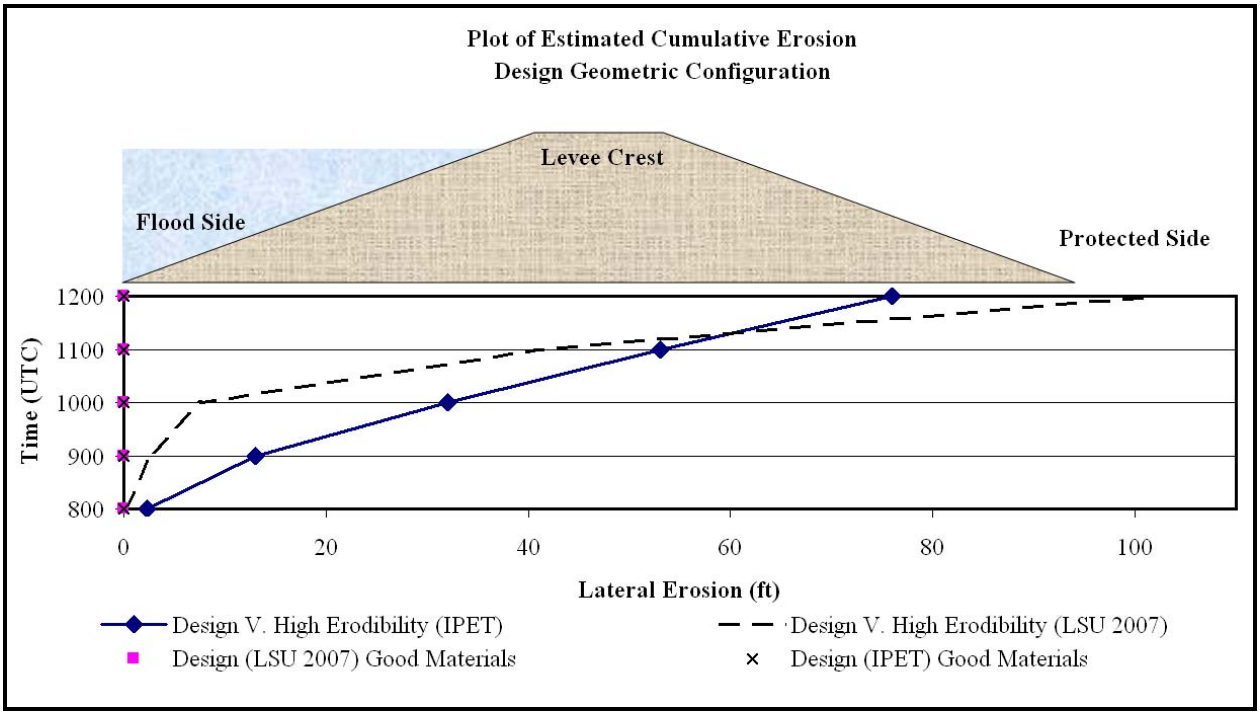


Figure 105: Comparison of lateral erosion for the design EBSB configuration.

These analyses confirm that levees constructed of 'good' materials with low erodibility would have performed significantly better than one constructed of high erodibility materials. Subjected to the same wave impacts, the levee with 'good' materials would have experienced insignificant erosion. It is also highly likely that the levee would have performed very well during overtopping conditions as well.

Erosion analyses were also performed accounting for velocities parallel (or 'current) to the EBSB flood-face. These current velocities were generated as a result of water flow through the MRGO and GIWW towards the IHNC and Lake Pontchartrain. The magnitude of the current velocity was on the order of 0.5 to 1 ft/s (Kok et al., 2008) at the face of the EBSB. Figure 106 shows the result of inclusion of the current velocities. There was no significant impact of this velocity component.

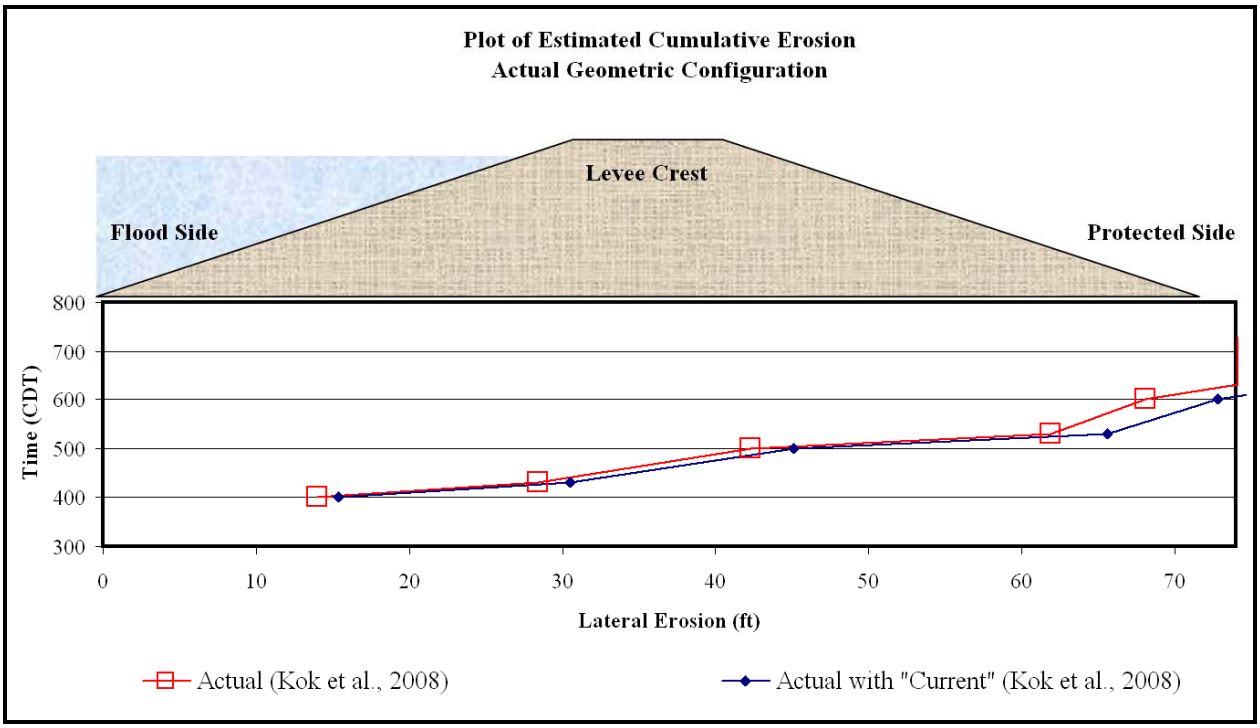


Figure 106: Comparison of lateral erosion with and without storm surge currents for the Kok et al., 2008 hydrodynamics. The storm surge currents negligibly increase the magnitude of lateral EBSB erosion.

XII. REVIEW OF POSSIBLE MR-GO WAVE-INDUCED EROSION SITES

Determination of Wave-Induced Erosion

This section of the report outlines features and characteristics associated with wave-induced erosion. Figure 107 shows a conceptual cross-sectional overview of wave-induced erosion in the EBSB (constructed with erodible materials).

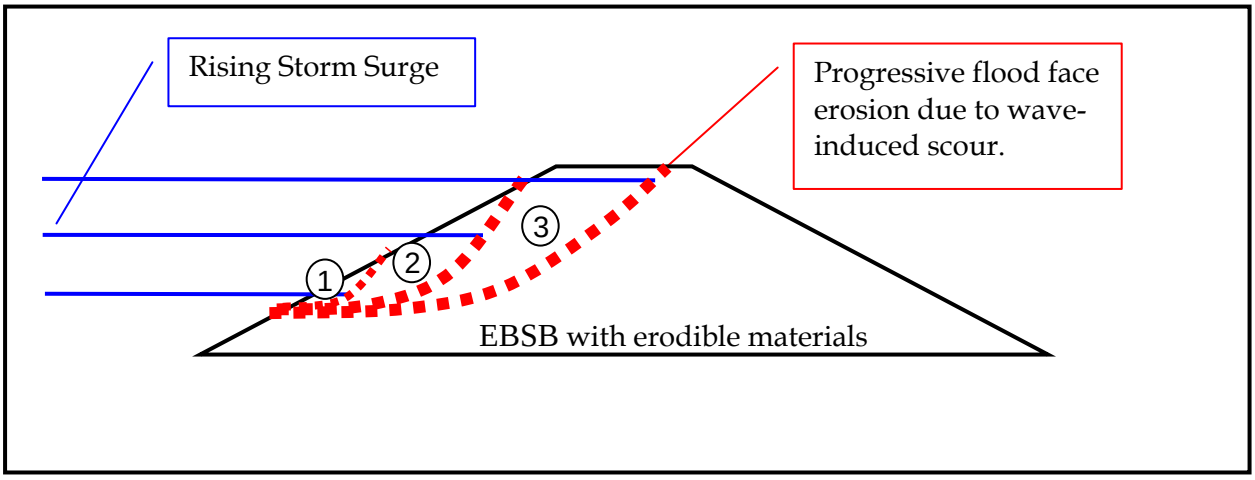


Figure 107: Scalping and notching of the EBSB flood side face, eventually resulting in breaching as waves impact the EBSB face during the rising hurricane storm surge.

A progressive failure horizon develops as the storm surge elevation increases with the approach of the hurricane. At step (1), the incident waves are small and the magnitude of erosion is small. As the storm surge rises, the erosion envelope grows until the storm surge reaches the crest of the levee step (3) and the EBSB is breached from a combination of wave-induced erosion and overtopping.

This potential coastal levee/EBSB failure mode was also identified in Bruun (1985). Figure 108 shows the progressive wave-induced erosion from wave attack. The longer the earthen levees are exposed to wave attack, the more erosion is incurred and the more damage the levee receives.

Overtopping induced erosion was treated as a separate failure mechanism from wave-induced attack.

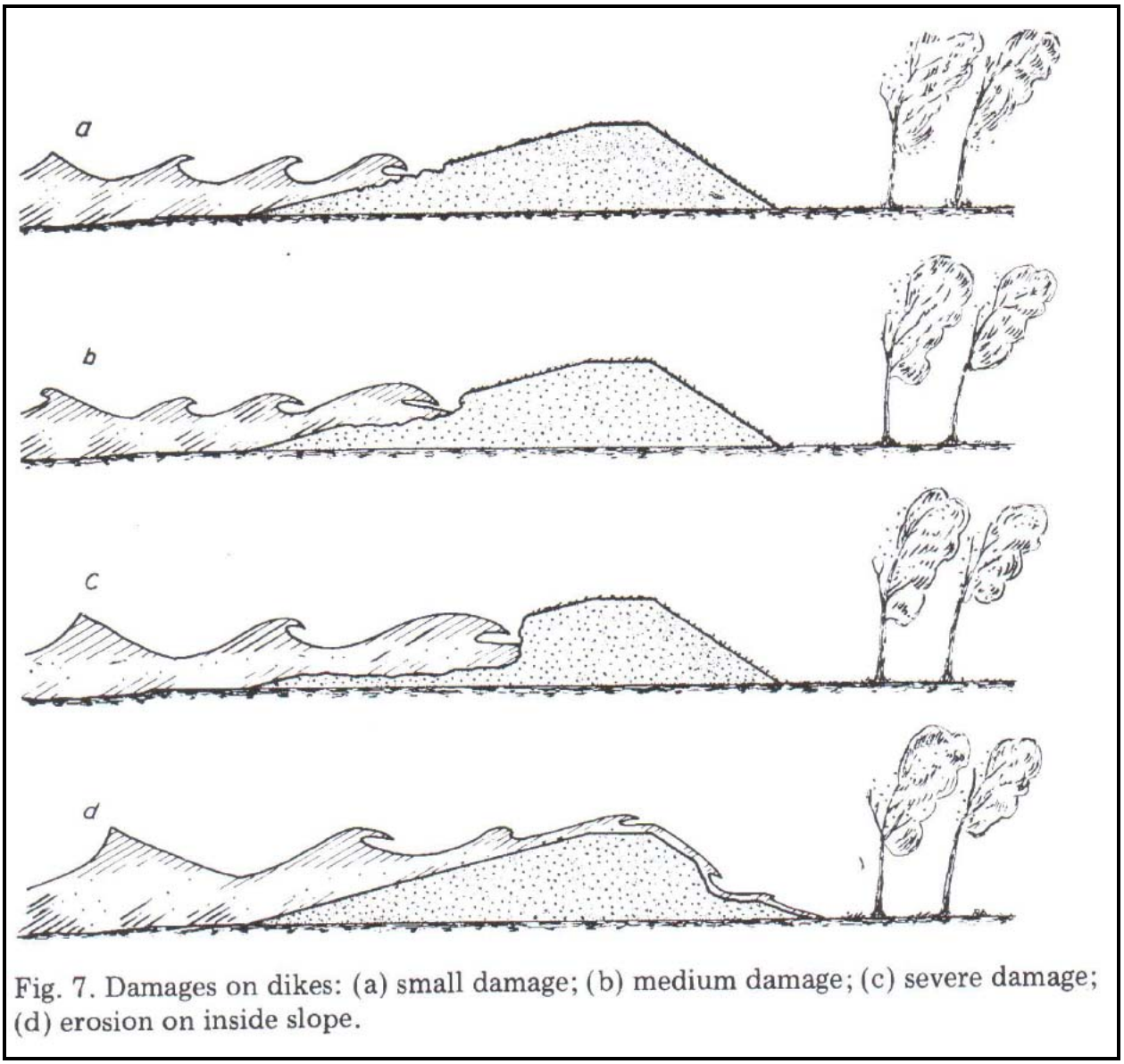


Fig. 7. Damages on dikes: (a) small damage; (b) medium damage; (c) severe damage; (d) erosion on inside slope.

Figure 108: Failure progression on flood face of coastal levees due to wave-induced notching and erosion (Bruun,1985).

IPET identified a four-stage progressive erosion development profile (Figure 109) for overtopping-induced erosion. This failure mechanism results in a 'ridge' on the flood side of the

levee. EBSBs that experienced wave-induced erosion would have an intact protected side and scoured flood side (as shown in Figure 110).

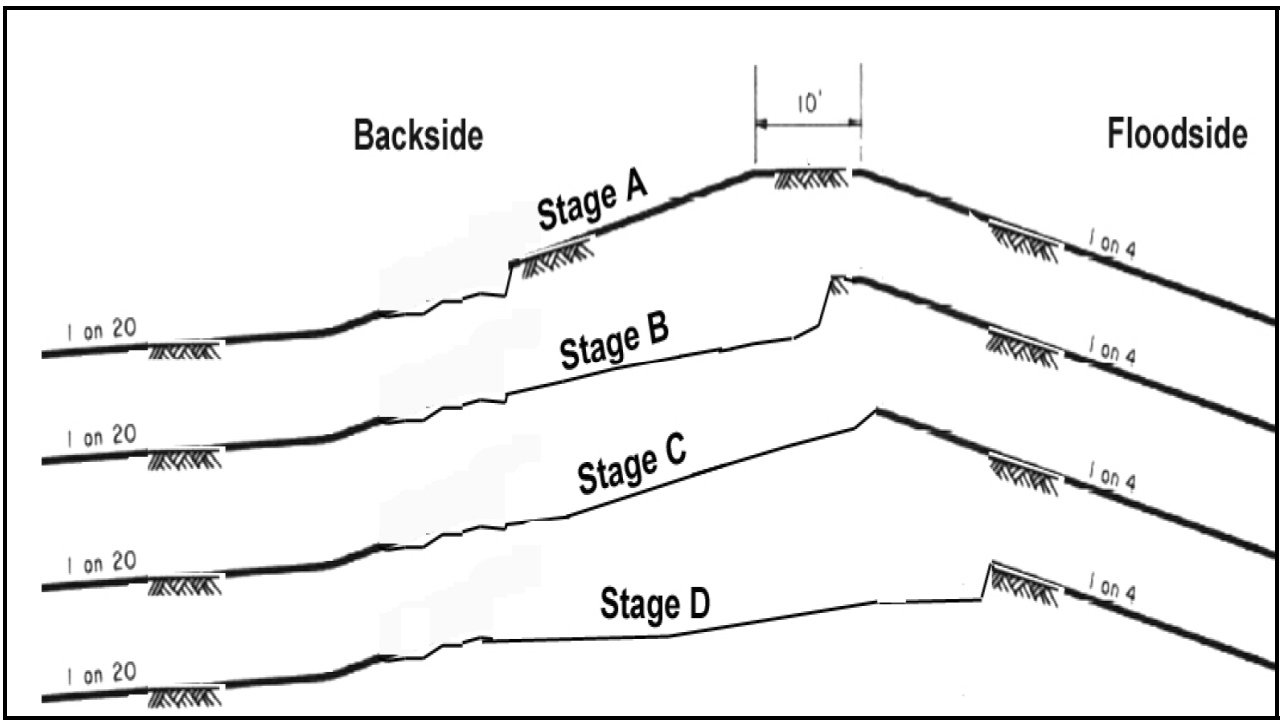


Figure 109: IPET provided an overtopping erosion development profile. Notice the remains of a 'ridge' on the flood side of the 'levee' following Stage D of overtopping induced erosion. This ridge is not present when erosion is initiated on the flood side of the EBSB (IPET, 2007d).

IPET (2007d) identified a location where only flood side notching occurred (Figure 110). This photograph clearly shows damage to the flood side of the EBSB and no visible damage on the protected side of the EBSB. This confirms it is possible and, in fact, wave induced erosion did occur on the MR-GO EBSB. The extent and prevalence of wave-induced erosion is still debatable since the required physical evidence has been 'washed' away. Thus, wave-induced erosion is a very possible occurrence and the photo-documentation demonstrates its occurrence during Hurricane Katrina.



Figure 110: IPET identified that there were locations where wave-induced erosion was observed with no overtopping-induced erosion. The location of this photograph was not specified by IPET (IPET, 2007d).

Insights into breaching mechanisms can be gained by the configuration of the study location following the hurricane (Figure 111). A healthy vegetative cover was observed after the hurricane. This vegetative cover extended past both the flood side and protected side EBSB toes of the 3.5:1 (horizontal:vertical) slopes.

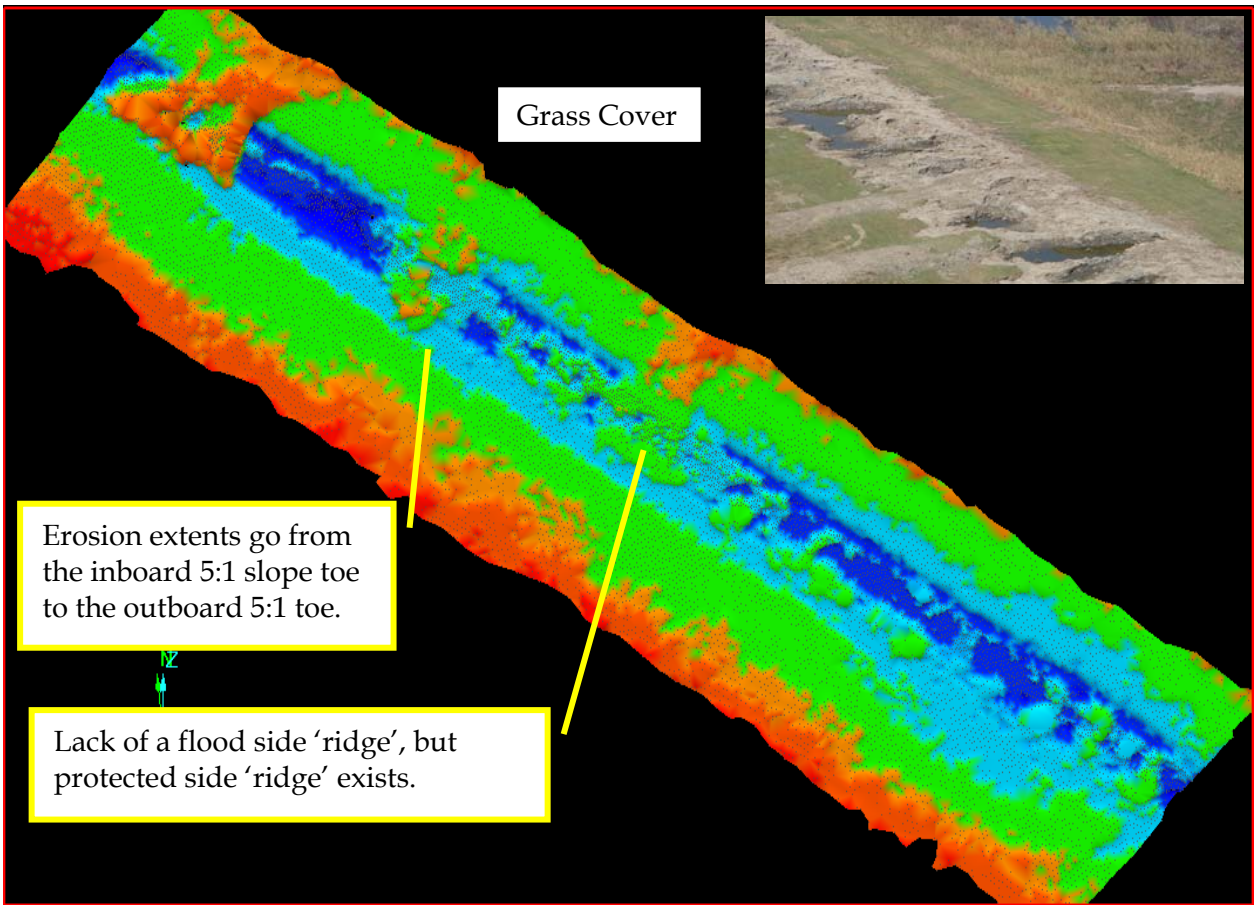


Figure 111: Aerial oblique view of a section of MR-GO EBSB that suffered extreme erosion and scour. This EBSB was constructed from highly erodible materials.

Topographic data collected by aerial LiDAR (Figure 111) confirms that major erosion occurred within the main body of the EBSB only, not on the outer shallow EBSB slope. There are locations where the flood side of the EBSB has been eroded all the way down to the flood side toe, but the protected side of the EBSB was not eroded all the way down to the toe. This implies that overtopping was not the main failure mode at this location as the protected side EBSB toe would be the first location eroded during overtopping conditions.

Possible Wave-Induced Erosion Sites

Locations along the MR-GO EBSB where scour and erosion occurred outboard of the EBSB centerline were considered possible wave-induced erosion sites. An examination of the 2005 aerial LiDAR surveys was conducted to identify these areas (Figure 112a) (Morris 2008). Based on our review, we found many sites possible wave-induced erosion sites. Detailed study of the aerial LiDAR survey data and photographs of the breach features (scarps, erosion paths) combined with results from the analyses detailed here, we identified areas in which there were features that suggested a combination of overtopping and wave action induced breaching. See Figure 112b for these locations.

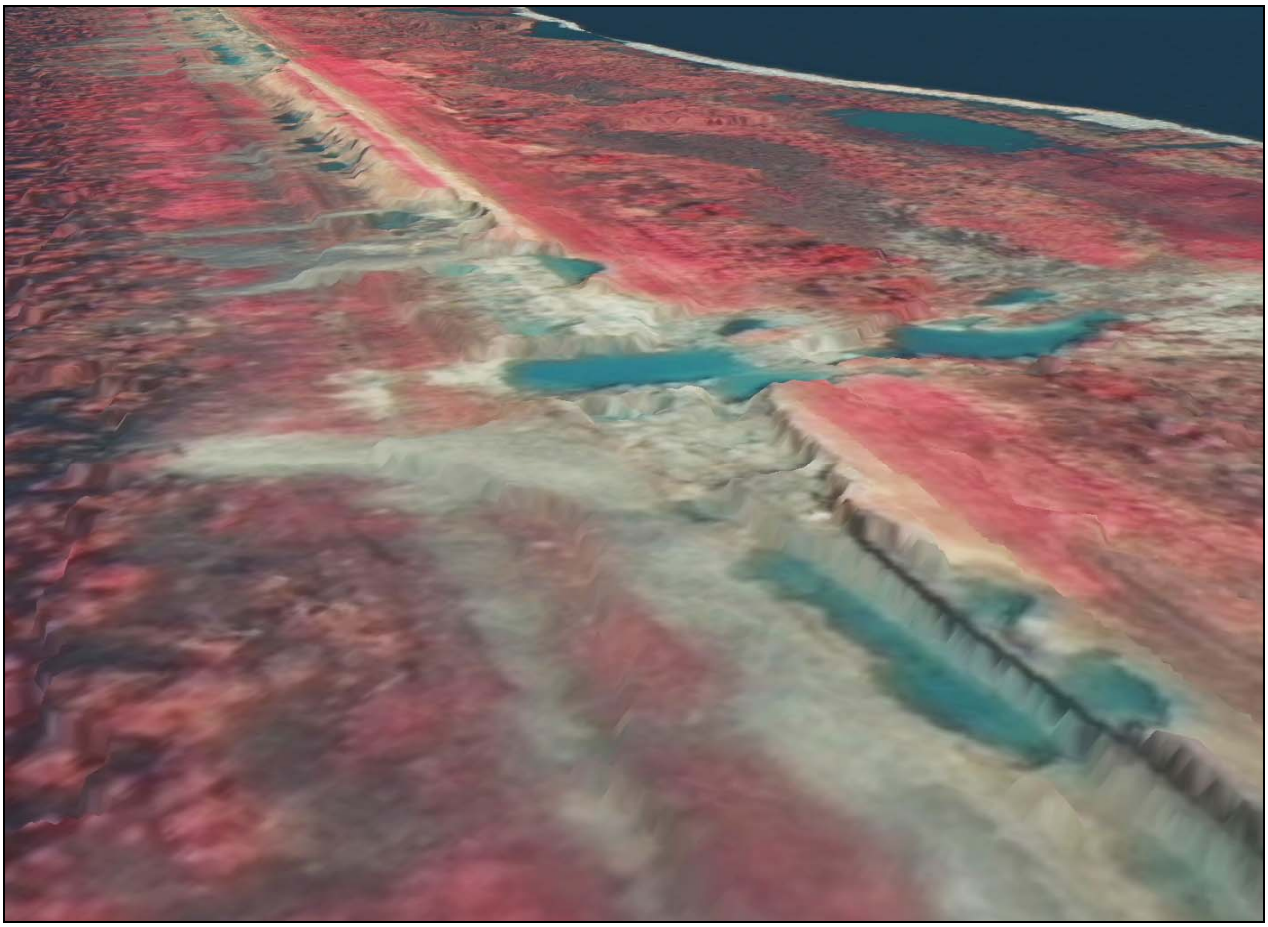


Figure 112a: Color Infra Red Photography Draped over Post Katrina LiDAR survey (Morris 2008).



Figure 112b: EBSB breach sites from wave-induced erosion and overtopping and wave erosion based on visual examinations of aerial LiDAR and photographic data.

Characteristics that were used to identify wave-induced erosion sites included regions with significant erosion but lack of a flood side EBSB toe ridge which would occur as a result of overtopping induced erosion creating a failure zone that propagates from the protected side EBSB to towards the flood side toe, areas with visible flood side notching, and zones with wider erosion extents on the flood side as compared with the protected side.

Analyses of the performance of the man-made flood protection structures located along MR-GO Reach 2 during Hurricane Katrina indicate that approximately 35 percent of the EBSBs along the Reach 2 alignment were breached due to attack by waves, 47 percent were breached by a combination of wave attack and surge overtopping – backside erosion (including sheet pile repair breaches), and 18 percent were overtopped but did not breach (sheet pile repair sections, Dupre and Bievenue navigation structures, some segments of the EBSBs). Analyses of the breaching that developed at the Bayou Dupre and Bayou Bienvenue navigation structure wing walls were determined to have been caused by overtopping erosion (section north of Dupre structure wing wall to EBSB connection) and by the combination of seepage, uplift and surge lateral forces (section south of Bievenue structure wing wall to EBSB connection).

XIII. COMPARISON WITH USACE ANALYSES

Results from this study were compared with draft results posted in a draft power point presentation prepared by Mr. Bruce Ebersole (USACE, Undated). Although the presentation did not have accompanying text, several of the graphics presented are useful to provide a basis of comparison.

As can be seen in Figure 113, there was evidence that wave-induced notching occurred without overtopping induced levee protected side erosion. Figure 114 clearly shows that even with overtopping conditions, the only ‘damage’ incurred to the levee at this (location not specified)

was on the outboard face. The erosion profile also well-resembles the erosion profile indicated in Figure 108 of this report.

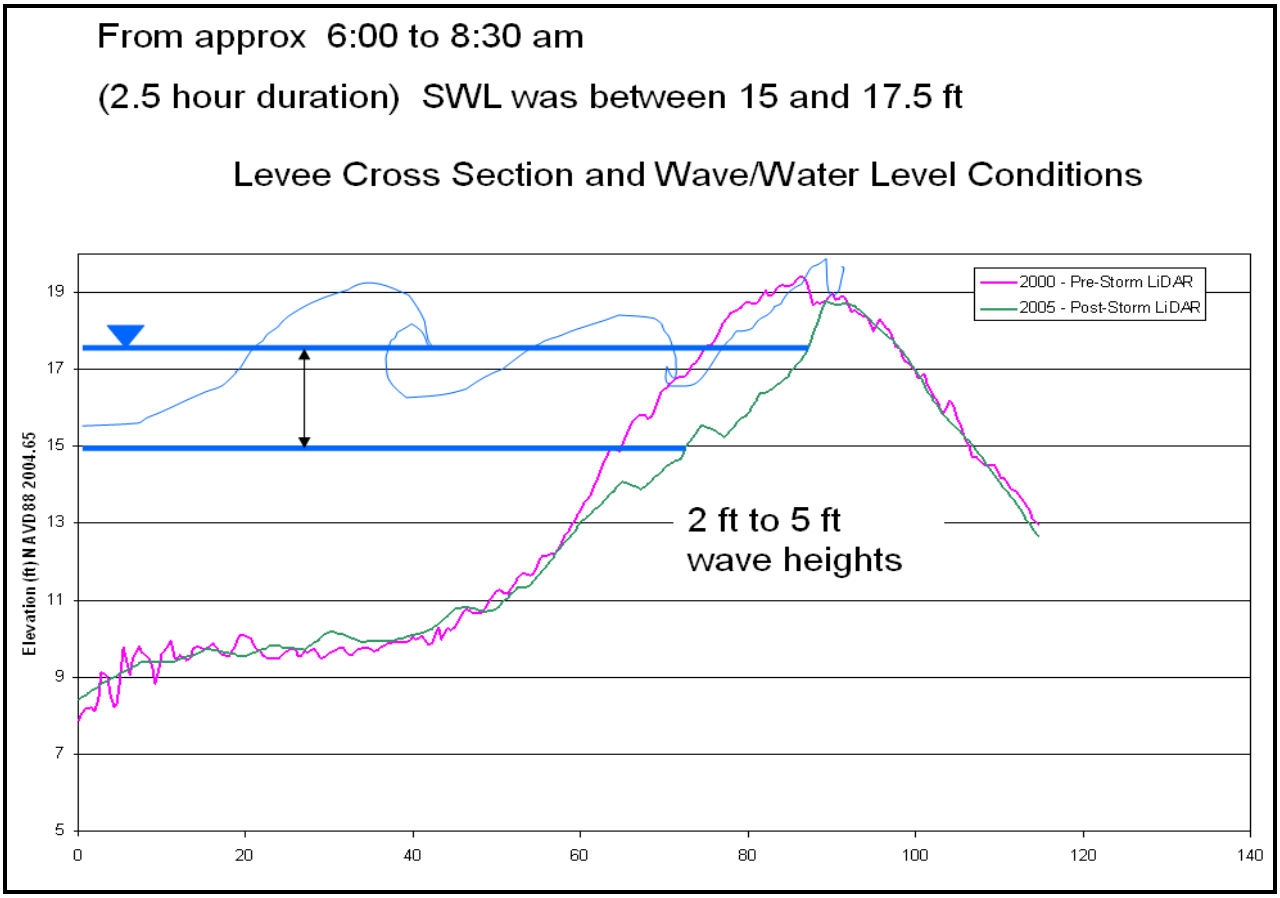
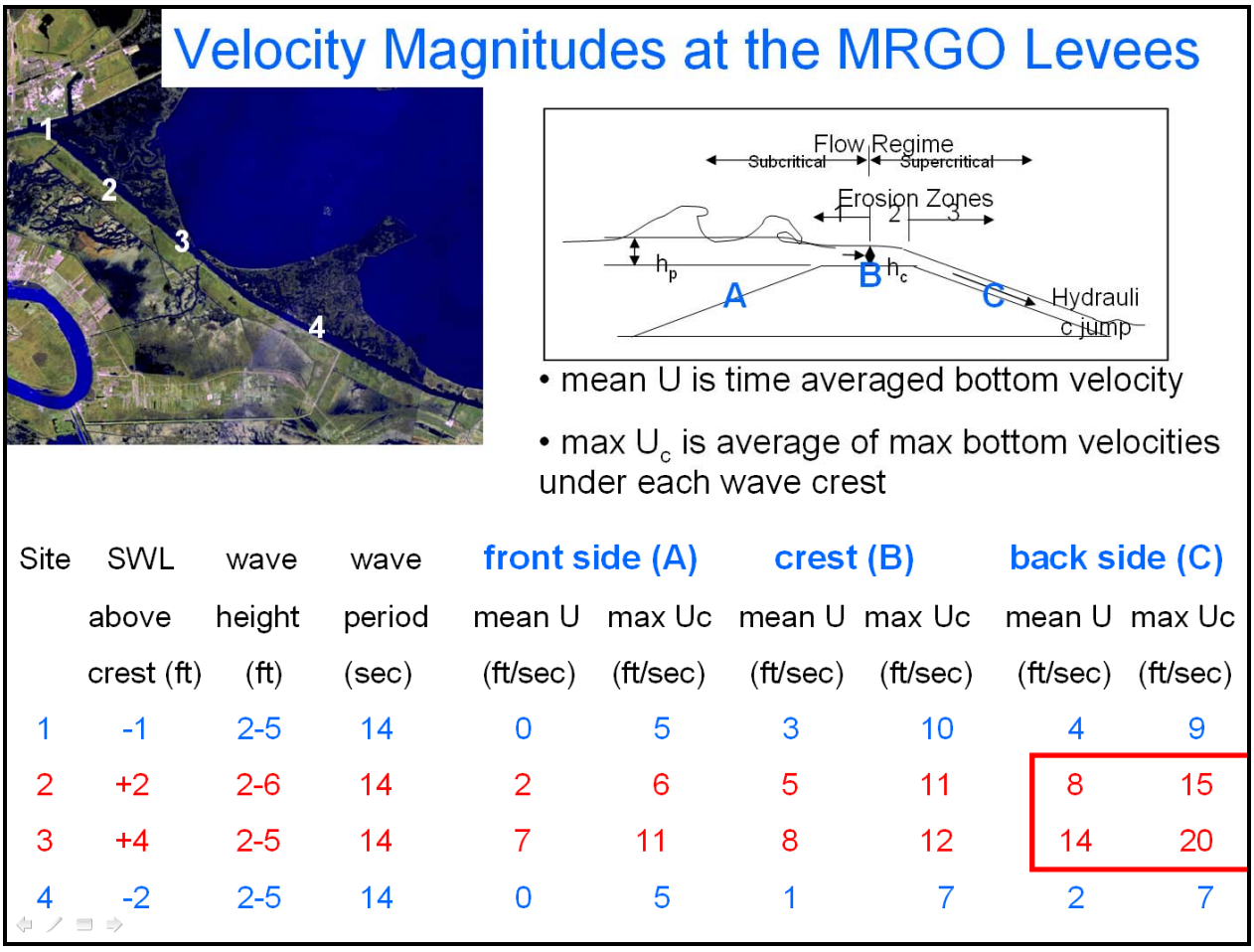


Figure 113: Pre and Post Aerial LiDAR are highlighted to show wave-induced notching of the levee (USACE, Undated).

An examination of the estimated velocities also match the results of our analyses for the considered storm sure still water elevations (Figure 114). It is important to note that our evaluations found that higher flood side velocities were encountered at lower storm surge elevations, where incident waves caused 'runup' and 'rundown' conditions, resulting in large transient levee face velocities (these 'runup' and 'rundown' velocities are also empirically validated based on Bruun, 1985).



Site	SWL above crest (ft)	wave height (ft)	wave period (sec)	front side (A) mean U (ft/sec)	front side (A) max Uc (ft/sec)	crest (B) mean U (ft/sec)	crest (B) max Uc (ft/sec)	back side (C) mean U (ft/sec)	back side (C) max Uc (ft/sec)
1	-1	2-5	14	0	5	3	10	4	9
2	+2	2-6	14	2	6	5	11	8	15
3	+4	2-5	14	7	11	8	12	14	20
4	-2	2-5	14	0	5	1	7	2	7

Figure 114: Velocity ranges for the flood side, crest, and protected sides of the levee as calculated by the USACE (USACE, Undated) for storm surge elevations near the levee crest elevation.

These independently derived conclusions by the USACE appear to confirm the analytic results found in this study. As noted in Section XV, additional model calibration and validation studies should be commissioned to validate the analyses based on actual field data as opposed to simulated and scaled-laboratory testing results.

XIV. MODEL CALIBRATION AND VALIDATION

No detailed site-specific model calibration was performed for this study due to the lack of actual data during Hurricane Katrina. The primary means for model validation was the actual

performance of the EBSB in the study area coupled with available pre- and post-storm data such as estimated hydrodynamics, topography (based on Aerial LiDAR surveys in 2000 and 2005), soil borings, design documentation, and construction drawings.

Velocities determined by LSDYNA were compared with velocity estimates from IPET (2007a) and were found to be in general agreement. IPET found protected side velocities to be on the order of 5-10 ft/s, which match well with our predicted range of 5-10 ft/s. IPET did not calculate wave-induced erosion, so it was not possible to compare our calculated erosion magnitudes with IPET estimates.

To validate the magnitude of LSDYNA simulated peak runup/rundown velocities, empirical correlations (Bruun, 1985) were used. The peak empirical wave runup/rundown velocity was compared with the peak LSDYNA wave runup/rundown velocity (from all monitored node elevations). The velocity at 0830 CDT was not evaluated as the EBSB had been overtopped by this time. The comparison is presented in Table 32 for the Scenario 1 hydrodynamics and Table 33 for the Scenario 2C hydrodynamics.

Table 32: Comparison of LSDYNA Peak Velocities with Empirical Correlations for Scenario 1 (Actual MR-GO) hydrodynamics

Time (CDT)	**Storm Surge Elevation (ft)**	**LSDYNA Peak Velocity (ft/s)**	**Empirical Peak Velocity (ft/s)**	**Velocity Agreement**
0430	+10.1	10	14.4	Underpredicts
0530	+12.0	12	16.8	Underpredicts
0630	+14.2	15**	18.4	Underpredicts
0730	+16.6	14**	20.0	Underpredicts

Table 33: Comparison of LSDYNA Peak Velocities with Empirical Correlations for Scenario 2C (Neutral MR-GO) hydrodynamics

Time (CDT)	Storm Surge Elevation (ft)	LSDYNA Peak Velocity (ft/s)	Empirical Peak Velocity (ft/s)	Velocity Agreement
0430	+9.9	4	10.1	Underpredicts
0530	+11.8	6	11.3	Underpredicts
0630	+14.0	4**	12.5	Underpredicts
0730	+16.2	3**	12.8	Underpredicts

The majority of LSDYNA simulated cases developed wave runup/rundown peak velocities below the maximum velocity predicted by empirical methods. For high storm surges (that result in active wave-overtopping and noted with a ** in the above tables), the LSDYNA velocity values greatly underpredict the maximum velocity. This is a result of the geometric configuration of the EBSB. The Brunn values assume no overtopping (and resulting dissipation of energy), whereas the actual modeled condition results in active overtopping, thus resulting in decreased maximum uprush/downrush velocities. For those storm surge elevations where there is no wave-induced overtopping, the LSDYNA and empirical velocity values are in very close agreement.

XV. REFERENCES

Bea, Robert Glenn. 2008a. "Robinson v. United States. Expert Report of Dr. Robert Glenn Bea. Engineering Forensic Studies of Performance of the Man-Made Features Bordering the Mississippi River-Gulf Outlet (MR-GO) during Hurricane Katrina." Dated July 11, 2008.

Bea, Robert Glenn. 2008b. "Robinson v. United States. Expert Report of Dr. Robert Glenn Bea. Engineering Forensic Studies of Performance of the Man-Made Features Bordering the Mississippi River-Gulf Outlet (MR-GO) during 'Neutral' MR-GO Hurricane Katrina Conditions." Dated July 11, 2008.

Bruun, Per. 1985. Design and Construction of Mounds for Breakwaters and Coastal Protection. Developments in Geotechnical Engineering; 37. Elsevier Science Publishers, B.V. Amsterdam.

Coastal Environments, Inc (CEI). 1984. "The Mississippi River Gulf Outlet: A Study of Bank Stabilization." Prepared for: St. Bernard Parish Police Jury, Ashley Henderson, President; U.S. Department of Commerce, National Oceanic and Atmospheric Administration; and State of Louisiana, Department of Natural Resources, Coastal Management Section. Dated December, 1984.

de Wit, L., B. Maaskant, M. Kok, and J.K. Vrijling. "Flow Modeling New Orleans – Mississippi River Gulf Outlet, Hurricane Katrina, August 2005." TU Delft and SVASEK. Final Draft Rev2 Report. May 30, 2008. Ref: LdW/1474/08202/B.

Gautier, C., M. Kok, and J.K. Vrijling. "Wave Modeling New Orleans – Mississipi River Gulf Outlet, Hurricane Katrina August 2005. SWAN Results Scenario 1B (=with FINEL water levels)." TU Delft and SVASEK. May 30, 2008a. Ref: cg/1474/08209.

Gautier, C., M. Kok, and J.K. Vrijling. "Wave Modeling New Orleans – Mississipi River Gulf Outlet, Hurricane Katrina August 2005. SWAN Results Scenario 2C." TU Delft and SVASEK. May 30, 2008b. Ref: cg/1474/08201.

Hewlett, H.W.M., L. A. Boorman, and M. E. Bramley. "Design of Reinforced Grass Waterways." Construction Industry Research and Information Association. London. 1987.

Independent Levee Investigation Team (ILIT). 2006. "Investigation of the Performance of the New Orleans Flood Protection System in Hurricane Katrina on August 29, 2005." University of California, Berkeley. Dated July 31, 2006. Available from: www.ce.berkeley.edu/~new_orleans. Date accessed: August 20, 2007.

Interagency Performance Evaluation Team. 2007a. "Performance Evaluation of the New Orleans and Southeast Louisiana Hurricane Protection System. Final Report of the Interagency Performance Evaluation Task Force. Volume IV – The Storm. Final." Dated March 29, 2006. Available from: https://ipet.wes.army.mil/.

_____. 2007b. "Performance Evaluation of the New Orleans and Southeast Louisiana Hurricane Protection System. Final Report of the Interagency Performance Evaluation Task Force. Volume IV – The Storm – Technical Appendix. Final." Dated March 29, 2006. Available from: https://ipet.wes.army.mil/.

_____. 2007c. "Performance Evaluation of the New Orleans and Southeast Louisiana Hurricane Protection System. Final Report of the Interagency Performance Evaluation Task Force.

Volume II – Geodetic Vertical and Water Level Datums. Final." Dated March 26, 2006. Available from: https://ipet.wes.army.mil/.

_____. 2007d. "Performance Evaluation of the New Orleans and Southeast Louisiana Hurricane Protection System. Final Report of the Interagency Performance Evaluation Task Force. Volume V – The Performance – Levees and Floodwalls. Final." Dated June 2007. Available from: https://ipet.wes.army.mil/.

_____. 2007e. "Performance Evaluation of the New Orleans and Southeast Louisiana Hurricane Protection System. Final Report of the Interagency Performance Evaluation Task Force. Volume V – The Performance – Levees and Floodwalls. Appendices 16 - 23. Final." Dated June 2007. Available from: https://ipet.wes.army.mil/.

Kok, M., B. Maaskant and L. de Wit. "Flow Modeling New Orleans MRGO. Katrina Event August 2005 – Preliminary Results." TU Delft and Svasek Hydraulics. April 18, 2008.

Lematire, J. and Desmorat, R. (2005). *Engineering Damage Mechanics*, Springer Verlag, New York.

Livermore Software Technology Corporation (LSTC) . 2007. "LS-DYNA." Available from: www.lstc.com. Date accessed: August 20, 2007.

Louisiana State University (LSU). "What to tell your students for Bob Bea 27th November 2007." Primary author: Dr. Ivor van Heerden. 2007.

Louisiana State University (LSU). "Hydrograph 1 - Katrina Hydrographs constructed from composite High Water Marks, ADCIRC S08 Model, Lockmasters Staff, Partial gage data." Primary author: Dr. Ivor van Heerden. April 2008.

Morris, C. A. (2008). *Survey and Spatial Data In the Vicinity of the Mississippi River Gulf Outlet (MR-GO),* Report prepared for Plaintiffs in Robinson v. United States, CMor Consulting LLC, Baton Rouge, Louisiana.

Munson, Bruce R., Donald F. Young, and Theodore H. Okiishi. 1998. Fundamentals of Fluid Mechanics. Third Edition. John Wiley and Sons. New York.

National Engineering Science Company (NESCO). 1966. "Storm Surge Effects of the Mississippi River Gulf Outlet, Study A." Contract No. DA-16-047-CIVENG-66-316. NESCO Report SN-326-A. September 9, 1966.

Seijffert, Jan Willem and Hank Verheij. 1999. "Chapter 14. Grass Covers and Reinforcement Measures." Rijkswaterstaat, Hydraulic Engineering Division, Delft. Pages 289 – 302.

Technical Advisory Committee for Flood Defense in the Netherlands (TAW). 1999. "Grass Cover as a Dike Revetment."

United States Army Corps of Engineers. 1958a. "Geologic Investigation of the Mississippi River Gulf Outlet." Miscellaneous Paper No. 3-259. February 1958.

_____. 1958b. "Mississippi River Gulf Outlet Design Memorandum No. 1-B, Channels, Mile 39.01 to Mile 63.77."

_____. 1965. "Report on Hurricane Betsy, September 8-11, 1965 in the U.S. Army Engineer District, New Orleans." November 1965.

_____. 1966a. "Lake Pontchartrain, LA and Vicinity, Chalmette Area Plan, Design Memorandum No. 3, General Design." Prepared by Waldemar S. Nelson & Company, Inc., Engineers & Architects, New Orlenas, LA and U.S. Army Engineer District, New Olreans, Corps of Engineers, U.S. Army, New Orleans, LA. November 1966.

_____. 1966b. "Lake Pontchartrain and Vicinity, Louisiana, Design Memorandum No. 12, Sources of Construction Materials." Prepared in the office of the District Engineer, New Orleans District, Corps of Engineers, New Orleans, Louisiana. June 1966.

_____. 1967a. "Hurricane Protection Levee, First Lift, Sta 594+00 - Sta 770+11." DACW29-67-B-0136.

_____. 1967b. "Hurricane Protection Levee, First Lift, Sta 368+00 - Sta 570+00." DACW29-67-B-0134.

_____. 1968. "Hurricane Protection Levee, First Lift, Sta 387+40 - Sta 523+00 (Not Continuous)." DACW29-68-B-0064.

_____. 1970. "Report on Hurricane Camille, 14-22, August 1969." New Orleans, Louisiana. May 1970.

_____. 1972. "Hurricane Protection Levee, Chalmette Area Plan, Sta 370+00 to Sta 682+00." DACW29-72-B-0137.

_____. 1980. "Hurricane Protection Levee, First Enlargement, Sta 360+70 to Sta 699+00 (non continuous)." DACW29-80-B-0151.

_____. 1983. "Hurricane Protection Levee, Bayou Bienvenue to Bayou Dupre Levee Closures, Orleans and St. Bernard Parish, LA." DACW29-83-5-0012.

_____. 1985. "Hurricane Protection Levee Second Enlargement MR-GO B/L Sta 380+50 to Sta 692+50." DACW29-85-B-0073.

_____. 1987. "Chalmette Area Plan, Hurricane Protection Levee Closures, MR-GO B/L Sta 367+60 to Sta 1005+49." DACW29-87-B-0014.

_____. 1992. "Lake Pontchartrain Louisiana and Vicinity Chalmette Area Plan, Hurricane Protection Levee Closures, Sta 366+00 C/L to Sta 1007+91 CL." DACW29-92-B-0061.

_____. 2004. Computer Program: CORPSCON 6.0.1. Developed by Engineer Research and Development Center, Topographic Engineering Center. Available from: www.tec.army.mil.

_____. 2005. "Lake Pontchartrain Louisiana and Vicinity Chalmette Area Plan, Hurricane Protection Levee, Emergency Restoration B/L Sta 383+00 to Sta 704+00." Solicitation No. W912P8-05-R-0063.

_____. 2006. "Lake Pontchartrain Louisiana and Vicinity Chalmette Area Plan Emergency Restoration, Levee Restoration East of Bayou Dupre, MR-GO B/L Sta 714+55 to Sta 1007+91." Solicitation No. W912P8-06-R-0002.

_____. 2006b. "Coastal Engineering Manual: Part II, Chapter 1, Water Wave Mechanics." EM 1110-2-1100.

_____. 2006c. "Coastal Engineering Manual: Part VI, Chapter 5, Fundamentals of Design." EM 1110-2-1100.

_____. Undated. "Draft – in progress work. Hydrodynamic Loadings and Levee/Wall Response Along the Navigation Channels." Power Point Presentation. Prepared by Bruce Ebersole. Coastal Hydraulics Laboratory.

United States Department of Transportation (FHWA). 1988. Design of Roadside Channels with Flexible Linings. Hydraulic Engineering Circular No. 15. Publication No. FHWA-IP-87-7. Research, Development, and Technology, Turner –Fairbank Highway Research Center, 6300 Georgetown Pike, McLean, Virginia.

United States Geological Survey. 1951. "Chalmette Quardrangle, Louisiana." 7.5-Minute Series (Topographic).

_____. 1967. "Chalmette Quardrangle, Louisiana." 7.5-Minute Series (Topographic).

_____. 1972. "Chalmette Quardrangle, Louisiana." 7.5-Minute Series (Topographic).

University of California, Berkeley. 2006. "UC Berkeley ILIT MR-GO Borings." – Unpublished.

XVI. APPENDIX A – PARAMETRIC STUDIES OF EBSB EROSION

IPET and LSU (2007) Hydrodynamic Conditions

IPET Hydrodynamics

Wave impact modeling was performed by IPET (2007a) along the MR-GO EBSB and the hydrodynamic results from these numerical analyses were used as input to our wave-induced erosion/scour analyses. Additional hydrodynamic studies were performed by LSU (2007) in the Lake Borgne area. These two sources of hydrodynamic characteristics were used for this study.

Information on IPET (2007a) derived hydrodynamics were linearly interpolated to develop site specific characteristics. IPET calculated the storm surge elevation (still water level), significant wave height, and wave periods at four locations (Station 430+00; Station 540+00; Station 670+00; and Station 880+00) along the MR-GO reach.

The study site for these analyses is located at approximately Station 497+00, so the interpolated value between the IPET (2007b) results at Station 430+00 and Station 540+00 (which is approximately Station 485+00) was used. This approach assumes that a linear relationship exists for the storm surge and peak wave period between Stations. A summary of the storm surge elevations, peak wave periods, as well as velocity calculations from IPET (2007b) at Station 430+00 and Station 540+00 are presented in Figures C1 and C2, respectively. Plots of the interpolated IPET-based significant wave height, wave period, and storm surge are presented in Figures C3 through C5.

The LSU hydrodynamics were developed by using peak wave period and significant wave heights as determined by van Heerden (LSU, 2007) and scaling the IPET hydrodynamic time histories to match these peak values. The resulting hydrodynamics are shown in Figures C6 through C8.

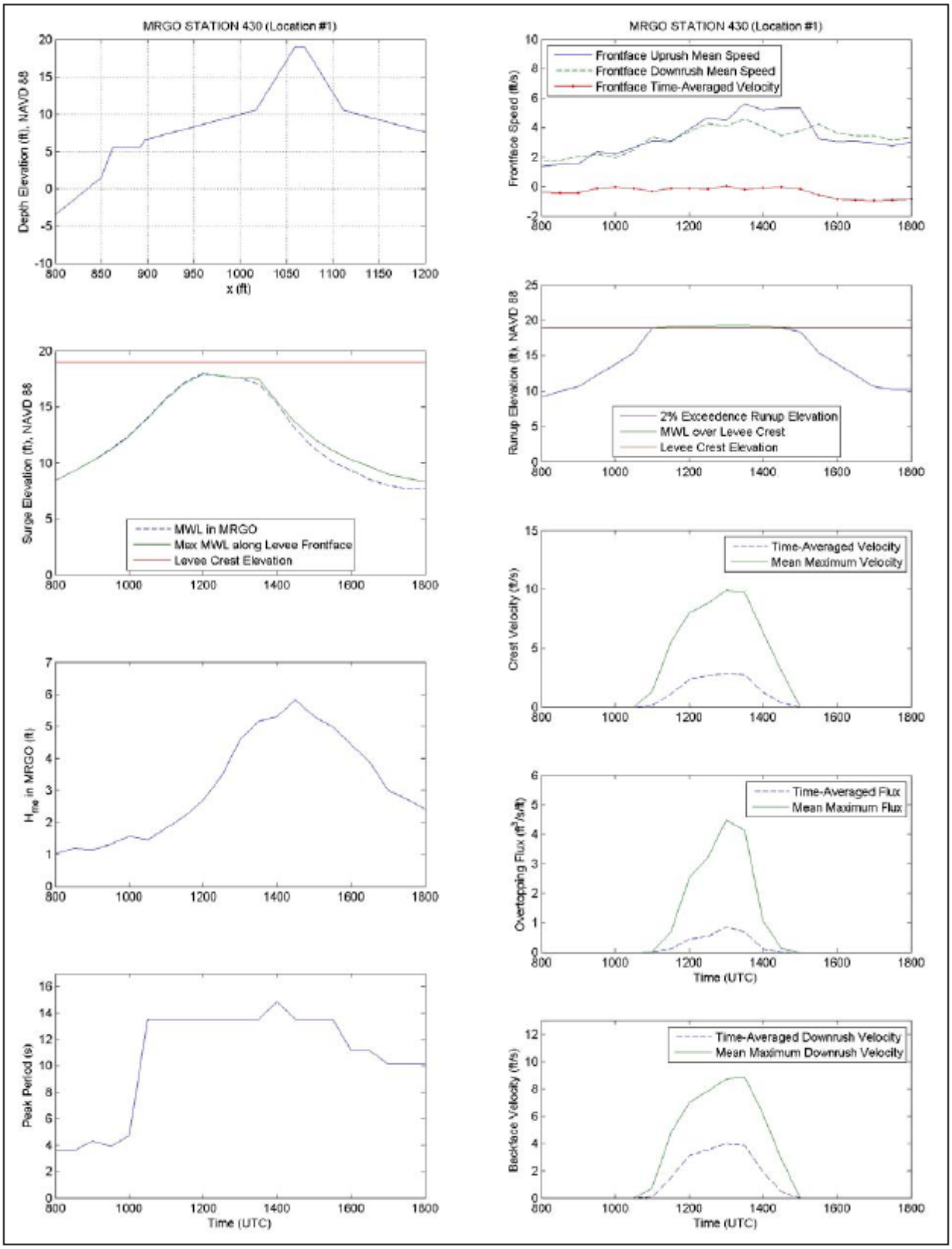


Figure C1: A summary of hydrodynamic calculations at MR-GO Station 430+00 (IPET, 2007b).

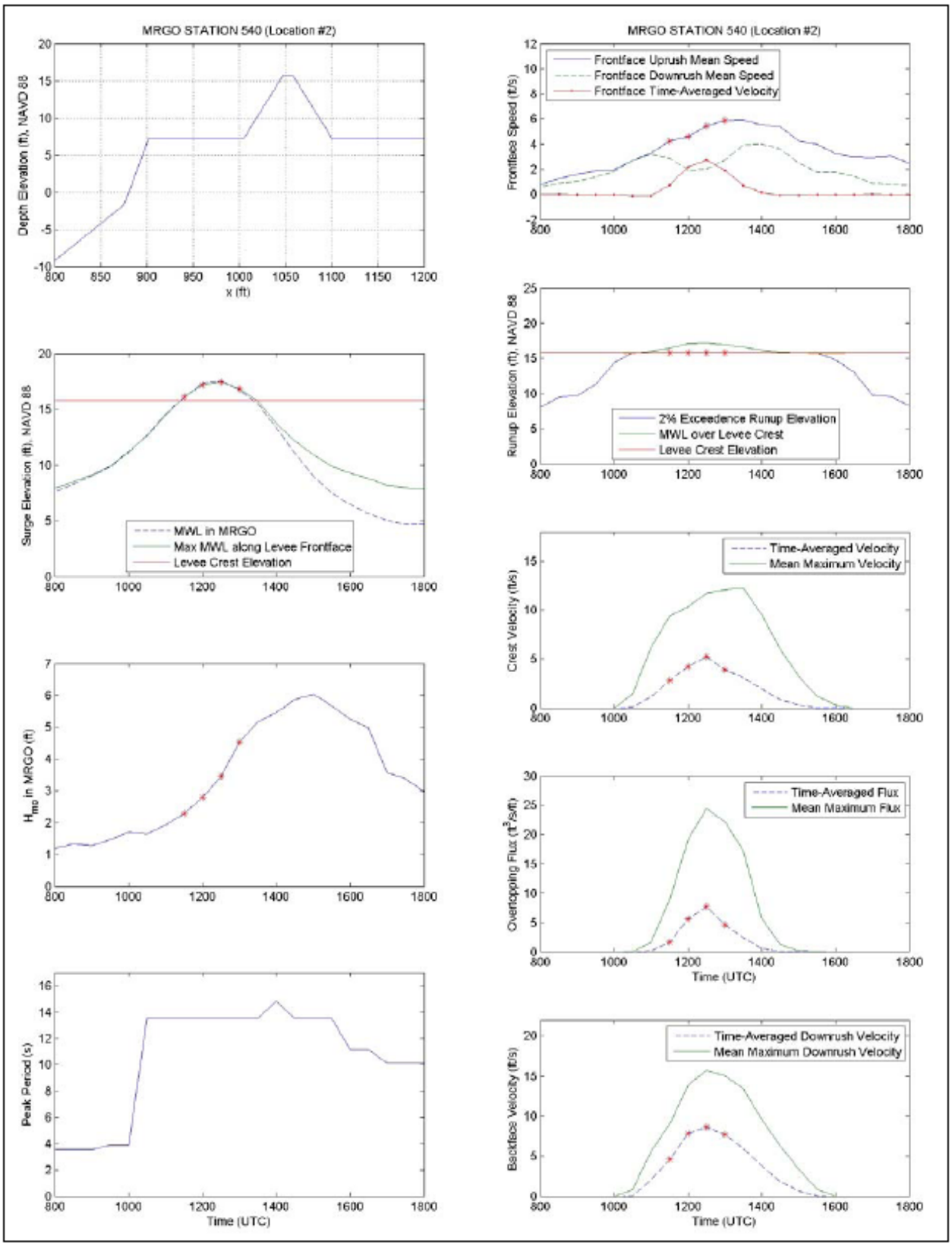


Figure C2: A summary of hydrodynamic calculations at MR-GO Station 540+00 (IPET, 2007b).

According to the IPET (2007a) study, hurricane storm surge levels were taken from a combination of ADCIRC time series calculations and measured high watermark elevations. The ADCIRC modeling was found to be an average of 2.6 feet lower than the measured high watermarks, so IPET (2007a) linearly increased the ADCIRC values starting 2 hours before the peak of the storm (0 feet) to the ADCIRC value plus 2.6 feet at the peak of the storm, then back down to the ADCIRC calculated value beyond 2 hours after the peak of the storm.

Incident wave conditions were based on the 95 percent STWAVE modeling results just offshore of the MR-GO levees. Wave conditions at select times between 0630 and 1500 (UTC) on August 29, 2005 were used as the basis for simulation of quasi-semi steady state conditions.

The topography of the EBSBs and surrounding terrain used by IPET (2007a) in their hydrodynamic modeling was based on geometry defined in the "Lake Pontchartrain, LA and Vicinity Design Memorandum No. 3," dated November 1966. The EBSB profiles were shifted vertically to match the EBSB crest elevations from pre-Katrina LiDAR surveys.

As previously mentioned, the study site for these analyses is located at approximately Station 497+00, so the IPET (2007a) results at Station 430+00 and Station 540+00 were linearly interpolated to determine values at the study Station (497+00).

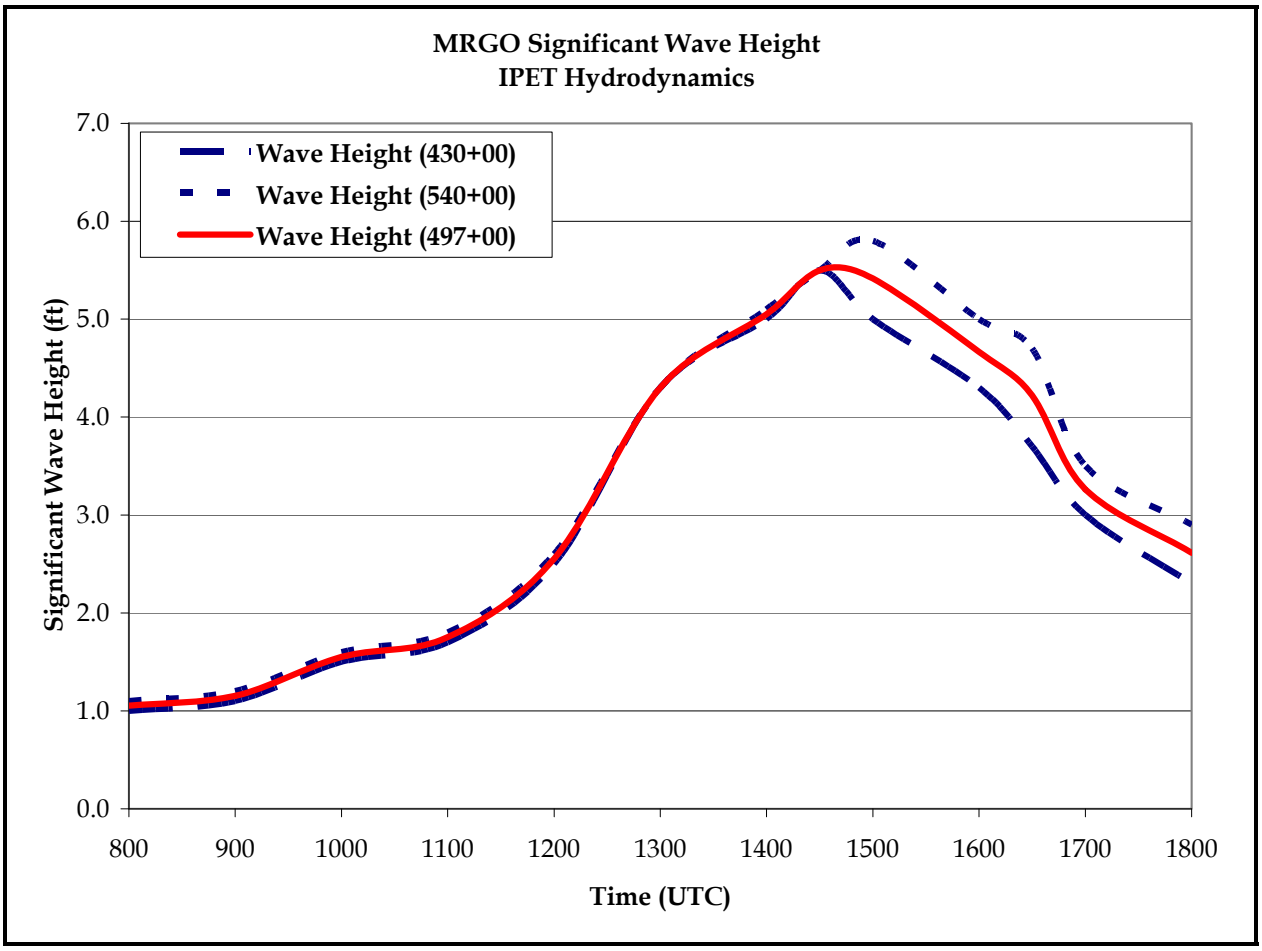


Figure C3: Significant wave height time history as determined based on IPET (2007a).

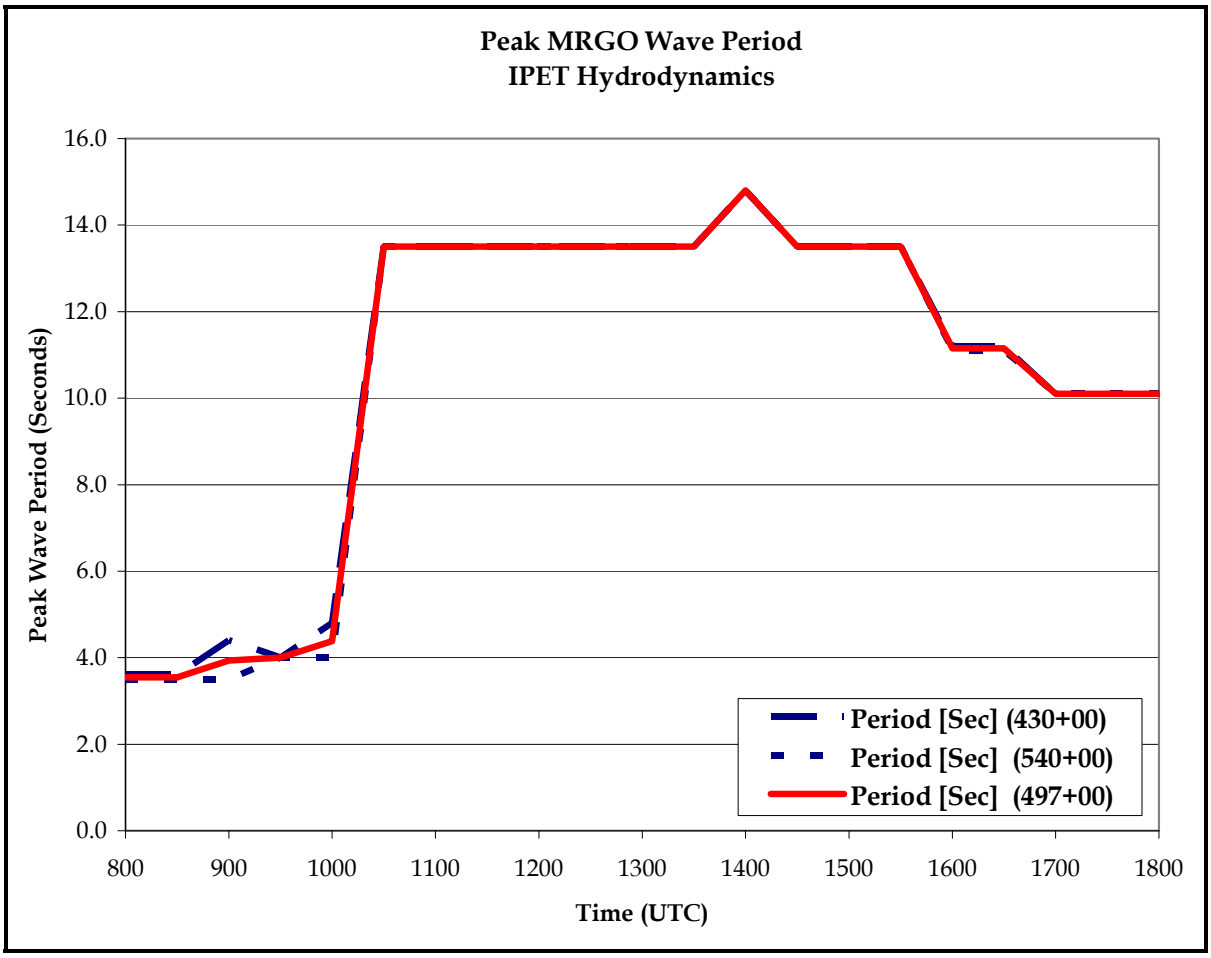


Figure C4: Wave period time history as determined based on IPET (2007a).

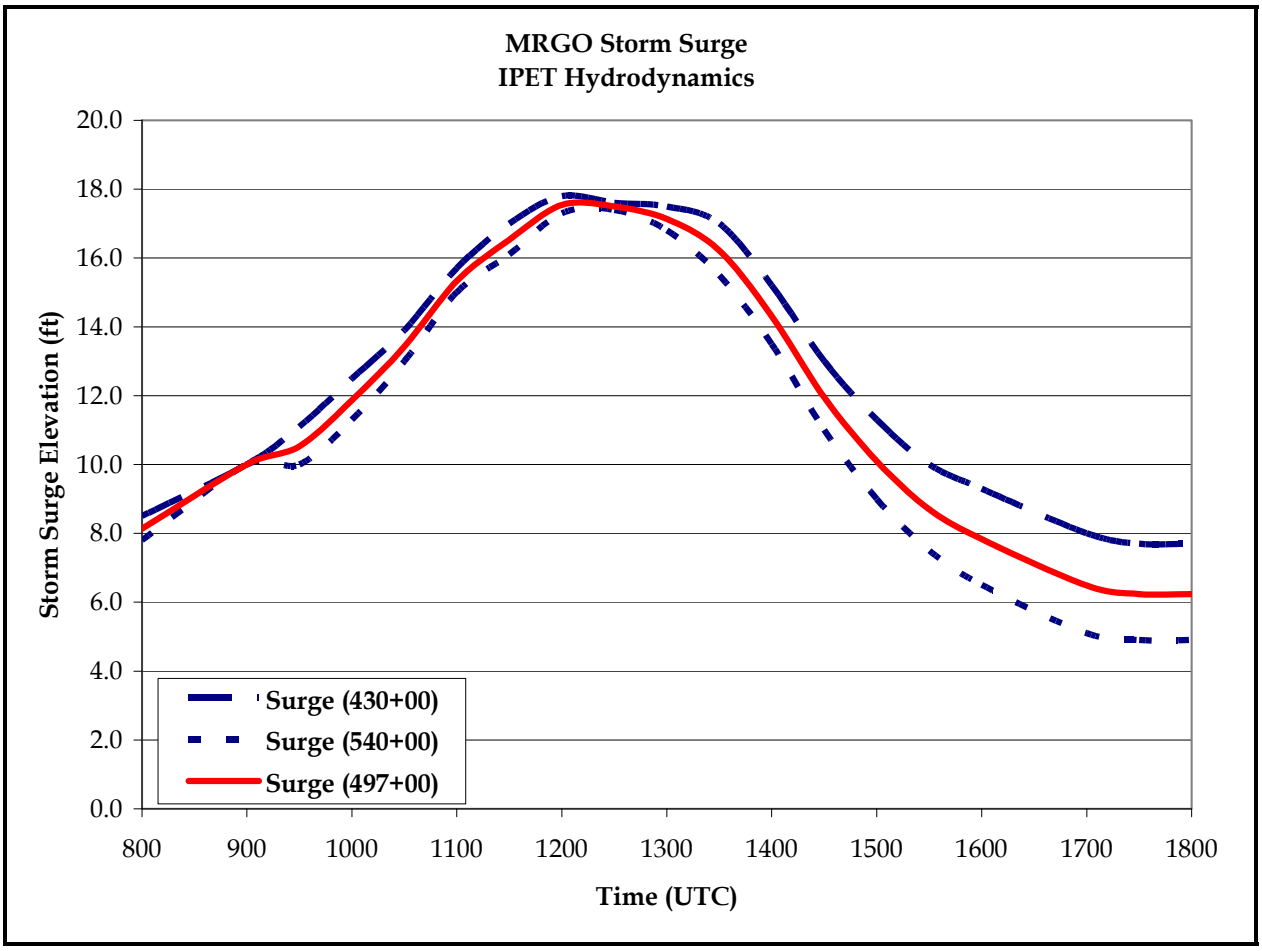


Figure C5: Storm surge time history as determined based on IPET (2007a).

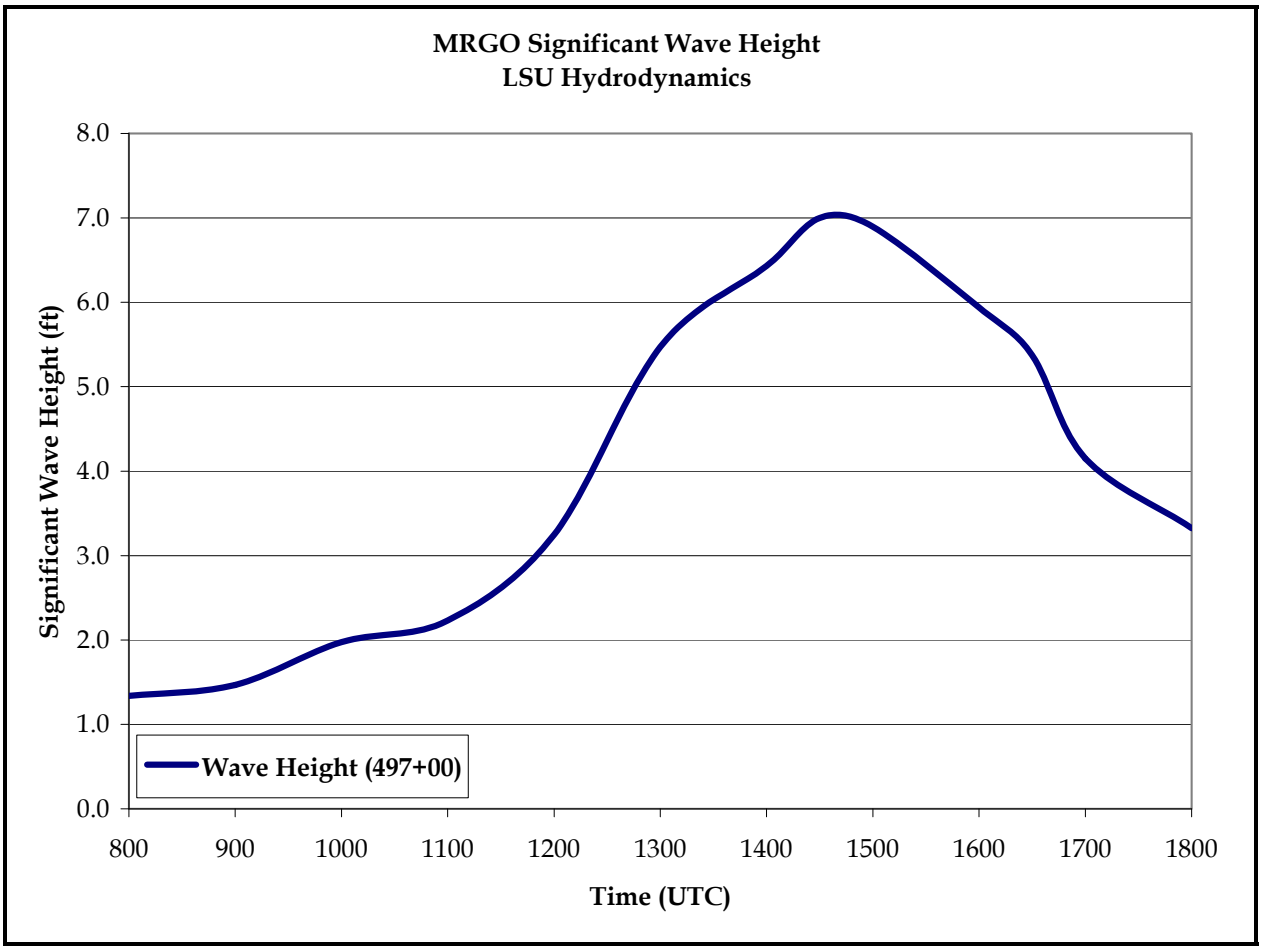


Figure C6: Significant wave height time history as determined using the LSU (2007) scaling factors.

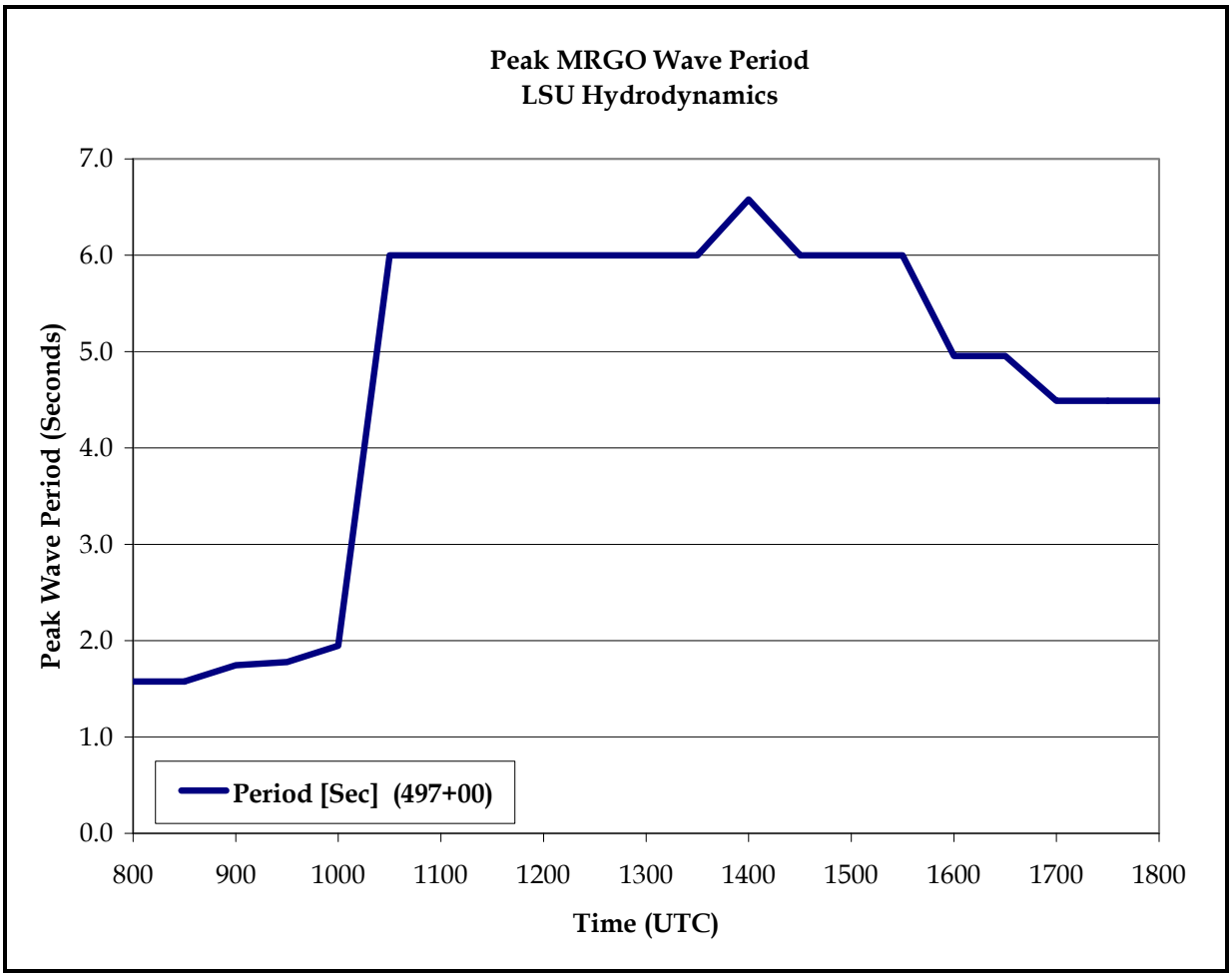


Figure C7: Wave period time history as determined using the LSU (2007) scaling factors.

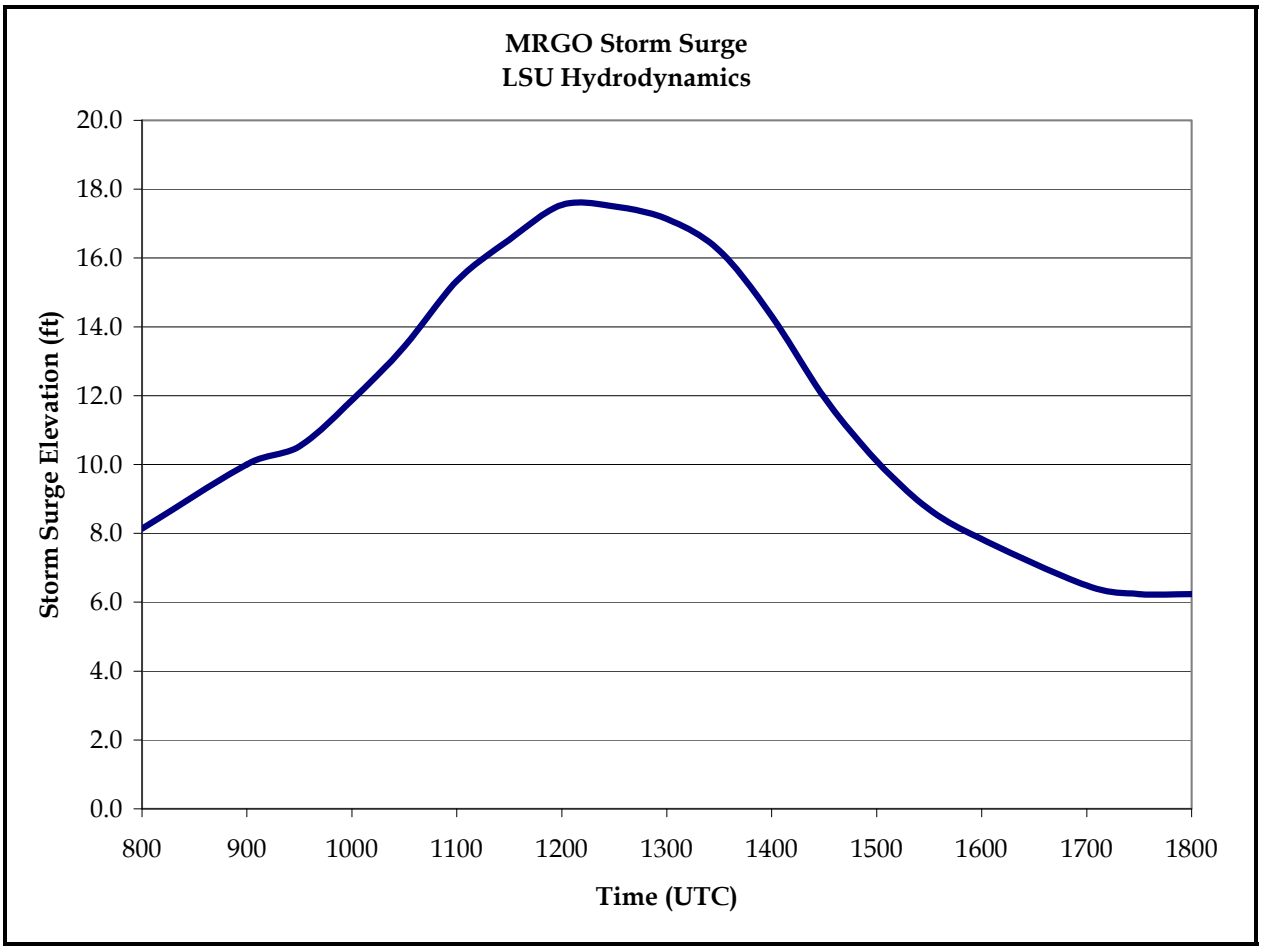


Figure C8: Storm surge time history as determined using the LSU (2007) scaling factors.

Model Configuration and Conditions

Interaction shear velocities between the storm surge and the earthen levees were evaluated for a selection of storm surge elevations. Simulations were also performed using the design geometric EBSB configuration and the actual EBSB configuration (as determined based on the available Aerial LiDAR data from 2000). For each storm surge elevation a numerical simulation was conducted for 150 seconds using the hydrodynamic characteristics as defined by IPET (IPET, 2006). This simulation time was selected in order to optimize computing time, while achieving 'steady state' wave impact conditions (interaction shear stresses and velocities) in the model. The initial 20 seconds of numerical simulation were dedicated to 'initializing' the run (gravity initialization and generating the hurricane waves).

A total of twelve numerical simulations were conducted for this evaluation. Snapshots of interaction shear velocities were calculated for each analysis case. Table C1 presents a summary of the wave analysis conditions.

Table C1: Summary of Wave Analysis Conditions

Case	Hydro-dynamics	EBSB Geometry	Storm Surge Elevation	Significant Wave Height (H_{mo})	Wave Period	Overtopping Rate ($ft^3/s/ft$)
I	IPET	Actual	+8 ft	1.1 ft	3.5 s	0.0
II	IPET	Actual	+12 ft	1.6 ft	4.4 s	0.0
III	IPET	Actual	+17.5 ft	2.6 ft	13.5 s	0.19
IV	LSU	Actual	+8 ft	1.3 ft	2.0 s	0.0
V	LSU	Actual	+12 ft	2.0 ft	2.0 s	0.0
VI	LSU	Actual	+17.5 ft	3.2 ft	6.0 s	0.19
VII	IPET	Design	+8 ft	1.1 ft	3.5 s	0.0
VIII	IPET	Design	+12 ft	1.6 ft	4.4 s	0.0
IX	IPET	Design	+17.5 ft	2.6 ft	13.5 s	0.07
X	LSU	Design	+8 ft	1.3 ft	2.0 s	0.0
XI	LSU	Design	+12 ft	2.0 ft	2.0 s	0.0
XII	LSU	Design	+17.5 ft	3.2 ft	6.0 s	0.07

The storm surge elevations, significant wave heights, wave periods, and overtopping rates were obtained from IPET (2007a) as described in Section 8. A minimum wave period of 2.5 s was required to generate acceptable waves in the numerical model. The predicted wave period of 1.6 s and 1.9 s was not drastically modified.

The development of the geometric configuration of the EBSB (Figure C9) was based on the design section (USACE, 1966a). The flood side EBSB toe begins at Elevation +4 ft, runs at a

slope of 1 on 5 for 5 ft to Elevation + 5 ft, then runs on a slope of 1 on 30 for 120 ft to Elevation + 9 ft, then runs at a slope of 1 on 5 for 42.5 ft to Elevation +17.5 ft. The crest has a width of 10 ft. The protected side EBSB slope runs on a slope of 1 on 5 for a distance of 42.5 ft to Elevation +9 ft. For these analyses, the model was terminated at Elevation +9 ft. The primary focus of the model is to determine fluid/ EBSB interaction shear velocities on the flood side face of the EBSB, not evaluating the overtopping velocities down the protected side of the EBSB.

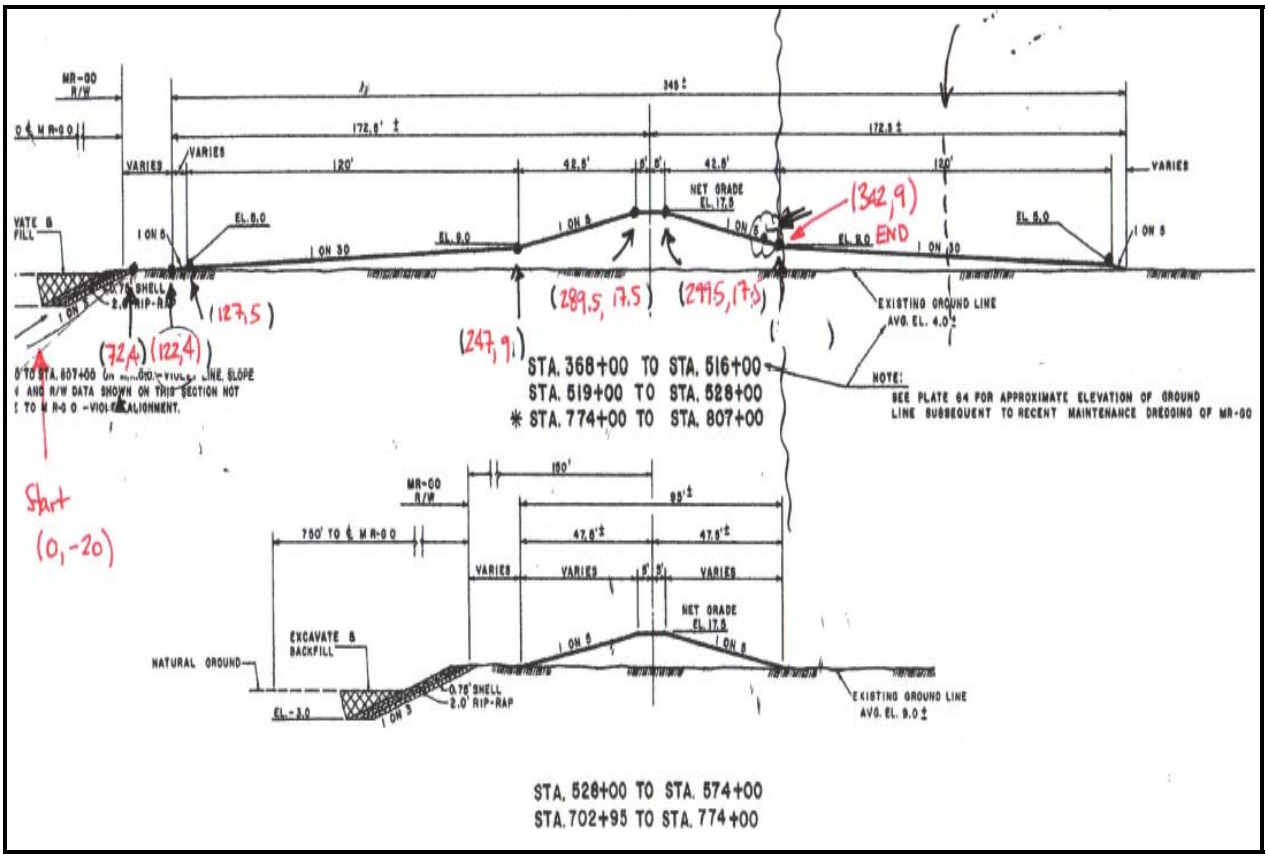


Figure C9: The design EBSB configuration was used as the basis for the geometric configuration of the EBSB (USACE, 1966a).

As previously mentioned, the design EBSB configuration was not the actual configuration of the EBSB at the time Hurricane Katrina hit the New Orleans area. The crest elevation at Station 497+00 was approximately +16.0 feet, 1.5 feet lower than the target design elevation.

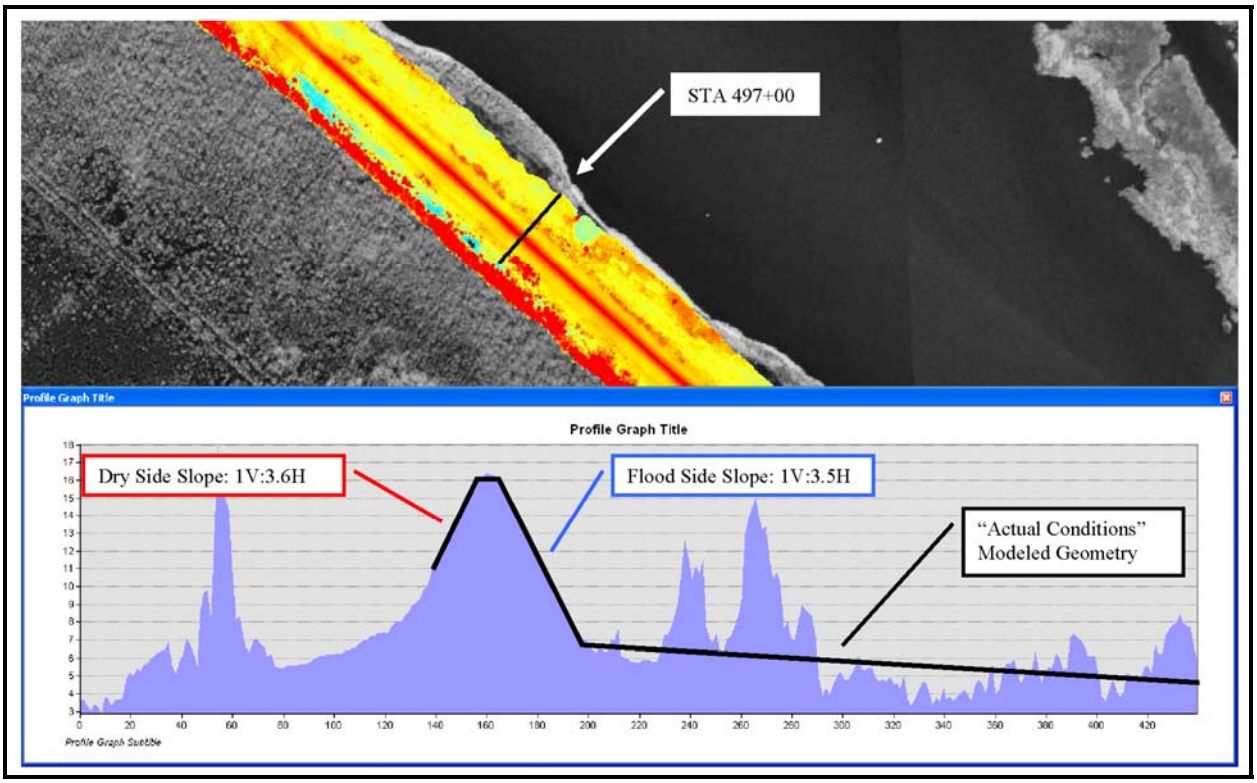


Figure C10: The EBSB profile used to model 'actual' geometry.

The development of the actual geometric configuration of the EBSB (Figure C10) was based on available Aerial LiDAR data. The flood side EBSB toe begins at Elevation +5 ft, runs at a slope of about 1 on 66 for 130 ft to Elevation + 7 ft, then runs on a slope of 1 on 3.5 for 31 ft to Elevation + 16 ft. The crest has a width of 10 ft. The protected side EBSB slope runs on a slope of 1 on 3.6 to Elevation +9 ft. For these analyses, the model was terminated at Elevation +9 ft.

In order to fully develop the hurricane waves, a portion of the MR-GO channel was incorporated in to the model to provide additional depth adjacent to the wave generator. The actual distance from the edge of the MR-GO channel to the flood side toe of the EBSB is approximately 258 ft, however, for this simulation the modeled distance was 50 ft (to reduce the numerical computation time). This modification is not expected to have a significant impact to the

calculated interaction shear velocities since wave damping is not implemented in the model. It is important to note that the presence of flood side vegetation acts to attenuate and damp incident wave energy and this wave damping has not been captured by the numerical simulation (nor was it accounted for in the hydrodynamic characterization developed by IPET, 2006). As a result of not capturing wave damping through the flood side vegetation, calculated interaction shear stresses and velocities predicted by the model will be on the higher bound of actual forces experienced by the EBSB during the hurricane. This is an area of active continuing research.

The model was created using a grid size of approximately 1.0 ft (meaning a node was located at a spacing of one foot). The x-axis runs longitudinal and the y-axis represents the model elevation. The z-axis runs along the width of the model (which was set to be 1-foot).

Velocities were determined by tracking the velocity profiles at selected nodes using the *DATABASE_HISTORY_NODE option (nodout) for the actual (Figure C11) and design (Figure C12) EBSB geometries. This option generates an ASCII database output with a time-history summary of velocity components and resultants for the selected nodes. The location of the velocity corresponds to the location of the node.

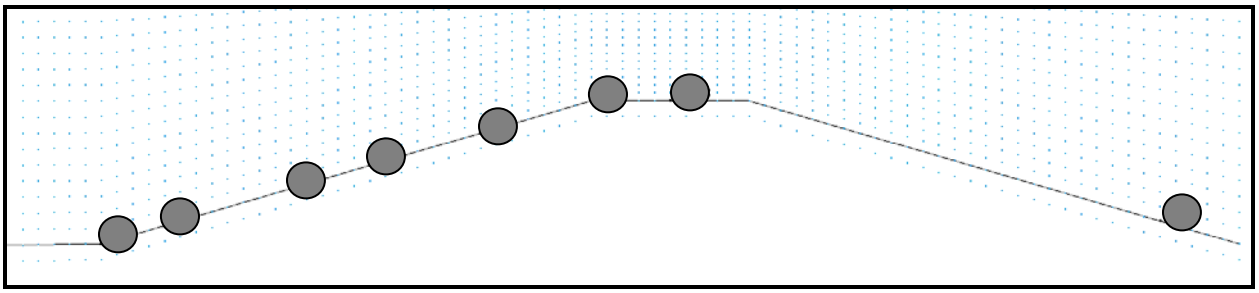


Figure C11: An overview of 'monitoring' nodes used to calculate shear velocities for the actual EBSB configuration.

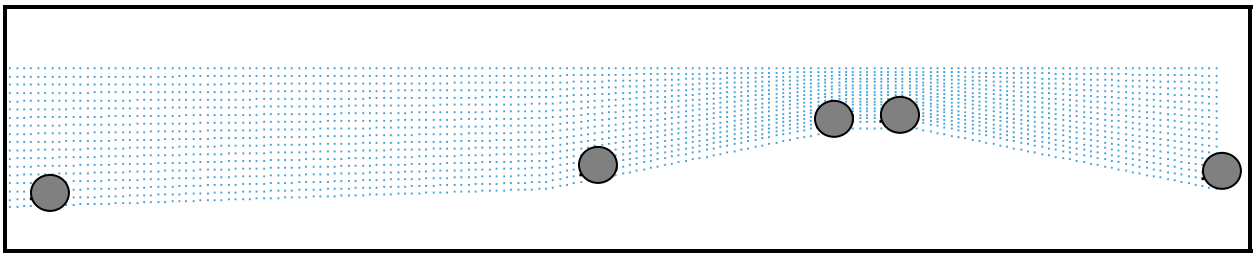


Figure C12: An overview of 'monitoring' nodes used to calculate shear velocities for the design EBSB configuration.

The imposed interaction shear velocities calculated by the LSDYNA numerical simulation were compared against the erosion/scour soil limits (capacity) as estimated based on the Erodibility Function Apparatus and EBSB soil composition. The EBSB at Station 497+00 was characterized to consist of semi-compacted hydraulic fill (high erodibility material).

The analyses were oriented to determining the likelihood of EBSB breaching due primarily to wave impact prior to EBSB overtopping. As a result, the analysis time frame was limited to the time before the storm surge overtopped the EBSB. Once overtopping occurred, the high-erodibility materials would have been extremely susceptible to erosion due to the high velocities and low material erosion resistance.

Table C2: Summary of Anticipated Erosion/Scour for Evaluated Cases on EBSB Flood Side Face

Case	Configuration	Hydro-dynamics	Storm Surge Elevation	Peak Velocity (ft/s)	Erosion/Scour Anticipated?
I	Actual Geometry	IPET	+8 ft	2.3	Likely
II			+12 ft	8.5	Very Likely
III			+17.5 ft	10.0	Very Likely
IV		LSU	+8 ft	1.8	Unlikely
V			+12 ft	5.0	Very Likely
VI			+17.5 ft	8.8	Very Likely
VII	Design Geometry	IPET	+8 ft	3.2	Likely
VIII			+12 ft	8.0	Very Likely
IX			+17.5 ft	26.2	Very Likely
X		LSU	+8 ft	1.9	Unlikely
XI			+12 ft	2.4	Likely
XII			+17.5 ft	20.8	Very Likely

Table C2 summarizes the results of the twelve storm surge cases; six for the actual EBSB configuration and six for the 'design' configuration. As seen in this chart, erosion/scour on the flood side face of the EBSB is possible for the majority of cases evaluated.

It was determined that no significant erosion or scour would occur with the storm surge at an elevation near + 8 ft (9.5 ft below the target crest elevation) for the 'design' and actual EBSB

geometry. For all other cases, erosion based on the magnitude of shear velocities was determined to be likely to very likely.

Table C3 presents a summary of error between the hydrodynamic conditions (significant wave height and wave period) between the IPET (2007a) and LSU (2007) estimates and the LSDYNA modeled conditions.

Table C3: Error Determination of DYNA Generated Waves for Scenario 1 Hydrodynamics

Time (CDT)	**Storm Surge Elevation (ft)**	**Significant Wave Height (H_{mo})**	**Wave Period (s)**	**DYNA Wave Height (H)**	**DYNA Wave Period (s)**	**Percent Error**
I	+8 ft	1.1 ft	3.5 s	1.1 ft	3.5 s	0% (0%)
II	+12 ft	1.6 ft	4.4 s	1.7 ft	4.5 s	6% (2%)
III	+17.5 ft	2.6 ft	13.5 s	2.5 ft	13.5 s	4% (0%)
IV	+8 ft	1.3 ft	2.0 s	1.4 ft	2.5 s	7% (20%)
V	+12 ft	2.0 ft	2.0 s	1.9 ft	3.0 s	5% (33%)
VI	+17.5 ft	3.2 ft	6.0 s	3.0 ft	6.0 s	7% (0%)
VII	+8 ft	1.1 ft	3.5 s	1.1 ft	3.5 s	0% (0%)
VIII	+12 ft	1.6 ft	4.4 s	1.8 ft	4.5 s	11% (2%)
IX	+17.5 ft	2.6 ft	13.5 s	2.6 ft	13.5 s	0% (0%)
X	+8 ft	1.3 ft	2.0 s	1.3 ft	2.5 s	0% (20%)
XI	+12 ft	2.0 ft	2.0 s	2.0 ft	3.0 s	0% (33%)
XII	+17.5 ft	3.2 ft	6.0 s	3.6 ft	6.0 s	11% (0%)

A discussion of the predicted shear velocities for the twelve evaluated cases is presented below.

IPET and LSU (2007) Velocity Simulation Results

Analysis Case I

Case I (Figure C13) consisted of an EBSB crest elevation of +16 ft (actual geometry) and IPET-based hydrodynamics consisting of a storm surge elevation of +8 ft, a wave period of 3.5 s, and a significant wave height of 1.1 ft. There was no overtopping.



Figure C13: Initial conditions for analysis Case I.

At Elevation +8 ft, the storm surge had reached the flood side toe of the EBSB. A plot of the shear velocities is presented in Figure C14. The peak shear velocity was determined to be 2.25 ft/s.

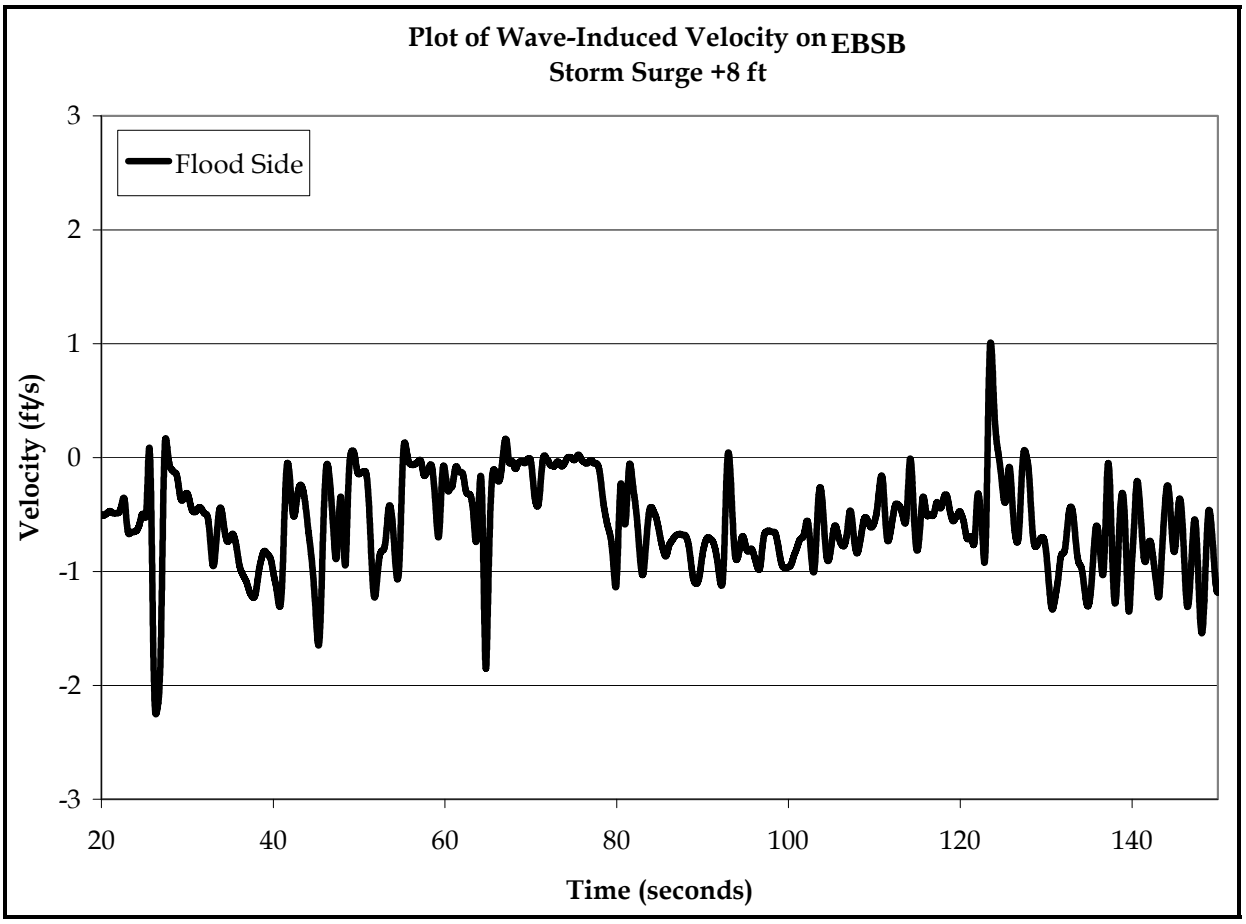


Figure C14**:** A plot of the velocity time history on the flood side face of the EBSB with the storm surge at +8 ft.

Figure C15 (below) provides a graphical representation of water movement over time. With the hurricane storm surge at El. +8 ft, the actual geometric configuration of the EBSB induces a tendency for the waves to exhibit a primarily 'runup' and 'rundown' behavior. Because the slope is very shallow, the wave energy is greatly damped and no wave 'impacts' are experienced by the EBSB.

Storm Surge Elevation: +8 ft Crest Elevation: +16 ft

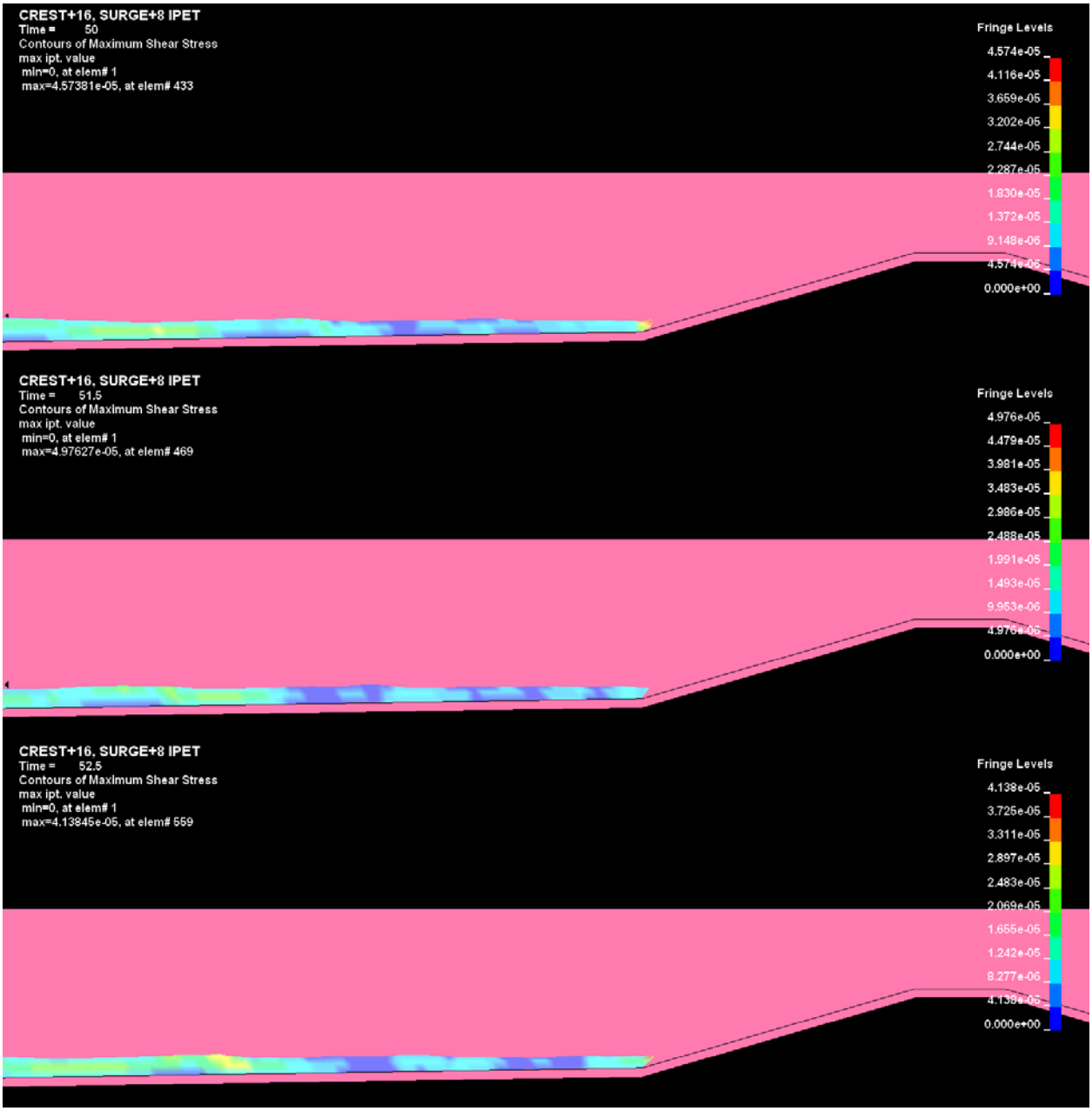


Figure C15**:** With the hurricane storm surge at El. +8 ft, the actual geometric configuration of the EBSB induces a tendency for the waves to exhibit a primarily 'runup' and 'rundown' behavior. Because the slope is very shallow, the wave energy is greatly damped and no wave 'impacts' are experienced by the EBSB.

Analysis Case II

Case II (Figure C16) consisted of a crest elevation of +16 ft (actual geometry) and IPET-based hydrodynamics consisting of a storm surge elevation of +12 ft, a wave period of 4.4 s, and a significant wave height of 1.6 ft. There was no overtopping.

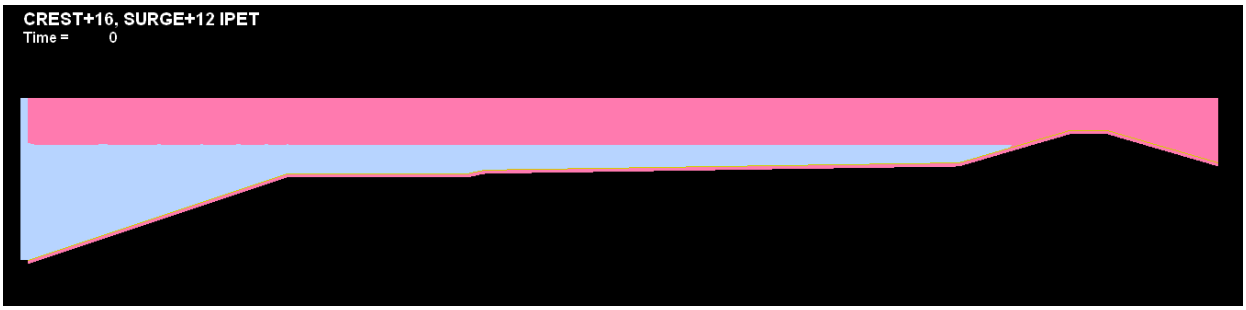


Figure C16: Initial conditions for analysis Case II.

At Elevation +12 ft, the storm surge had reached the main EBSB 1 on 3.5 flood side slope. This slope was vegetated at the time of the hurricane, so some erosion resistance was provided by the grassy cover. A plot of shear velocities is presented in Figure C17. Based on the velocity profile, the majority of the velocities significantly exceed the critical erosion values, so this implies that erosion/scour would occur as a result of wave impact at this elevation. The peak velocity was determined to be 8.5 ft/s.

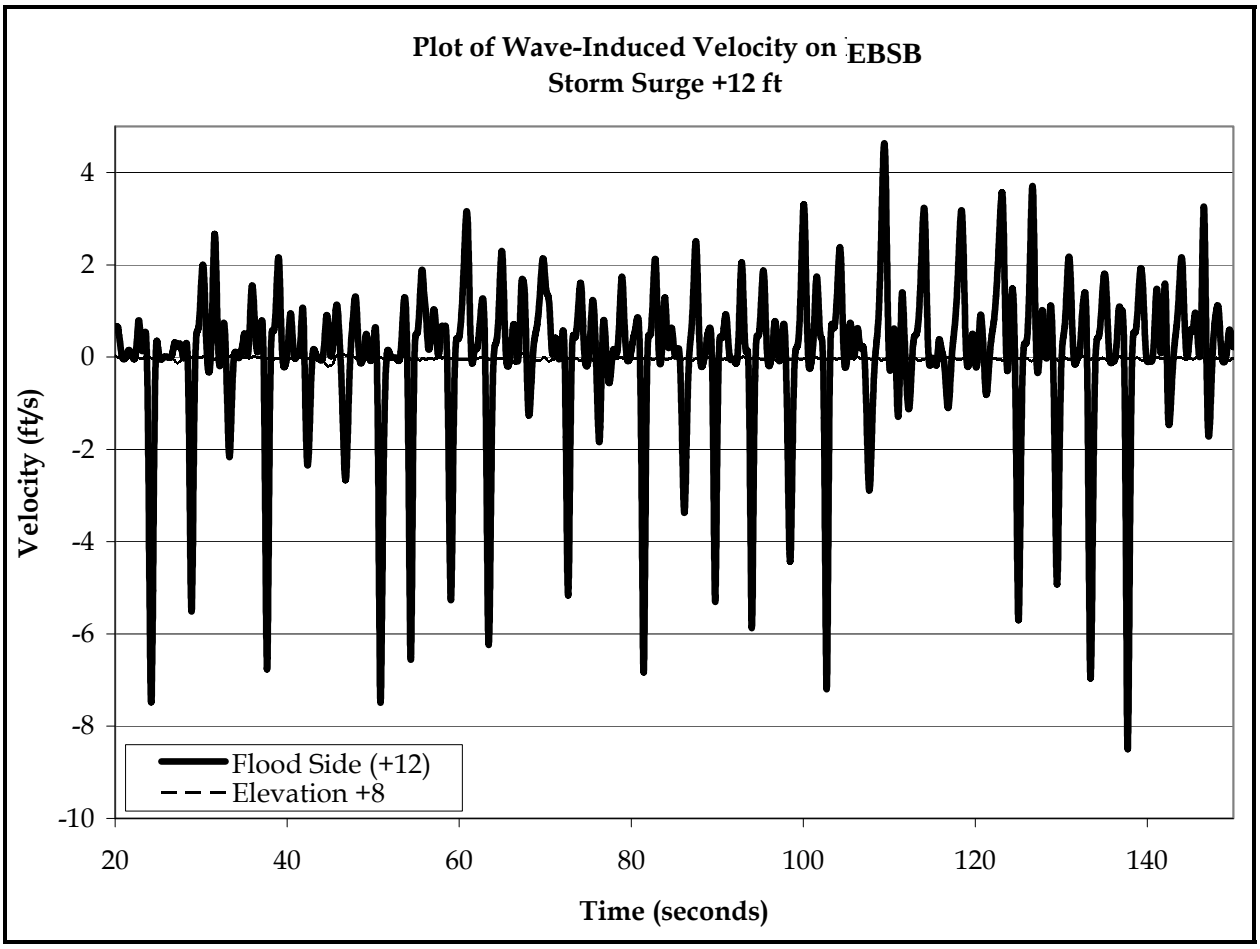


Figure C17: Time history plot of shear velocities for the storm surge at Elevation +12 ft.

Figure C18 (below) provides a graphical representation of water movement over time. With the hurricane storm surge at El. +12 ft, the actual geometric configuration of the EBSB induces a tendency for the waves to exhibit a primarily 'runup' and 'rundown' behavior, with moderate to major wave impacts.

Storm Surge Elevation: +12 ft Crest Elevation: +16 ft

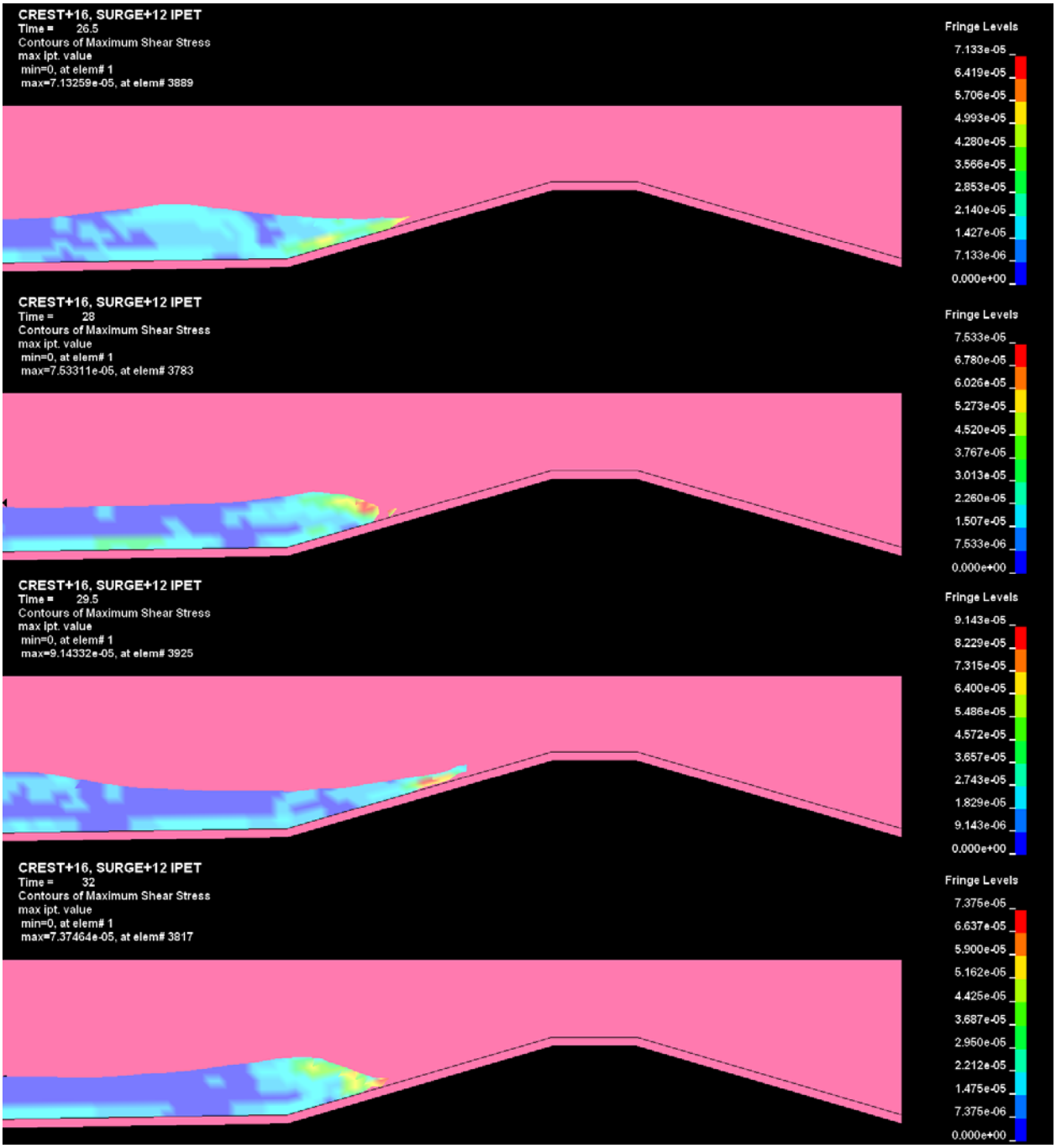


Figure C18**:** With the hurricane storm surge at El. +12 ft, the actual geometric configuration of the EBSB induces a tendency for the waves to exhibit a primarily 'runup' and 'rundown' behavior with moderate to major wave impacts.

Analysis Case III

Case III (Figure C19) consisted of a crest elevation of +16 ft (actual geometry) and IPET-based hydrodynamics consisting of a storm surge elevation of +17.5 ft, a wave period of 13.5 s, and a significant wave height of 2.6 ft. There was active overtopping.

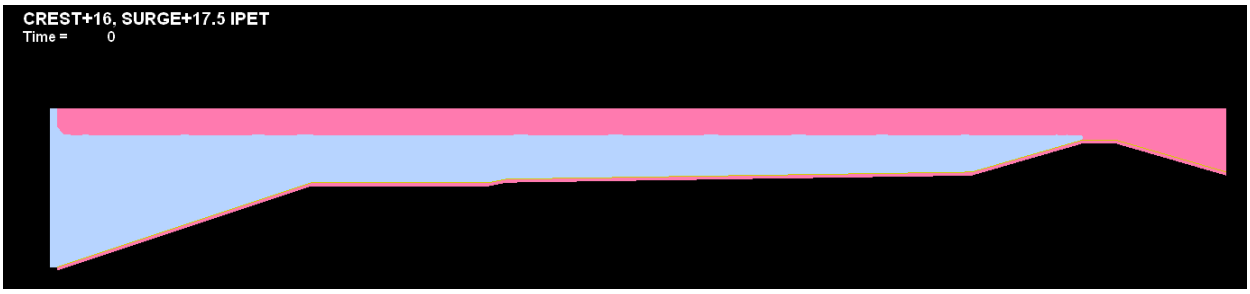


Figure C19**:** Initial conditions for analysis Case III.

At Elevation +17.5 ft, the storm surge had reached the crest of the EBSB and active overtopping was occurring. A plot of shear velocities is presented in Figure C20. Based on the velocity profile, the majority of the velocities exceed the critical erosion values, so this implies that major erosion would occur as a result of wave impact at this elevation. The peak velocity was determined to be 10.0 ft/s.

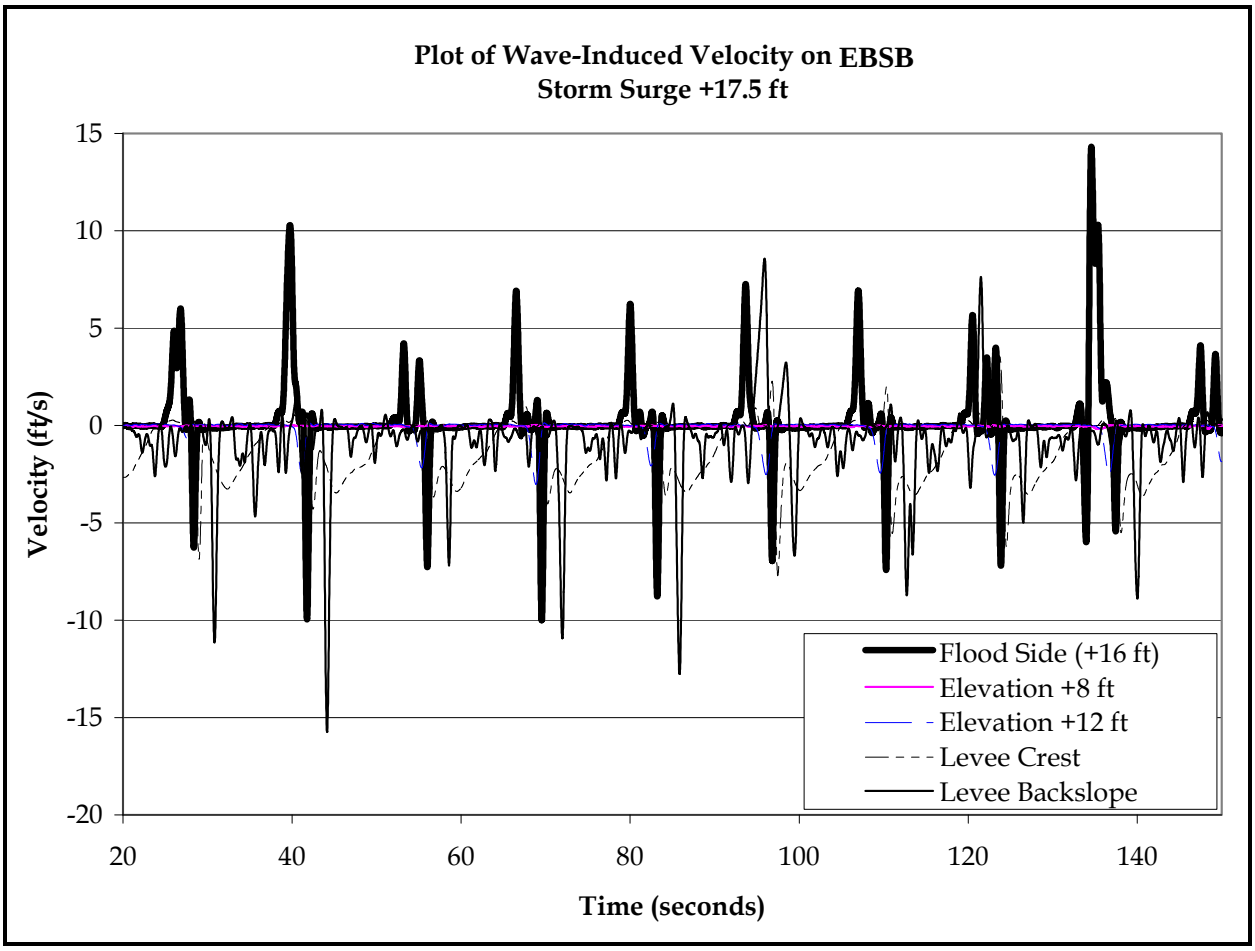


Figure C20: Time history plot of shear velocities for the storm surge at Elevation +17.5 ft.

Figure C21 (below) provides a graphical representation of water movement over time. With the hurricane storm surge at El. +17.5 ft, the geometric configuration of the EBSB appears to not promote direct wave impacts, but rather induces a tendency for the waves to 'spill over' the top of the EBSB, contributing significantly to overtopping erosion.

Storm Surge Elevation: +17.5 ft Crest Elevation: +16 ft

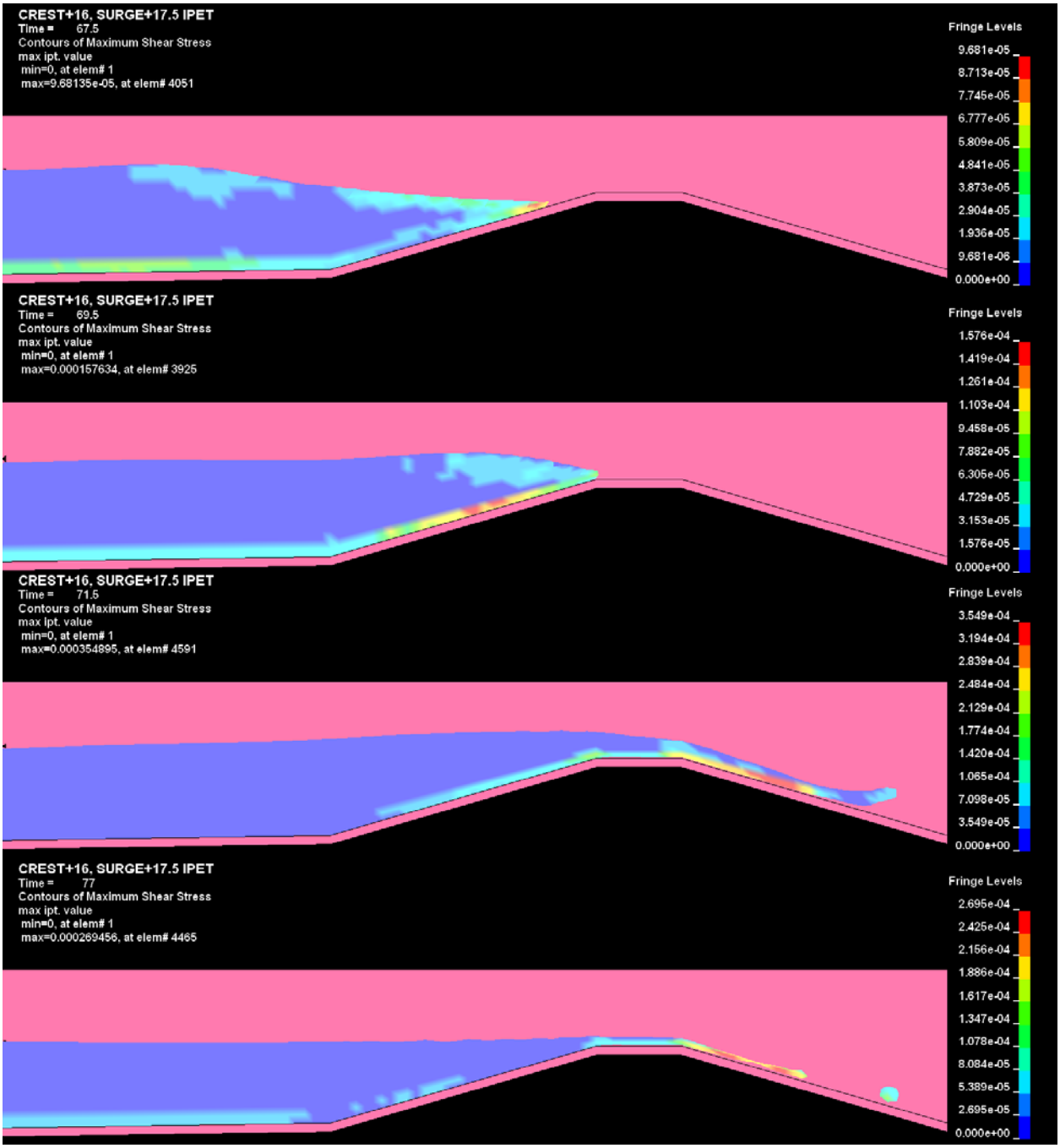


Figure C21**:** With the hurricane storm surge at El. +17.5 ft, waves induce predominantly overtopping erosion.

Analysis Case IV

Case IV (Figure C22) consisted of a crest elevation of +16 ft (actual geometry) and LSU-based hydrodynamics consisting of a storm surge elevation of +8 ft, a wave period of 2.0 s, and a significant wave height of 1.3 ft. There was no overtopping.

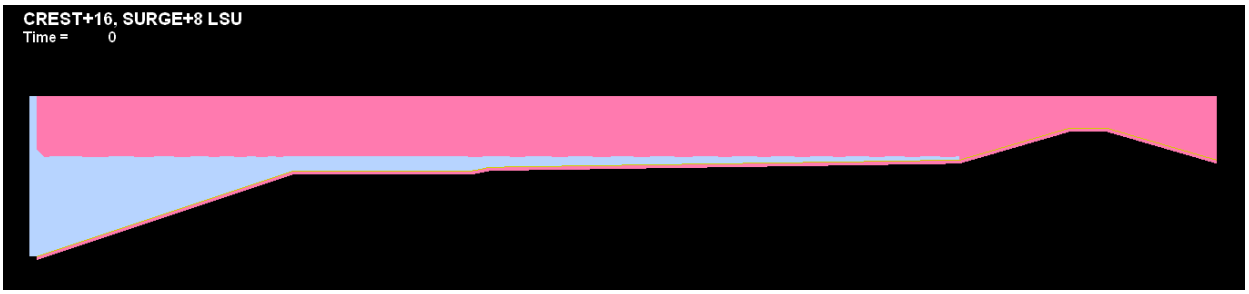


Figure C22: Initial conditions for analysis Case IV.

At Elevation +8 ft, the storm surge had reached the flood side toe of the EBSB. A plot of the shear velocities is presented in Figure C23. The peak shear velocity was determined to be 1.8 ft/s. This slope was vegetated at the time of the hurricane, so some erosion resistance was provided by the grassy cover. Based on the velocity profile, the calculated velocities do not exceed the critical erosion values, so this implies that negligible erosion would occur as a result of wave impact at this elevation.

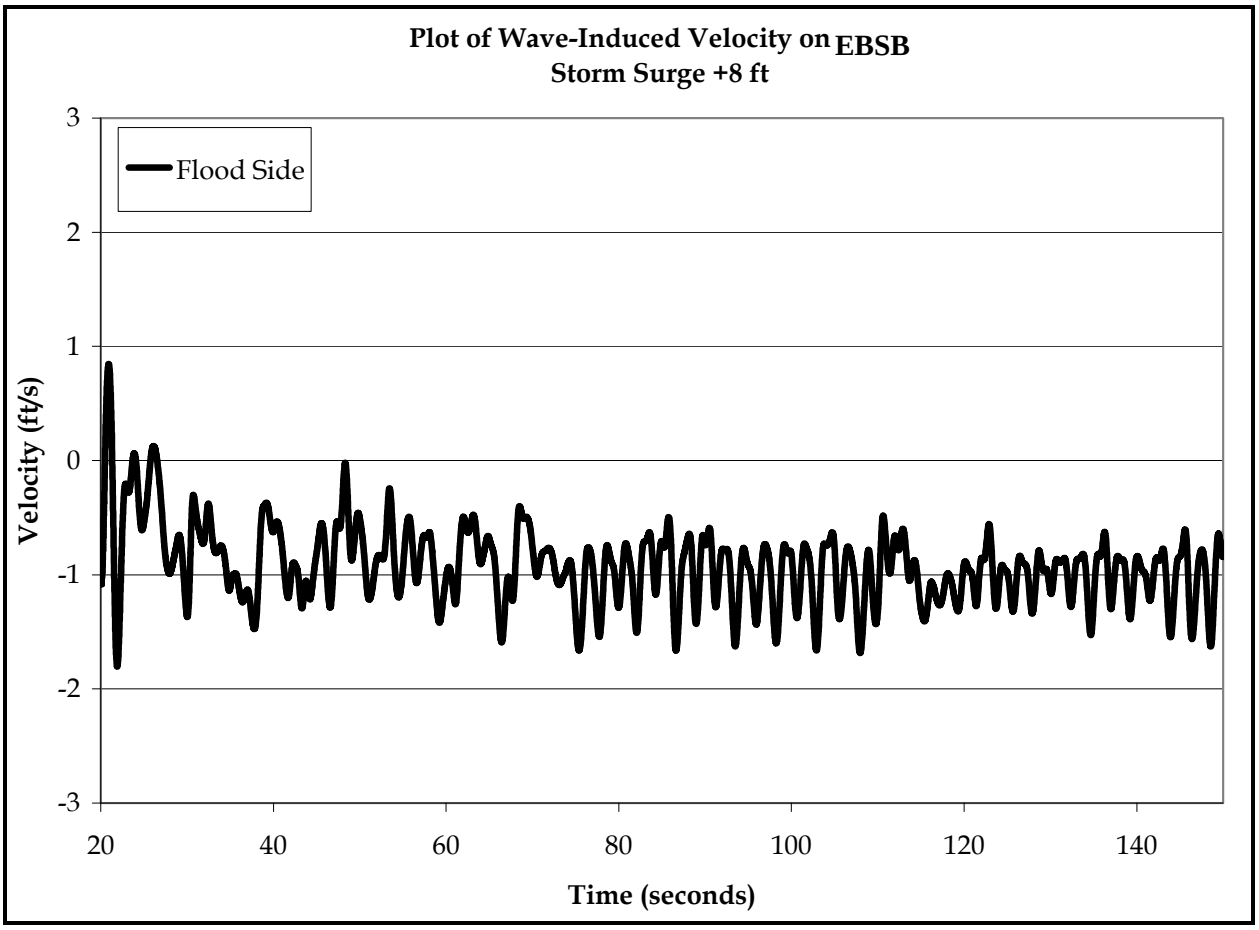


Figure C23: Time history plot of shear velocities for the storm surge at Elevation +8 ft.

Figure C24 (below) provides a graphical representation of water movement over time. With the hurricane storm surge at El. +8 ft, the geometric configuration of the EBSB induces a tendency for the waves to exhibit a primarily 'runup' and 'rundown' behavior, with minor to moderate wave impacts.

Storm Surge Elevation: +8 ft Crest Elevation: +16 ft



Figure C24**:** With the hurricane storm surge at El. +8 ft, the geometric configuration of the EBSB induces a tendency for the waves to exhibit a primarily ‘runup’ and ‘rundown’ behavior with negligible wave impacts.

Analysis Case V

Case V (Figure C25) consisted of a crest elevation of +16 ft (actual geometry) and LSU-based hydrodynamics consisting of a storm surge elevation of +12 ft, a wave period of 2.0 s, and a significant wave height of 2.0 ft. There was no overtopping.

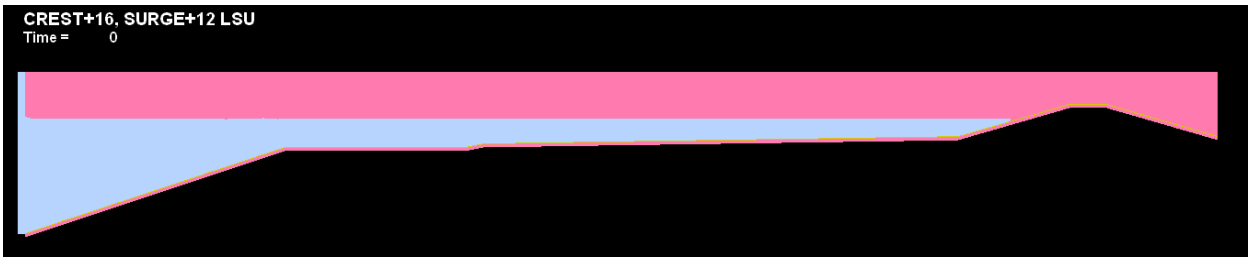


Figure C25: Initial conditions for analysis Case V.

At Elevation +12 ft, the storm surge had reached the main EBSB 1 on 5 flood side slope. This slope was vegetated at the time of the hurricane, so some erosion resistance was provided by the grassy cover. A plot of shear velocities is presented in Figure C26. Based on the velocity profile, the majority of the velocities exceed the critical erosion values, so this implies that minor to moderate erosion/scour would occur as a result of wave impact at this elevation. The peak velocity was determined to be 5.0 ft/s.

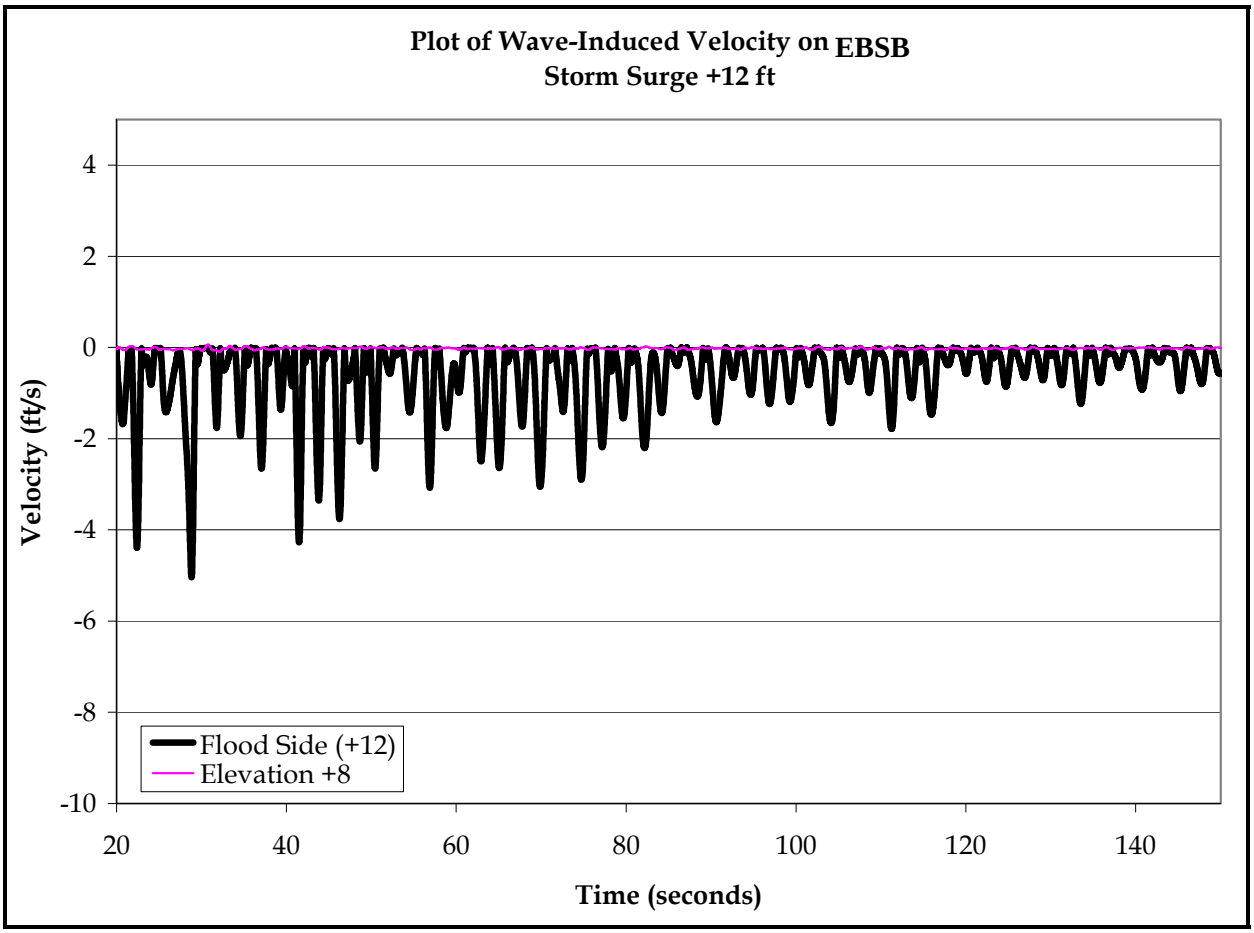


Figure C26: Time history plot of shear velocities for the storm surge at Elevation +12 ft.

Figure C27 (below) provides a graphical representation of water movement over time. With the hurricane storm surge at El. +12 ft, the design geometric configuration of the EBSB induces a tendency for the waves to exhibit a primarily 'runup' and 'rundown' behavior, with minor to moderate wave impacts.

Storm Surge Elevation: +12 ft Crest Elevation: +16 ft

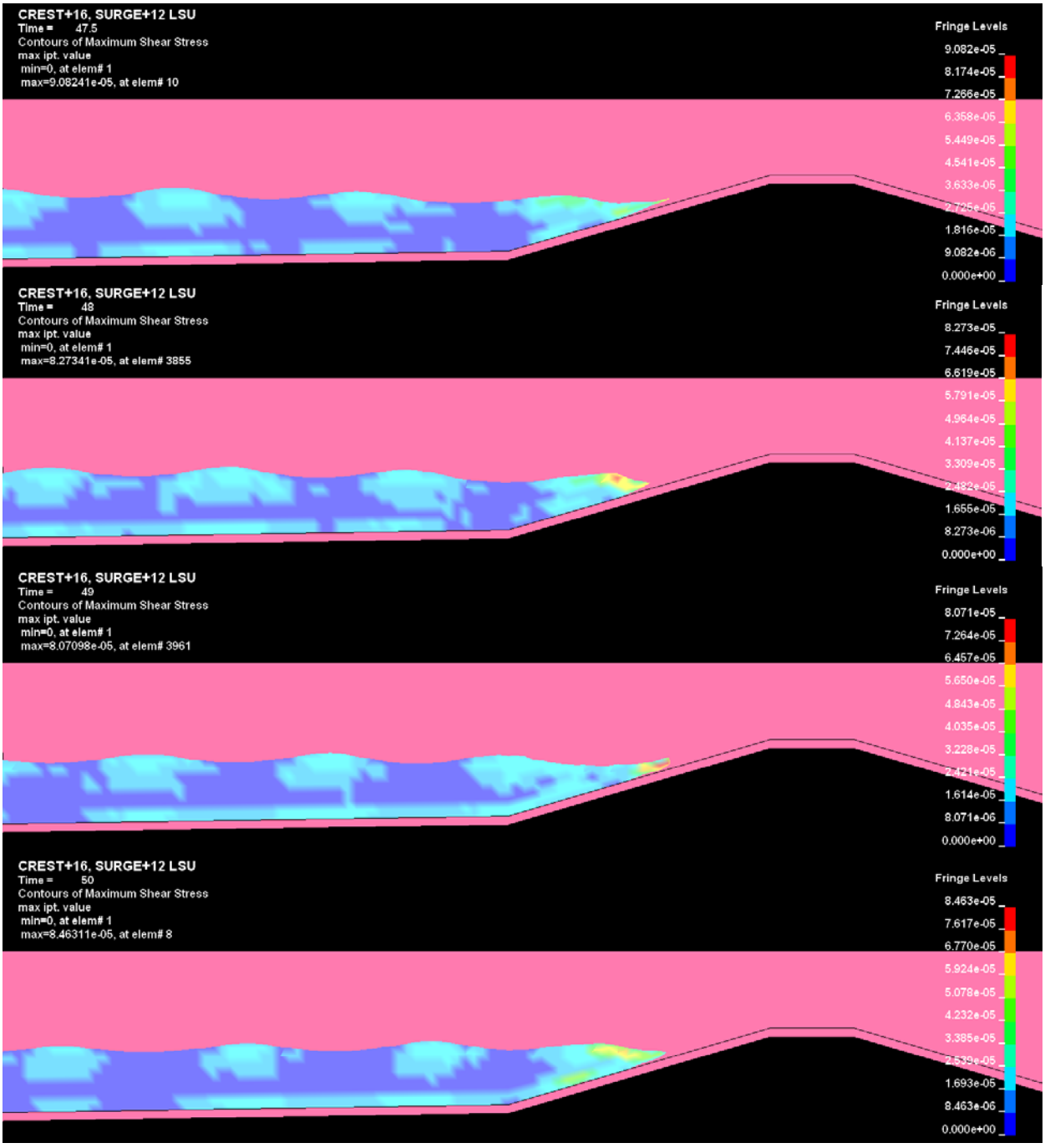


Figure C27**:** With the hurricane storm surge at El. +12 ft, the design geometric configuration of the EBSB induces a tendency for the waves to exhibit a primarily 'runup' and 'rundown' behavior with minor to moderate wave impacts.

Analysis Case VI

Case VI (Figure C28) consisted of a crest elevation of +16 ft (actual geometry) and LSU-based hydrodynamics consisting of a storm surge elevation of +17.5 ft, a wave period of 3.2 s, and a significant wave height of 6.0 ft. There was active overtopping.



Figure C28: Initial conditions for analysis Case VI.

At Elevation +17.5 ft, the storm surge had reached the crest of the EBSB and active overtopping was occurring. A plot of shear velocities is presented in Figure C29. Based on the velocity profile, the majority of the velocities exceed the critical erosion values, so this implies that major erosion would occur as a result of wave impact at this elevation. The peak velocity was determined to be 8.8 ft/s.

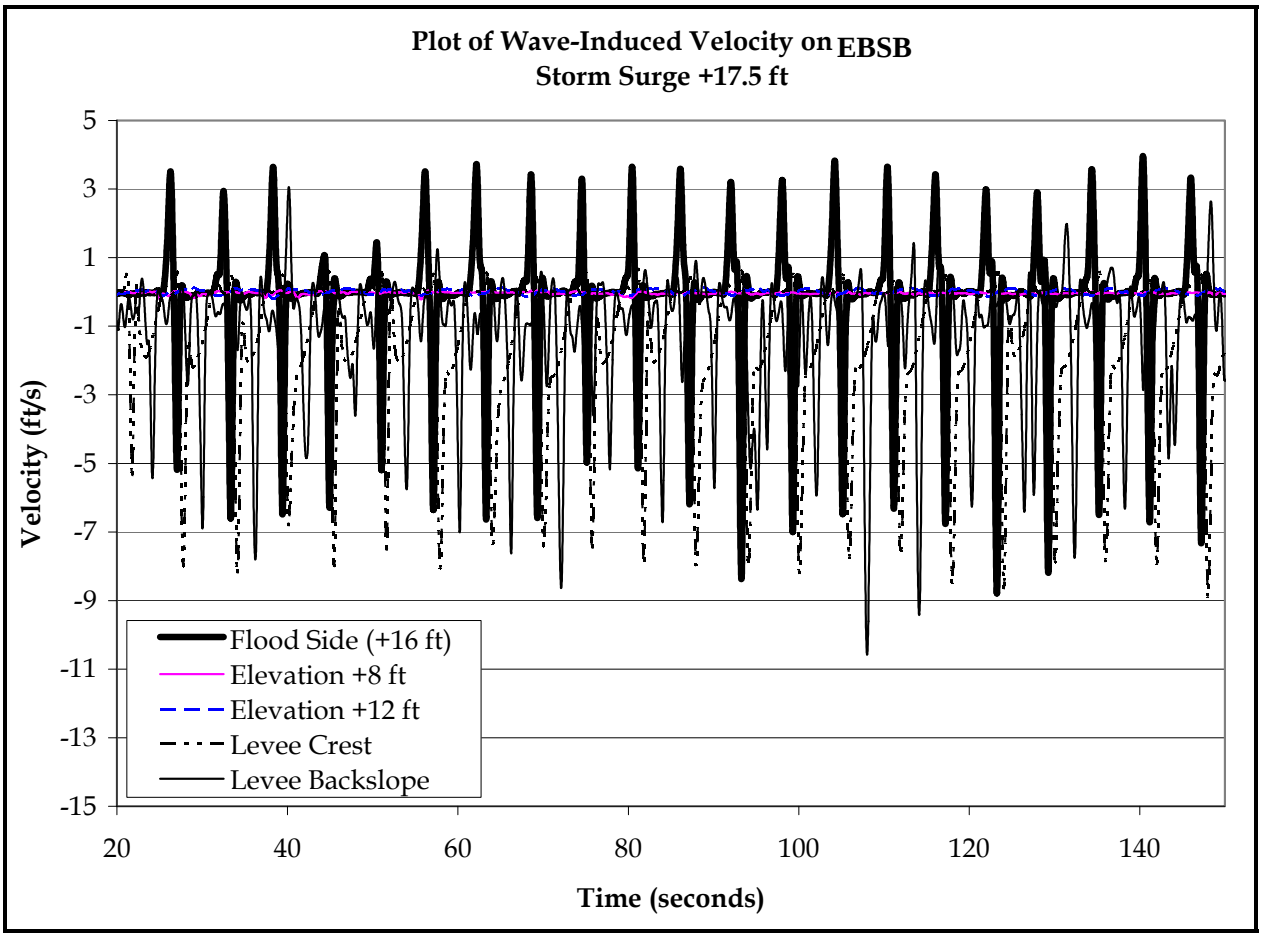


Figure C29**:** Time history plot of shear velocities for the storm surge at Elevation +17.5 ft.

Figure C30 (below) provides a graphical representation of water movement over time. With the hurricane storm surge at El. +17.5 ft, the geometric configuration of the EBSB appears to not promote direct wave impacts, but rather induces a tendency for the waves to 'spill over' the top of the EBSB, contributing significantly to overtopping erosion.

Storm Surge Elevation: +17.5 ft Crest Elevation: +16 ft

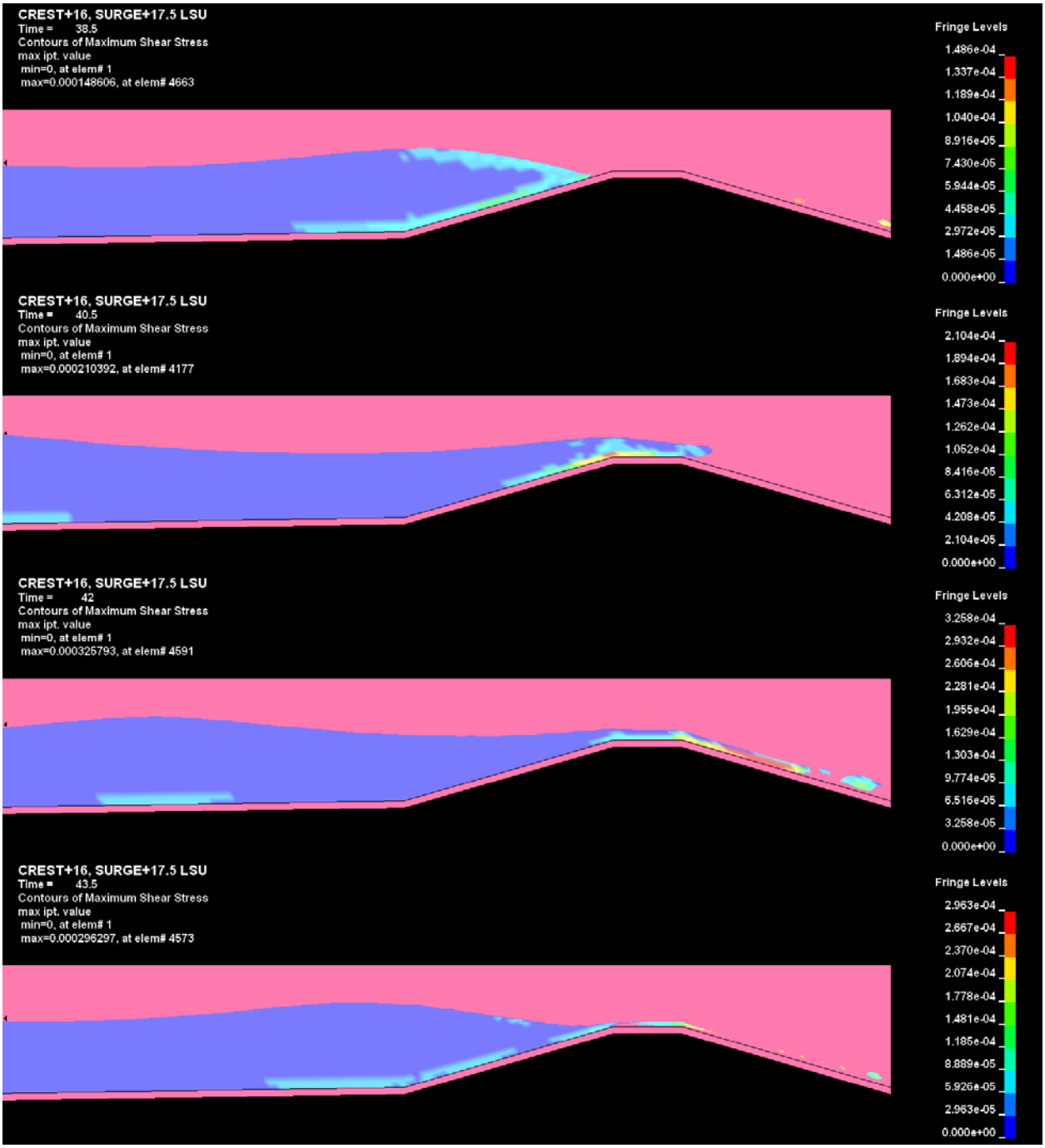


Figure C30**:** With the hurricane storm surge at El. +17.5 ft, waves induce predominantly overtopping erosion.

Analysis Case VII

Case VII (Figure C31) consisted of a crest elevation of +17.5 ft (design geometry) and IPET-based hydrodynamics consisting of a storm surge elevation of +8 ft, a wave period of 3.5 s, and a significant wave height of 1.1 ft. There was no overtopping.



Figure C31: Initial conditions for analysis Case VII.

At Elevation +8 ft, the storm surge reaches the 1 on 30 wave berm. This slope was vegetated at the time of the hurricane, so some erosion resistance was provided by the grassy cover. A plot of shear velocities is presented in Figure C32. Based on the velocity profile, the majority of the velocities exceed the critical erosion values, so this implies that minor to moderate erosion/scour would occur as a result of wave impact at this elevation. The peak velocity was determined to be 3.3 ft/s.

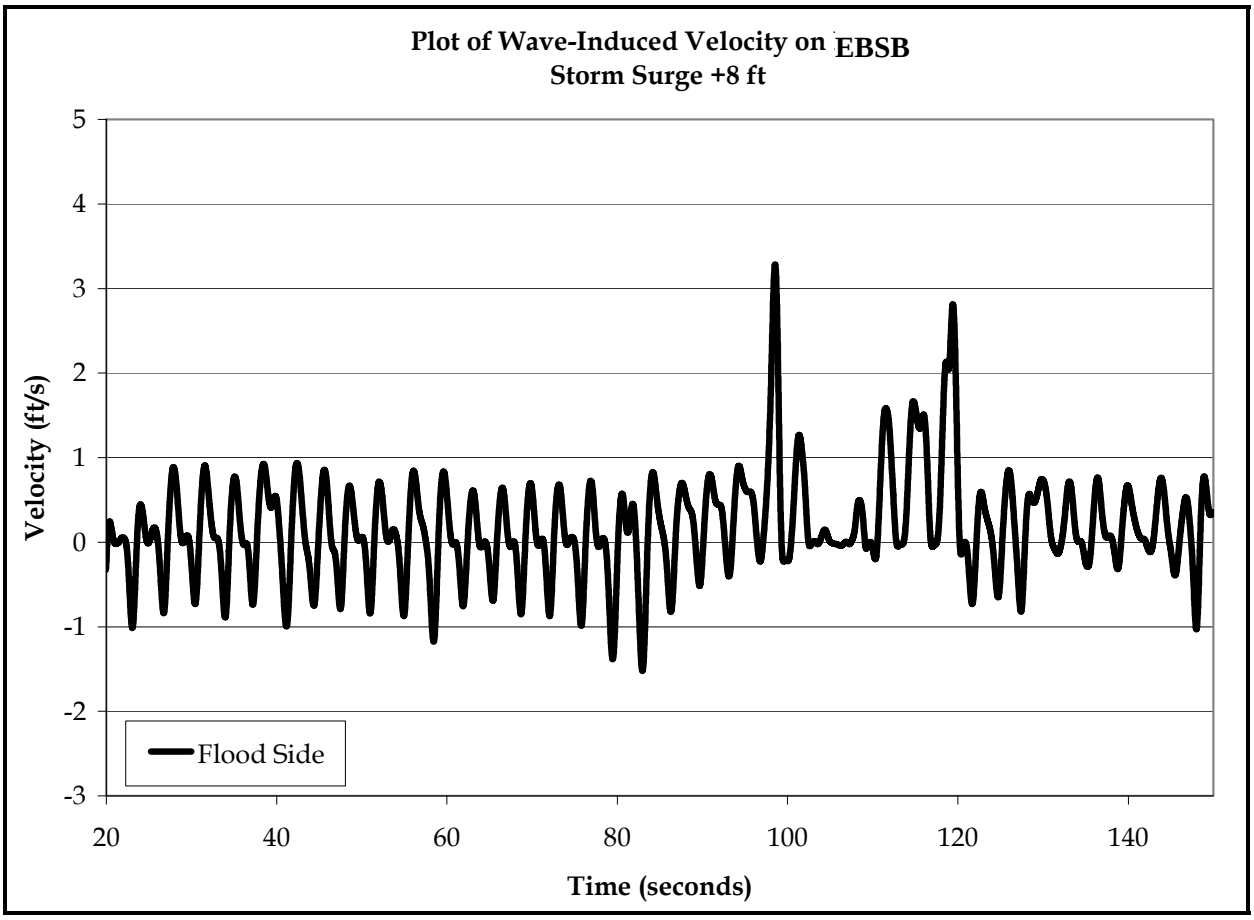


Figure C32**:** Time history plot of shear velocities for the storm surge at Elevation +8 ft.

Figure C33 (below) provides a graphical representation of water movement over time. With the hurricane storm surge at El. +8 ft, the design geometric configuration of the EBSB induces a tendency for the waves to exhibit a primarily 'runup' and 'rundown' behavior, with negligible wave impacts.

Storm Surge Elevation: +8 ft Crest Elevation: +17.5 ft



Figure C33**:** With the hurricane storm surge at El. +8 ft, the design geometric configuration of the EBSB induces a tendency for the waves to exhibit a primarily 'runup' and 'rundown' behavior with negligible wave impacts.

Analysis Case VIII

Case VIII (Figure C34) consisted of a crest elevation of +17.5 ft (design geometry) and IPET-based hydrodynamics consisting of a storm surge elevation of +12 ft, a wave period of 4.4 s, and a significant wave height of 1.6 ft. There was no overtopping.

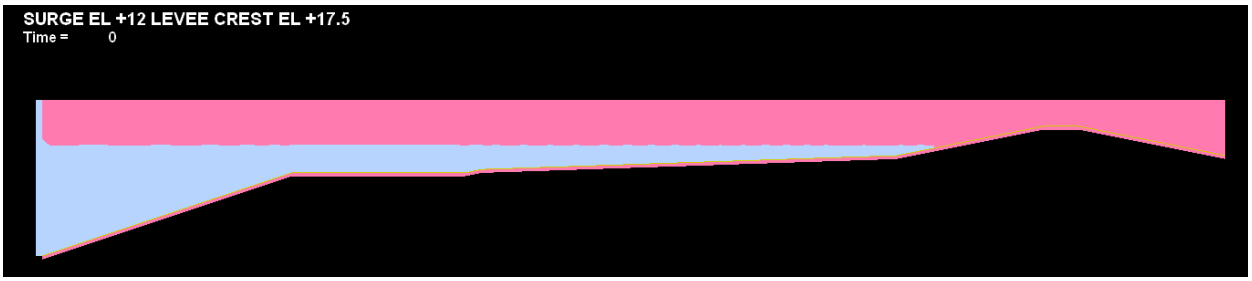


Figure C34: Initial conditions for analysis Case VIII.

At Elevation +12 ft, the storm surge reaches the main EBSB 1 on 5 flood side slope. A plot of shear velocities is presented in Figure C35. Based on the velocity profile, the majority of the velocities significantly exceed the critical erosion values, so this implies that erosion/scour would occur as a result of wave impact at this elevation. The peak velocity was determined to be 8.0 ft/s.

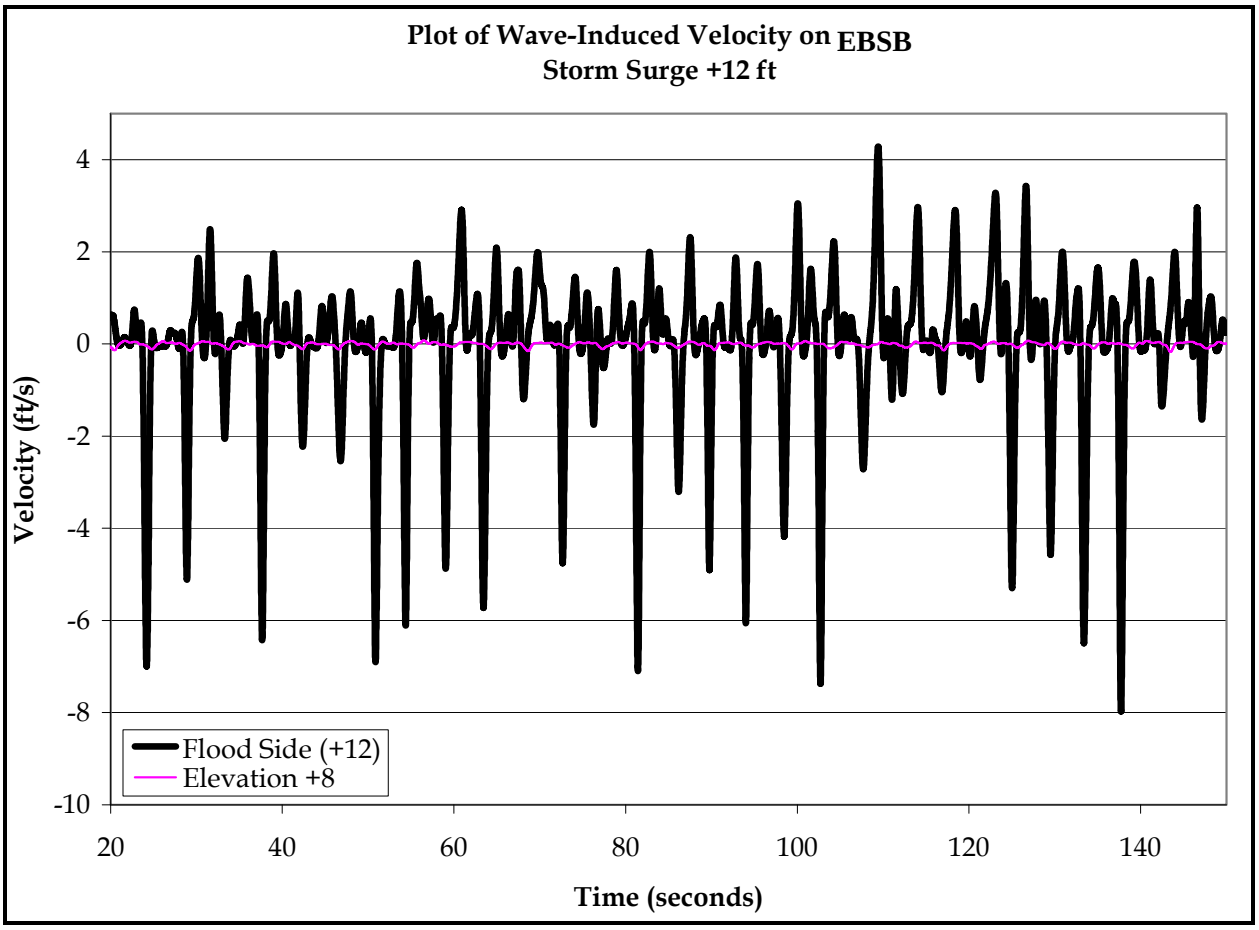


Figure C35**:** Time history plot of shear velocities for the storm surge at Elevation +12 ft.

Figure C36 (below) provides a graphical representation of water movement over time. With the hurricane storm surge at El. +12 ft, the design geometric configuration of the EBSB induces a tendency for the waves to exhibit a primarily 'runup' and 'rundown' behavior, with minor to moderate wave impacts.

Storm Surge Elevation: +12 ft Crest Elevation: +17.5 ft

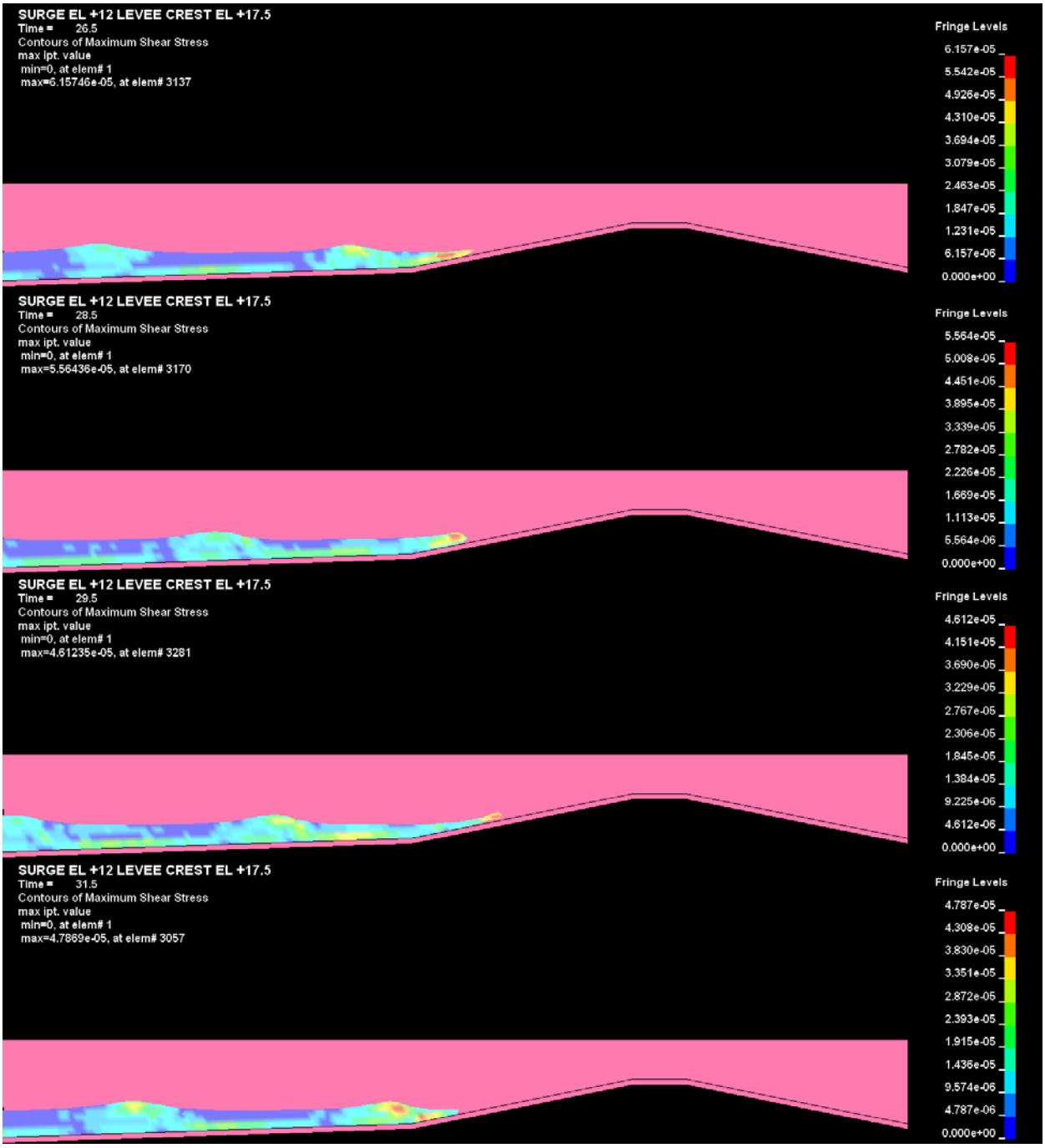


Figure C36**:** With the hurricane storm surge at El. +12 ft, the design geometric configuration of the EBSB induces a tendency for the waves to exhibit a primarily ‘runup’ and ‘rundown’ behavior with minor to moderate wave impacts.

Analysis Case IX

Case IX (Figure C37) consisted of a crest elevation of +17.5 ft (design geometry) and IPET-based hydrodynamics consisting of a storm surge elevation of +17.5 ft, a wave period of 13.5 s, and a significant wave height of 2.6 ft. Active overtopping was also included in the modeling.

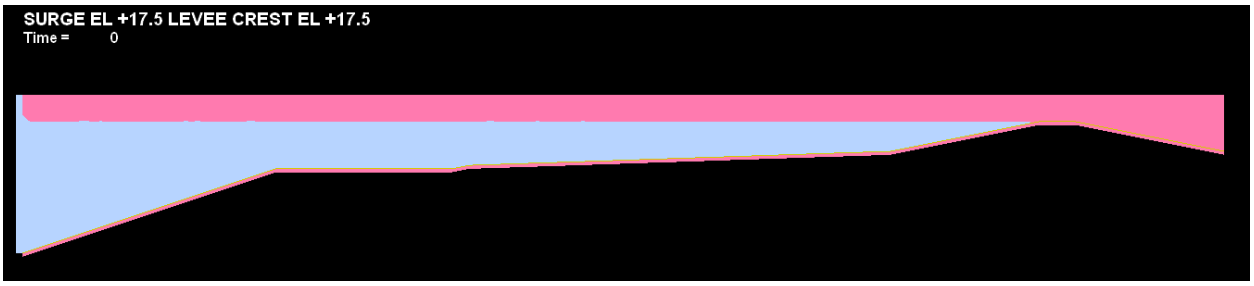


Figure C37**:** Initial conditions for analysis Case IX.

At Elevation +17.5 ft, the storm surge reaches the EBSB crest. A plot of shear velocities is presented in Figure C38. Based on the velocity profile, the majority of the velocities exceed the critical erosion values, so this implies that minor to moderate erosion/scour would occur as a result of wave impact at this elevation. The peak velocity was determined to be 26.2 ft/s.

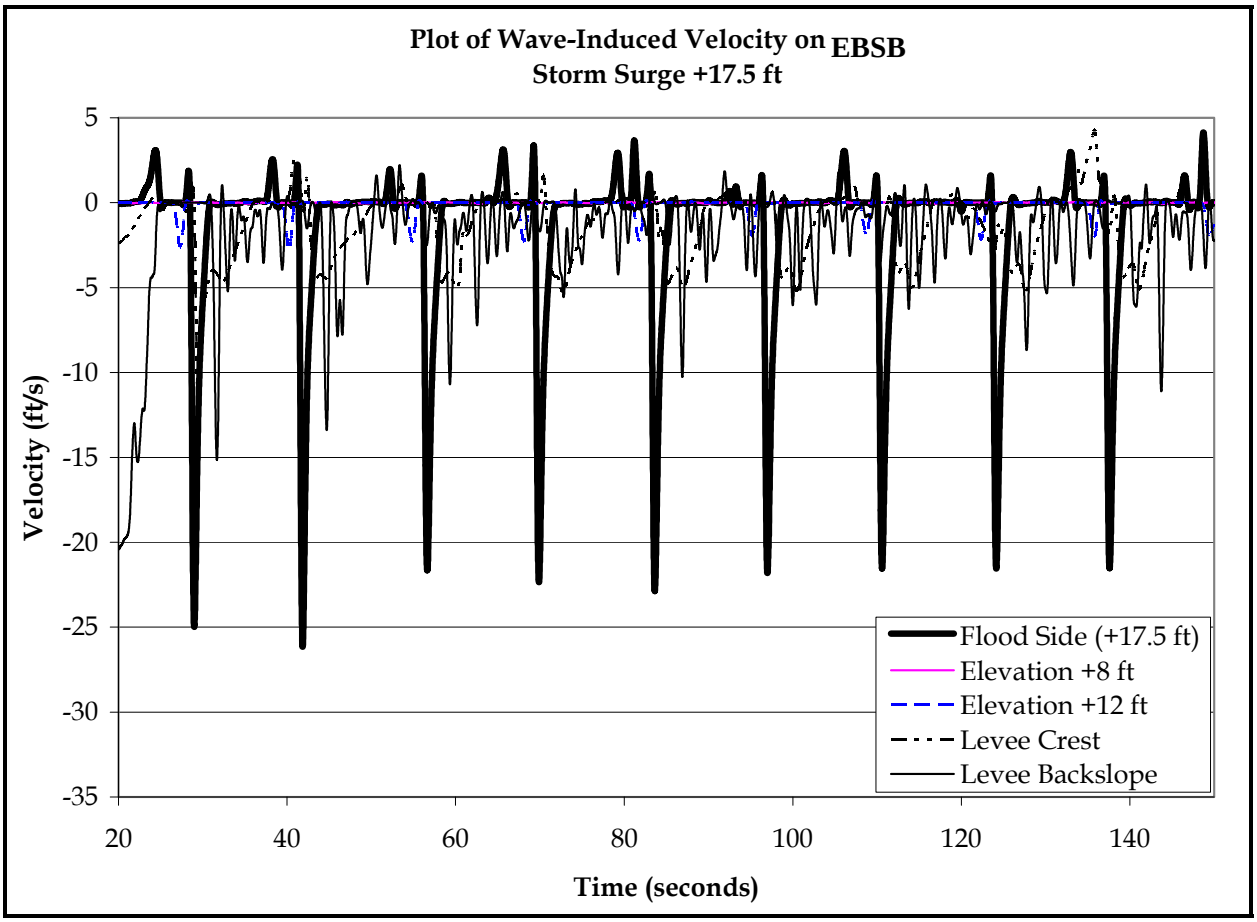


Figure C38: Time history plot of shear velocities for the storm surge at Elevation +17.5 ft.

Figure C39 (below) provides a graphical representation of water movement over time. With the hurricane storm surge at El. +17.5 ft, waves break on the EBSB face and spill over the crest until the wave pulse cascades down the back slope of the EBSB.

Storm Surge Elevation: +17.5 ft Crest Elevation: +17.5 ft

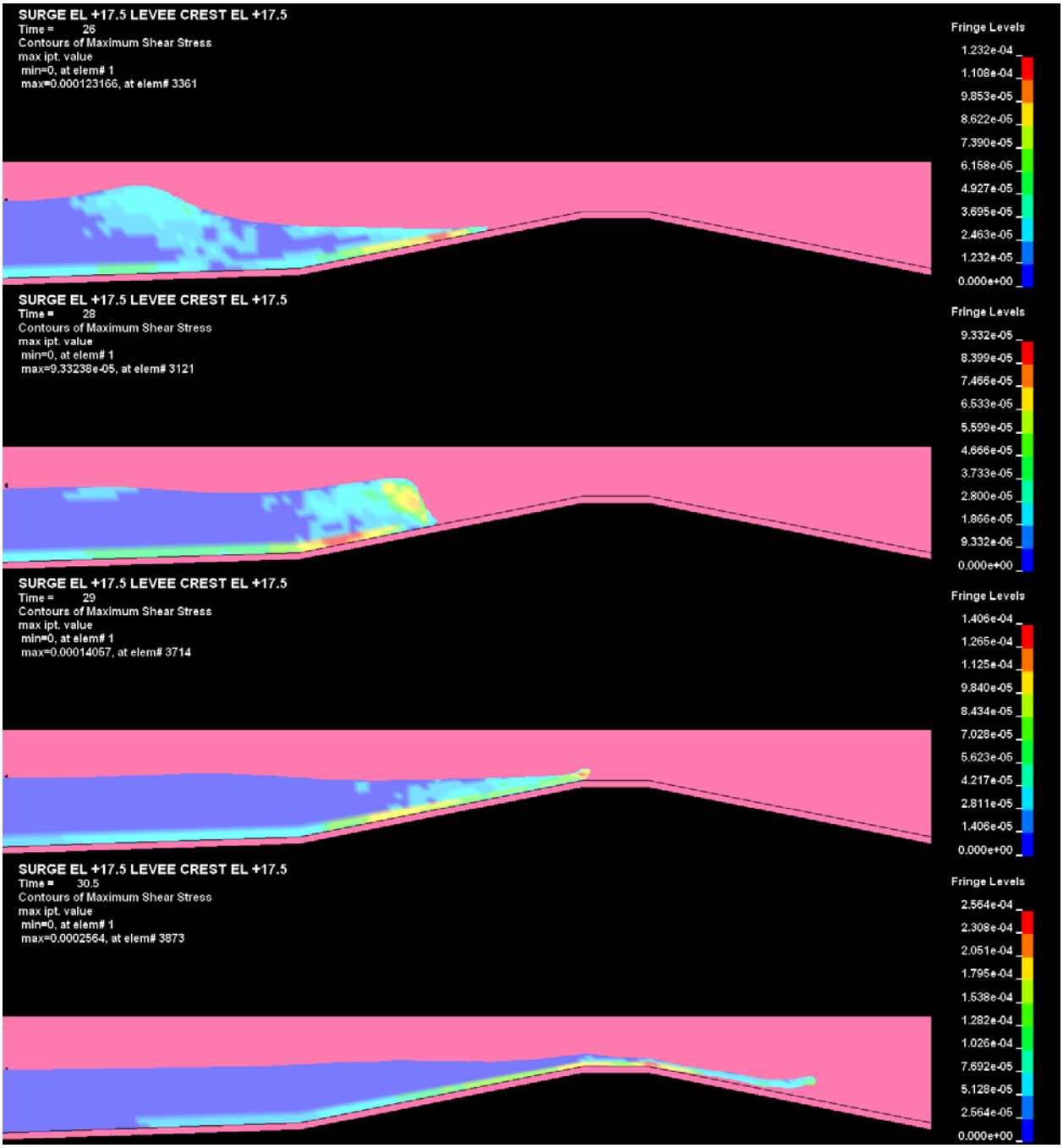


Figure C39**:** With the hurricane storm surge at El. +17.5 ft, waves break on the EBSB face and spill over the crest until the wave pulse cascades down the back slope of the EBSB.

Analysis Case X

Case X (Figure C40) consisted of a crest elevation of +17.5 ft (design geometry) and LSU-based hydrodynamics consisting of a storm surge elevation of +8 ft, a wave period of 2.0 s, and a significant wave height of 1.3 ft. No overtopping was included in the modeling.



Figure C40**:** Initial conditions for analysis Case X.

At Elevation +8 ft, the storm surge had reached the flood side toe of the EBSB. A plot of the shear velocities is presented in Figure C41. The peak shear velocity was determined to be 1.9 ft/s. This slope would have been vegetated at the time of the hurricane, so some erosion resistance was provided by the grassy cover. Based on the velocity profile, the calculated velocities do not exceed the critical erosion values, so this implies that negligible erosion would occur as a result of wave impact at this elevation.

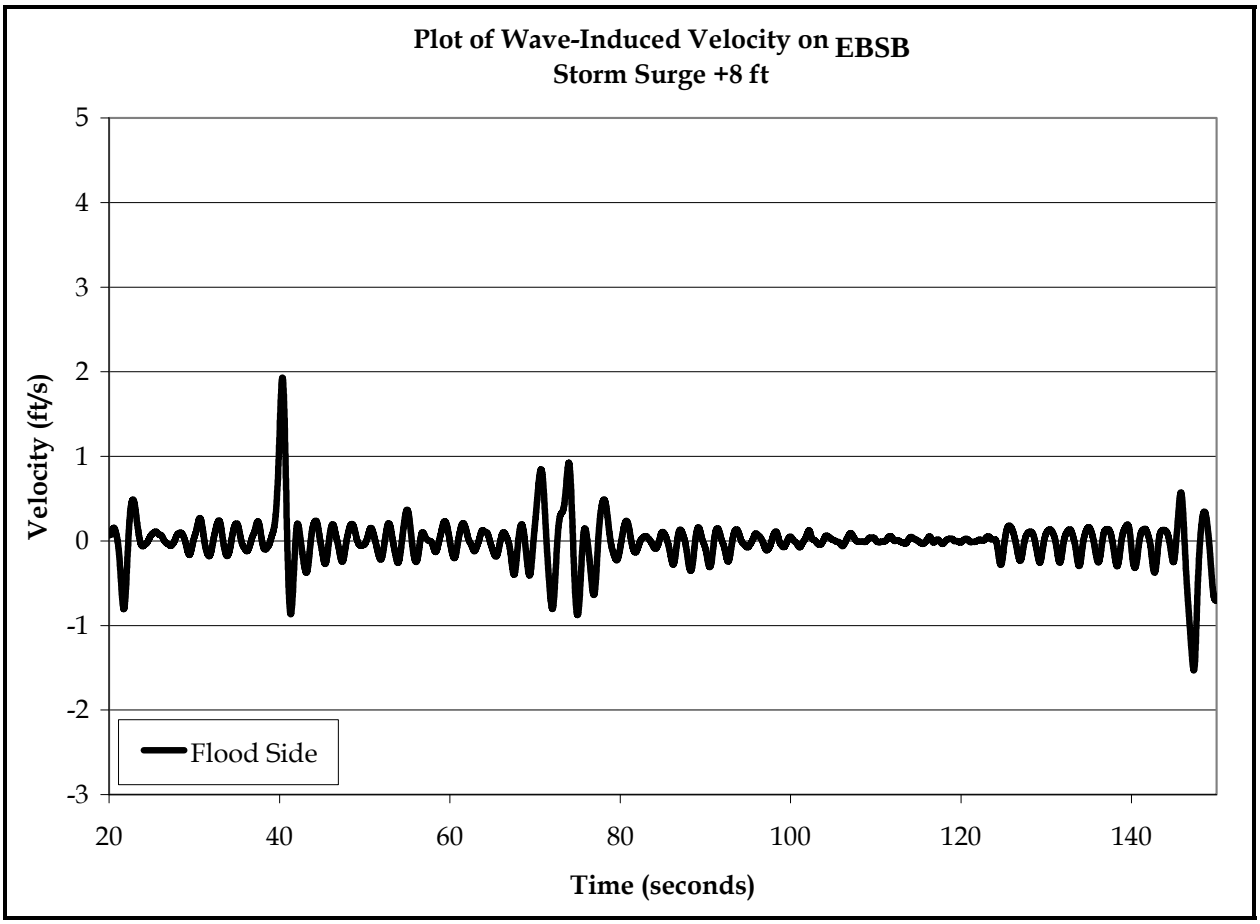


Figure C41: Time history plot of shear velocities for the storm surge at Elevation +8 ft.

Figure C42 (below) provides a graphical representation of water movement over time. With the hurricane storm surge at El. +8 ft, the design geometric configuration of the EBSB induces a tendency for the waves to exhibit a primarily 'runup' and 'rundown' behavior, with negligible wave impacts.

Storm Surge Elevation: +8 ft Crest Elevation: +17.5 ft



Figure C42: With the hurricane storm surge at El. +8 ft, the design geometric configuration of the EBSB induces a tendency for the waves to exhibit a primarily 'runup' and 'rundown' behavior with negligible wave impacts.

Analysis Case XI

Case XI (Figure C43) consisted of a crest elevation of +17.5 ft (design geometry) and LSU-based hydrodynamics consisting of a storm surge elevation of +12 ft, a wave period of 2.0 s, and a significant wave height of 2.0 ft. No overtopping was included in the modeling.

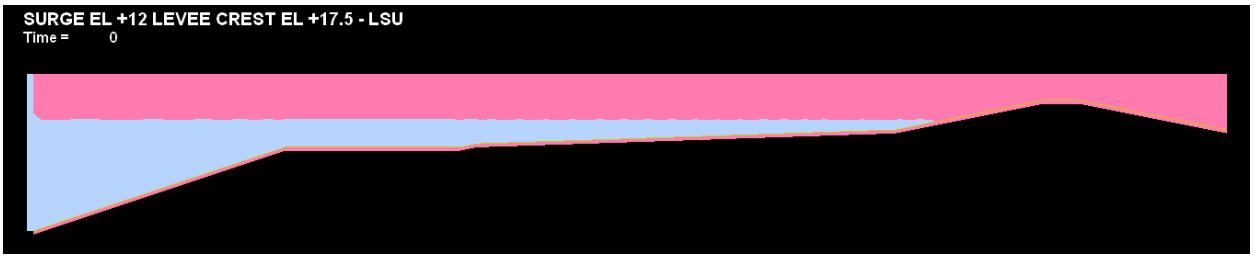


Figure C43: Initial conditions for analysis Case XI.

At Elevation +12 ft, the storm surge had reached the main EBSB 1 on 5 flood side slope. This slope would have been vegetated at the time of the hurricane, so some erosion resistance was provided by the grassy cover. A plot of shear velocities is presented in Figure C44. Based on the velocity profile, the majority of the velocities do not exceed the critical erosion values (including erosion protection offered by grass coverings), so this implies that minor erosion/scour would occur as a result of wave impact at this elevation. The peak velocity was determined to be 2.4 ft/s.

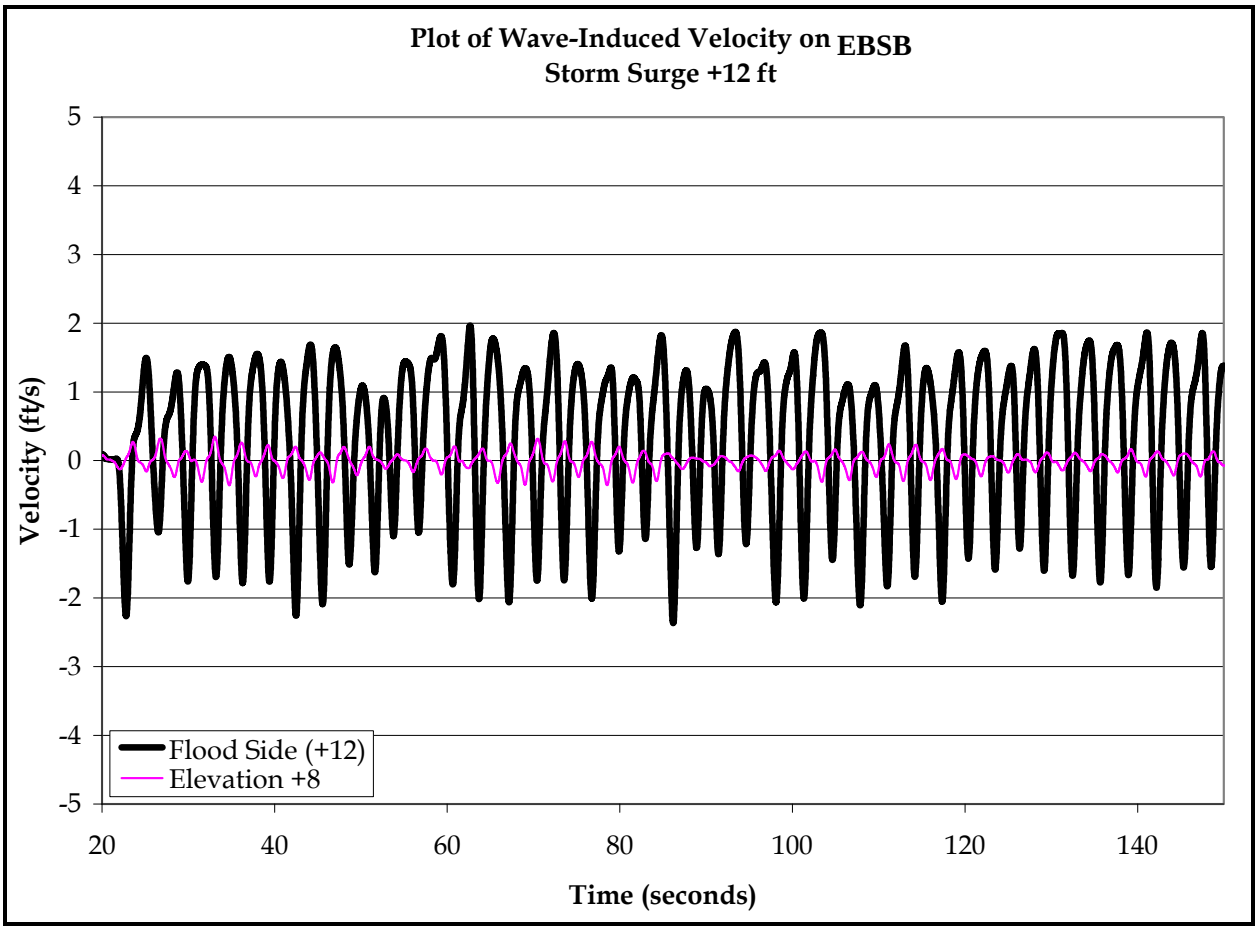


Figure C44: Time history plot of shear velocities for the storm surge at Elevation +12 ft.

Figure C45 (below) provides a graphical representation of water movement over time. With the hurricane storm surge at El. +12 ft, the design geometric configuration of the EBSB induces a tendency for the waves to exhibit a primarily 'runup' and 'rundown' behavior, with minor wave impacts.

Storm Surge Elevation: +12 ft Crest Elevation: +17.5 ft

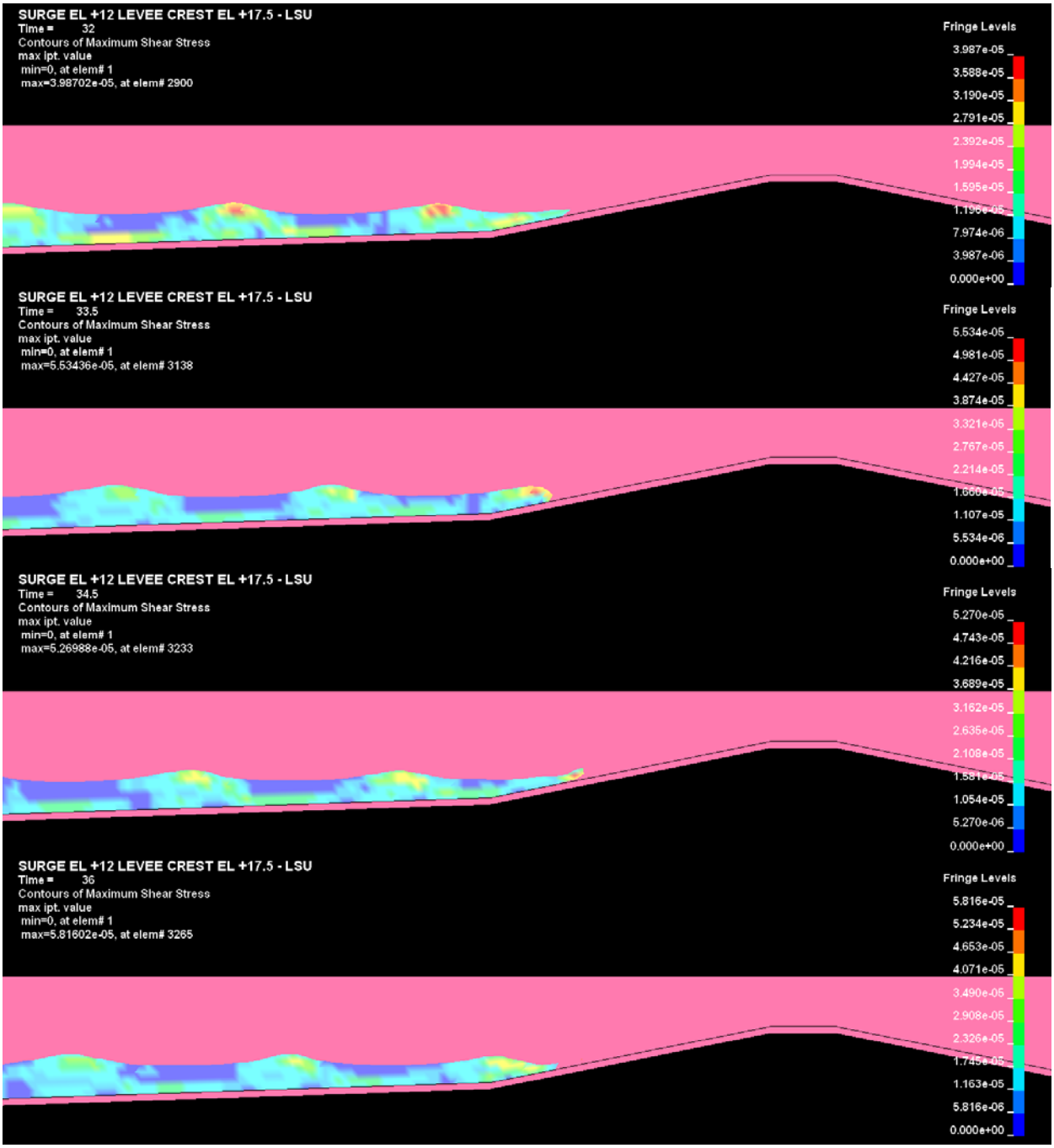


Figure C45: With the hurricane storm surge at El. +12 ft, the design geometric configuration of the EBSB induces a tendency for the waves to exhibit a primarily 'runup' and 'rundown' behavior with minor wave impacts.

Analysis Case XII

Case XII (Figure C50) consisted of a rest elevation of +17.5 ft (design geometry) and LSU-based hydrodynamics consisting of a storm surge elevation of +17.5 ft, a wave period of 6.0 s, and a significant wave height of 3.2 ft. Active overtopping was also included in the modeling.

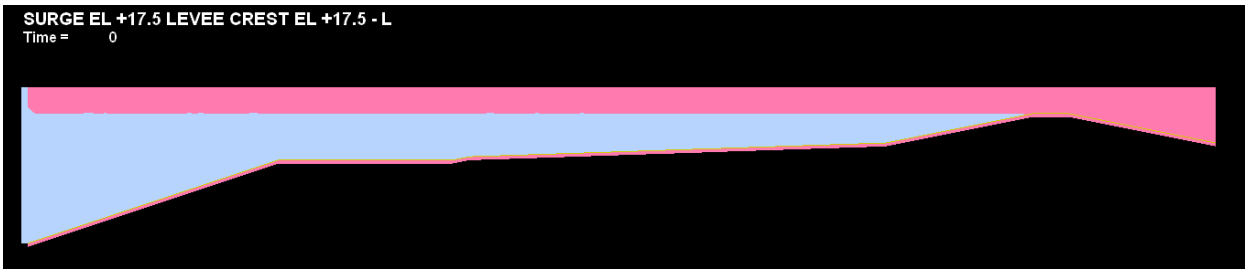


Figure C50**:** Initial conditions for analysis Case XII.

At Elevation +17.5 ft, the storm surge reaches the EBSB crest. A plot of shear velocities is presented in Figure C51. Based on the velocity profile, the majority of the velocities exceed the critical erosion values, so this implies that significant erosion/scour would occur as a result of wave impact at this elevation. The peak velocity was determined to be 20.8 ft/s.

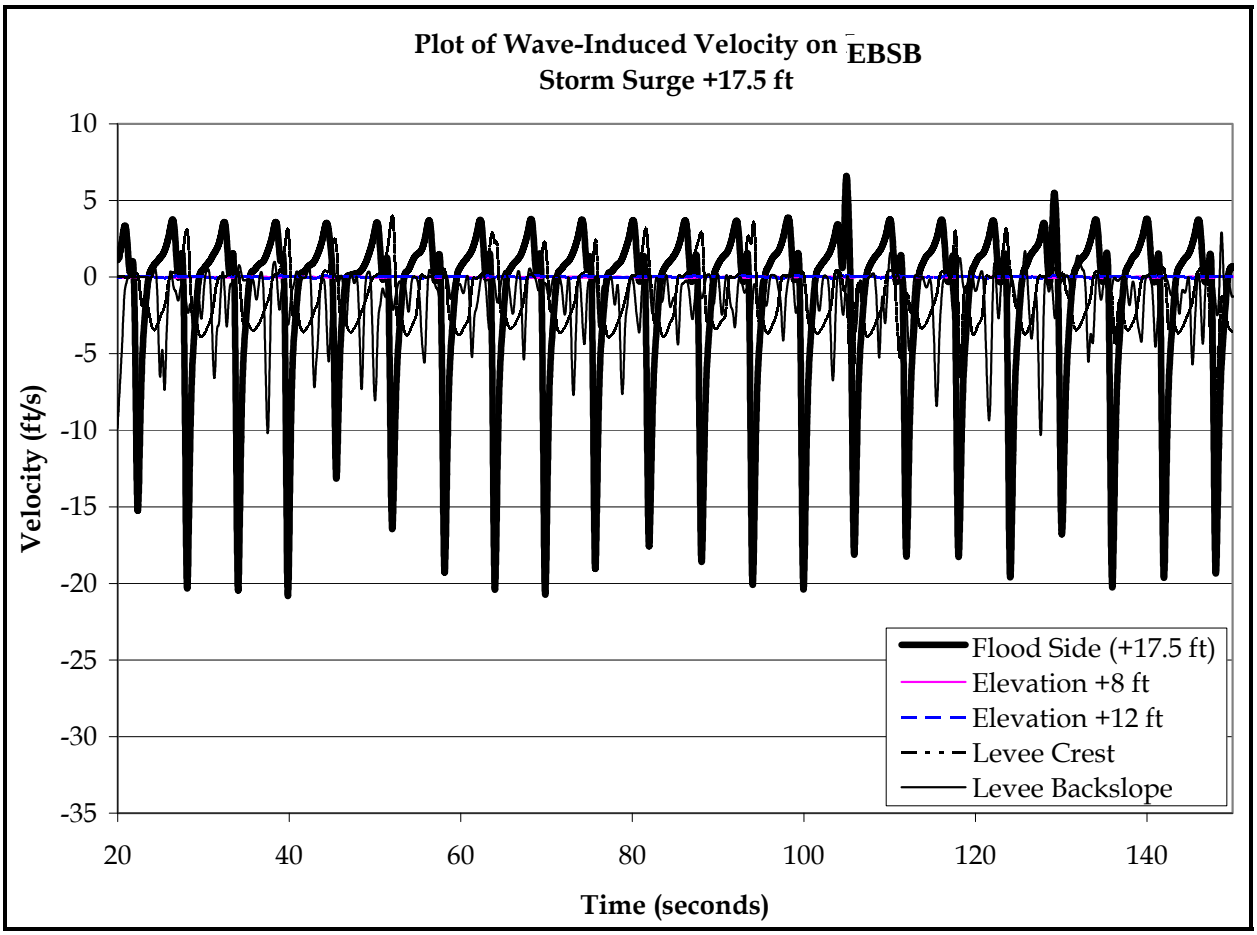


Figure C51**:** Time history plot of shear velocities for the storm surge at Elevation +17.5 ft.

Figure C52 (below) provides a graphical representation of water movement over time. With the hurricane storm surge at El. +17.5 ft, the design geometric configuration of the EBSB induces a tendency for the waves to exhibit a primarily 'runup' and 'rundown' behavior, with minor to moderate wave impacts.

Storm Surge Elevation: +17.5 ft Crest Elevation: +17.5 ft

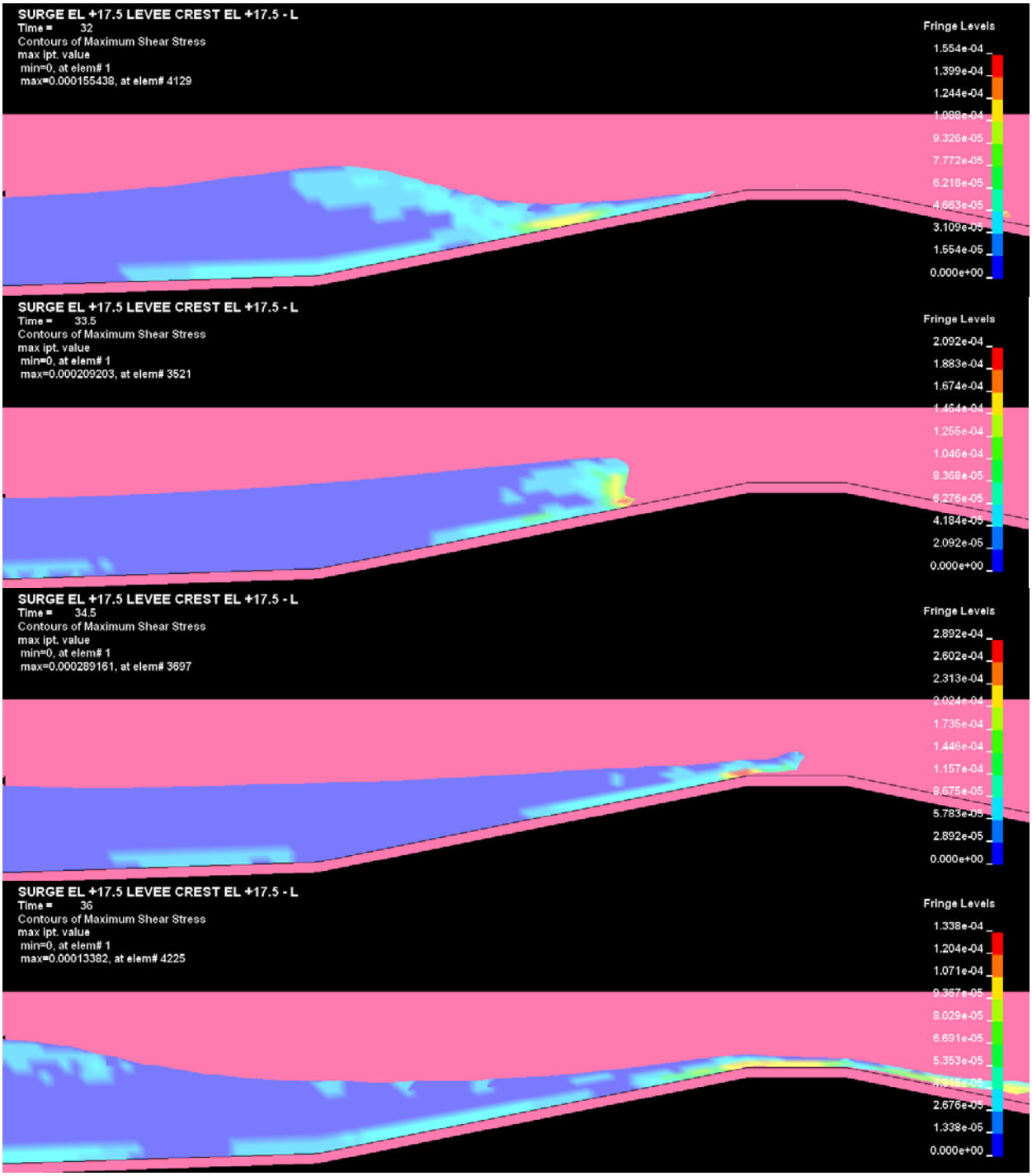


Figure C52**:** With the hurricane storm surge at El. +17.5 ft the EBSB experiences significant wave impacts.

Estimation of EBSB Breach due to Wave Impacts

Wave-induced cumulative erosion of EBSB materials (E) was calculated using an integrated time-step function (Eq C4) based on the erodibility of the EBSB material (estimated based on the procedure described in Section 8) at the time step being evaluated (where the erodibility of the time step is determined by the time-average shear velocities calculated at the defined storm surge elevations). The erodibility at the time step ($\dot{e}(v)$) is then multiplied by the value of the time step to calculate the lateral extent of erosion.

$$E = \sum \dot{e}(v(t))\Delta t \qquad \text{[Eq C4]}$$

Since the numerical simulation only has an effective time duration of 130 seconds (eliminating the first 20 numerical simulation time required to 'initiate' the model), the cumulative erosion for the 130 second period was extrapolated to the remainder of the time interval (i.e. multiplied by 3600s/130s or 27.74).

Tables C4-C7 presents a summary of the estimated lateral erosion between 0800 and 1200 (UTC). It was assumed (due to the high runup/rundown velocities) that no vegetative cover existed on the EBSB slope following the peak of the storm surge at 1200 (UTC). For overtopping conditions, erosion over the EBSB crest and overtopping induced erosion were not included in the lateral erosion calculations.

Table C4: Determination of Erosion on EBSB Flood Face, IPET Hydrodynamics, Actual Geometry

Time (UTC)	Storm Surge Elevation	Calculated Lateral Erosion (ft)	Cumulative Lateral Erosion (ft)
0800	+8 ft	0.7	0.7
0900	+10 ft	10.9	11.6
1000	+12 ft	21.0	32.6
1100	+15.3 ft	19.5	52.2
1200	+17.5 ft	18.0	70.2

Table C5: Determination of Erosion on EBSB Flood Face, LSU Hydrodynamics, Actual Geometry

Time (UTC)	Storm Surge Elevation	Calculated Lateral Erosion (ft)	Cumulative Lateral Erosion (ft)
0800	+8 ft	0.0	0.0
0900	+10 ft	4.5	4.5
1000	+12 ft	9.0	13.5
1100	+15.3 ft	15.5	29.0
1200	+17.5 ft	22.0	51.0

Table C6: Determination of Erosion on EBSB Flood Face, IPET Hydrodynamics, Design Geometry

Time (UTC)	Storm Surge Elevation	Calculated Lateral Erosion (ft)	Cumulative Lateral Erosion (ft)
0800	+8 ft	2.3	2.3
0900	+10 ft	10.7	13.0
1000	+12 ft	19.0	32.0
1100	+15.3 ft	21.0	53.0
1200	+17.5 ft	23.0	76.0

Table C7: Determination of Erosion on EBSB Flood Face, LSU Hydrodynamics, Design Geometry

Time (UTC)	Storm Surge Elevation	Calculated Lateral Erosion (ft)	Cumulative Lateral Erosion (ft)
0800	+8 ft	0.1	0.1
0900	+10 ft	2.5	2.6
1000	+12 ft	5.0	7.6
1100	+15.3 ft	33.0	40.6
1200	+17.5 ft	61.0	101.6

Based on these analyses, we can conclude that it was very possible for the EBSB to have been breached through the crest solely as a result of wave-induced erosion of the highly erodible materials used to construct the EBSB. By 1200 (UTC), the storm surge was above the EBSB crest (resulting in active overtopping of the EBSB) and the calculated cumulative erosion would have been sufficient to erode past the 10-ft wide EBSB crest.

Figure C53 shows a plot of lateral erosion induced from wave-attack on the actual and design geometric EBSB configurations. The EBSB crest is breached between 1100 and 1200 UTC (based on IPET and LSU hydrodynamics).

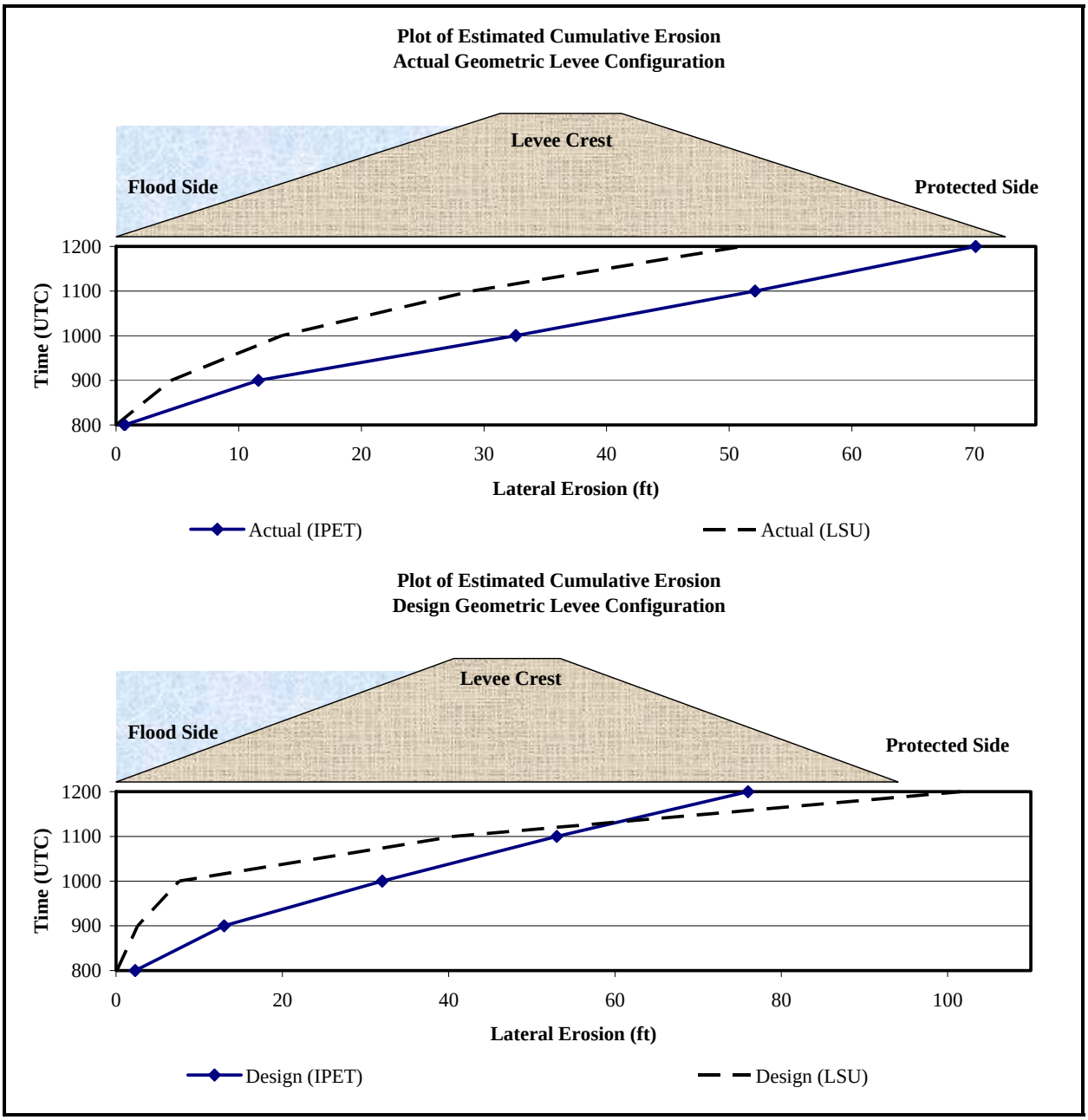


Figure C53: A plot of lateral erosion induced from wave-attack on the actual and design geometric EBSB configurations.

Wave Damage on EBSBs Constructed with ‘Good’ Materials

To evaluate wave-induced erosion on a EBSB with the same geometric configuration and hydrodynamic loading, the same wave-induced erosion (E) amount was calculated as Station 497+00 site, but the erodibility characteristics of a low erodibility EBSB material was selected from the MR-GO EBSBs north of Bayou Bienvenue.

Tables C8-C11 presents a summary of the estimated lateral erosion between 0800 and 1200 (UTC), when the storm surge elevations were above +8 ft for a levee constructed with ‘good’ materials. Shear velocities at storm surge elevations other than those modeled were selected based on linear interpolation. For overtopping conditions, erosion over the levee crest and overtopping induced erosion were not included in the lateral erosion calculations.

Table C8: Determination of Erosion on Levee Flood Face, IPET Hydrodynamics, Actual Geometry

Time (UTC)	Storm Surge Elevation	Calculated Lateral Erosion (ft)	Cumulative Lateral Erosion (ft)
0800	+8 ft	0.0	0.0
0900	+10 ft	0.0	0.0
1000	+12 ft	0.0	0.0
1100	+15.3 ft	0.0	0.0
1200	+17.5 ft	0.0	0.0

Table C9: Determination of Erosion on Levee Flood Face, LSU Hydrodynamics, Actual Geometry

Time (UTC)	Storm Surge Elevation	Calculated Lateral Erosion (ft)	Cumulative Lateral Erosion (ft)
0800	+8 ft	0.0	0.0
0900	+10 ft	0.0	0.0
1000	+12 ft	0.0	0.0
1100	+15.3 ft	0.0	0.0
1200	+17.5 ft	0.0	0.0

Table C10: Determination of Erosion on Levee Flood Face, IPET Hydrodynamics, Design Geometry

Time (UTC)	Storm Surge Elevation	Calculated Lateral Erosion (ft)	Cumulative Lateral Erosion (ft)
0800	+8 ft	0.0	0.0
0900	+10 ft	0.0	0.0
1000	+12 ft	0.0	0.0
1100	+15.3 ft	0.0	0.0
1200	+17.5 ft	0.0	0.0

Table C11: Determination of Erosion on Levee Flood Face, LSU Hydrodynamics, Design Geometry

Time (UTC)	Storm Surge Elevation	Calculated Lateral Erosion (ft)	Cumulative Lateral Erosion (ft)
0800	+8 ft	0.0	0.0
0900	+10 ft	0.0	0.0
1000	+12 ft	0.0	0.0
1100	+15.3 ft	0.0	0.0
1200	+17.5 ft	0.0	0.0

Based on these analyses, we can conclude that a levee constructed of 'good' materials with low erodibility would have performed significantly better than one constructed of high erodibility materials. Subjected to the same wave impacts, the levee with 'good' materials would have experienced insignificant erosion. It is also highly likely that the levee would have performed very well during overtopping conditions as well.

Figure C54 shows a plot of lateral erosion induced from wave-attack on the actual and design geometric levee configurations. No breaching occurs for a levee constructed of 'good' materials (0 ft of lateral erosion for both IPET and LSU hydrodynamics).

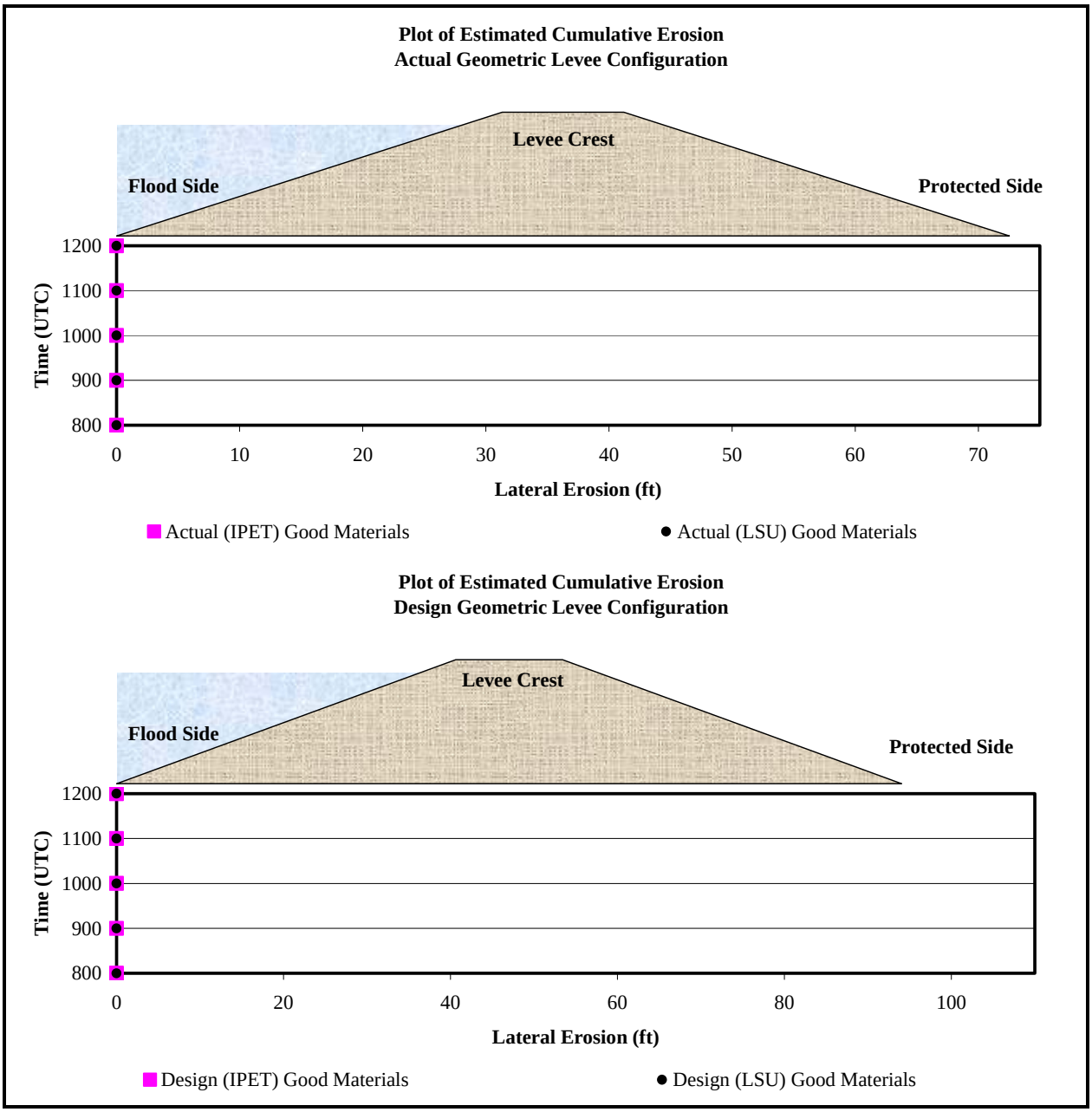


Figure C54: A plot of lateral erosion induced from wave-attack on the actual and design geometric levee configurations.

Validation

Velocities determined by LSDYNA were compared with velocity estimates from IPET (2007a) and were found to be in general agreement. IPET found protected side velocities to be on the order of 5-10 ft/s, which match well with our predicted range of 5-10 ft/s. IPET did not calculate wave-induced erosion, so it was not possible to compare our calculated erosion magnitudes with IPET estimates.

To validate the magnitude of LSDYNA simulated peak runup/rundown velocities, empirical correlations (Brunn, 1985) were used. The peak empirical wave runup/rundown velocity was compared with the peak LSDYNA wave runup/rundown velocity. This comparison is presented in Table C12.

Table C12: Comparison of LSDYNA Peak Velocities with Empirical Correlations

Case	Storm Surge Elevation	LSDYNA Peak Velocity (ft/s)	Empirical Peak Velocity (ft/s)	Velocity Agreement
I	+8 ft	2.3	1.8	Good
II	+12 ft	8.5	11.5	Fair
III	+17.5 ft	10.0	34.8	Underpredicts
IV	+8 ft	1.8	0.6	Overpredicts
V	+12 ft	5.0	4.8	Good
VI	+17.5 ft	8.8	15.2	Underpredicts
VII	+8 ft	3.2	13.1	Underpredicts
VIII	+12 ft	8.0	15.8	Underpredicts
IX	+17.5 ft	26.2	19.4	Overpredicts
X	+8 ft	1.9	7.1	Underpredicts
XI	+12 ft	2.4	7.2	Underpredicts
XII	+17.5 ft	20.8	22.3	Good

The majority of LSDYNA simulated cases developed wave runup/rundown peak velocities below the maximum velocity predicted by empirical methods. This is most likely a result of the selected 'monitoring' nodes not being situated within the maximum runup/rundown velocity zone. Incorporation of additional 'monitoring' nodes could be used to correct this problem, however, addition of these extra nodes was not possible within the allocated project completion time. The LSDYNA predicted velocities, however, are within a factor of two with the empirical values.

There were two instances where the LSDYNA wave runup/rundown peak velocities were greater than the empirical peak velocities. These instances occurred with the wave impacting the outside EBSB crest. The empirical peak velocities were developed for a sloping surface, not the crest of a 'levee,' so the empirical correlation may not accurately reflect the potential peak velocity due to the changes in geometric configuration. The magnitude of the overprediction is relatively small, with a maximum overprediction velocity of 7 ft/s (or 26%).

Supplemental Wave Impact Modeling (SWAN & LSU (2008) Hydrodynamics)

Interaction shear velocities between the storm surge and the EBSBs were evaluated for eight supplemental synthetic storm surge elevations and associated hydrodynamics developed by LSU (2008) and Kok et al. (2008). Simulations were performed using the actual EBSB configuration (as determined based on the available Aerial LiDAR data from 2000). For each storm surge elevation a numerical simulation was conducted for 150 seconds using the hydrodynamic characteristics as defined by LSU (2008) and Kok et al. (2008). Table C13 presents a summary of the wave analysis conditions. Table C14 presents the wave generation parameter inputs for the simulations.

Table C13: Summary of Wave Analysis Conditions

Case	Time (CDT)	Storm Surge Elevation (ft) NAVD88	Significant Wave Height, H_{mo} (ft)	Wave Period (s)	Overtopping Rate ($ft^3/s/ft$)
A	04:00	10.2	3.9	3.3	0.0
B	04:30	11.1	4.5	3.5	0.0
C	05:00	12.0	5.2	3.8	0.0
D	05:30	12.8	5.9	4.0	0.0
E	06:00	13.8	6.6	4.2	0.0
F	06:30	14.8	7.3	4.5	0.2
G	07:00	16.0	7.9	4.7	0.3
H	07:30	17.1	7.6	4.9	0.3

Table C14: Wave Generation Parameters

Case	Time (CDT)	Storm Surge Elevation (ft) NAVD88	Wave Height Parameter (v)	Wave Period Parameter (ω)	Overtopping_ Velocity ($ft^3/s/ft$)
A	04:00	10.2	2.285	1.80	0.0
B	04:30	11.1	2.685	1.80	0.0
C	05:00	12.0	2.950	1.57	0.0
D	05:30	12.8	3.255	1.57	0.0
E	06:00	13.8	2.950	1.26	0.0
F	06:30	14.8	4.080	1.35	0.2
G	07:00	16.0	4.200	1.20	0.3
H	07:30	17.1	4.120	1.35	0.3

The relative error between the simulated DYNA waves and the specified hydrodynamics (Kok et al., 2008) is presented in Table C15. In general, there was very close (less than 15% error) agreement between the modeled and specified wave (note that relative error for wave period is presented in "()").

Table C15: Calculated Error of LSDYNA Simulated Waves

Case	Storm Surge Elevation (ft) NAVD88	Significant Wave Height, H_{mo} (ft)	Wave Period (s)	DYNA Wave Height (H)	DYNA Wave Period	Percent Error
A	10.2	3.9	3.3	3.7	3.5	5% (6%)
B	11.1	4.5	3.5	4.1	3.5	9% (0%)
C	12.0	5.2	3.8	4.9	4.0	6% (5%)
D	12.8	5.9	4.0	6.0	4.0	2% (0%)
E	13.8	6.6	4.2	6.9	5.0	5% (19%)
F	14.8	7.3	4.5	7.4	4.5	1% (0%)
G	16.0	7.9	4.7	8.0	5.0	1% (6%)
H	17.1	7.6	4.9	7.4	5.0	3% (2%)

Results

The imposed interaction shear velocities calculated by the LSDYNA numerical simulation were compared against the erosion/scour soil limits (capacity) as estimated based on the Erodibility Function Apparatus and EBSB soil composition. The EBSB at Station 497+00 was characterized to consist of semi-compacted hydraulic fill (high erodibility material).

The analyses determined the likelihood of EBSB breaching due to wave impact during the rise of the hurricane storm surge. As a result, the analysis time frame was limited to the time before the storm surge overtopped the EBSB. Once overtopping occurred, the high-erodibility materials

would have been extremely susceptible to erosion due to the high velocities and low material erosion resistance. Wave-induced cumulative erosion of EBSB materials (E) was calculated using an integrated time-step function (Eq C4, as presented in Section XI) based on the erodibility of the EBSB material at the time step being evaluated (where the erodibility of the time step is determined by the time-average shear velocities calculated at the defined storm surge elevations).

Since the numerical simulation only has an effective time duration of 130 seconds (eliminating the first 20 numerical simulation time required to 'initiate' the model), the cumulative erosion for the 130 second period was extrapolated to the remainder of the 30-time interval (i.e. multiplied by 1800s/130s or 13.87).

Table C16 presents a summary of the estimated lateral erosion between 0400 and 0730 (CDT). For overtopping conditions, erosion over the EBSB crest and overtopping induced erosion were not included in the lateral erosion calculations.

Table C16: Determination of Erosion on EBSB Flood Face, Kok et al. (2008) Hydrodynamics, Actual Geometry

Time (CDT)	**Storm Surge Elevation (ft) NAVD88**	**Calculated Lateral Erosion (ft)**	**Cumulative Lateral Erosion (ft)**
04:00	10.2	14.0	14.0
04:30	11.1	14.4	28.4
05:00	12.0	13.9	42.3
05:30	12.8	19.6	61.9
06:00	13.8	6.2	68.1
06:30	14.8	6.0	74.1
07:00	16.0	0	74.1
07:30	17.1	0.4	74.5

Figure C55 shows a plot of lateral erosion induced from wave-attack on the actual and design geometric EBSB configurations. Based on these simulations, and the assumed EBSB geometric configuration and materials, the EBSB crest is breached around 0500 CDT. After 0530 CDT, the magnitude of lateral erosion dramatically reduces as the outboard EBSB face is fully submerged by the storm surge (which occurs around 0600 CDT). Because the EBSB face is submerged, there is no wave-induced runup/rundown, minimizing velocity magnitudes on the EBSB face.

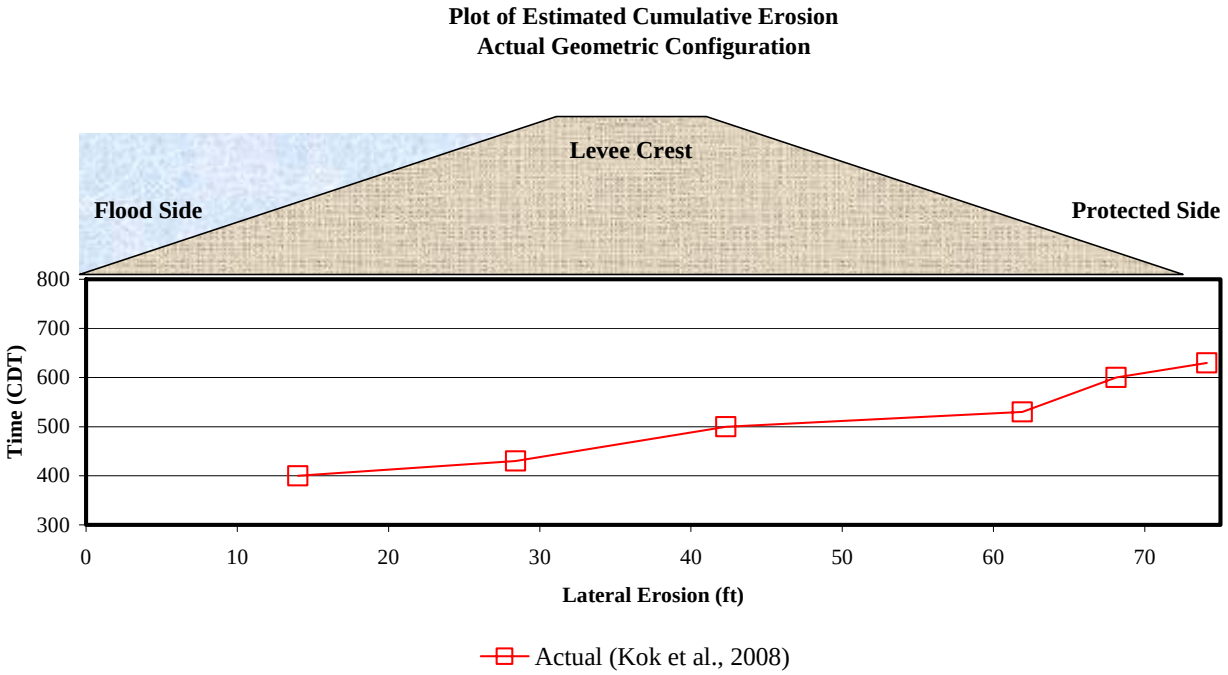


Figure C55: Estimate of cumulative lateral wave-induced levee erosion between 0400 and 0700 CDT based on Kok et al., (2008) hydrodynamics. Erosion through the levee crest is estimated to have occurred at 0500 CDT.

A comparison between the supplemental analysis and previous analyses using IPET and LSU hydrodynamics is presented in Figure C56. The Kok et al. (2008) hydrodynamics imply that more wave-induced erosion occurred on the EBSB than wave-induced erosion as determined by the LSU (2007) and IPET (2007a) hydrodynamics. However, all three hydrodynamic profiles indicate that the EBSB would have been breached as a result of wave-induced erosion.

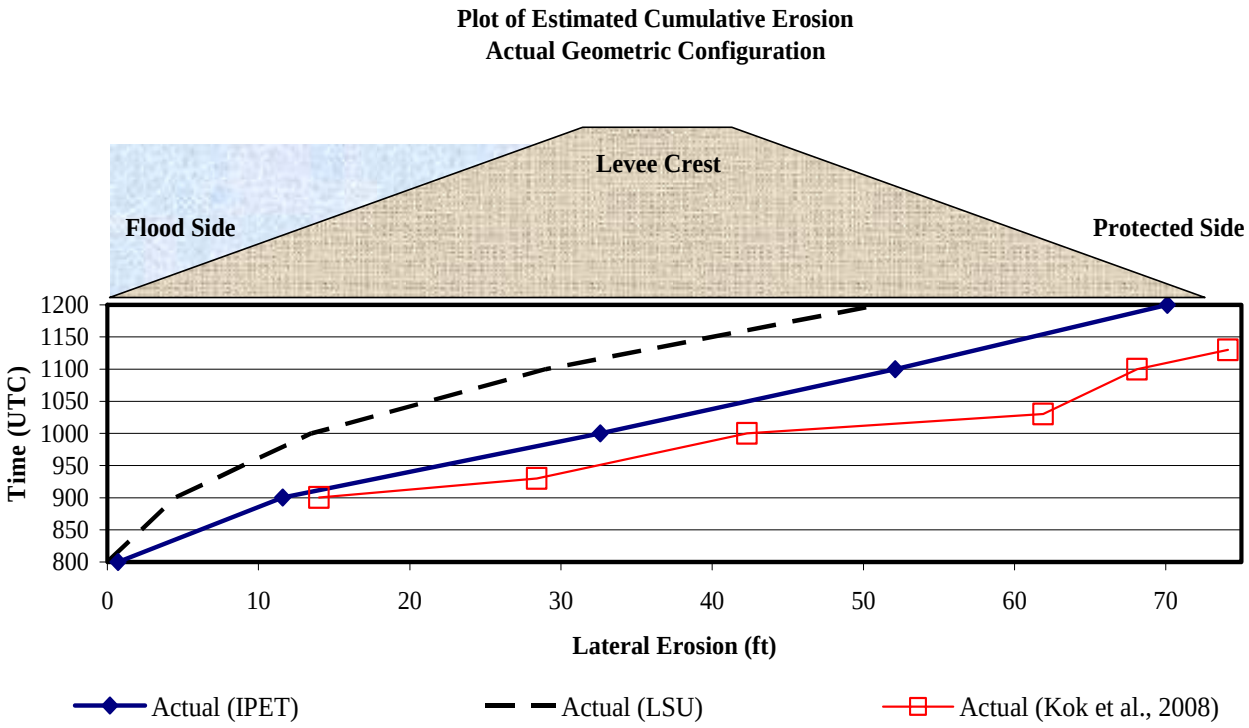


Figure C56: Comparison of lateral erosion estimates based on IPET (2007a), LSU (2007), and Kok et al., (2008) hydrodynamics. All three hydrodynamic profiles result in breaching of the EBSB due to wave-induced erosion.

Erosion analyses were also performed accounting for velocities parallel (or 'current) to the EBSB flood-face. These current velocities were generated as a result of water flow through the MRGO and GIWW towards the IHNC and Lake Pontchartrain. The magnitude of the current velocity was on the order of 0.5 to 1 ft/s (Kok et al., 2008) at the face of the EBSB. Figure C57 shows the result of inclusion of the current velocities. There was no significant impact of this velocity component.

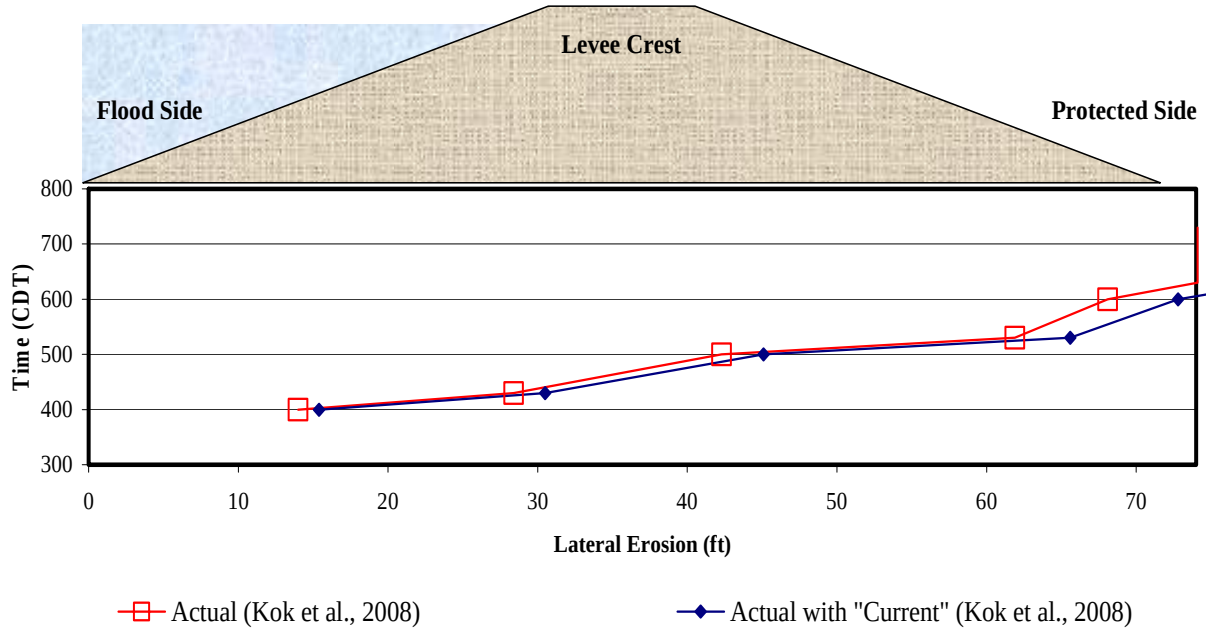


Figure C57: Comparison of lateral erosion estimates based on IPET (2007a), LSU (2007), and Kok et al., (2008) hydrodynamics, with and without current velocity contributions.

Results of Supplementary Simulation Runs

A case-by-case breakdown of simulated results is presented in this section. Simulations spanned from 0400 CDT to 0730 CDT and were performed every 30 minutes.

Analysis Case A (0400 CDT)

Case A (Figure C58) consisted of a storm surge elevation of +10.2 ft (NAVD88), a wave period of 3.3 s, and a significant wave height of 3.9 ft. There was no overtopping.

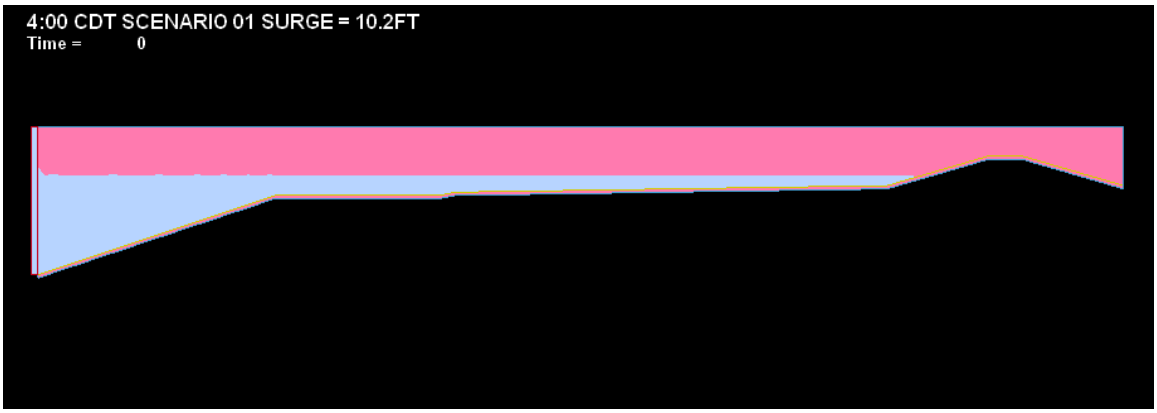


Figure C58: Initial conditions for analysis Case A.

At Elevation +10.2 ft, the storm surge had reached the flood side toe of the EBSB. A plot of the shear velocities is presented in Figure C59. The peak shear velocity was determined to be 13.1 ft/s.

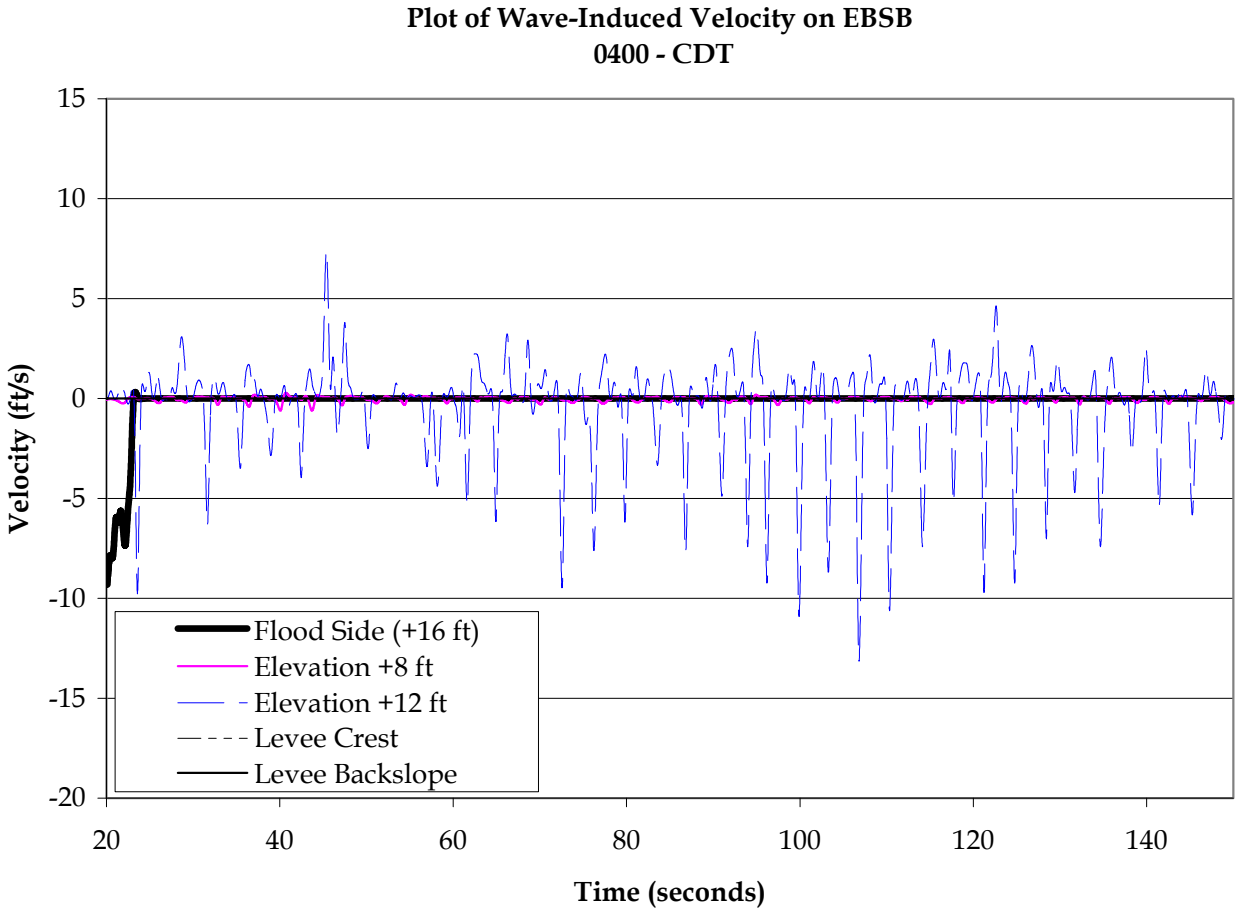


Figure C59**:** A plot of the velocity time history on the flood side face of the EBSB with the storm surge at +10.2 ft (NAVD88).

Figure C60 (below) provides a graphical representation of water movement over time. With the hurricane storm surge at El. +10.2 ft (NAVD88), the actual geometric configuration of the EBSB induces a tendency for the waves to exhibit a primarily 'runup' and 'rundown' behavior.

Storm Surge Elevation: +10.2 ft (NAVD88) Crest Elevation: +16 ft

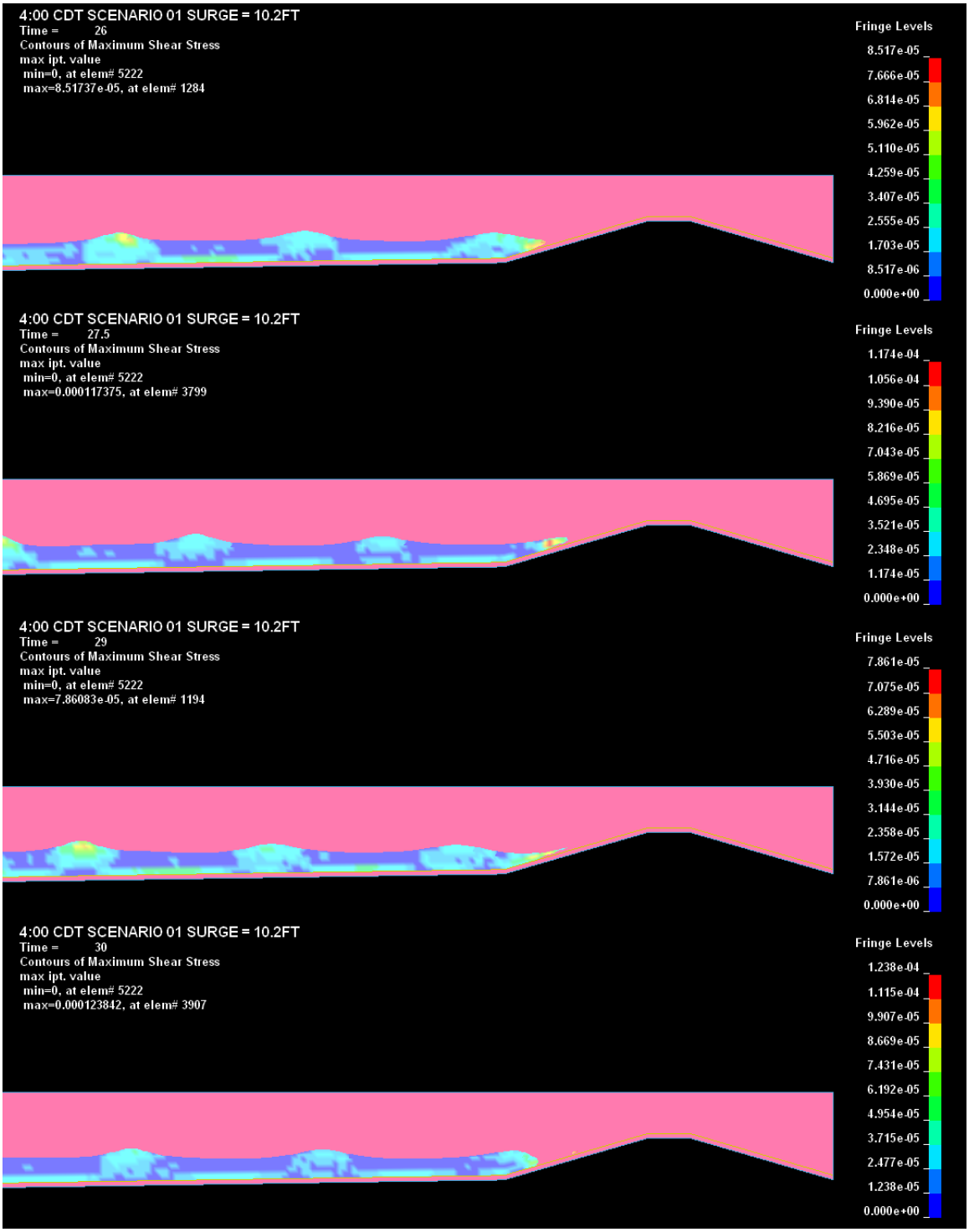


Figure C60**:** With the hurricane storm surge at El. +10.2 ft (NAVD88), the actual geometric configuration of the EBSB induces a tendency for the waves to exhibit a primarily 'runup' and 'rundown' behavior.

Analysis Case B (0430 CDT)

Case B (Figure C61) consisted of a storm surge elevation of +11.1 ft (NAVD88), a wave period of 3.5 s, and a significant wave height of 4.5 ft. There was no overtopping.

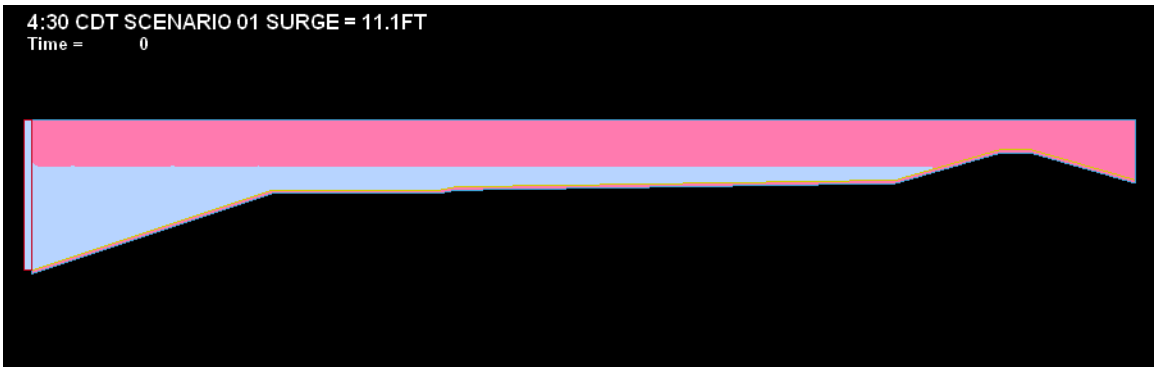


Figure C61: Initial conditions for analysis Case B.

A plot of the shear velocities is presented in Figure C62. The peak shear velocity was determined to be 11.3 ft/s.

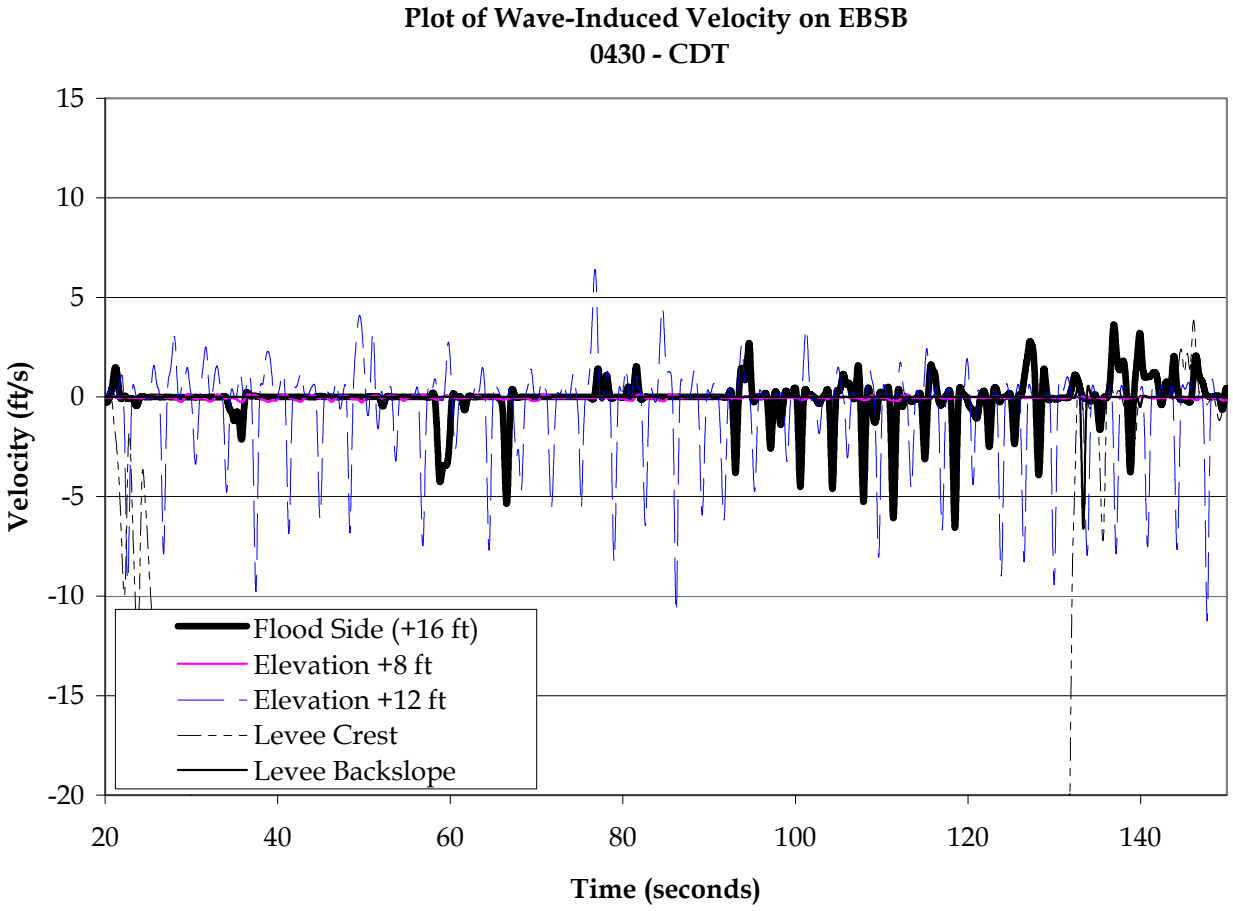


Figure C62**:** A plot of the velocity time history on the flood side face of the EBSB with the storm surge at +11.1 ft (NAVD88).

Figure C63 (below) provides a graphical representation of water movement over time. With the hurricane storm surge at El. +11.1 ft (NAVD88), the actual geometric configuration of the EBSB induces a tendency for the waves to exhibit a primarily 'runup' and 'rundown' behavior.

Storm Surge Elevation: +11.1 ft (NAVD88) Crest Elevation: +16 ft

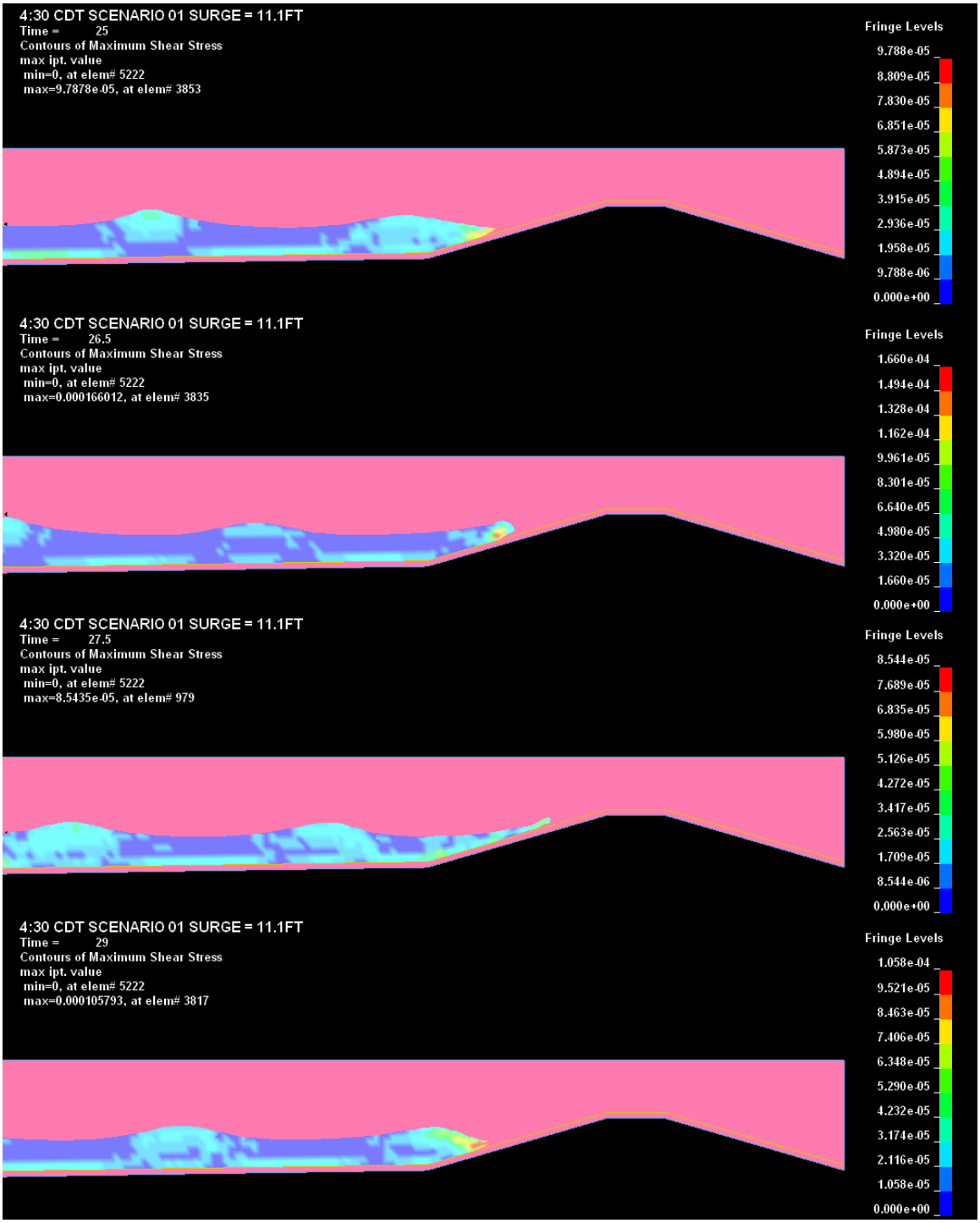


Figure C63**:** With the hurricane storm surge at El. +11.1 ft (NAVD88), the actual geometric configuration of the EBSB induces a tendency for the waves to exhibit a primarily 'runup' and 'rundown' behavior.

Analysis Case C (0500 CDT)

Case C (Figure C64) consisted of a storm surge elevation of +12.0 ft (NAVD88), a wave period of 3.8 s, and a significant wave height of 5.2 ft. There was no overtopping.

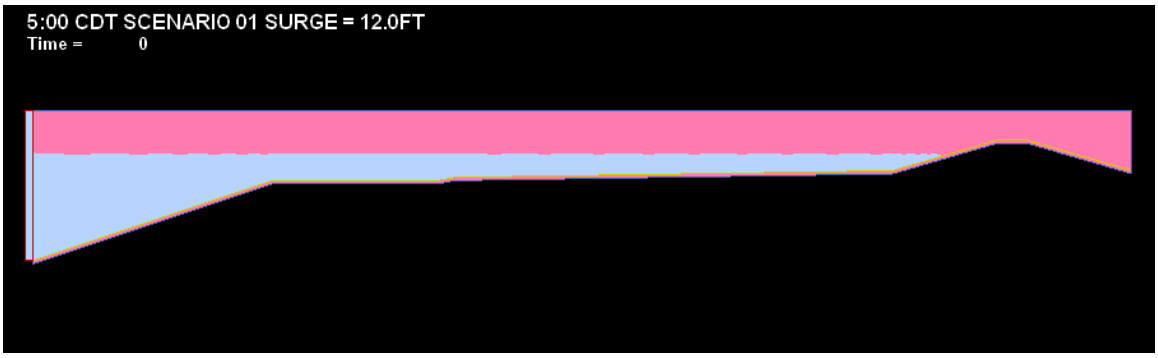


Figure C64: Initial conditions for analysis Case C.

A plot of the shear velocities is presented in Figure C65. The peak shear velocity was determined to be 7.2 ft/s.

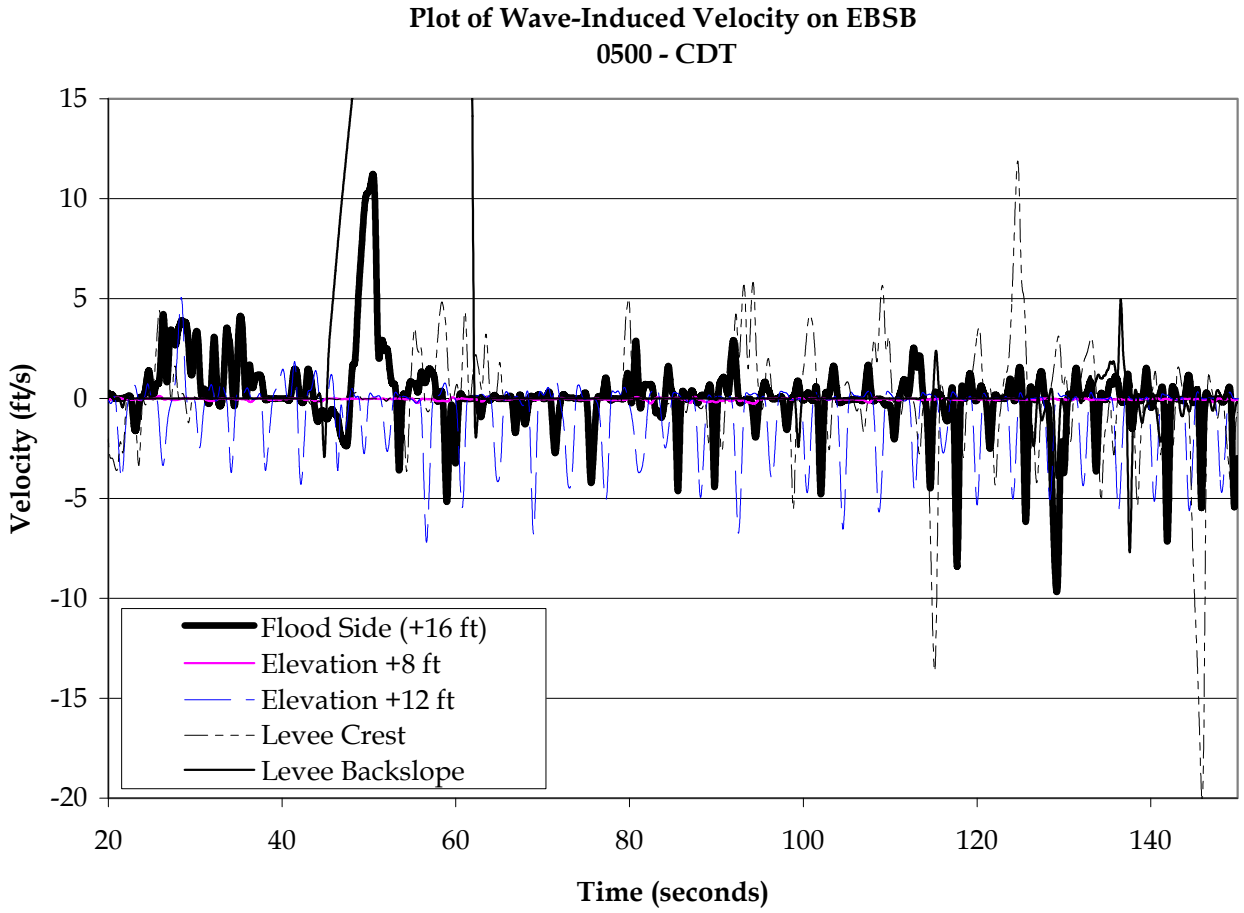


Figure C65**:** A plot of the velocity time history on the flood side face of the EBSB with the storm surge at +12.0 ft (NAVD88).

Figure C66 (below) provides a graphical representation of water movement over time. With the hurricane storm surge at El. +12.0 ft (NAVD88), the actual geometric configuration of the EBSB induces a tendency for the waves to exhibit a primarily 'runup' and 'rundown' behavior.

Storm Surge Elevation: +12.0 ft (NAVD88) Crest Elevation: +16 ft

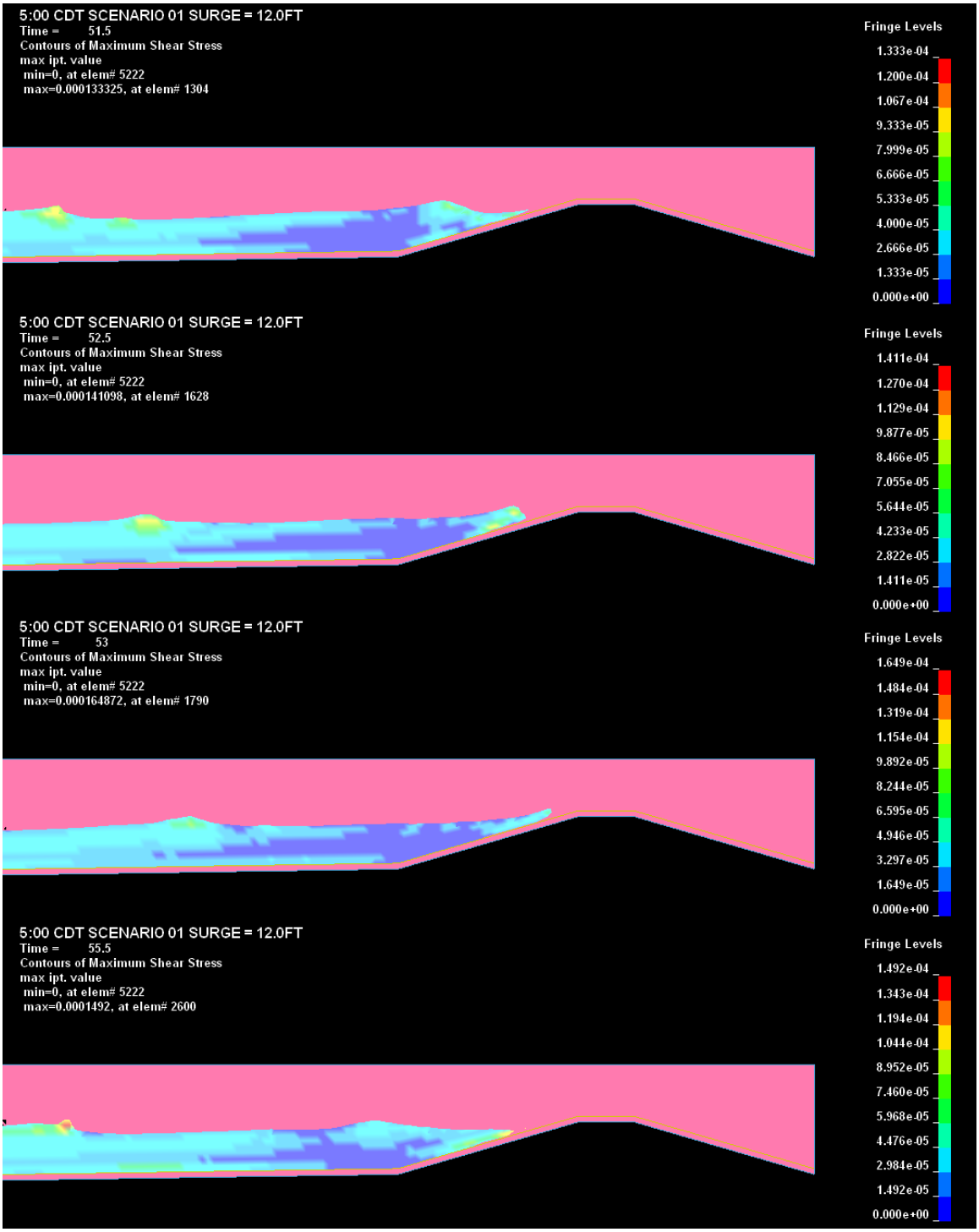


Figure C66**:** With the hurricane storm surge at El. +12.0 ft (NAVD88), the actual geometric configuration of the EBSB induces a tendency for the waves to exhibit a primarily ‘runup’ and ‘rundown’ behavior.

Analysis Case D (0530 CDT)

Case D (Figure C67) consisted of a storm surge elevation of +12.8 ft (NAVD88), a wave period of 4.0 s, and a significant wave height of 5.9 ft. There was no overtopping.

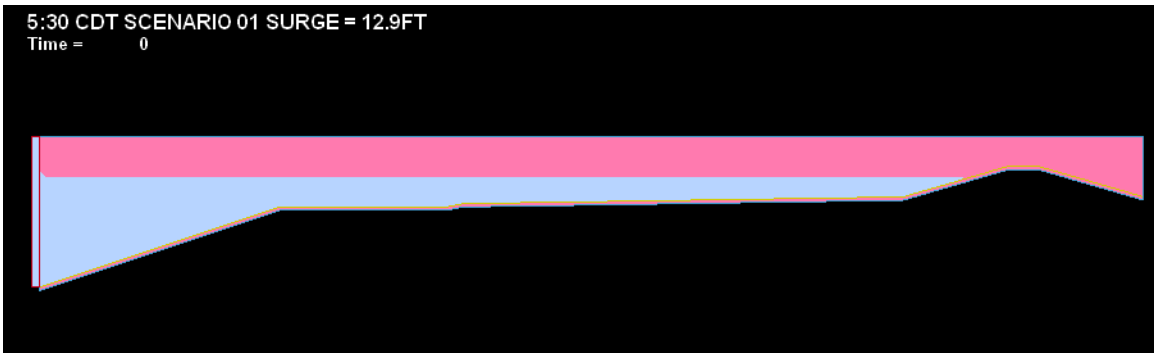


Figure C67: Initial conditions for analysis Case D.

A plot of the shear velocities is presented in Figure C68. The peak shear velocity was determined to be 12.3 ft/s.

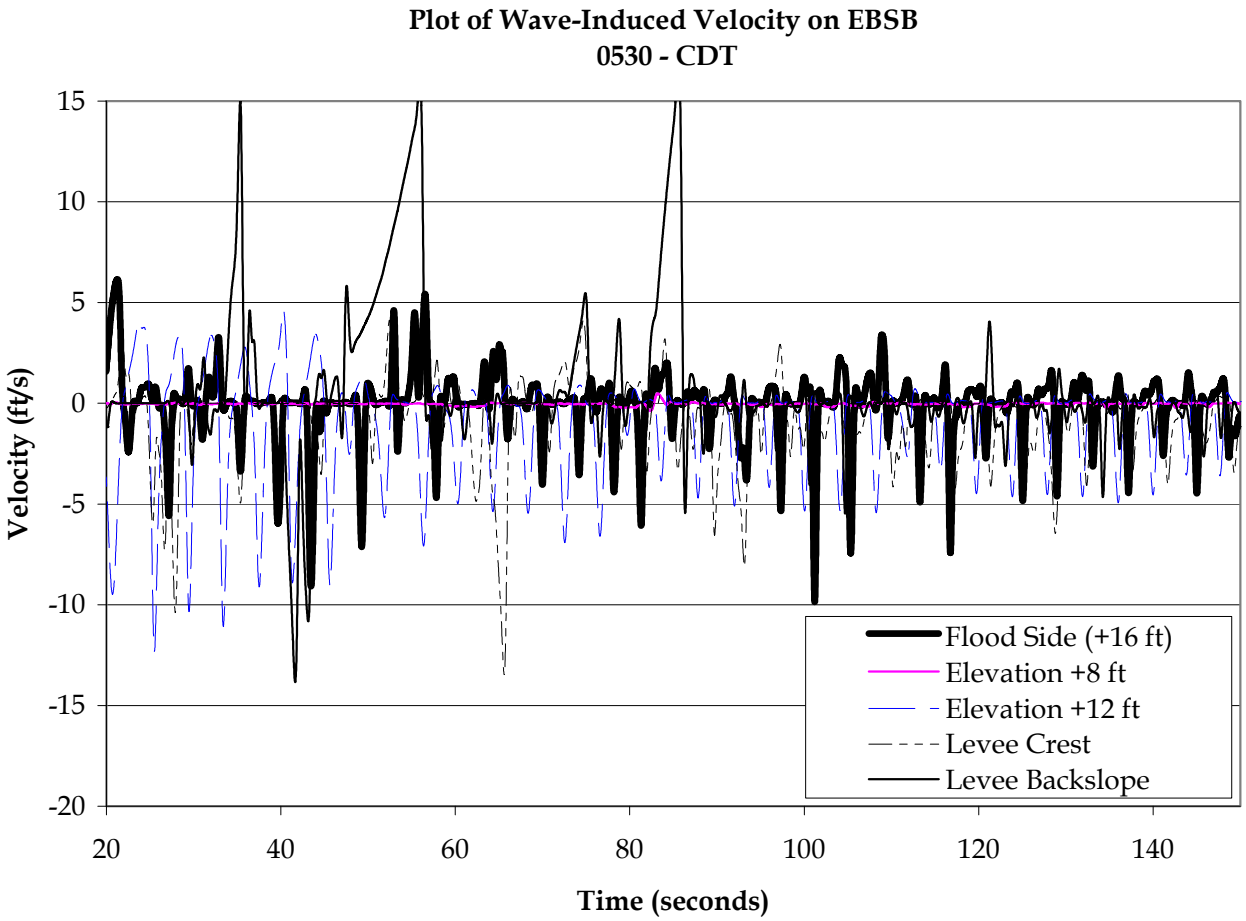


Figure C68**:** A plot of the velocity time history on the flood side face of the EBSB with the storm surge at +12.8 ft (NAVD88).

Figure C69 (below) provides a graphical representation of water movement over time. With the hurricane storm surge at El. +12.8 ft (NAVD88), the actual geometric configuration of the EBSB induces a tendency for the waves to exhibit a primarily 'runup' and 'rundown' behavior.

Storm Surge Elevation: +12.8 ft (NAVD88) Crest Elevation: +16 ft

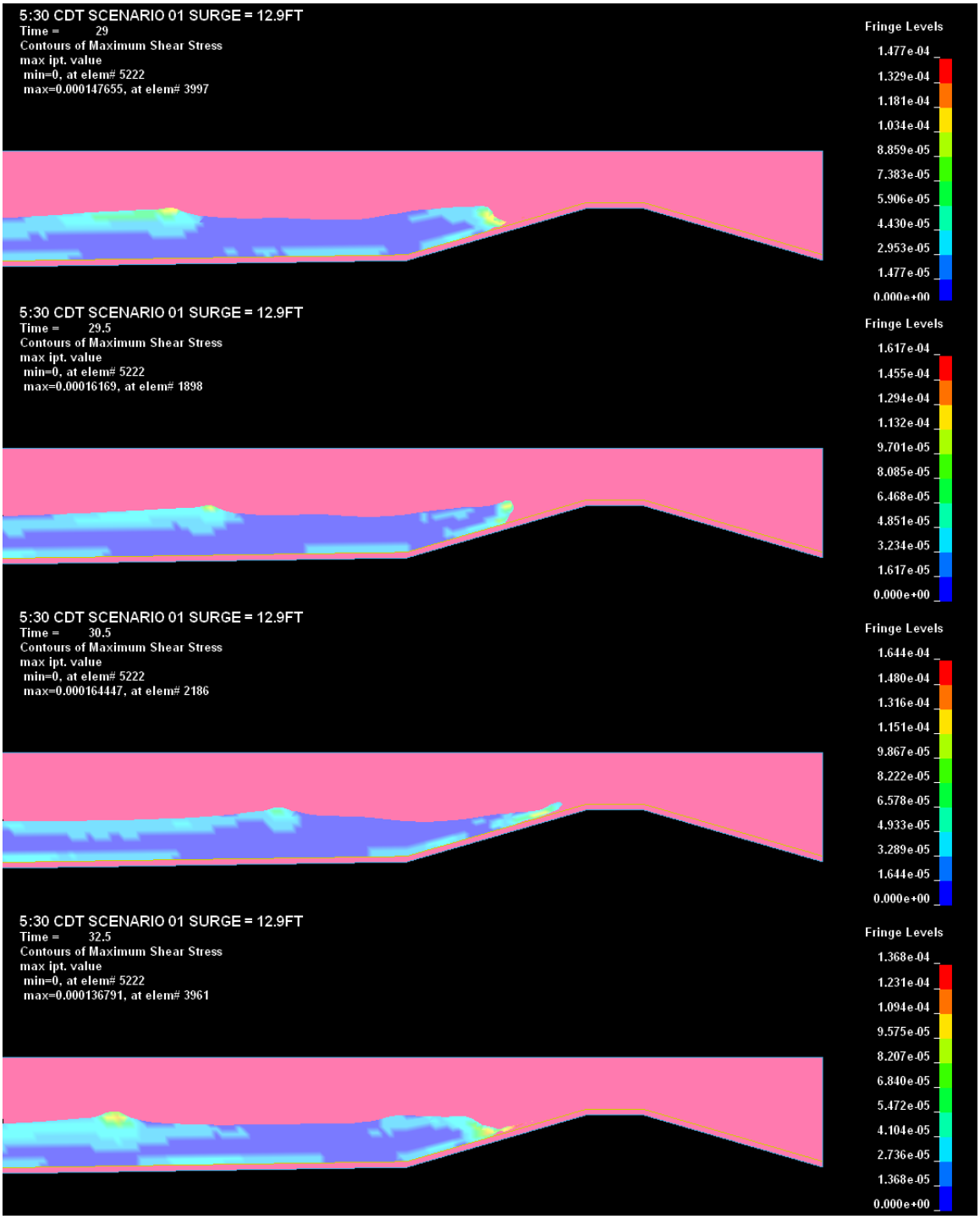


Figure C69**:** With the hurricane storm surge at El. +12.8 ft (NAVD88), the actual geometric configuration of the EBSB induces a tendency for the waves to exhibit a primarily 'runup' and 'rundown' behavior.

Analysis Case E (0600 CDT)

Case E (Figure C70) consisted of a storm surge elevation of +13.8 ft (NAVD88), a wave period of 4.2 s, and a significant wave height of 6.6 ft. There was minor wave-induced overtopping.

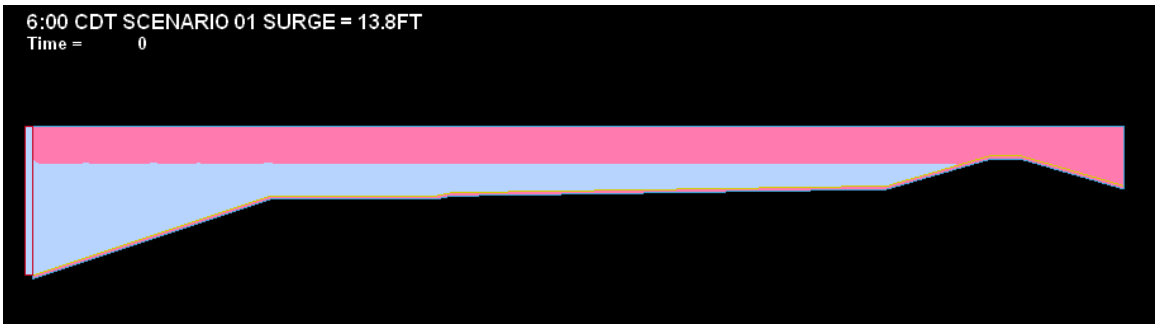


Figure C70: Initial conditions for analysis Case E.

At Elevation +10.2 ft, the storm surge had reached the flood side toe of the EBSB. A plot of the shear velocities is presented in Figure C71. The peak shear velocity was determined to be 6.2 ft/s.

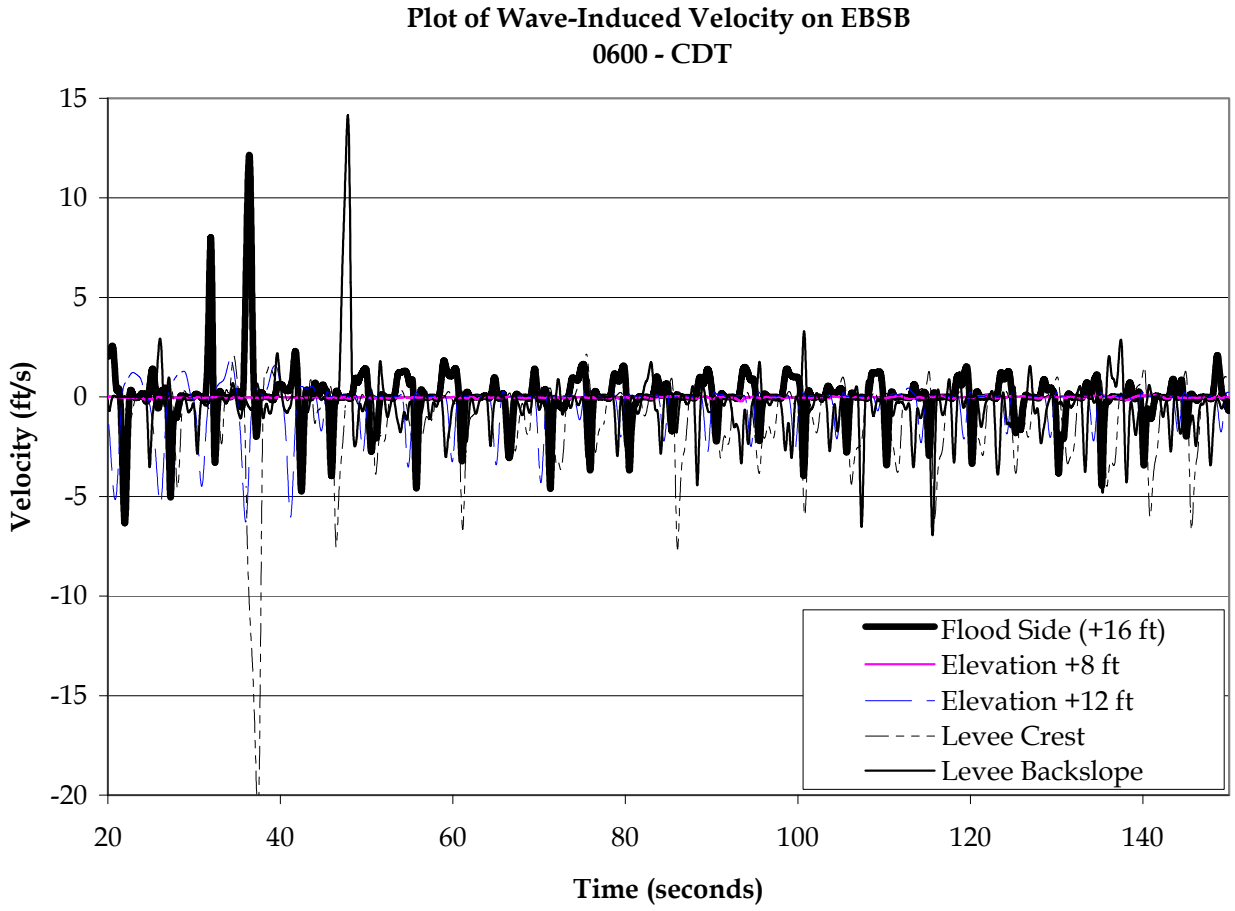


Figure C71**:** A plot of the velocity time history on the flood side face of the EBSB with the storm surge at +13.8 ft (NAVD88).

Figure C72 (below) provides a graphical representation of water movement over time. With the hurricane storm surge at El. +13.8 ft (NAVD88), the actual geometric configuration of the EBSB induces a tendency for the waves to exhibit a primarily 'runup' and 'rundown' behavior, with some wave-induced EBSB overtopping.

Storm Surge Elevation: +13.8 ft (NAVD88) Crest Elevation: +16 ft

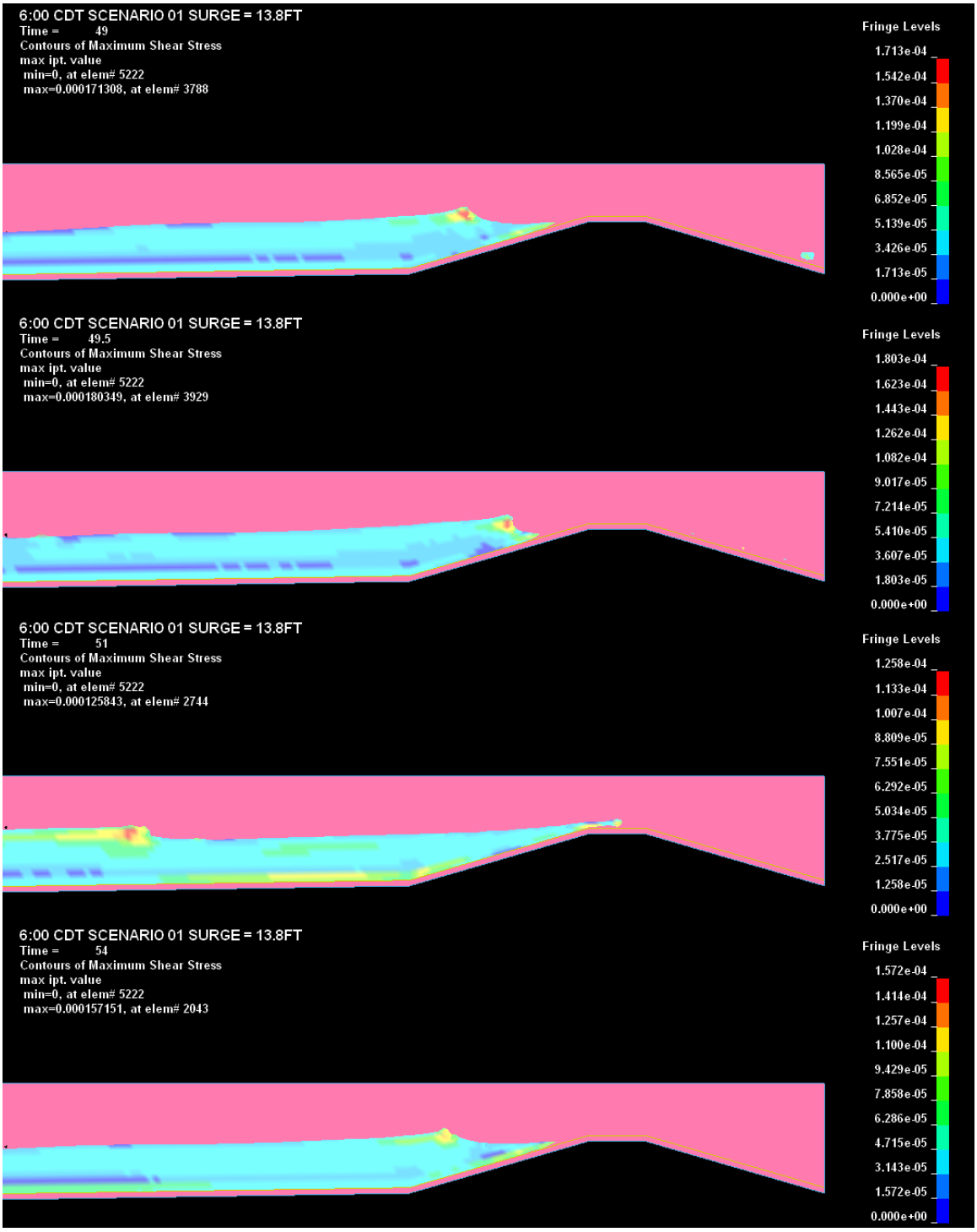


Figure C72**:** With the hurricane storm surge at El. +13.8 ft (NAVD88), the actual geometric configuration of the EBSB induces a tendency for the waves to exhibit a primarily ‘runup’ and ‘rundown’ behavior.

Analysis Case F (0630 CDT)

Case F (Figure C73) consisted of a storm surge elevation of +14.8 ft (NAVD88), a wave period of 4.5 s, and a significant wave height of 7.3 ft. There was wave-induced EBSB overtopping.

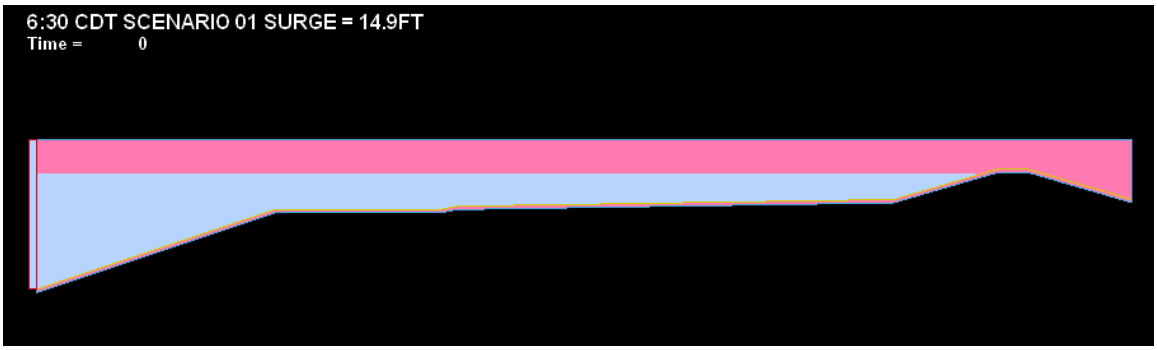


Figure C73: Initial conditions for analysis Case F.

At Elevation +14.8 ft, the storm surge was near the crest of the EBSB. A plot of the shear velocities is presented in Figure C74. The peak shear velocity was determined to be 6.0 ft/s.

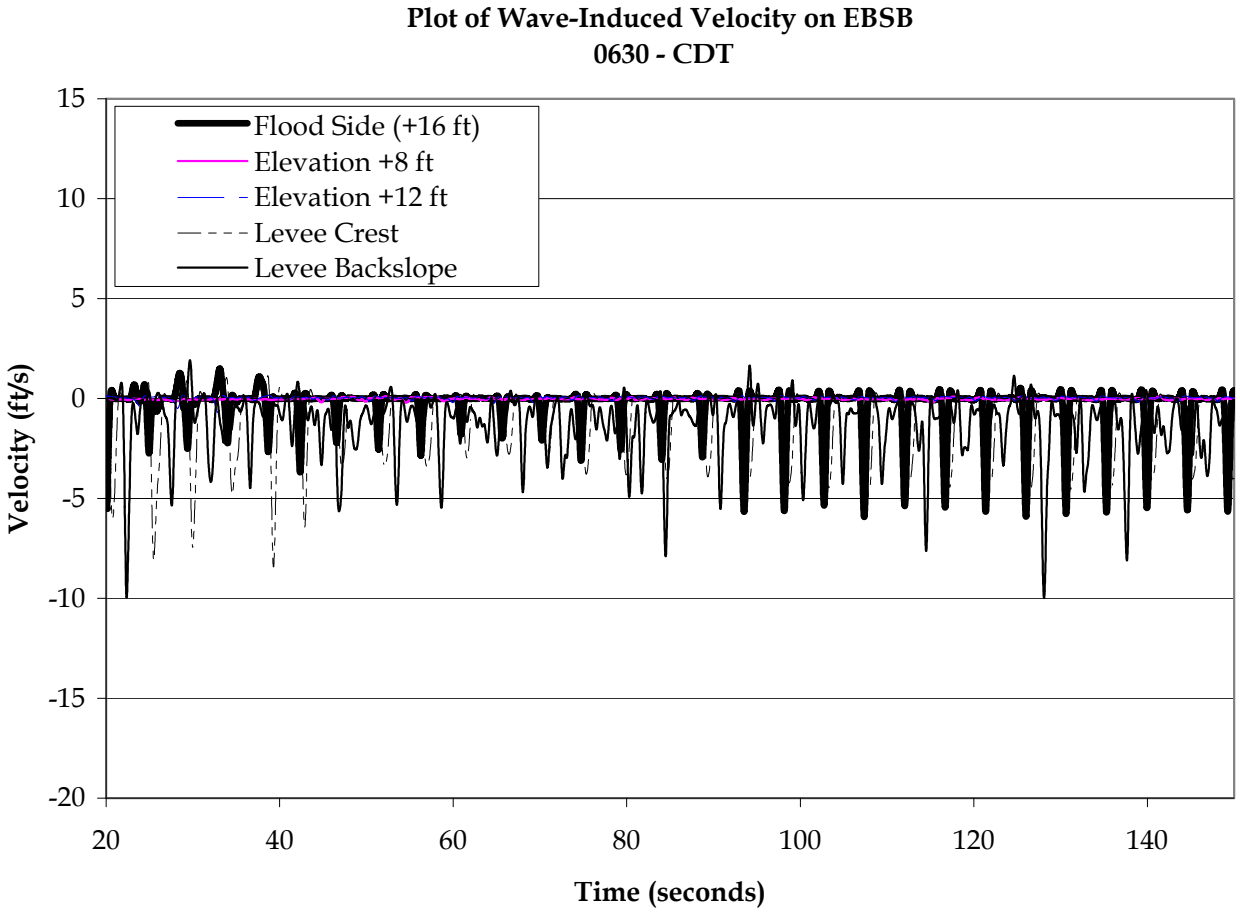


Figure C74**:** A plot of the velocity time history on the flood side face of the EBSB with the storm surge at +14.8 ft (NAVD88).

Figure C75 (below) provides a graphical representation of water movement over time. With the hurricane storm surge at El. +14.8 ft (NAVD88), the actual geometric configuration of the EBSB induces a tendency for the waves to exhibit a primarily 'runup' and 'rundown' behavior, but with wave-induced overtopping as well.

Storm Surge Elevation: +14.8 ft (NAVD88) Crest Elevation: +16 ft

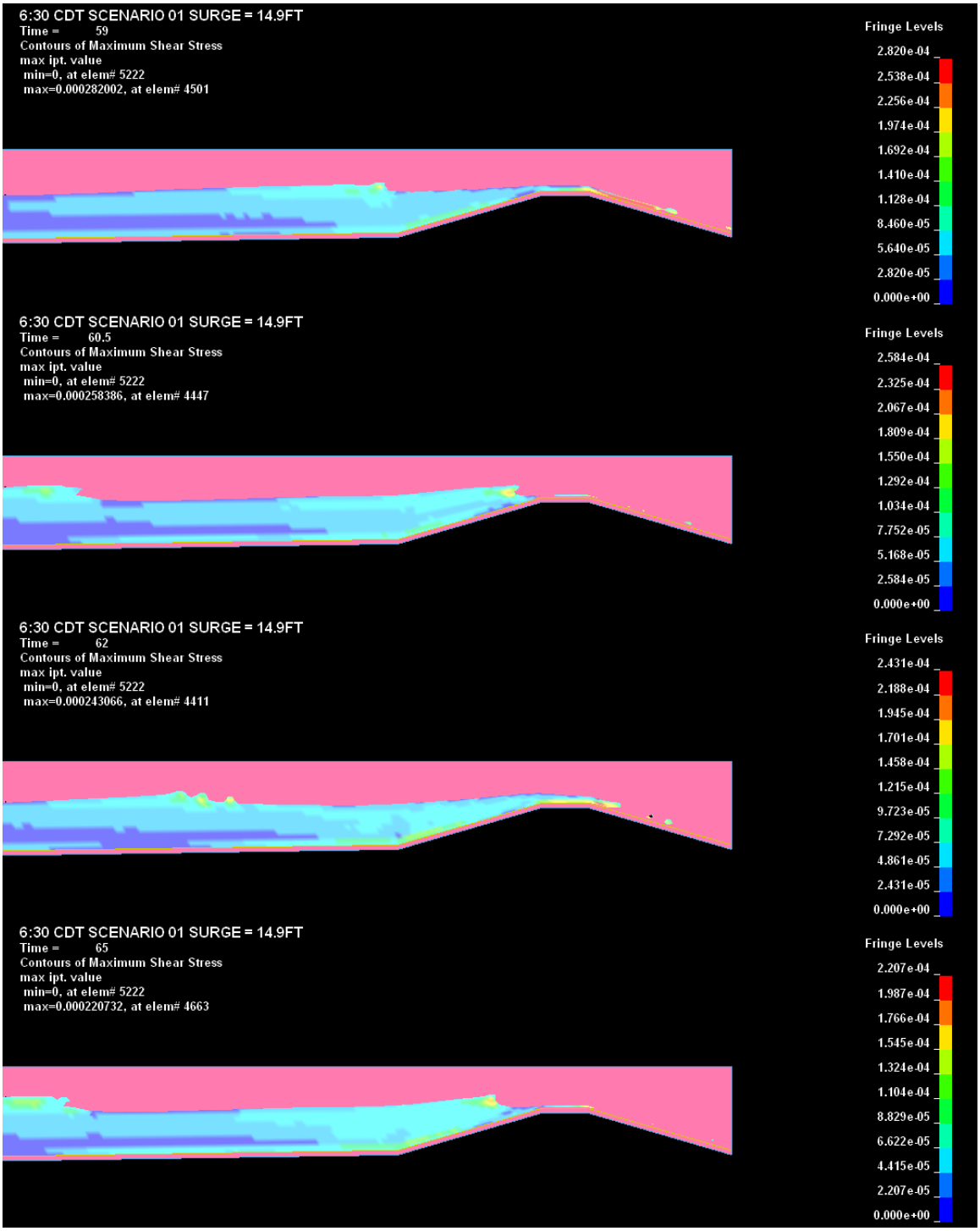


Figure C75**:** With the hurricane storm surge at El. +14.8 ft (NAVD88), the actual geometric configuration of the EBSB induces a tendency for the waves to exhibit a primarily 'runup' and 'rundown' behavior with wave-induced overtopping.

Analysis Case G (0700 CDT)

Case G (Figure C76) consisted of a storm surge elevation of +16.0 ft (NAVD88), a wave period of 4.7 s, and a significant wave height of 7.9 ft. There was active overtopping.



Figure C76: Initial conditions for analysis Case G.

At Elevation +16.0 ft, the storm surge had reached the flood side toe of the EBSB. A plot of the shear velocities is presented in Figure C77. The peak shear velocity on the ESBS face was determined to be about 0 ft/s (at the monitoring node situated at Elevation +16 ft), due to the buffering of water movement due to the high surge elevation. Velocities across the crest and backside are high, with a peak velocity of over 10 ft/s rushing down the backside of the levee.

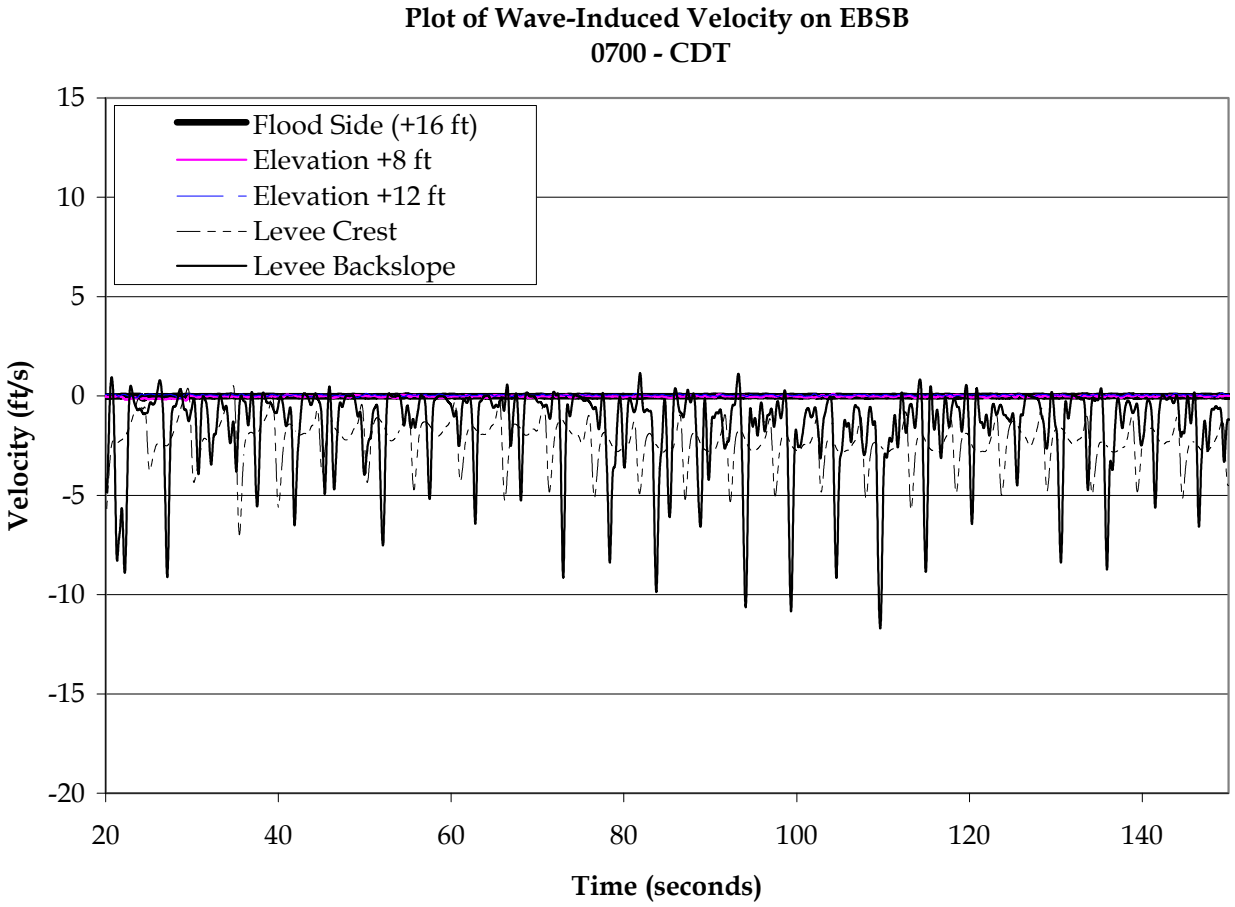


Figure C77**:** A plot of the velocity time history on the flood side face of the EBSB with the storm surge at +16.0 ft (NAVD88).

Figure C78 (below) provides a graphical representation of water movement over time. With the hurricane storm surge at El. +16.0 ft (NAVD88), the actual geometric configuration of the EBSB results in active overtopping by incident waves.

Storm Surge Elevation: +16.0 ft (NAVD88) Crest Elevation: +16 ft

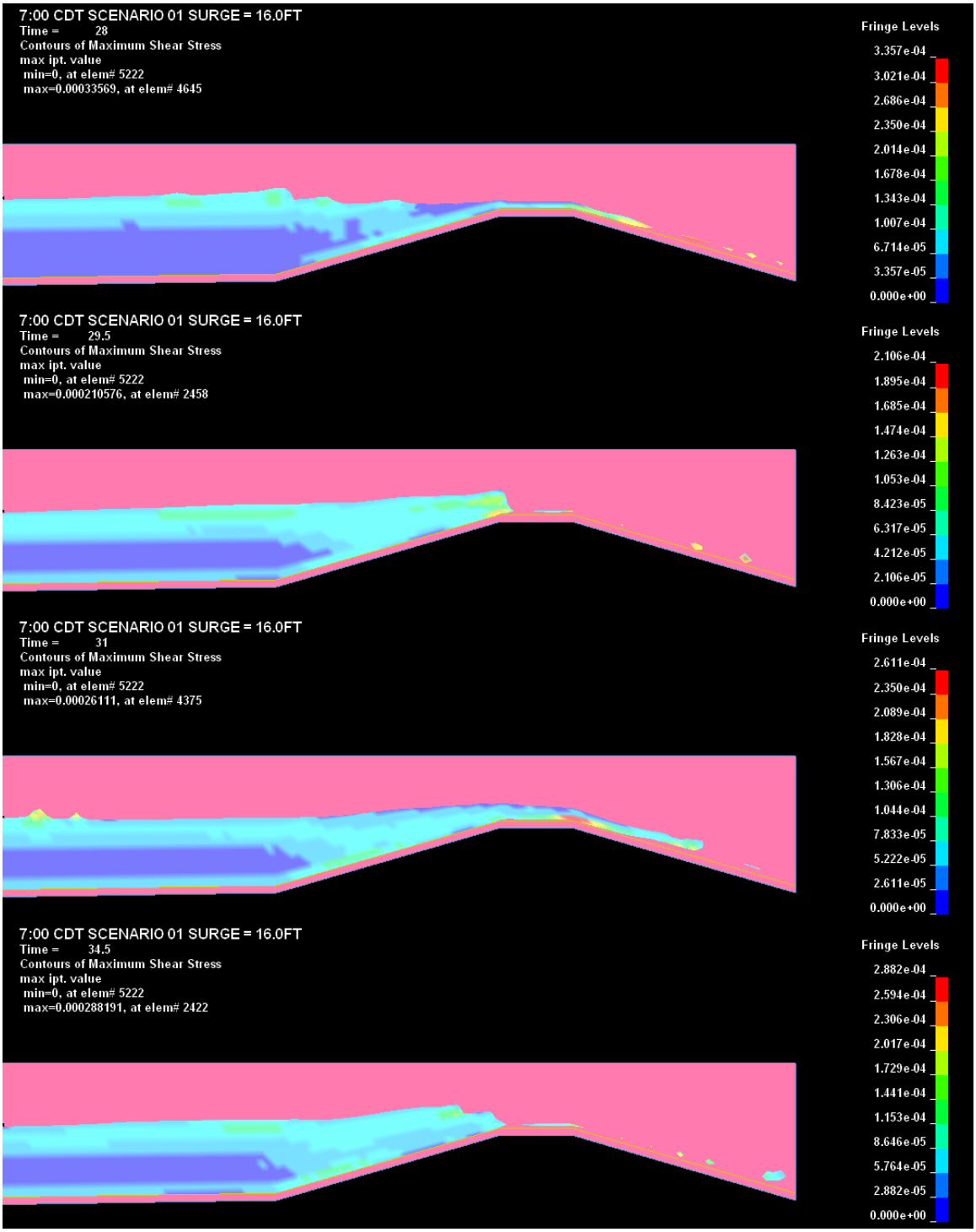


Figure C78**:** With the hurricane storm surge at El. +16.0 ft (NAVD88), the actual geometric configuration of the EBSB induces steady overtopping due to incident waves.

Analysis Case H (0730 CDT)

Case H (Figure C79) consisted of a storm surge elevation of +17.1 ft (NAVD88), a wave period of 4.0 s, and a significant wave height of 7.6 ft. There was active overtopping.

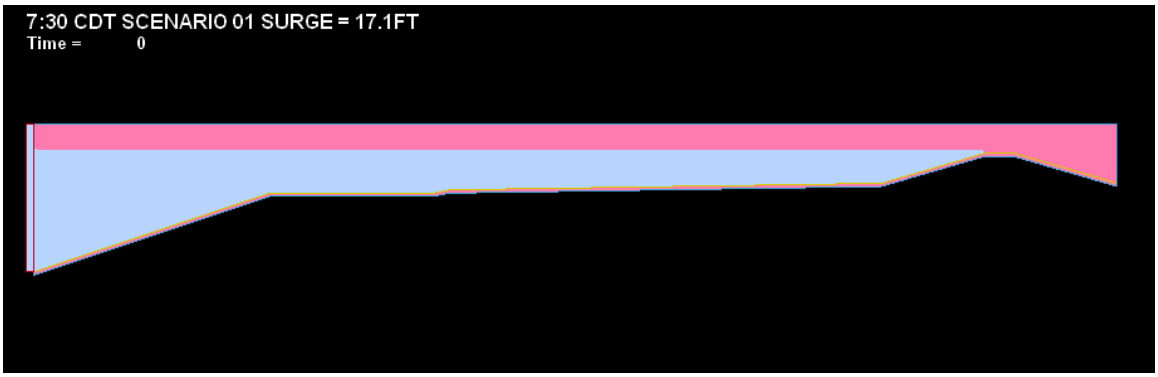


Figure C79: Initial conditions for analysis Case H.

At Elevation +17.1 ft (NAVD88), the storm surge had reached the crest of the EBSB and there was active overtopping. A plot of the shear velocities is presented in Figure C80. The peak shear velocity on the ESBS face was determined to be 0.4 ft/s.

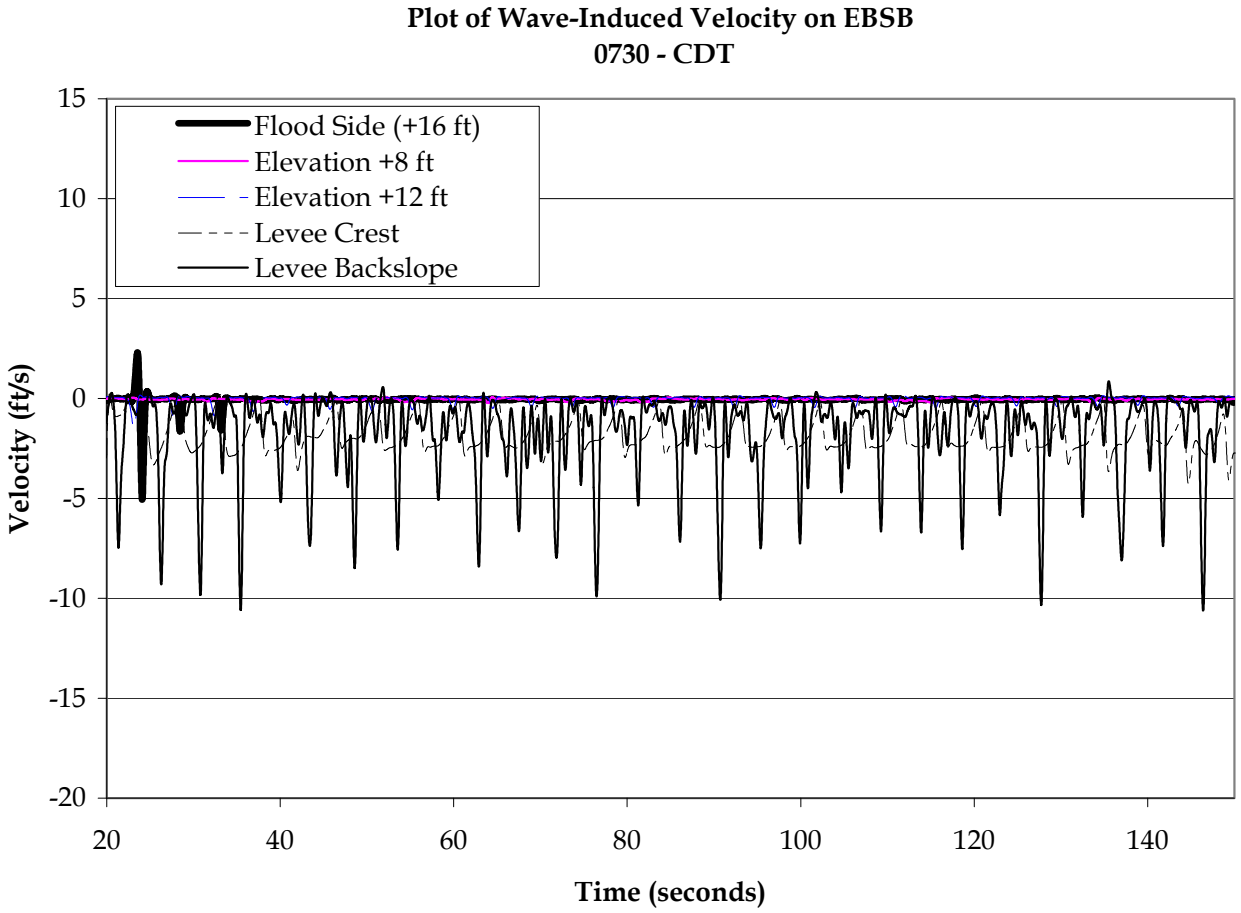


Figure C80**:** A plot of the velocity time history on the flood side face of the EBSB with the storm surge at +17.1 ft (NAVD88).

Figure C81 (below) provides a graphical representation of water movement over time. With the hurricane storm surge at El. +17.1 ft (NAVD88), the storm surge still water elevation actively overtops the actual geometric configuration of the EBSB.

Storm Surge Elevation: +17.1 ft (NAVD88) Crest Elevation: +16 ft

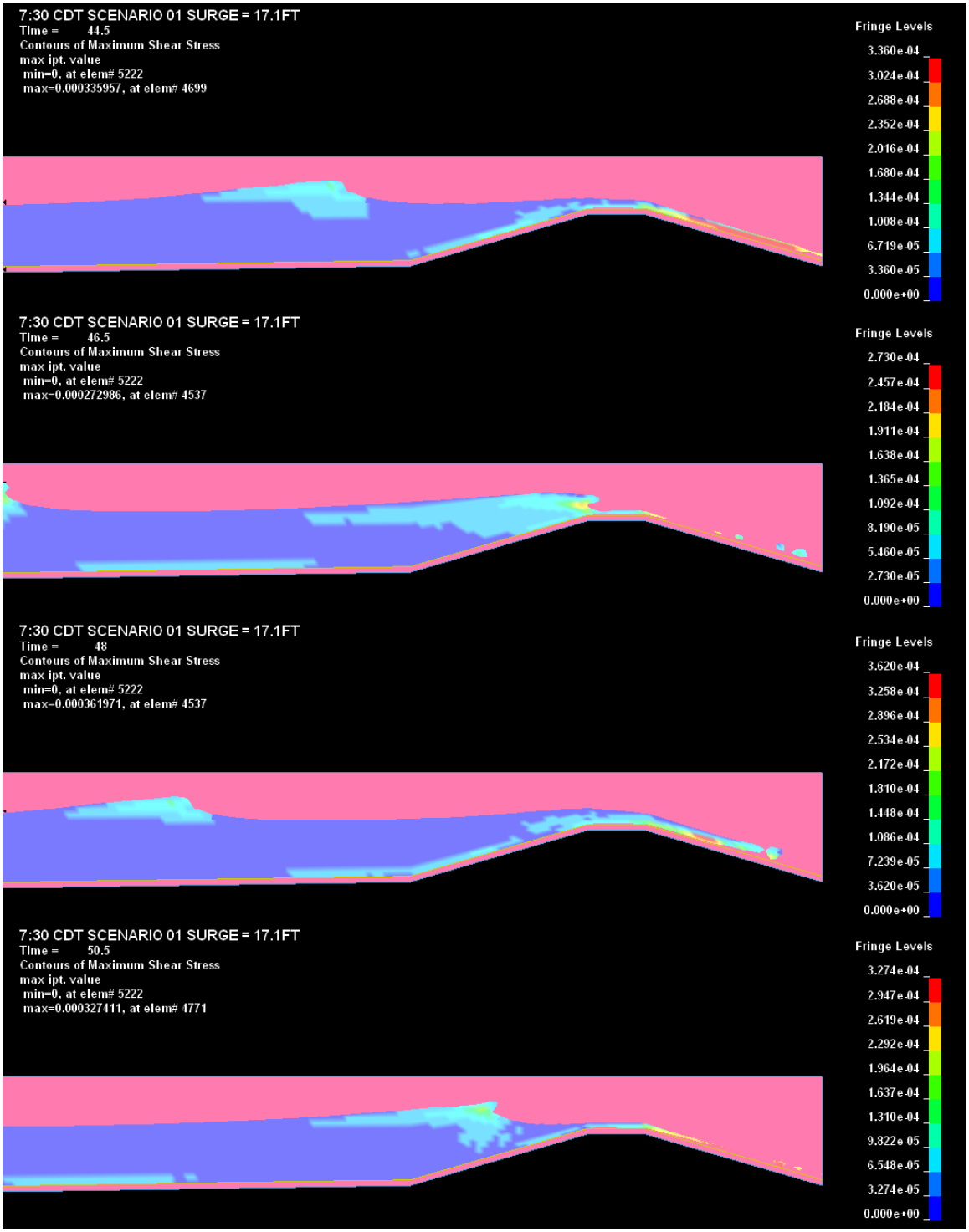


Figure C81: With the hurricane storm surge at El. +17.1 ft (NAVD88), the EBSB is actively overtopped as a result of both the still water storm surge and incident wind waves.